Molecular characterisation of the mechanism of target-dependant microRNA degradation

Semih Cetin

UNIVERSITÉ DE STRASBOURG

ÉCOLE DOCTORALE DES SCIENCES DE LA VIE ET DE LA SANTÉ

UPR 9002

THÈSE

présentée par :

Semih CETIN

soutenue le : **12 septembre 2016**

pour obtenir le grade de : **Docteur de l'université de Strasbourg**

Discipline / Spécialité :

Sciences du vivant / Aspects moléculaire et cellulaire de la biologie

Caractérisation moléculaire du mécanisme de dégradation des microARN par un transcrit cible

THÈSE dirigée par :

Mr PFEFFER Sébastien	Directeur de recherche CNRS, Université de Strasbourg

RAPPORTEURS :

Mr BRODERSEN Peter	Associate Professor, Université de Copenhague
Mme VANACOVA Stěpánka	Associate Professor, Université de Masaryk

---

AUTRES MEMBRES DU JURY :

Mr GAGLIARDI Dominique	Directeur de recherche CNRS, Université de Strasbourg
Mr FILIPOWICZ Witold	Professeur, Friedrich Miescher Institute for Biomedical Research

Acknowledgements

I would like to first of all thank Sébastien for giving me the opportunity to do my thesis in his laboratory. I am very grateful to have been a part of his team, the members of which he chooses so well to form a very diverse and interesting bunch that creates a very enjoyable learning and growing environment. Thank you for being so supportive and always accessible to talk science or any other subject. Being supervised by Sebastien was very enriching experience for which I will forever be grateful, rich in learning and experiences not only through my main work in the lab but also through the collaborations he allowed me to take part in as well as the teaching missions that he encouraged me to pursue at the faculty.

I would also like to thank the members of the jury, Peter Brodersen, Stěpánka Vanacova and Dominique Gagliardi for accepting to judge my work and for their invaluable feedback through the very interesting and stressful scientific discussion during my defence.

I would like to thank Joern Pütz for inspiring me to follow my scientific adventure in Strasbourg after my year as an Erasmus student, and for helping and supporting me tremendously along the way.

I would like to thank all the former and present members of the Pfeffer laboratory; Gabrielle, Mélanie, Erika, Aurélie, Maud, Béatrice, Ramy, Diane, Guillaume, Lee, Ali, Ilyass, Mathieu, Antoine and Olivier, with whom we shared a great deal of time inside and outside of the laboratory. Thank you all for your support during these years and helping me grow personally and professionally. You have made this adventure very enjoyable and very memorable and I feel very lucky and grateful to have shared my time with you all.

I am thankful to my family who have always been there for me and supported me in every way since the start, never failing to encourage me along the way. Finally, I would like to thank my girlfriend Nevcin, for being ever present, through our adventures from our Erasmus year abroad to our thesis studies. She has been the source of tremendous support during these times and the invaluable constant in my life.

TABLE OF CONTENTS

TABLE OF FIGURES

TABLES INDEX

INTRODUCTION

1. Biogenesis of miRNAs

1.1 Canonical biogenesis of mammalian miRNA

The biogenesis of miRNAs has been extensively studied over the years and we now have quite a good understanding of the different mechanisms involved in this process, although some aspects of it still require further investigation. In this part, I will focus on the current knowledge of the canonical mammalian miRNA biogenesis, but will also mention work performed on invertebrates like *Drosophila* and *C. elegans* as they have contributed to our current knowledge on mammalian miRNA biogenesis.

1.1.1 Generation of miRNA precursor and export into the cytoplasm

miRNAs derive from large primary transcripts (pri-miRNAs) that are generally transcribed by RNA polymerase II. These pri-miRNAs resemble regular coding transcripts as they are capped and polyadenylated (Cai et al., 2004; Lee et al., 2004). Pri-miRNAs can be found in introns and exons from protein coding genes or expressed as their own independent transcription unit (Baskerville and Bartel, 2005; Kim and Kim, 2007; Rodriguez et al., 2004). In other rare cases they can also be transcribed by RNA polymerase III (Pfeffer et al., 2005) (Figure 1). The pri-miRNA transcript contains regions that fold back into imperfect stem-loop structures, these stem-loops can be recognized and excised by an Rnase III ribonuclease called Drosha in the nucleus (Lee et al., 2003) (Figure 1, 2 and 3)). Several sequence and structural determinants exist on pri-miRNAs that make them good substrates for Drosha processing. Hence, pri-miRNAs present an imperfect stem-loop structure of three helical turns (~33bp), flanked by a terminal loop and single stranded segments (Han et al., 2006). The single stranded segments are important, as Drosha will cleave by measuring 11 bp from the basal junction (Auyeung et al., 2013). Additionally, other sequence determinants are important for efficient Drosha processing, the basal motifs UG at position -13 from the cleavage site and CNNC at position +17, and to some extent the apical motif GUG/UGU (Auyeung et al., 2013; Fang and Bartel, 2015) (Figure 2-A, 2-B). The importance of these sequence motifs varies from one pri-miRNA to the next though, as one fifth of all mammalian pri-miRNA do not possess any of them.

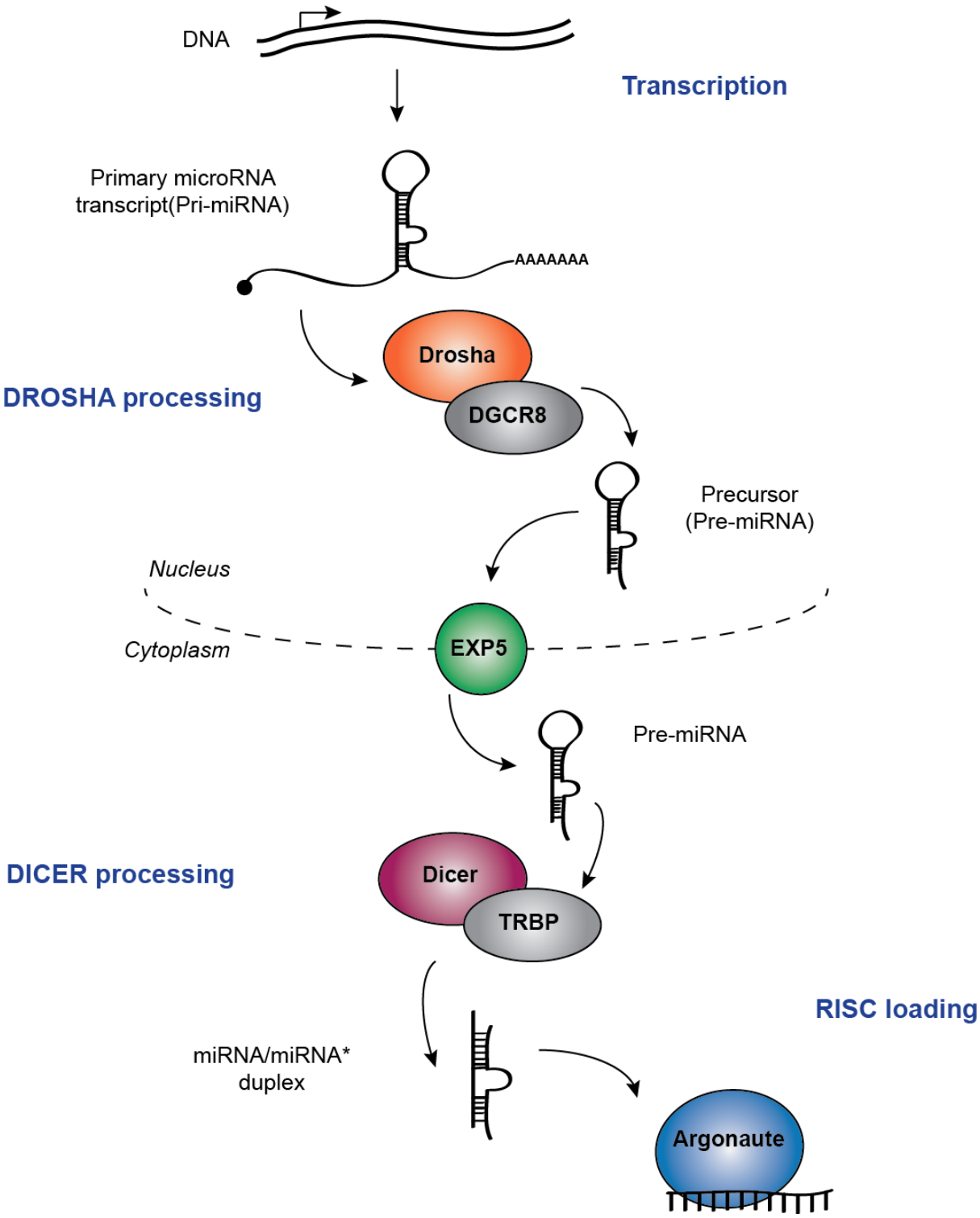

Figure 1: Biogenesis of miRNAs

Schematic representation of miRNA biogenesis in mammals. After the primary transcript of a miRNA (pri-miRNA) is produced, two sequential processing events occur, first by Drosha to produce the miRNA precursor (pre-miRNA) followed by its export to the cytoplasm by EXP5 (exportin-5), then by DICER, which will generate the mature miRNA/miRNA* duplex. One of the two strands of the duplex is then loaded into an Argonaute protein to form the RNA-induced silencing complex (RISC).

Drosha is part of a protein complex called the Microprocessor, the other essential cofactor found in this complex is the diGeorge Syndrome Critical Region Gene 8 (DGCR8) protein (Denli et al., 2004; Gregory et al., 2004; Han et al., 2004; Landthaler et al., 2004). A recent study shows that a dimer of DGCR8 and one monomer of Drosha constitute the Microprocessor (Nguyen et al., 2015) (Figure 2-B and 3-B). DGCR8 recognizes the apical stem of the pri-miRNA hairpin with the UGU motif and DROSHA positions itself by recognizing the basal UG motif, resulting in the cleavage of the pri-miRNA by measuring 11 bp from the basal junction, a feature that was recently confirmed by the resolution of Drosha crystal structure (Kwon et al., 2016; Nguyen et al., 2015) (Figure 2-B and 3-C).

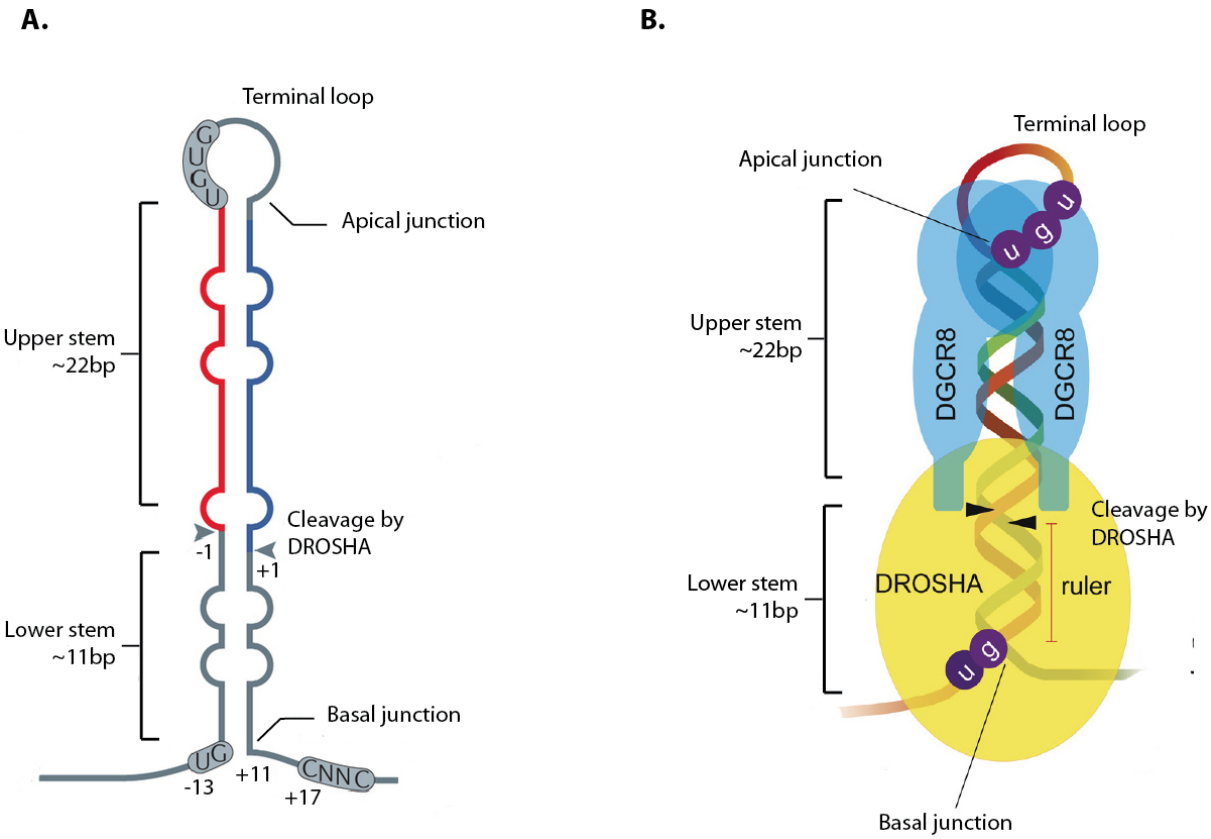

Figure 2: Structure of primary miRNA and the organization of the Microprocessor
A. Schematic representation of a typical pri-miRNA organization, ~33 bp stem-loop and sequence determinants present in the apical loop and single strand flanking regions are key features for Drosha recognition. **B.** Model of the organization of the microprocessor on the pri-miRNA composed of a dimer of DGCR8 and one DROSHA. DROSHA cleaves by measuring ~11bp from the basal junction. Adapted from (Ha and Kim, 2014; Nguyen et al., 2015).

The cleavage by the Microprocessor releases the stem-loop precursor RNA (pre-miRNA) and leaves a 2nt overhang and hydroxyl group at its 3' extremity, typical of Rnase III cuts (Lee et

al., 2002). Once the pre-miRNA has been released by Drosha, it is transported to the cytoplasm by the Ran-GTP dependent nuclear export factor Exportin-5 (Bohnsack et al., 2004; Lund et al., 2004; Yi et al., 2003) (Figure 1). The 3'OH and 2nt overhang present on the pre-miRNA is the feature that is recognized and required for Exportin-5 binding (Zeng and Cullen, 2004). Exportin-5 also contributes to the protection of pre-miRNAs from degradation by binding to both its 5' and 3' extremities (Okada et al., 2009).

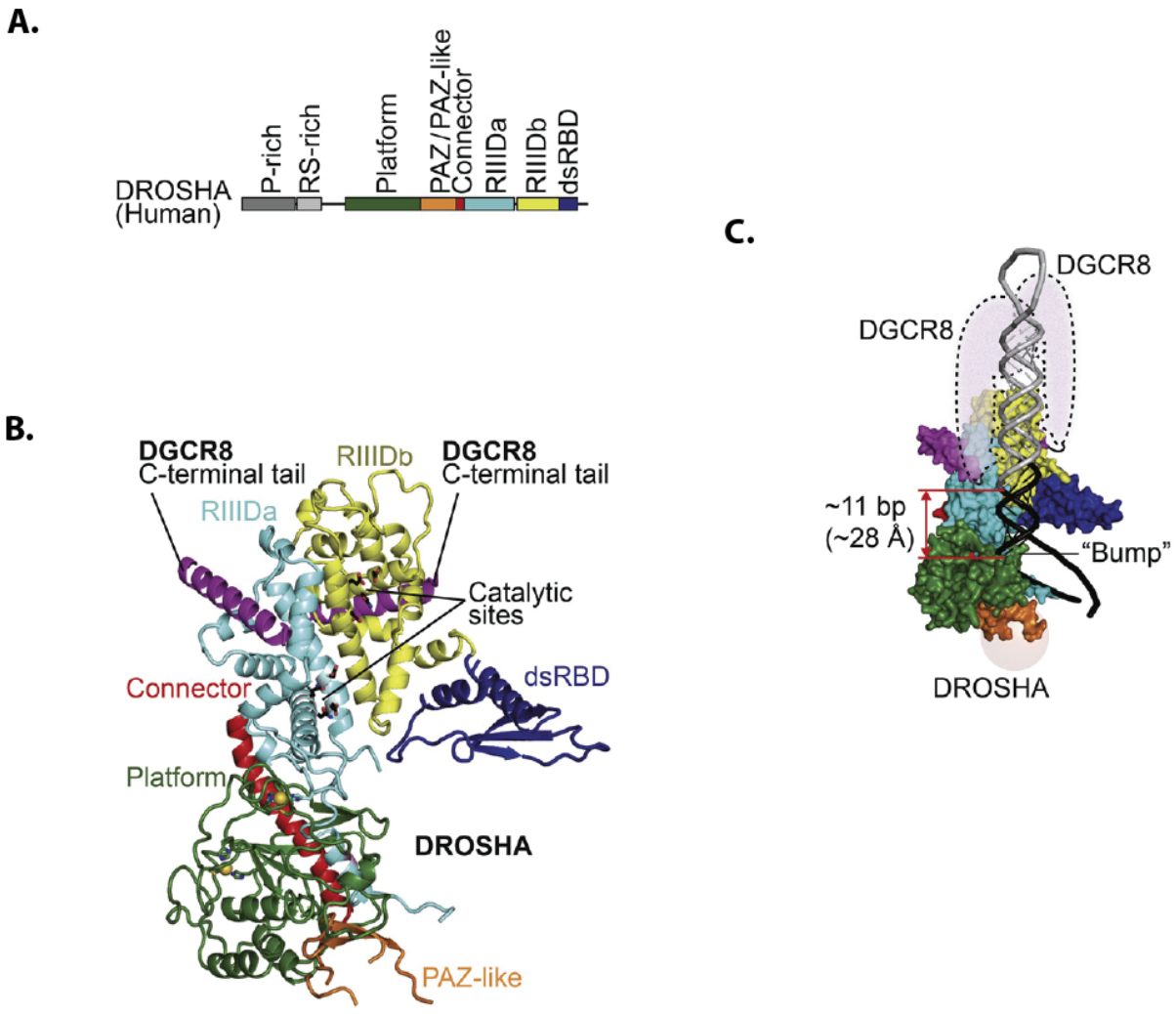

Figure 3: Structure of Drosha

A. Domain organization of human Drosha. The structure of a fragment of Drosha (390-1365) was resolved in complex with the C-terminal tail of DGCR8 which have been previously shown to be sufficient for pre-miRNA processing (Nguyen et al., 2015) **B.** The domains are colored as in A. **C.** model for human Microprocessor binding to pre-miRNA, confirming the stoichiometry of the microprocessor with one Drosha and two DGCR8 molecules. Taken from (Kwon et al., 2016).

1.1.2 Dicing of the pre-miRNA into miRNA/miRNA* duplex

Once in the cytoplasm the pre-miRNA will be recognized and processed by a second Rnase III enzyme called Dicer, this maturation step will produce the mature miRNA duplex (Hutvágner et al., 2001). The first model of DICER cleavage described the recognition of the 3' overhang of the pre-miRNA by the PAZ (Piwi Argonaute Zwille) domain and the cleavage near the apical loop after measuring 22 bp, creating a new 3'OH terminal 2nt overhang (Macrae et al., 2006; Zhang et al., 2004). More recently though, it was demonstrated that Dicer also anchors the 5' end of the pre-miRNA by recognizing the 5' terminal phosphate group in addition to its 3'OH, and the cleavage site is designated by measuring 22 bp from this end for most pre-miRNA (Park et al., 2011) (Figure 4).

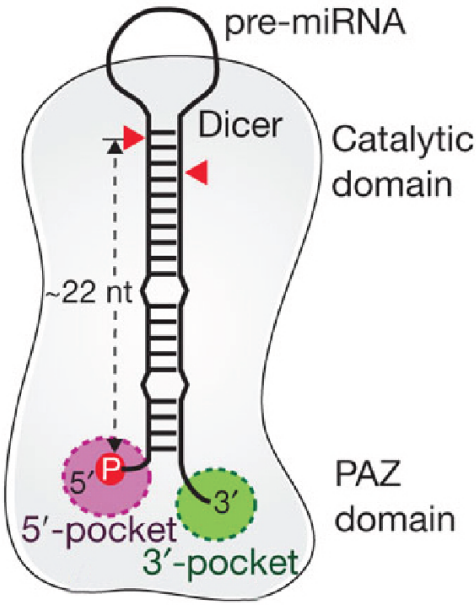

Figure 4: Schematic representation of Dicer pre-mi-RNA processing.
5' and 3' binding pockets in the PAZ domain recognize the 5' phosphate and the 3'OH of the pre-miRNA respectively. DICER then measures 22 bp after the 5'P and cleaves to produce the miRNA/miRNA* duplex. Taken from (Park et al., 2011).

Dicer is found in complex with a cofactor called TRBP (Transactivation region (Tar) RNA binding protein) (Chendrimada et al., 2005; Haase et al., 2005) and also another one called PACT (Protein activator of PKR) (Lee et al., 2006). In the absence of TRBP the expression level of miRNAs do not change, however Dicer cleavage becomes less accurate, shifting the start and end of mature miRNAs by several nucleotides (Kim et al., 2014b). However, in the

absence of PACT the miRNA levels or accurate processing of pre-miRNA do not differ from wild-type cells, raising the question of its importance in pre-miRNA processing (Kim et al., 2014b).

TRBP and PACT have other roles beyond their implication in the biogenesis of miRNA pathway, which are reviewed in (Heyam et al., 2015; Svobodova et al., 2016). Notably, they have antagonistic roles in the interferon pathway, their binding to Dicer being mutually exclusive as they share the same binding residues (Wilson et al., 2015), these cofactors might be at the origin of a crosstalk between Dicer and the interferon pathway.

The duplex of miRNA formed after Dicer cleavage will be loaded in the effector complex called RNA induced silencing complex (RISC), which will invariably contain a protein from the Piwi/Argonaute family (Carmell et al., 2002). There are four Argonaute proteins (AGO1-4) in mammals capable of loading miRNAs, but only AGO2 has the slicer activity allowing the endonucleolytic cleavage of the target RNA (Liu et al., 2004; Meister et al., 2004).

1.2 Non canonical biogenesis of miRNA

Although the canonical biogenesis pathway accounts for the maturation of the vast majority of miRNAs, there are several examples of miRNAs that do not rely on the canonical maturation machinery. A recent study by Narry Kim's laboratory looked at the effects of individual knockouts of Drosha, Exportin 5 and Dicer on miRNA expression in human cells and divided the non-canonical miRNA maturation in a total of five different groups (Kim et al., 2016b) (Figure 5).

Several examples of miRNAs exist which skip the Drosha-mediated cleavage, as they are already expressed into a structure mimicking that of a pre-miRNA or another enzyme catalyses the production of the pre-miRNA. One of the earliest discovered group of Drosha-independent miRNAs are called mirtrons. These pre-miRNA derive from intronic loci and their extremities are defined by the splicing event therefore precluding the need of further cleavage, they then join the canonical pathway at the level of nuclear export (Berezikov et al., 2007; Okamura et al., 2007; Ruby et al., 2007) (Figure 5). Compared to the canonical miRNAs, the numbers of mirtrons is quite low. A likely explanation for this is the existence of a pathway counteracting the emergence of new mirtrons by signaling them for degradation by non-templated nucleotide addition, as recently reported in *Drosophila* (Bortolamiol-Becet et al., 2015; Reimão-Pinto et al., 2015).

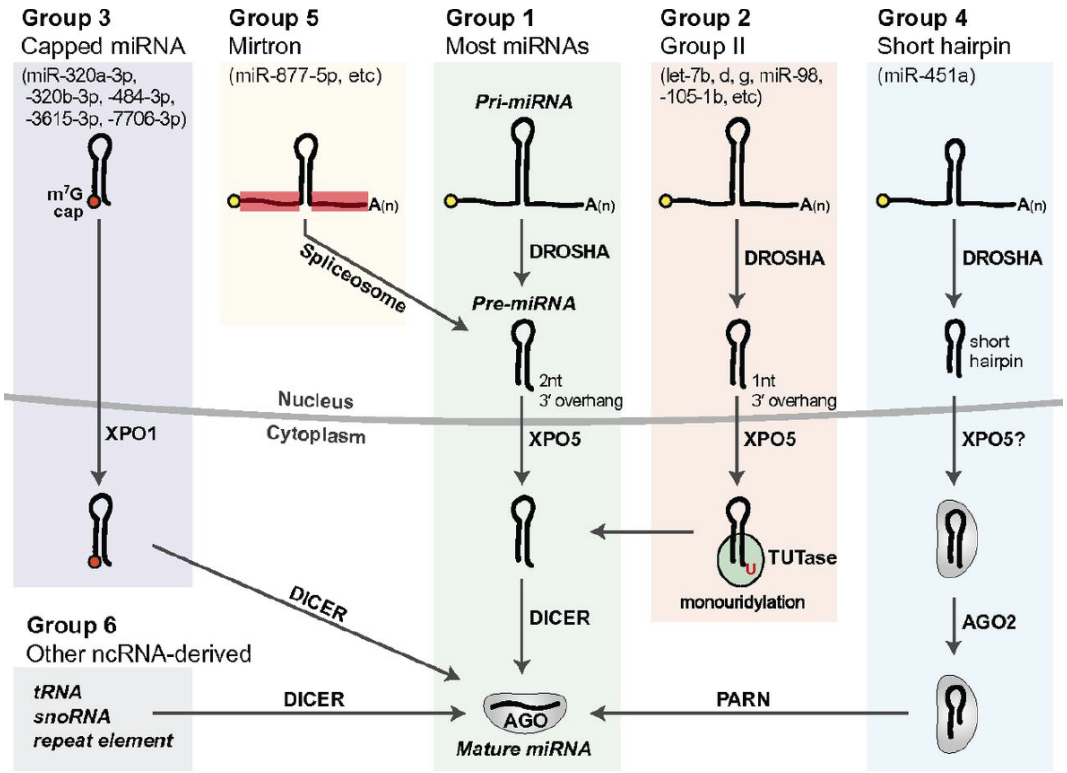

Figure 5: Biogenesis pathways of miRNAs.
Most miRNAs follow the canonical miRNA biogenesis pathway (group 1) requiring both Drosha and Dicer processing. The majority of let-7 family members as well as miR-105 require TUTases activity to get the correct 2nt 3' overhang (group 2) before Dicer processing (Heo et al., 2012). Other groups follow their biogenesis independently of Drosha or Dicer processing. Taken from (Kim et al., 2016b).

Another example of Drosha independent miRNAs is called 5'capped pre-miRNA. These pre-miRNAs are produced by RNA polymerase II, are capped at 5' extremity and their 3' end is believed to be defined by premature transcription termination. These pre-mRNAs are exported by Exportin-1 and processed by Dicer. One particularity of these miRNAs is that only the 3p arm of the pre-miRNA can be loaded into AGO, as the cap interferes with loading, thereby allowing a new experimental strategy for expressing exogenous si/miRNA with only one functional arm (Xie et al., 2013) (Figure 5).

Non-coding RNA like tRNAs and snoRNAs can also be a source of miRNAs that are independent of Drosha (Babiarz et al., 2008; Ender et al., 2008). Some herpesviruses have also been shown to express Drosha-independent miRNAs, such as the mouse herpesvirus MHV68, which expresses miRNAs from tRNAs that are processed by RNAseZ (Bogerd et al., 2010; Pfeffer et al., 2005) (Figure 5 and 6-A). Another example is the herpesvirus saimiri, which uses an snRNA-like RNA as a precursor and the integrator complex to release the pre-miRNA (Cazalla et al., 2011) (Figure 5 and 6-B).

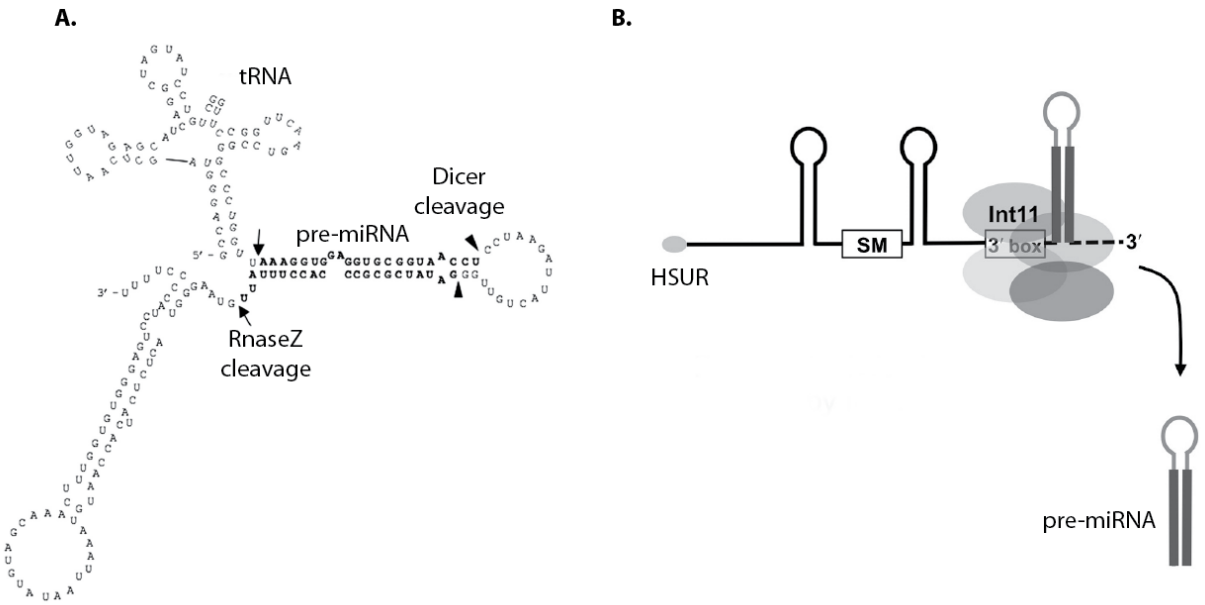

Figure 6: Examples of Drosha independent group 6 miRNA biogenesis
A. structure of pri-miR-M1-7 expressed by MHV68 that contains a tRNA, the pre-miR-M1-7 and another stem-loop. RNAseZ cleavage sites are shown by arrows and Dicer cleavage sites by triangles. Taken from (Bogerd et al., 2010). **B.** The structure of several HSURs expressed by *Herpervirus saimiri*. The 3' box is recognized and cleaved by the Integrator complex, creating a pre-miRNA and a pre-snRNA. The pre-miRNA is exported to the nucleus for Dicer processing. Taken from (Cazalla et al., 2011).

miR-451 to date is the only known miRNA to present a Dicer-independent maturation. After Drosha-mediated cleavage, it is directly loaded into AGO2, which slices its 3'arm (Cheloufi et al., 2010; Cifuentes et al., 2010; Yang et al., 2010). The resulting longer 5p miRNA arm is trimmed by the exonuclease PARN (Poly(A)-Specific Ribonuclease) resulting in the mature miR-451 (Yoda et al., 2013) (Figure 5). Similar to miR-451, pre-miRNAs previously were shown load onto AGO (Diederichs and Haber, 2007; Liu et al., 2012). Recently, it was shown that 5p miRNAs were less affected than 3p miRNAs in Dicer knockout cells, this is due to the loading of pre-miRNAs to AGO and their maturation by slicing and trimming like miR-451 (Kim et al., 2016b).

1.3 Formation of functional miRISC

Whether their biogenesis depends on Drosha and Dicer or not, all functional miRNAs get loaded onto an Argonaute protein to form effector complexes called RISC in order to exert their function. The formation of RISC is a multistep process consisting of the loading of the duplex, unwinding of the two strands and passenger strand ejection. The loading of the mature

miRNA duplex takes place in the so called RISC Loading Complex (RLC), which contains Dicer, an Argonaute protein and TRBP (Chendrimada et al., 2005; Gregory et al., 2005; Maniataki and Mourelatos, 2005). After loading of the duplex into AGO, one of the strands is discarded, it is refered to as the passenger strand or miRNA* sequence, whereas the one that is kept is called the guide strand (miRNA).

Argonaute proteins possess four domains called N, PAZ, MID and PIWI, the 5' phosphate end of the miRNA is bound by the 5' binding pocket located at the interface of N and MID domains (Ma et al., 2004; Parker et al., 2005) while the 3' hydroxyl end of the miRNA is anchored in the PAZ domain (Lingel et al., 2004; Yan et al., 2003) (Figure 7-A and 7-B). The PIWI domain folds like an Rnase H endonuclease that is catalytically active for target RNA cleavage only in the case of AGO2 in mammals (Meister et al., 2004; Schwarz et al., 2004; Song et al., 2004).

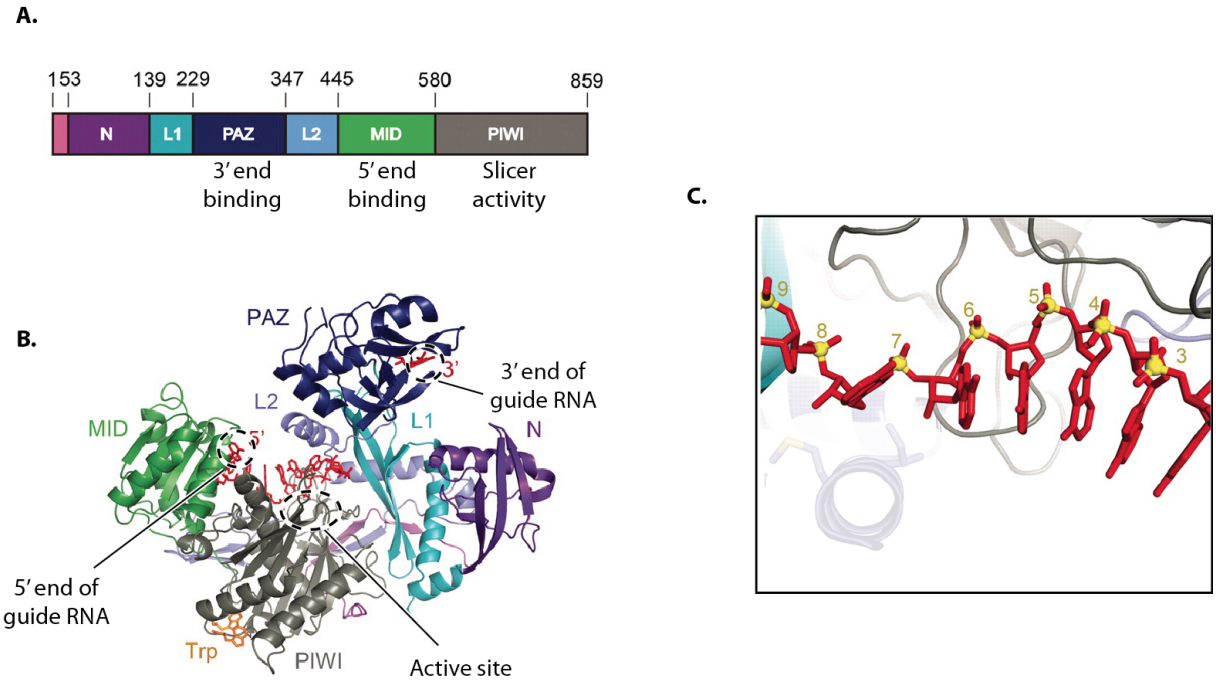

Figure 7: Domain organization and structure of AGO2.

A. Domain organization of human AGO2. **B**. Structure of human AGO2 and a guide RNA (in red). Tryptophan residue binds to hydrophobic pockets in the PIWI domain. **C.** Zoom on the seed region that is exposed and organized in a helix ready to engage with target RNA. Taken from (Schirle and MacRae, 2012).

The loading of the mature miRNA duplex is a dynamic process, as it requires ATP hydrolysis. The ATP-dependent step is when the mature duplex of miRNA is loaded onto AGO, with the help of the chaperones Hsp70/Hsp90 (Iwasaki et al., 2010; Johnston et al., 2010). The proposed model of action of Hsp70/Hsp90 on duplex loading is called 'energy slope' model, where Hsp70/Hsp90 will stabilize AGO in an open, duplex-loading capable conformation,

which is thermodynamically less favorable, until the loading of the miRNA duplex, where it comes back to a stable conformation (Kobayashi and Tomari, 2016). The following steps of loading are ATP-independent. The choice of the guide strand is asymmetric and depends on the thermodynamic stability of the 5' of miRNA duplex, the strand with the least stable pairing at its 5' end will be kept (Khvorova et al., 2003; Schwarz et al., 2003). In mammals, although Dicer and TRBP are found associated with the RISC loading complex, they do not contribute to the strand selection process (Betancur and Tomari, 2012; Kim et al., 2014b). AGO alone is able to sense the thermodynamic stability of a miRNA duplex as it is prying away the guide strand by its 5'end from the passenger strand (Suzuki et al., 2015). The unwinding then functionally involves the N domain of AGO this time on the 3' end of the guide strand, resulting finally in the ejection of the passenger strand (Kwak and Tomari, 2012). Some miRNA duplexes, like siRNA duplexes in Drosophila, use passenger strand cleavage for facilitating the guide strand loading and passenger strand ejection, although this requires the slicer activity of AGO2 (Shin, 2008). However, for most miRNA duplexes, the ejection happens by slicer-independent unwinding of the passenger strand, as most miRNA duplexes have mismatches in central position that facilitate the unwinding and are incompatible with AGO2-mediated cleavage (Kawamata et al., 2009).

2. Mode of action and Function of miRNAs

2.1 Target recognition of miRNAs

Once the mature RISC is formed, the miRNA will guide this complex to target messenger RNAs and direct their post-transcriptional repression. In animals, although it is uncommon, when there is extensive complementarity between the miRNA and its target mRNA, AGO2-containing RISC can direct cleavage of the messenger (Yekta et al., 2004). For most miRNA and their respective mRNA targets, the complementarity will be non-extensive and RISC will direct translational repression by diverse mechanisms (discussed in the next part).

The fact that animal miRNAs find their targets only by partial complementarity poses a big problem when it comes to identify their potential targets. However, not all residues within the miRNA sequences are equally important and various evidence pointed out that the most prominent sequence determinant of miRNA targeting is at 5' proximal nucleotides 2 to 8 so-called the 'seed' region (Lewis et al., 2003). The seed region alone is sufficient for translational repression as G-U wobbles in the seed hinder targeting and 3' region binding is hardly determinant (Brennecke et al., 2005; Doench and Sharp, 2004). This observation is supported by crystal structure analysis of AGO2 loaded with miRNA, showing the positions

2-6 of the miRNA exposed and free to engage in base pair formation with target RNAs (Elkayam et al., 2012; Schirle and MacRae, 2012) (Figure 7-B and 7-C). Although the pairing of the seed is necessary and sufficient for miRNA-mediated regulation, some examples of supplementary and compensatory pairing to the seed exist in the literature (reviewed in (Bartel, 2009; Pasquinelli, 2012)). Since in animals, most miRNA interact with target mRNAs within their 3'UTR region, several miRNA target prediction tools were developed focalizing on seed sequences and conserved binding sites on homologous 3'UTRs. These prediction algorithms, which can be of great value, produce however varying results with many false positives (reviewed in (Min and Yoon, 2010). Recently, several high-throughput experiments were designed to biochemically identify large number of targets. These usually rely on crosslink and immunoprecipitation of Argonaute proteins followed by deep sequencing of the isolated target RNAs. These studies showed, in addition to the classic seed match- 3'UTR interactions, other kind of interactions involving the coding sequence and 5' UTR region, thereby potentially broadening our understanding of miRNA target sites (Chi et al., 2009; Hafner et al., 2010; Leung et al., 2011a).

2.2 Influence of target site context

miRNAs guide the RISC to target mRNA with limited specificity, usually by the recognition of a seed-match sequence. As such, thousands of mRNAs have been found to be under pressure to maintain their miRNA binding sites (Brennecke et al., 2005; Krek et al., 2005; Lewis et al., 2005). At the same time, some messenger RNAs are also subjected to selective avoidance, a mechanism in which 50% of messengers expressed in the same tissue as some abundant miRNAs are devoid of seed matches for these miRNA (Farh et al., 2005; Stark et al., 2005). However, the avoidance of seed matches is not complete, as these mRNAs still contain seed-match sites, meaning that every miRNA binding does not have the same regulatory potential as others might. Other determinants probably exist in the surroundings of seed matches on the target mRNA influencing miRNA mediated regulation. Indeed, one study demonstrated through extensive mutational analysis that most of the 3'UTR of c*og-1* mRNA in *C.elegans* is important for miRNA repression, showing that a seed match alone is not a sufficient predictor of functional miRNA interaction (Didiano and Hobert, 2008).

In a study by Grimson *et al.*, the authors demonstrated that the accessibility of miRNA binding site is playing a major role in the efficacy of repression exerted by miRISC. They put forward several determinants such as the proximity to AU-rich sequences, creating less

secondary structures and easy access, avoidance of the region 15nt downstream of the stop codon to prevent competition with the ribosome and preference of the extremities of the UTR as the middle would have more chances to form occluding structures (also shown by (Gaidatzis et al., 2007)) . The number of adjacent miRNA binding sites present in a 3'UTR for the same or different miRNAs also affects the efficacy of repression, as miRNAs have been shown to have cooperative and combinatorial effects (Broderick et al., 2011; Grimson et al., 2007; Saetrom et al., 2007).

Other characteristics of the 3'UTR context influencing miRISC activity include binding of RBPs (RNA binding proteins) on or near a miRNA binding site. The effects of these RBP on the activity of miRISC will be discussed in the section 3.2.2.

2.3 Mechanism of action of miRNAs

As seen above, depending on the complementarity level between a miRNA and its target mRNA, the messenger will follow one of two different fates: cleavage and subsequent degradation by exonucleases when there is perfect complementarity (Hutvagner et al., 2004; Liu et al., 2004; Meister et al., 2004); translational repression when there is only partial complementarity. In the latter case, the target will be regulated upon recruitment of several factors by AGO, mediating a combination of mechanisms resulting in mRNA silencing. The key connector protein recruited in this case is GW182, which has been extensively studied as a partner of AGO proteins (Jonas and Izaurralde, 2015).

The silencing mechanism mediated by miRNAs has been extensively studied over the years, it occurs as a result of the combinatorial effect of translational repression and accelerated mRNA decay comprising deadenylation, decapping and 5' to 3' degradation (Figure 8). Another aspect of miRNA-mediated silencing is the sequestration of targeted mRNAs in cytoplasmic loci called GW182 containing bodies (GW bodies) or mRNA processing bodies (P-Bodies) restricting their availability to the translation machinery (Eulalio et al., 2007; Liu et al., 2005a; Pillai et al., 2005; Sen and Blau, 2005).

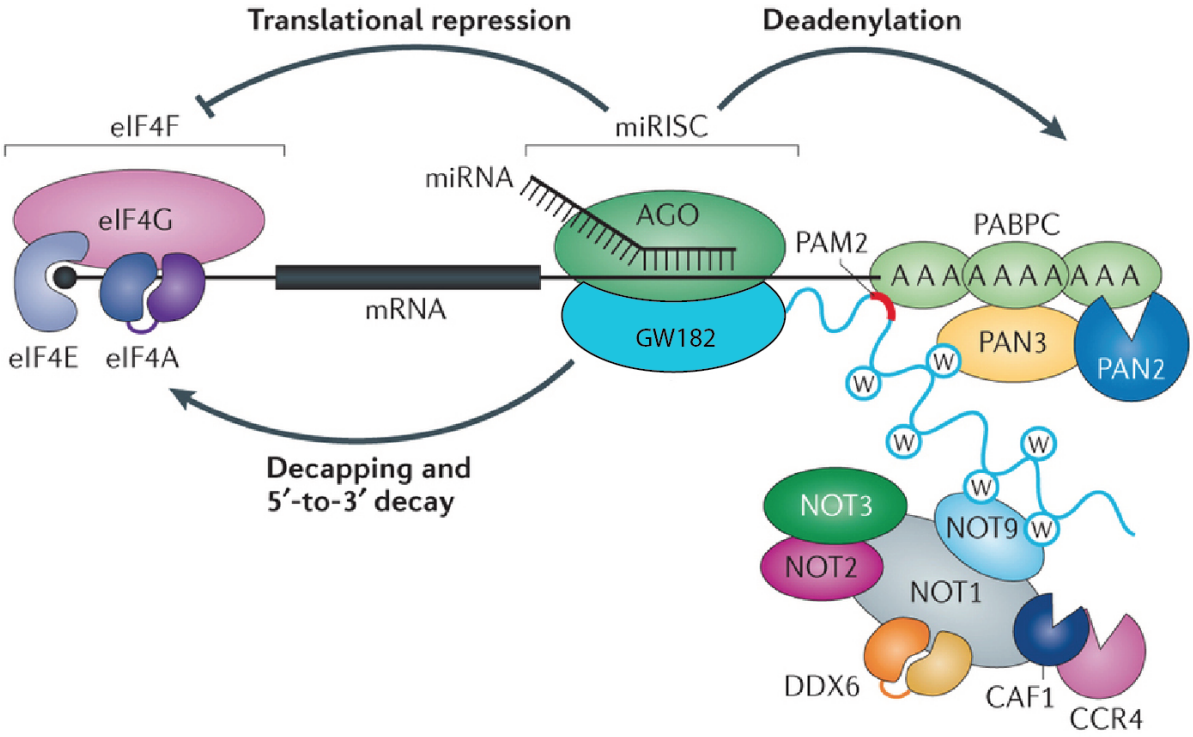

Figure 8: miRNA mediated gene silencing in animals.
Following AGO recognition of a target mRNA, it recruits GW182, which acts as a platform to interact with PABPC (cytoplasmic poly(A)-binding protein) and the deadenylase complexes PAN2-PAN3 and CCR4-NOT. Once deadenylated the mRNA gets rapidly decapped and degraded by XRN1 (5' to 3' exoribonuclease 1). In addition, miRNA also induce translational repression, although the exact mechanism is less clear. PAM2: PABP-interacting motif, W: Tryptophan repeats recruiting various complexes to RISC. Taken from (Jonas and Izaurralde, 2015).

The steps of translational inhibition and of mRNA decay as well as their sequence of events and their relative contribution to silencing have long been a source of debate in the field, due to the contradictory results obtained from different studies. The subject over the years has been covered numerous times in reviews that summarized the progress in the understanding of miRNA mediated silencing (Eulalio et al., 2008; Fabian and Sonenberg, 2012; Huntzinger and Izaurralde, 2011; Pillai et al., 2007). However, it is now well established that most of the silencing (66-90%) is due to mRNA decay as assessed by ribosome profiling studies (Eichhorn et al., 2014; Guo et al., 2010). Translation repression accounts for the rest of miRNA mediated silencing, however it is only observed at early time points after miRNA action, very rapidly mRNA decay becomes the dominant mechanism (Bazzini et al., 2012; Eichhorn et al., 2014).

As mentioned above, the central actor recruited by Argonaute proteins to induce repression is GW182. Indeed, the disruption of this recruitment impedes miRNA-induced silencing (Jakymiw et al., 2005; Liu et al., 2005b; Meister et al., 2005). Moreover, tethering GW182

alone to an mRNA will induce its repression (Lazzaretti et al., 2009; Zipprich et al., 2009). Three paralogues of GW182 protein exist in mammals, trinucleotide repeat containing 6 (TNRC6) A (also known as GW182), TNRC6B and TNRC6C. GW182 proteins take their name from GW repeats that they contain, these repeats are unstructured and participate in binding to AGO (Pfaff et al., 2013; Lian et al., 2009; Till et al., 2007) and poly-A binding protein (PABP) (Jinek et al., 2010; Zekri et al., 2009) (Figure 8). PABP and GW182 interaction is important for miRNA mediated silencing as mutating GW182 in its binding motif to PABP (PAM2) impairs its silencing activity (Huntzinger et al., 2010).

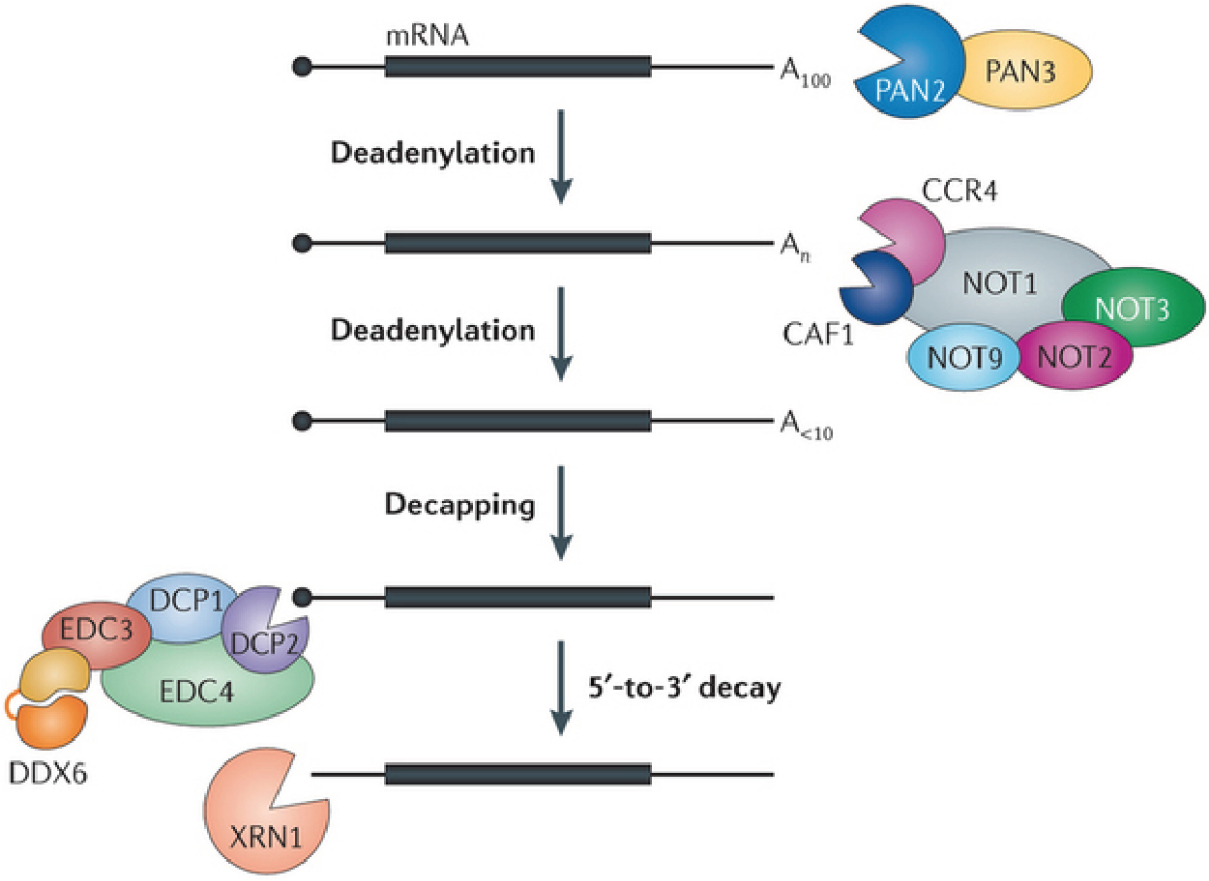

Figure 9: Cellular mRNA decay pathway

The majority of mRNA decay is triggered by deadenylation. The PAN2-PAN3 complex is responsible for the first stage of deadenylation which is then taken over by CCR4-NOT complex, although in the absence of PAN2-PAN3, CCR4-NOT can function by itself (Wahle and Winkler, 2013). Following deadenylation, decapping of the mRNA is induced. Several proteins participate in decapping, DCP1, EDC3, EDC4, DDX6 and PATL1 (not shown) (Chen et al., 2014; Jonas and Izaurralde, 2013; Mathys et al., 2014). DDX6 and PATL1 are interacting directly with CCR4-NOT1 complex creating a physical link between deadenylation and decapping (Jonas and Izaurralde, 2013). EDC4 in turn interacts with XRN1, recruiting the nuclease to the now decapped and deadenylated mRNA (Braun et al., 2012). Taken from (Jonas and Izaurralde, 2015).

Moreover, GW182 acts as a platform for other proteins and through the various interactions it triggers will cause the targeted mRNA to enter into the 5'to 3' mRNA decay pathway by bringing onto the mRNA the deadenylase complexes PAN2-PAN3 and CCR4-NOT (Braun et al., 2011; Chekulaeva et al., 2011; Fabian et al., 2011) (Figure 8 and 9). After deadenylation, decapping and 5' to 3' degradation will ensue.

Translational repression is another important part of miRNA-mediated silencing. Two models of translational repression were proposed, either acting at the initiation of translation or post-initiation steps. Again ribosomal profiling experiments shed light on this subject and excluded the involvement of post initiation steps (Guo et al., 2010). Rather, it seems that the predominant mechanism is the inhibition of translation initiation through interference with the activity of the eIf4F complex, reviewed in (Jonas and Izaurralde, 2015).

2.4 Function of miRNAs

More than half of protein coding genes have been found under selective pressure to maintain miRNA binding sites (Friedman et al., 2009). Consequently, it is not hard to imagine every cellular process being subjected to regulation by miRNAs. Unsurprisingly, aberrant expression profiles of miRNA are found in a wide variety of diseases. Notably, cancer researchers have reported extensively that some miRNAs can be oncogenic or tumor-suppressive when expressed abnormally (Esquela-Kerscher and Slack, 2006; Hammond, 2007). In addition, global levels of miRNA expression has also been found to be reduced in some cancers (Lu et al., 2005; Thomson et al., 2006). This reduction has been linked to low levels of Drosha or Dicer expression and to mutations in *TARBP2* or *XPO5* (Melo et al., 2009, 2010; Merritt et al., 2008).

Knock-out experiments in mice of central proteins in the miRNA pathway result in embryonic lethality. Mice with a null mutation in *Dicer*, the microprocessor components or *Ago2* die in early stages of development (Bernstein et al., 2003; Fukuda et al., 2007; Liu et al., 2004; Wang et al., 2007). These observations indicate the incompatibility of life with the complete loss of miRNA pathway. Nonetheless, most individual miRNA knockouts show moderate or no evident phenotypes, and only a couple of miRNAs have been linked to disease in humans (Mencia et al., 2009; de Pontual et al., 2011). This trend seems to be conserved in mouse (Park et al., 2012) and holds true for *C.elegans* as well, since only 10% of miRNAs are required for development and viability of the animal (Miska et al., 2007).

Typically, the inactivation of a given miRNA will only cause up to a two-fold increase in the expression level of its targets (Baek et al., 2008). Expect for a few miRNAs that can act as regulatory switches by strongly repressing a limited set of targets that result in a clear phenotypic outcome (Olsen and Ambros, 1999; Reinhart et al., 2000), most miRNAs are thought to reinforce the robustness of biological processes. They do so by helping to fine-tune gene expression in the face of challenges like transcriptional noise and environmental perturbations thereby enabling the cell to execute the decisions that it takes by other regulatory mechanisms (Bartel and Chen, 2004; Ebert and Sharp, 2012). One observation that reinforces this theory comes from the study of individual miRNA knockouts in *C.elegans* that showed a phenotype only in a sensitized background where other regulatory pathways are weakened (Brenner et al., 2010).

3. Regulation of miRNA expression

Given that miRNA are implicated in almost all cellular functions, their aberrant expression can be at the root of several conditions and diseases. What dictates ultimately the level of expression of a given miRNA is a combination of many factors, and it is therefore not surprising that at every level of the miRNA biogenesis from its transcription to the stability of the mature form, several molecular mechanisms are in action to ensure that the miRNA accumulates at the right level.

3.1 Regulation of miRNA biogenesis

3.1.1 Transcriptional regulation

Most of the miRNA genes are transcriptionally regulated in the same way as their mRNA counterparts, as they are similarly transcribed by RNA Pol II (Cai et al., 2004; Lee et al., 2004). This means that any regulatory mechanisms involved in the control of coding transcripts (transcription factors, enhancers, repressors, epigenetic modifications), are also involved in miRNA gene transcription regulation. Although for intergenic miRNA transcripts, this clearly holds true, ChIP-seq (chromatin immunoprecipitation followed by sequencing) experiments have shown that intronic miRNAs (but not mirtrons), may also use their own

promoter in addition to sharing their host mRNA's promoter (Monteys et al., 2010; Ozsolak et al., 2008), thus adding to the complexity of miRNA transcription regulation.
Transcription factors (TFs) play an important role in the expression of miRNA transcripts, they work to adjust positively or negatively the miRNA expression profile in a tissue or developmental time specific manner. Several examples of TFs regulating miRNA expression have been discovered in studies of miRNA expression in cancer. The tumor suppressor protein P53 has been shown for example to induce the expression of the miR-34 family (reviewed in (He et al., 2007)). Another example is the transcription factor c-Myc, a proto-oncogene, which has been involved in the induction of the miR-17-92 family (O'Donnell et al., 2005) and miR-9 (Ma et al., 2010) and also has been shown to down-regulate the expression of several tumor suppressor miRNA (Chang et al., 2008).

3.1.2 Regulation of miRNA processing

After production of the primary miRNA transcript, the sequential action of Drosha and Dicer will generate the final mature miRNA. Acting on these two steps as well as the export step represents a logical way to influence the accumulation level of the active miRNA. Protein components of these steps have been shown to be regulated post-translationally, thereby representing a way to influence globally on miRNA profile. Additionally, cofactors can also modulate the substrate preference of these enzymes, or in a more restricted manner, interact directly with the pri- or pre-miRNA sequence, to influence specifically (either negatively or positively) their processing efficiency.

3.1.2.1 Regulation of the Microprocessor

The regulation of the maturation by the Microprocessor of pri-miRNA is crucial for several reasons, in addition to the fact that the efficiency of this cleavage will affect the abundance of a miRNA, this cleavage also defines the extremities of the mature miRNA. The fidelity of this cleavage is therefore crucial to ensure the production of accurate mature miRNAs and restrict their targeting by constricting their seed sequence.
Drosha and its cofactor DGCR8 are part of a complex autoregulatory loop, where DGCR8 stabilizes DROSHA by way of protein-protein interactions on one hand, and where Drosha destabilizes DGCR8 mRNA by cleaving it at a hairpin structure on the other (Han et al., 2009;

Triboulet et al., 2009; Yeom et al., 2006). This ensures the preservation of homeostatic levels of the two proteins in the cell.

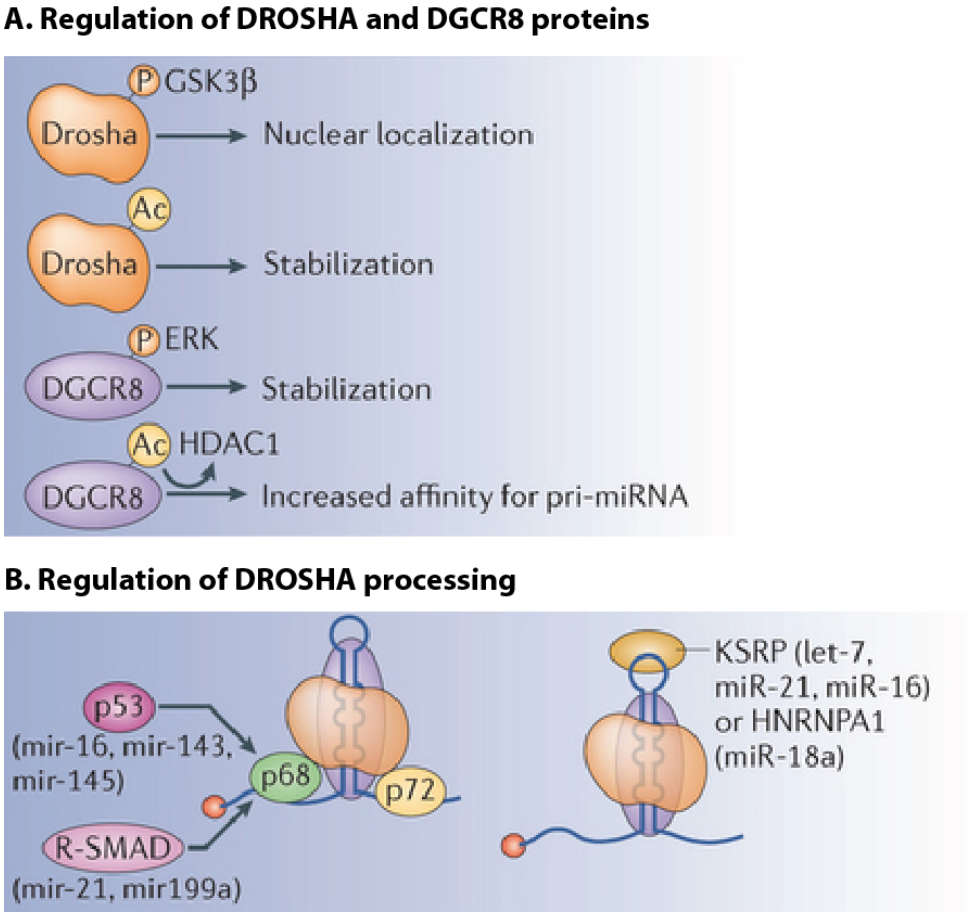

Figure 10: Examples of pri-miRNA processing regulation
A. Some example of the post-translational modifications on DROSHA and DGCR8 affecting in different ways the activity of the Microprocessor. **B.** Regulation of a subset of pri-miRNA processing by RNA binding proteins. Taken from (Ha and Kim, 2014).

Other mechanisms have been found to regulate the Microprocessor's activity. These include post-translational modifications of Drosha and DGCR8 and protein factors interacting with the Microprocessor or the pri-miRNA itself to modulate its processing efficiency. Post-translational modifications of the Microprocessor include: phosphorylation of Drosha by glycogen synthase kinase 3β (GSK3β), which is required for nuclear localization of DROSHA (Tang et al., 2010, 2011) and of DGCR8, which increases its stability (Herbert et al., 2013); Drosha can also be acetylated and this increases its stability by competing with its ubiquitination (Tang et al., 2013); finally DGCR8 can be deacetylated, which modulates positively its affinity towards pri-miRNAs (Wada et al., 2012) (Figure 10-A).

Several RNA-binding proteins regulate the Microprocessor activity positively or negatively by engaging in protein-protein interactions with Drosha and/or protein-RNA interactions with the pri-miRNAs. The helicases p68 and p72 (also known as DDX-5 and DDX-17 respectively) are part of the Microprocessor and have been shown to upregulate the processing of a subset of pri-miRNAs (Fukuda et al., 2007). Moreover, these helicases can act as platforms to recruit other proteins that in turn can stimulate the processing of other pri-miRNAs. The p53 and p68 interaction stimulates the processing of miR-16, miR-143 and miR-145 in response to DNA damage (Suzuki et al., 2009). R-SMAD proteins can interact with p68 or directly with the pri-miRNA through a consensus sequence in the stem to promote the processing of miR-21 and miR-199 (Davis et al., 2008, 2010) (Figure 10-B).
Terminal loop of pri-miRNA represents another opportunity for proteins to modulate the processing of pri-miRNAs. HNRNPA1 can bind to the loop of pri-miR-18 but not to other pri-miRNAs found in the same cluster and thereby promoting the processing of pri-miR-18 (Guil and Caceres, 2007; Michlewski et al., 2008). KSRP binds to the terminal loop of pri-miRNAs that possess GGG triplets and promotes their processing (Ruggiero et al., 2009; Trabucchi et al., 2009) (Figure 10-B). Proteins can also negatively influence pri-miRNA processing, for example LIN28 binds to the loop of pri-let-7 and represses its processing (will be discussed in the section 4.1.2).

3.1.2.2 Export regulation

Exportin-5 did not receive as much attention as the other factors implicated in miRNA biogenesis, however some examples of regulation of its activity have been described. The expression of Exportin-5 has been found to be post-transcriptionally upregulated during the entry into cell cycle, resulting in a global increase in miRNA levels (Iwasaki et al., 2013). Moreover, the activity of Exportin-5 increases after DNA damage carrying more pre-miRNA into the cytoplasm, this is due to the increased interaction of XPO5 with a phosphorylated NUP153, a component of the nucleopore complex (Wan et al., 2013). Analysis of several tumors showed a mutation in the *Xpo-5* gene producing a C-terminal truncated protein, which results in a global decrease of miRNA levels (Melo et al., 2010). Another example of regulation of Exportin-5 activity comes from adenovirus infection, where a highly structured viral non-coding RNA VA1 is expressed at very high levels causing the saturation of Exportin-5 by outcompeting cellular pre-miRNA for transport to the cytoplasm, effectively blocking pre-miRNA processing (Lu and Cullen, 2004). The blocking of Exportin-5 activity

by the latter mechanism or by its depletion leads to the downregulation of Dicer expression, which revealed Exportin-5 to be responsible for Dicer mRNA export from the nucleus (Bennasser et al., 2011), uncovering a crosstalk similarly to Drosha and DGCR8 between these two central factors in the miRNA pathway.

Other than Exportin-5, only Exportin-1 is known to also transport pre-miRNA, although this activity is restricted to non-canonical 5'-cap-miRNA precursor (Xie et al., 2013). A recent study from Narry Kim's laboratory showed however that Exportin-5 was not indispensable for pre-miRNA transport as knockout cells for Exportin-5 only showed modest reduction in the levels of mature miRNA, indicating that other transport mechanisms and factors might exist (Kim et al., 2016b). It would be of interest to investigate these alternate mechanisms as well as other possible regulatory partners of Exportin-5.

3.1.2.3 Regulation of Dicer processing

As for the Microprocessor, the level of expression of Dicer is crucial for miRNA processing. Like the Microprocessor, Dicer and its partner TRBP are also found in an autoregulation loop. A decrease in TRBP levels translates in a decrease in Dicer levels and pre-miRNA processing (Chendrimada et al., 2005; Melo et al., 2009; Paroo et al., 2009). In addition, Dicer mRNA possesses a Let-7 target site in its coding region, creating a feedback loop affecting miRNA biogenesis in physiological or cancer conditions (Forman et al., 2008). These regulatory loops are contributing to the regulation of homeostatic Dicer activity.

Phosphorylation of TRBP stabilizes itself as well as Dicer, resulting in the upregulation of growth-stimulating miRNAs and in a decrease of Let-7, although the mechanism for the specificity to those miRNA is unknown (Paroo et al., 2009).

Finally, Dicer activity can also be modulated indirectly by RBPs. KSRP is promoting the biogenesis of a subset of miRNAs by binding to the loop of their pre-miRNA (Trabucchi et al., 2009). LIN28 proteins bind specifically to pre-Let-7 and impede Dicer processing through the recruitment of Terminal Uridylyl Transferases (TUTases) (will be discussed in more detail in the 4.1.2).

3.2 Regulation of RISC action

miRNA exert their function by assembling into effector RISC complexes which invariably contain Argonaute proteins. One obvious target for regulation of miRNA activity would thus be at the level of the RISC, so it is not surprising that several regulatory processes acting on Argonaute proteins' levels or function exist. These aspects will be introduced in this following part. Alternatively, other mechanisms also exist that act on the miRNA itself, affecting its stability or specificity that will be discussed in separate chapters.

3.2.1 Regulation at the level of Argonaute proteins

Argonaute proteins and miRNAs again are part of an autoregulation loop whereby Argonaute proteins when not loaded with a small RNA are unstable (Martinez and Gregory, 2013; Smibert et al., 2013), conversely over-expression of Argonaute proteins cause an increase in miRNA abundance (Diederichs and Haber, 2007), indicating that miRNAs are in excess compared to Argonaute proteins and thereby that unloaded miRNA are not stable either. This regulation loop ensures the homeostatic control of functional RISC complexes in the cell.
Mechanisms are also in place in the cell to actively control the levels of Argonaute proteins. While the chaperone HSP90 stabilizes unloaded AGO2 waiting to be loaded by a miRNA duplex (Johnston et al., 2010), in mouse cells LIN41 (TRIM71) has been shown to induce ubiquitination and proteasomal degradation of AGO2 (Rybak et al., 2009).
The degradation of AGO proteins when they are empty of miRNAs have been proposed to happen by autophagy as inhibition of lysosomes resulted in the rescue of AGO levels (Martinez and Gregory, 2013). Indeed, previously AGO2 and Dicer have been shown to be degraded by autophagy (Gibbings et al., 2012). Autophagy also known as macroautophagy is a major cellular process that contributes to cell's homeostasis, by degrading cellular components by way of their engulfment as cargo in membrane structures called autophagosomes. These autophagosomes then merge with lysosomes to degrade their cargo. Knockdown of major components of autophagy resulted in increased levels of miRNA-free Dicer and AGO2 and activation of autophagy resulted in a decrease in their levels (Gibbings et al., 2012). Long term inhibition of autophagy resulted in diminished levels of miRNA, suggesting a role for autophagy in the removal of Dicer and AGO proteins when free of miRNA. Similarly, in *C.elegans*, autophagy selectively degrades GW182 homolog AIN-1, regulating miRNA mediated repression (Zhang and Zhang, 2013).

Argonautes do not escape from the regulation by post-translational modifications. AGO2 has been shown to be prolyl 4-hydroxyled by C-P4H(I) increasing its stability and its localization to P-bodies (Qi et al., 2008; Wu et al., 2011). Phosphorylation of AGO2 at Ser387 by MAPK-activated protein kinase 2 (MAPKAPK2) or RACγ Ser/Thr protein kinase (AKT3) has also been shown to contribute to P-body localization (Horman et al., 2013; Zeng et al., 2008). Tyr529 of AGO2 is phosphorylated resulting in decreased miRNA loading and target repression (Mazumder et al., 2013; Rüdel et al., 2011). Phosphorylation of AGO2 under hypoxia at Tyr 393 is shown to result in its dissociation from Dicer and a decrease in pre-miRNA processing of som miRNAs (Shen et al., 2013). Moreover the activity of RISC can be decreased by its poly-ADP-ribosylation induced upon various stresses or viral infections (Leung et al., 2011b; Seo et al., 2013) (Figure 11).

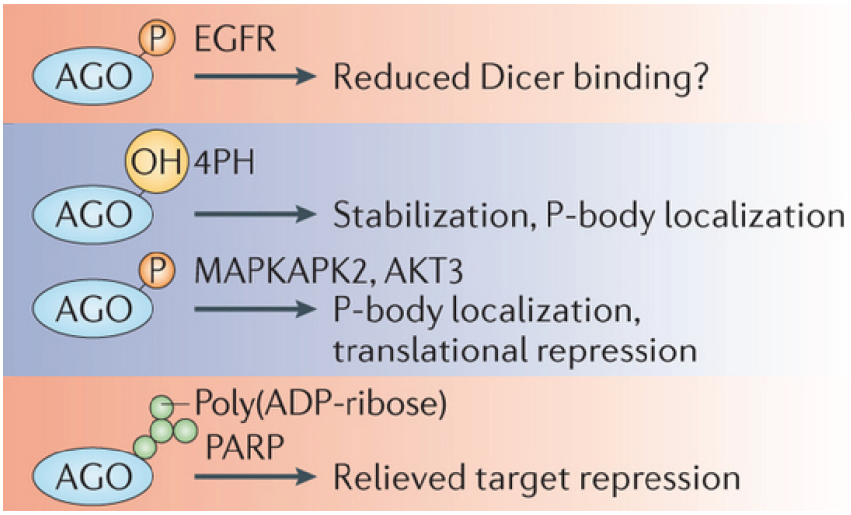

Figure 11: Examples of Argonaute protein regulation by post-translational modifications
Adapted from (Ha and Kim, 2014).

3.2.2 Regulation of the activity of Argonaute proteins by RNA binding proteins

3'UTRs of mRNAs can possess binding sites for RBPs, which can modulate positively or negatively the activity of miRISC. mRNAs containing binding sites for HuR or Pumilio family proteins were also found to be enriched for miRNA binding sites (Galgano et al., 2008; Mukherjee et al., 2011). Under various conditions, RBPs will move on their target mRNAs

and will affect the activity of miRISC by facilitating or hindering the binding of miRISC to the target mRNA or by acting on miRISC components directly (Figure 12).

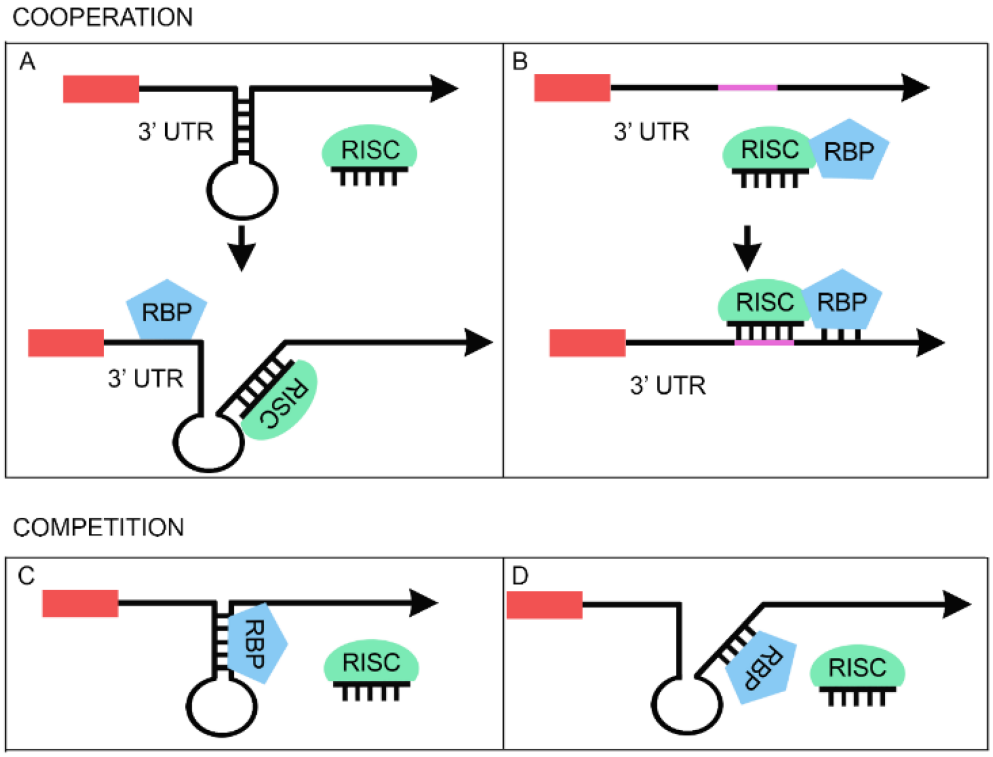

Figure 12: Functional interactions between RISC and RNA-binding proteins
A. An RBP can enhance the activity of RISC on a common mRNA by opening an occluding secondary structure. **B.** RISC transport to its target mRNA can be facilitated by an RBP. **C.** Competition can arise when the binding of an RBP changes the secondary structure of the mRNA and impedes the binding of RISC. **D.** RBPs can also share the same binding site on the target and reduce the efficacy of RISC by competing for binding (Loffreda et al., 2015).

One such RBP is HuR (also known as ELAV1), normally involved in the protection of mRNAs that contain AU rich sequences causing their rapid turnover (Meisner and Filipowicz, 2011). The binding of HuR on the 3'UTR of *CAT1* mRNA in human hepatoma cells during stress conditions, abolishes the miRNA mediated silencing already in place on the mRNA (Bhattacharyya et al., 2006). HuR achieves this by promoting the dissociation of RISC from the mRNA (Kundu et al., 2012). An opposite example also exist, where HuR is required for the repression by Let-7 of the *MYC* transcript, HuR binding is thought to facilitate the access of RISC to the adjacent miRNA binding site (Kim et al., 2009).
The DND1 protein (Dead End 1), expressed in the germline, antagonizes the activity of miR-372 family loaded RISC by binding to several target mRNAs, the binding site for DND1 overlaps with the miRNA binding site thereby preventing RISC binding (Kedde et al., 2007).

The tumor suppressor p27 is an inhibitor of cell-cycle progression, its repression induces cell cycle entry. Its mRNA possesses in its 3'UTR a binding site for miR-221 and miR-222 as well as one for PUM1. These two binding sites form a hairpin making the miR-221/222 binding site unavailable for RISC. Upon growth stimulation, PUM1 gets upregulated and phosphorylated and binds to the hairpin to expose miR-221/222 binding site. The resulting downregulation of p27 by miR-221/222 induces cell cycle re-entry (Kedde et al., 2010).
In serum starved cells or non-growing conditions, AGO2 bound to the AU rich sequences of TNFα mRNA 3'UTR, recruits Fragile-X-Related protein (FXR1). This recruitment induces the translational activation of TNFα mRNA instead of miRNA mediated repression (Vasudevan and Steitz, 2007; Vasudevan et al., 2007).
The number of RBPs expressed in the cell warrants the discovery of more of these kinds of antagonistic or synergistic effects of RBPs on miRISC during different conditions of stress or cell program. Other examples of RBP-miRISC interactions are reviewed in (Jiang and Coller, 2012; van Kouwenhove et al., 2011).

4. RNA intrinsic regulation affecting miRNA expression and targeting

Although so far, I have mostly introduced regulatory mechanisms acting through proteins involved in the miRNA pathway, there are also other mechanisms that act by modifying the miRNA transcript sequence, which in turn results in the modulation of the expression or the targeting capacity of miRNAs. Sequence modifications can occur at the pri-miRNA, pre-miRNA or mature miRNA level either in the core or at the extremities of these transcripts. The advent of deep-sequencing allowed us to discover new miRNAs but also led to the appreciation of heterogeneity in the mature miRNA sequence and length. These miRNA variants are called isomiRs (Morin et al., 2008) and they differ from their reference sequence in miRBase (Figure 13). The sequence variations in isomiRs can be due to imprecise Drosha or Dicer processing in which case it will be a templated modification, whereas RNA editing will produce an RNA that differs from the DNA sequence from which it is transcribed, which is therefore a non-templated modification (Figure 13). RNA editing is a cellular process that acts at the level of mRNA, tRNA and rRNA and involves nucleobase substitutions like cytidine to uracil (C to U) or adenine to inosine (A to I) deamination and non-templated nucleotide additions (NTA). In this part, the effects of these miRNA sequence modifications will be introduced.

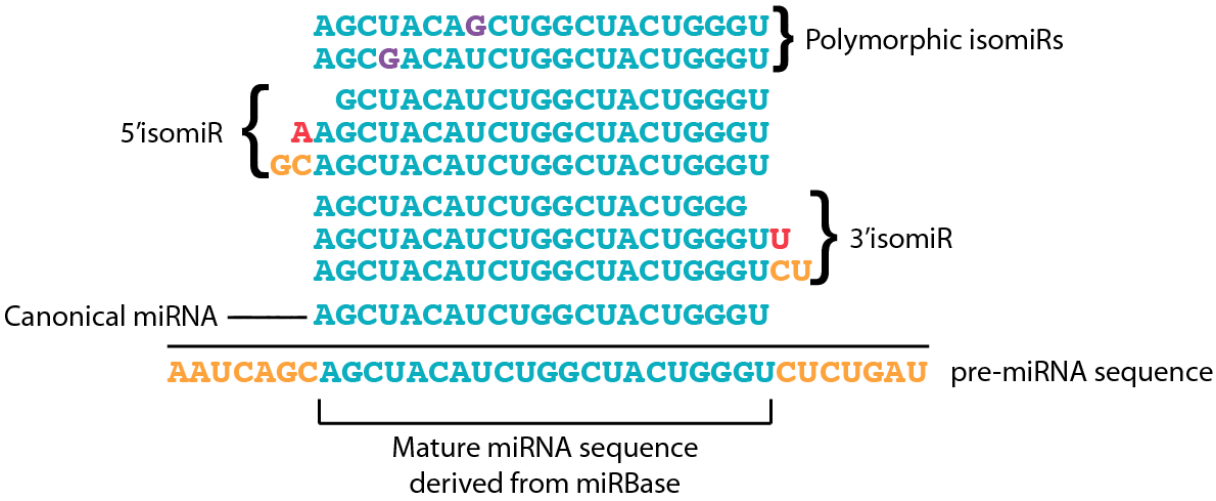

Figure 13: Example of miRNA heterogeneity.
The isoforms of human miR-222 are represented here to show isomiR heterogeneity. The canonical miR-222 sequence is represented in blue. The 5' and 3' isomiRs possess sequence heterogeneity at their 5' and 3' ends respectively, these sequence alterations can either be templated (yellow) or non-templated (red). Moreover, polymorphic isomiRs possess nucleotides that were acquired by nucleobase substitutions. Taken from (Neilsen et al., 2012).

4.1 Modifications on miRNA precursor sequences affecting their biogenesis and/or the targeting of miRNAs

4.1.1 Nucleobase substitutions on miRNA precursors

The most prevalent form of nucleobase substitution in eukaryotes is the A to I substitution by the deamination of adenine to inosine catalyzed by adenosine deaminase acting on RNA (ADAR) enzymes (Nishikura, 2010). The ADAR enzymes have been shown to edit specific pri-miRNA sequences in certain tissues (Luciano et al., 2004; Blow et al., 2006). The editing of a pri-miRNA sequence can affect the following processing steps or if the editing happens in the seed region, it can affect the target specificity of the resulting guide strand. Notably, upon editing of pri-miR-142, its processing by Drosha is suppressed (Yang et al., 2006). One similar example is the edition of pri-miR-151, although in this case Drosha processing is not affected, but the efficiency of Dicer cleavage of the pre-miRNA is diminished (Kawahara et al., 2007a). Regarding editing events that change the targeting specificity of a miRNA, one example is miR-376, in which editing of nucleotides in the seed region creates a set of targets different from the unedited miR-376 (Kawahara et al., 2007b). A comprehensive transcriptome analysis of RNA editing events identified 44 new miRNA editing sites of which

11 would fall in the seed region (Peng et al., 2012), making this mode of regulation by nucleotide substitution relatively rare. More information on ADAR mediated A to I substitutions in miRNA pathway can be found in the review by (Nishikura, 2016).
Similar to ADAR-mediated nucleobase substitution, single nucleotide polymorphisms (SNP) in miRNA genes can also alter miRNA sequence thereby affecting their biogenesis or resulting in changes in targeting specificity. In addition, some of these SNPs have been associated with cancer development (Calin et al., 2005; Jazdzewski et al., 2008, 2009; Ryan et al., 2010).While SNPs do not present an active regulatory process, they help demonstrating how changes in miRNA sequences can affect the expression and activity of a miRNA, making nucleobase substitutions an important regulatory process.

4.1.2 Regulation of let-7 biogenesis by non-templated nucleotide additions

The biogenesis of group II pre-miRNAs (Figure 5) is a good example of regulation by non-templated nucleotide additions. They possess a 3' overhang of only 1 nt after Drosha processing, and therefore require the addition of a single U nucleotide to form a 2nt 3' overhang than can be recognized by Dicer. This group contains most members of Let-7 family as well as miR-105 (Heo et al., 2012). The enzymes responsible for the mono-uridylation have been found to be TUTase2, TUTase4 and TUTase7 from the terminal uridylyl transferase (TUTase) family (these enzymes will be introduced in the next part) (Heo et al., 2012) (Figure 14). In addition to this mono-uridylation necessary for pre-let-7 processing, other post-transcriptional mechanisms exist for the regulation of Let-7 expression as its biogenesis is repressed during specific embryonic stages (Suh et al., 2004; Thomson et al., 2006). As mentioned earlier in the sections 3.1.2.1 and 3.1.2.3), the binding of LIN28 to the loop of pri-let-7 hinders its processing by Drosha (Newman et al., 2008; Viswanathan et al., 2008). Moreover, LIN28 has also been shown to be bound to the pre-let-7 and to impede its processing by Dicer (Heo et al., 2008; Rybak et al., 2008). It was later shown that LIN28 recruits the terminal uridylyl transferases TUTase4 and TUTase7 in order to trigger the oligouridylation of pre-Let-7 (Hagan et al., 2009; Heo et al., 2008, 2009). The oligo U tail added to the pre-Let-7 not only inhibits Dicer processing but also induces its decay by the 3'-5' exonuclease DIS3L2 (DIS-3 like 2) that recognizes the added U tail (Chang et al., 2013; Ustianenko et al., 2013) (Figure 14). LIN28 works as a molecular switch to turn the same TUTases that ensure the good processing of a pre-miRNA to negative modulators of biogenesis by changing their activity.

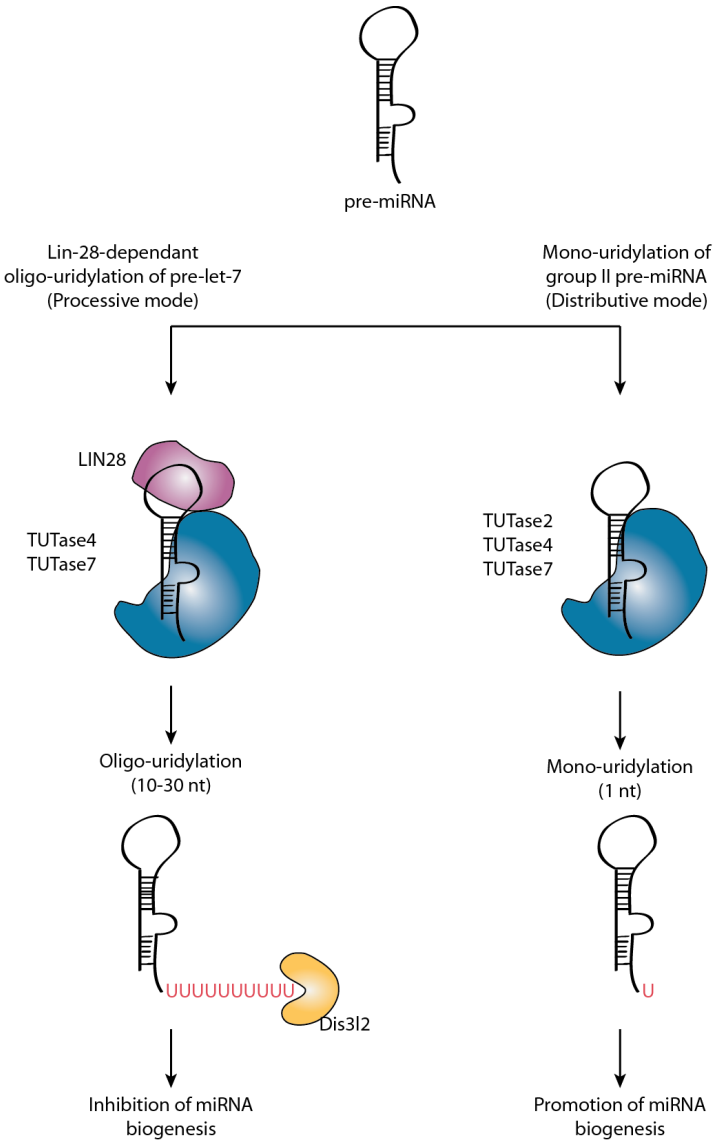

Figure 14: Regulation of pre-let-7 family biogenesis by TUTases
Group 2 pre-miRNAs acquire a single U residue on their 3' end, to form the canonical 3' 2 nt overhang recognized by Dicer, this mono-uridylation is due to the redundant action of TUTases 2/4/7. However, in undifferentiated cells, LIN28 binds to the loop of pre-Let-7 and through the action of TUTases 4/7, an oligo-U tail is added to the pre-miRNA. The oligo-uridylation prevents Dicer processing but is also recognized by the exonuclease Dis3l2 and quickly degraded. Adapted from (Kim et al., 2015).

An extensive analysis of pre-miRNAs demonstrated that LIN28-independent non-templated nucleotide additions, the most common being mono-U addition, are a frequent feature of many miRNA other than the Let-7 family (Newman et al., 2011). This suggests that regulation of pre-miRNAs by non-templated nucleotide additions can be a general feature of miRNA biogenesis. Of note, another function of oligo-uridylation by TUT4 and TUT7 has

been discovered more recently, where truncated or defective pre-miRNAs are uridylated. Truncated pre-miRNAs can be generated after their loading in AGO2 followed by slicing similar to miR-451 (Cheloufi et al., 2010; Cifuentes et al., 2010; Diederichs and Haber, 2007; Yang et al., 2010). These truncated pre-miRNAs are oligo-uridylated by TUT4 and TUT7 inducing their subsequent degradation (Kim et al., 2015; Liu et al., 2014). Degradation of these uridylated pre-miRNAs is performed by the exosome creating a quality control process for miRNA synthesis, keeping the pool of AGO and Dicer proteins free of defective pre-miRNAs.

4.2 Sequence modifications on mature miRNA (isomiRs)

The term isomiR was first coined in a paper by (Morin et al., 2008). Small RNA sequencing had already identified miRNAs exhibiting sequence variations compared to their reference sequence (Landgraf et al., 2007) but most of these were generally considered as artifacts of cloning or alignment (Hoon et al., 2010; Reese et al., 2010). However, the fact that isomiRs are loaded in AGO to form functional RISC implies that they are functionally relevant (Baran-Gale et al., 2013; Burroughs et al., 2010; Chan et al., 2013). Moreover, it was also suggested that isomiRs would work together with canonical miRNAs to even out off-target regulation (Cloonan et al., 2011). IsomiRs are created by several mechanisms; a shift in Drosha or Dicer processing would alter the mature miRNA sequence and change the seed sequence, nucleobase substitutions catalyzed by ADARs can create polymorphic isomiRs and potentially change the targeting of a miRNA (discussed previously) or enzymes like exoribonucleases or nucleotidyl transferases can create non-templated sequence modifications (Figure 13). Although the majority of isomiRs presents variation in its 3' extremity and therefore maintains the same seed sequence, there is also an unneglectable fraction of 5' isomiRs with a shifted seed (Guo and Chen, 2014).

4.2.1 5' isomiRs: shift in Drosha and/or Dicer cleavage

5' isomiRs are mostly due to an imprecise cleavage by Drosha or Dicer (Neilsen et al., 2012) (Figure 13). The shift will not only cause a change in the repertoire of mRNA targets because of the seed sequence change, but can also potentially result in a change in the selection of the guide strand that depends on the thermodynamic stability of the extremities of the duplex.

Notably, one study showed a change in the guide strand selection process for more than 10% of pre-miRNAs in at least one tissue (Cloonan et al., 2011). Although some 5' isomiRs can have a new set of targets, they will also to some degree regulate the same targets as their canonical counterparts (Guo and Chen, 2014), however their targeting efficiency might differ from their canonical counterparts (Chiang et al., 2010; Humphreys et al., 2012). Some accounts state that most of these isomiRs are products of imprecise cleavage by Dicer rather than Drosha suggesting a higher fidelity for the latter (Wu et al., 2009; Zhou et al., 2012).

4.2.2 3' IsomiRs: 3' heterogeneity

By far the most common type of isomiR is 3' modified isomiRs, with regard to the number and abundance of different miRNAs displaying this type of modification (Burroughs et al., 2010; Newman et al., 2011; Wyman et al., 2011). The structural analysis of AGO proteins shows that the 5' end of the miRNA is embedded in the MID domain whereas its 3' extremity is more accessible as it can go past the PAZ domain (Elkayam et al., 2012; Schirle and MacRae, 2012) (Figure 7-B). This accessibility therefore renders the action of modifying enzymes on the miRNA possible, exonucleases can shorten the miRNA and nucleotidyl-transferases can add non-templated nucleotides. The origins and effects of these miRNA isoforms will be discussed in the following part.

4.2.2.1 Exoribonucleases creating 3' isomiRs

In *Drosophila* an exoribonuclease called Nibbler (Nbr) has been found to act on miR-34 to create several templated isoforms. The 3'-5' exoribonuclease degrades the miRNA already loaded into AGO1 by trimming it from 24 to 21 nt. *Nbr* depletion showed that it acts on a larger set of miRNAs and it causes developmental defects in *Drosophila*, thereby demonstrating the importance of the production of these miRNA isoforms (Han et al., 2011; Liu et al., 2011). A similar process has also been discovered in *Neurospora crassa,* where the RNA exosome and an exonuclease called QIP trim the 3' end of miRNAs (Xue et al., 2012). The counterparts of these ribonucleases remain to be discovered in mammals. However, as introduced earlier, the exonuclease PARN, the human orthologue of Nibbler, is involved in the maturation of miR-451, acting by trimming down the pre-miR-451 to its final size after its

slicing by AGO2 (Yoda et al., 2013). Moreover, this same exoribonuclease is also involved in trimming and further degradation of miR-21 (Boele et al., 2014).

4.2.2.2 Non-templated nucleotide additions on mature miRNA by mammalian terminal uridylyl transferases (TUTases)

Non-templated nucleotide additions are catalyzed by nucleotidyl-transferases which are template independent polymerases acting on RNA (Martin and Keller, 2007; Stevenson and Norbury, 2006; Wilusz and Wilusz, 2008). The most classical example is the polyA polymerase (PAP) that catalyzes the polyadenylation of pre-mRNA. There are other similar enzymes called non-canonical PAPs that add shorter stretches of nucleotides than their canonical counterparts. The first reported example of such an enzyme is Cid1 in yeast (Wang et al., 2000). Seven non-canonical PAPs have been identified in mammals (called hereafter terminal uridylyl-transferase (TUTase)) (Martin and Keller, 2007; Stevenson and Norbury, 2006; Wilusz and Wilusz, 2008). Six of them have been implicated in miRNA 3' heterogeneity (Wyman et al., 2011). They possess uridylyl and/or adenylyltransferase activities (Kwak and Wickens, 2007; Rissland et al., 2007; Wickens and Kwak, 2008), which is concordant with the most frequent modifications on 3' isomiR being additions of adenines and uridines (Burroughs et al., 2010; Chiang et al., 2010). 3' isomiRs maintain the same 5' sequence, thus keeping the same subset of target mRNAs as their canonical counterparts, however non-templated nucleotide additions on mature miRNA can affect their stability and targeting efficiency. As we will see in the next part, TUTases have a range of different targets and functions.

4.2.2.3 Mammalian TUTase family and their function

TUTases belong to the superfamily of β-like nucleotidyl transferases. They all possess a functional catalytic motif composed of a nucleotidyl transferase and a PAP-associated domain (Figure 15) (Martin and Keller, 2007) and can function as uridyl and/or adenyltransferases on different types of RNA (Kwak and Wickens, 2007; Rissland et al., 2007; Wickens and Kwak, 2008). For historical reasons, these enzymes have acquired several aliases, and I will designate them here with their most recognized names (Figure 15).

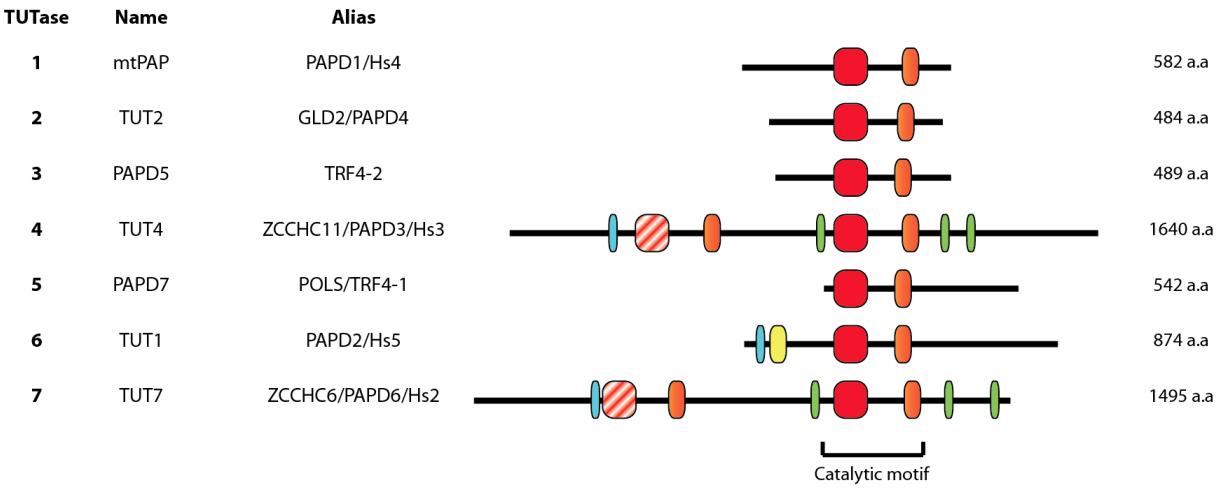

Figure 15: Schematic representation of domain organization of TUTases
Human TUTases 1-7 with their alternative aliases are represented. The nucleotidyl transferase domain (red box) and PAP-associated domain (orange box) constitute the catalytic motif. Hatched box designates a conserved nucleotidyl transferase domain that is inactive due to sequence variations. Blue boxes represent a C2H2-type zinc finger domain. Green boxes represent CCHC-type zinc finger domain. Yellow box corresponds to the RRM (RNA recognition motif). Adapted from (Heo et al., 2009).

A study by Wyman *et al.* reported on the contributions of six TUTases (all but PAPD7) to the 3' heterogeneity of miRNAs in different tissues of several organisms. They used a technique that is more amenable to the quantification of miRNA variants than classical sequencing called nCounter assay. It involves hybridization of fluorescent, bar-coded probes to miRNAs of interest, the quantification of the miRNA variant is performed by scanning and counting of the probes (Geiss et al., 2008; Wyman et al., 2011). This study first of all showed that nucleotide additions on miRNA are common but not universal and that some miRNAs have a higher propensity to acquire additions (Wyman et al., 2011). Adenosine addition is the most abundant modification with 50% of additions being mono-adenylation, while mono-uridylation accounts for 25 % of additions, confirming the findings of a previous study (Chiang et al., 2010; Wyman et al., 2011). Secondly, through individual knockdown of TUTases and quantification of miRNA variants, the study implicates 6 out of 7 TUTases in the formation of 3' heterogeneity of at least one miRNA variant. mtPAP, TUT2, PAPD5 and TUT4 are found to mostly add 3' A, TUT1 3' U or A and TUT7 3' U residues (Wyman et al., 2011), confirming a previous study that implicated TUT2, PAPD5 and TUT4 with 3' A additions (Burroughs et al., 2010). Lastly, the authors mention that the knockdown of a given TUTase can induce an increase in the expression of other TUTases, notably TUT2 knockdown induces PAPD5 expression. This warrants possible compensation of function of one TUTase by another, suggesting that this study might have underestimated the effects of

some TUTases on non-templated nucleotide additions. The fact that TUT4 and TUT7 redundantly oligouridylate pre-let7 following LIN-28 binding and together with TUT2 mono-uridylate group 2 pre-miRNAs supports this notion (see section 4.1.2).

TUT2 (also known as GLD-2 or PAPD4) is involved in the polyadenylation of dormant mRNAs in mouse oogenesis (Nakanishi et al., 2006). More recently however, TUT2 was also shown to add a single non-templated adenine at the 3' end of miR-122 in liver cells. This mono-adenylation stabilizes miR-122 and occurs after dicing. In its absence, miR-122 is destabilized (Katoh et al., 2009). Another study showed that additional miRNAs are also mono-adenylated and stabilized by TUT2 but the extent of stabilization depends on the sequence at the 3' end of the miRNA, notable examples being some of Let-7 family members (D'Ambrogio et al., 2012). Of note, the fly homolog of TUTase2 called WISPY, has been reported to adenylate maternally inherited miRNAs with one or two residues of adenine in early embryos and to help the clearance of maternal miRNAs (Lee et al., 2014). A similar clearance of host miRNAs has been observed during vaccinia virus infection, where the viral poly-A polymerase VP55, oligo-adenylates host miRNAs thereby inducing their degradation by the cellular machinery (Backes et al., 2012).

Apart from the redundant function of TUT4 and TUT7 on pre-let-7 mono and poly-uridylation (Heo et al., 2009, 2012; Thornton et al., 2012) (Figure 14), their other function is to mark mRNAs with short polyA tails by addition of a stretch of U residues to facilitate their decay (Lim et al., 2014). Moreover, TUT4 has also been demonstrated to mark the 3' end of histone mRNAs with uridines for degradation (Schmidt et al., 2011; Su et al., 2013). At the level of mature miRNAs, TUT4 was shown to uridylate the 3' end of mature miR-26a, which impairs its ability to regulate targets in the inflammatory response (Jones et al., 2009). Further studies showed another set of miRNAs to be substrates of TUT4 uridylation, again alleviating their repressive efficacy in growth hormone expression in mice (Jones et al., 2012). However, the uridylation of these miRNA does not seem to change their expression levels, rather it blocks their repressive activity by a yet to be described mechanism (Jones et al., 2012).

PAPD5 is implicated in the generation of some snoRNAs, by oligo-adenylating their 3' ends, which allows the recruitment of the exonuclease PARN for trimming to their mature size (Berndt et al., 2012). A similar synergy between PAPD5 and PARN has been reported for the oncogenic miR-21 in several tumors. PAPD5 adds a single A residue on the 3' end of miR-21, inducing its degradation by the nuclease PARN. The disruption of miR-21 regulation by adenylation and degradation has been found to be an attribute of several tumors (Boele et al., 2014).

TUT1, also known as Star-PAP or U6 TUTase was first reported to catalyze the addition of three uridines to the 3' end of U6 snRNA, which is involved in splicing, and to be involved in the recycling of U6 (Trippe et al., 2003, 2006). Moreover, it is also involved in the poly-adenylation of a set of mRNAs that are involved in cell survival (Li et al., 2012; Mellman et al., 2008) and oxidative stress response (Gonzales et al., 2008; Laishram and Anderson, 2010; Mellman et al., 2008). In the miRNA pathway, TUT1 globally regulates the abundance of miRNAs by an indirect mechanism that is independent of its nucleotidyl transferase activity (Knouf et al., 2013), pointing to a general stabilizing effect on miRNAs. However, the depletion of TUT1 was also associated with the loss of A and U residues from a subset of miRNA 3' ends that coincided with the acquisition of other nucleotides, possibly by the action of other TUTases (Knouf et al., 2013).

5. Mature miRNA turnover

Turnover at the level of mature miRNA received less attention compared to other aspects of miRNA pathway i.e. regulation of biogenesis or miRNA action. This might in part be due to the fact that for a long time mature miRNAs were perceived as quite stable molecules with their expression being detectable over periods as long as several days after their biogenesis is blocked (Baccarini et al., 2011; Bail et al., 2010; Gantier et al., 2011; Rooij et al., 2007). More recently however, some miRNAs were reported to show a rapid turnover under specific conditions. Thus, miR-29b decays faster in cycling mammalian cells than in mitosis arrested cells (Hwang et al., 2007; Zhang et al., 2011). Similarly, rapid decay of miR-16 family members has been observed in NIH-3T3 cells transitioning from G0 to G1 phase (Rissland et al., 2011). In neurons, miRNAs generally have a faster turnover rate than in other cell types. In primary human neuron cultures and post mortem brain tissue, some brain enriched miRNAs have short half-lives (Sethi and Lukiw, 2009). Similarly, another study showed the rapid degradation of members of the miR-183-96-182 cluster along with miR-204 and miR-211 during light to dark adaptation in mouse retina. The levels of these miRNAs decrease approximately by 50% of their levels before transition (Krol et al., 2010). In the neurons of the sea slug *Aplysia californica*, miR-124 and miR-184 are rapidly down-regulated following serotonin exposure (Rajasethupathy et al., 2009).

Some of these rapidly degraded miRNAs contain cis-acting sequence elements that have been mapped to the entire length of the miRNA, i.e. the seed, the central region or the 3' end. For the destabilisation of miR-29b, the uracil residues in the centre of the miRNA are necessary

but not sufficient (Hwang et al., 2007; Zhang et al., 2011). In the case of miR-503 from the extended family of miR-16, the residues important for destabilisation have been mapped to its seed and 3' end extremities (Rissland et al., 2011). In the case of rapidly destabilised miRNAs given so far, some are found to be inherently unstable and their level are susceptible to be regulated by the modulation of their expression and biogenesis (Krol et al., 2010; Rissland et al., 2011). However, for miR-29b, the destabilisation is independent from a modulation in its expression or maturation (Hwang et al., 2007). 3' modifications on a mature miRNA as mentioned in the previous chapter can also affect its stability positively or negatively (see section 4.2.2). Other trans-acting factors have been found to induce active mature miRNA degradation in different organisms; these factors are usually 5' to 3' or 3' to 5' exoribonucleases. Known factors in different organisms will be introduced in the following part.

5.1 Trans acting factor in miRNA turnover

5.1.1 miRNA turnover in plants

Active degradation of mature miRNAs was first reported in *Arabidopsis thaliana*. Small RNA degrading nucleases (SDNs) are responsible for the degradation of mature miRNAs (Figure 16-A). The depletion of SDN family members in *A. thaliana* causes developmental defects along with elevated levels of several miRNAs. Experiments showed that SDN1 can degrade a synthetic miRNA in the 3' to 5' direction, defining it a 3' to 5' exoribonuclease (Ramachandran and Chen, 2008). In plants, small RNAs are 2'-O-methylated at their 3' extremity by Hua enhancer 1 (HEN1) protecting them from exonucleolytic attack as well as 3' uridylation (Li et al., 2005; Yu et al., 2005). Although the methyl group slows degradation by SDN1 it does not completely prevent it (Ramachandran and Chen, 2008) (Figure 16-A). Of note, 3' oligo-uridylation of plant miRNAs is catalysed by HEN1 Suppressor1 (HESO1) when miRNAs are not protected by 2'-O-methylation, these oligo-uridylated miRNAs are then destabilised by an unknown mechanism (Ren et al., 2012; Zhao et al., 2012) that is distinct from SDN1 action as uridylation has been shown to slow down SDN1 action at least *in vitro* (Ramachandran and Chen, 2008).

5.1.2 miRNA turnover in Chlamydomonas reinhardtii

In the green algae *Chlamydomonas reinhardtii*, uridylation of miRNAs induces their degradation. A terminal nucleotidyl tranferase called MUT68 was shown to uridylate the 3' end of both miRNA and siRNA *in vivo*. In turn, this uridylation induces their degradation by ribosomal RNA-processing protein 6 (RRP6), a component of the exosome (Ibrahim et al., 2010). The depletion of RRP6 *in vivo* also results in an increase in the levels of mature miRNAs, suggesting a cooperative effect between MUT68 and RRP6 (Ibrahim et al., 2010) (Figure 16-B).

5.1.3 miRNA turnover in Caenorhabditis elegans

In *C. elegans*, two exoribonucleases have been implicated in miRNA degradation. These are the 5' to 3' exonucleases XRN1 and XRN2 (Chatterjee and Grosshans, 2009; Chatterjee et al., 2011) (Figure 16-C). The depletion of XRN2 by RNAi raised the expression level of several miRNAs at the mature but not pre-miRNA or pri-miRNA level (Chatterjee and Grosshans, 2009; Chatterjee et al., 2011). Interestingly, the action of XRN2 on mature miRNA creates a mechanism ensuring the loading of AGO with miRNAs that have regulatory potential, discussed further in section 5.2.1.

5.1.4 miRNA turnover in mammals

A study by Bail and colleagues reported the involvement of XRN1 and the exosome in miRNA degradation. They first of all looked globally at the half-lives of miRNAs and showed that 95%
of miRNAs stay stable over 8 hours. One of the unstable miRNAs, miR-382, is stabilised 1.5 fold after depletion of ribosomal RNA-processing protein 41 (RRP41), a component of the exosome and 1.3 fold after XRN1 depletion (Bail et al., 2010) (Figure 16-D). The degradation of miR-382 is dependent, at least *in vitro* in HEK293 lysates, on it being processed by Dicer, as a synthetic miR-382 decays at the same rate as another more stable miRNA. However, with this *in vitro* system, it was shown that the degradation of miR-382 is dependent on its 3' terminus sequence, more precisely nucleotides 16-22 (Bail et al., 2010).

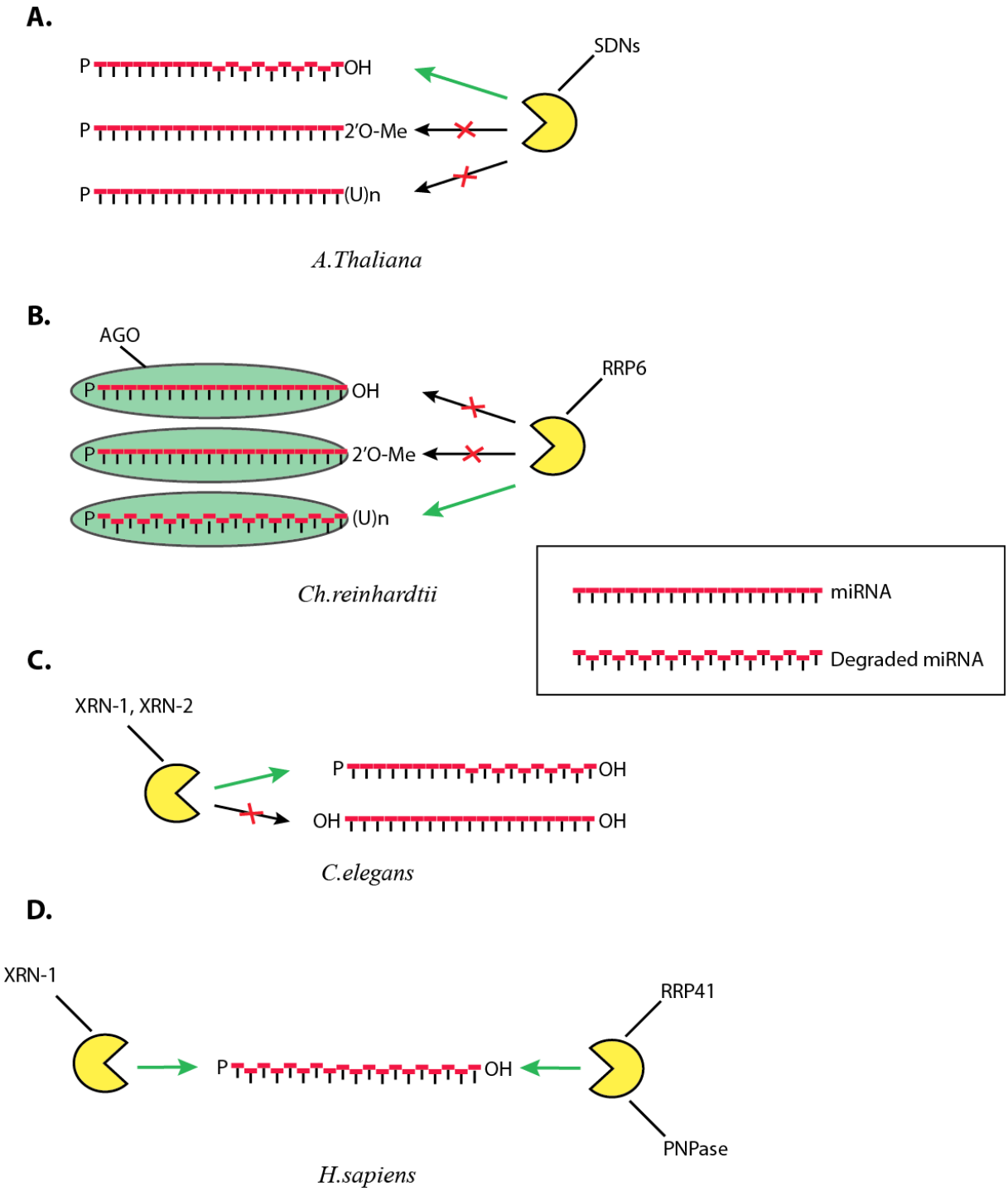

Figure 16: Exoribonucleases acting on mature miRNA in different organisms

A. SDNs act on mature miRNA when they are non-protected by 2'O-methylation in *A.thaliana* and oligo-uridylation impedes their activity (Ramachandran and Chen, 2008). **B**. *Ch.reinhardtii* RRP6 degrades AGO loaded miRNA after their oligo-uridylation but are impeded by OH or 2'O-Me on the 3' of the miRNA (Ibrahim et al., 2010). **C.** XRN1 and XRN2 degrade miRNA in *C.elegans* from the 5' en of the miRNA when the miRNA has a 5'P and not a 5'OH (Chatterjee and Grosshans, 2009; Chatterjee et al., 2011). **D.** In human cells, RRP41 and PNPase degrademiRNA in the 3' to 5' direction and XRN1 in the 5' to 3'direction (Bail et al., 2010; Das et al., 2010). Taken form (Ruegger et al., 2015).

Another study implicated a 3' to 5' exonuclease called the human polynucleotide phosphorylase (PNPase) or PNPT1 (polyribonucleotide nucleotidyltransferase 1) in the degradation of several mature miRNAs, including miR-221, miR-222 and miR-106b, without altering their pri- or pre-miRNA levels in melanoma cells (Figure 16-D). When added to total RNA from melanoma cells, *in vitro* translated PNPT1 is capable of degrading these miRNAs but does not affect other miRNAs demonstrating its sequence specificity (Das et al., 2010). However, PNPT1 is known to localize to mitochondria intermembrane space, leading to the question of where miRNA degradation would take place (Rüegger and Großhans, 2012).
The 3'-5' exoribonuclease Eri1has been shown to affect the stability of some miRNAs in mouse lymphocytes, inferred from the increase of miRNA levels in lymphocytes deriving from Eri1 knockout mice, however it is unknown if this enzyme acts directly on mature or precursor miRNAs or whether the observed effect results from an indirect consequence of the Eri1 deficiency (Thomas et al., 2012).

5.2 RNA-mediated miRNA turnover

Several 5' to 3' or 3' to 5' exoribonucleases have been implicated in miRNA degradation in different organisms. Although these enzymes are evolutionarily conserved, their functional conservation in miRNA degradation is not evident. Discovering nucleases that degrade miRNAs can be difficult due to the redundant action of several factors as is the case for SDNs in *A.thaliana* where depletion of several SDNs is needed to observe a phenotype (Ramachandran and Chen, 2008). Moreover, most of the studies that discovered these pathways are performed in specific tissues or conditions, which together with redundancy of pathways might have underestimated the extent to which these enzymes affect miRNA degradation. In addition, these nucleases have different kinds of RNA substrates, and the identity of co-factors that would give them specificity for miRNAs is currently unknown.
miRNA-mediated mRNA regulation can be achieved with different modes of action depending on the extent of complementarity between the miRNA and its target. Extensive complementarity results in endonucleolytic cleavage by slicing competent AGO proteins, which is the major mode of action for plant miRNAs (Jones-Rhoades et al., 2006). However, in metazoans, miRNAs mostly have a partial complementarity with their targets and induce translational repression (Bartel, 2009). Interestingly, in the recent years, the interaction between miRNAs and mRNAs has emerged as reciprocal, where targets can also have an influence on the stability of miRNA; which sometimes depends on the extent of interaction.

Not only mRNA target but also other types of RNA transcripts have been shown to affect miRNA turnover by stabilization or degradation and by relying on sequence specific interactions. Different examples will be discussed in the following part.

5.2.1 Target-mediated miRNA protection (TMMP)

As introduced previously, AGO proteins stabilize their associated miRNAs as over-expression of AGO proteins increase the levels of miRNA, showing that AGO protein level is a limiting factor for miRNA expression (Diederichs and Haber, 2007). In *C. elegans*, another regulation level exists that ensure functional miRNA levels by stabilizing miRNAs that possess an mRNA target and destabilizing those that do not. Experiments show that a reduction in the availability of target mRNAs decreases the levels of the miRNA that targets it and an increase in artificial target mRNA levels can stabilize that miRNA. This process termed target-mediated miRNA protection (TMMP), prevents miRNA decay by XRN1 and XRN2 by keeping them loaded into AGO (Chatterjee et al., 2011). On top of providing a way to keep the pool of AGO proteins loaded with functional miRNA, this mechanism can also, although to a lesser extent, provide a way for the evolution of new miRNAs that would derive from passenger strands of existing miRNA by acquiring target mRNAs.

5.2.2 Target RNA-mediated miRNA degradation

In contrast to TMMP, miRNA degradation can be induced by highly complementary interaction with target mRNAs on several instances. In *Drosophila*, Ameres and colleagues observed that after expression of a miRNA sensor bearing in its 3'UTR a perfect matching target site for a miRNA, the levels of that miRNA was reduced. This destabilization is accompanied by the appearance of longer (tailed with mostly A residues) and shorter (trimmed) isoforms of the miRNA. Moreover, the destabilization of the miRNA is dependent on high complementarity of its 3' half with the target mRNA whereas more classical seed only interaction did not cause any destabilization (Ameres et al., 2010). In *Drosophila,* siRNAs are loaded into AGO2 whereas miRNAs are loaded in AGO1 (Okamura et al., 2004) and siRNAs but not miRNAs are 2'O-methylated by HEN1 (Horwich et al., 2007). In mutant hen1 flies, AGO2 bound siRNAs become vulnerable to tailing and trimming, suggesting that 2'O-methylation is protecting siRNAs from RNA modifying enzymes (Ameres et al., 2010).

This is similar to plant miRNAs that are protected by the same modification, the loss of which results in tailing and trimming of plant miRNAs (Li et al., 2005; Yu et al., 2005). The tails that marks unmethylated miRNAs are mostly uridines and tailing also has been observed to occur on already trimmed miRNA (Li et al., 2005). These findings suggest that 2'O-methylation of the 3' end of miRNAs in plants and siRNAs in flies works to protect the small RNA from target-mediated degradation, as siRNAs and plant miRNAs are known to engage in extensive complementary interaction with their targets.

Ameres and colleagues also showed that the induction of tailing and trimming of miRNA can be achieved in human cell-lines by transfection of antagomiRs (Ameres et al., 2010). AntagomiRs are chemically modified RNA analogues that are antisense to the miRNA that they target, they have been instrumental to block miRNA function *in vitro* and *in vivo* (Hutvagner et al., 2004). These antagomiRs act at the level of RISC by blocking the cognate miRNA from recognizing its targets and also by decreasing the levels of the targeted miRNA (Hutvagner et al., 2004; Krutzfeldt et al., 2005). The decrease in cognate miRNA level after antagomiR transfection was shown to be accompanied by tailing, with adenines and uracils, and trimming of the miRNA (Ameres et al., 2010). This destabilisation of endogenous miRNA was also recapitulated *in vitro* by addition of an artificial mRNA with several highly complementary binding sites (Ameres et al., 2010). This was further demonstrated *in vivo*, by expressing a mRNA bearing several highly complementary sites, the destabilisation of the miRNA was again accompanied by addition of A and U residues, but the most abundant modified miRNA contained a single U residue on its 3' end (Baccarini et al., 2011). Target-mediated miRNA destabilisation is dependent on the extensive interaction of the mRNA with the miRNA as well as their relative abundance. The interaction at the 3' of the miRNA seems to be the most crucial for the induction of destabilisation as only a small number of mismatches can be tolerated for destabilisation to occur (Ameres et al., 2010; Baccarini et al., 2011; Xie et al., 2012). The importance of the interaction at the 3' end of the miRNA could be due to the fact that it might help to dislodge the end of the miRNA from the PAZ domain of AGO, making it accessible to exonucleases or nucleotidyl transferases (Wang et al., 2009). One can also imagine that after coming across a highly complementary target, the miRNA is unloaded from AGO and this makes the miRNA available for modification. *In vitro* experiments showed the unloading of miRNA from AGO after interacting with a highly complementary target and this was dependent on the interaction of the 3' end of the miRNA (De et al., 2013). Further experiments are needed to answer the question whether the modification of miRNA occurs before or after the unloading of the miRNA.

5.2.3 miRNA degradation and viral infections

Several natural examples of target-induced miRNA degradation exist in the literature; at present these examples only include viruses that make use of this mechanism to destabilize host miRNAs.

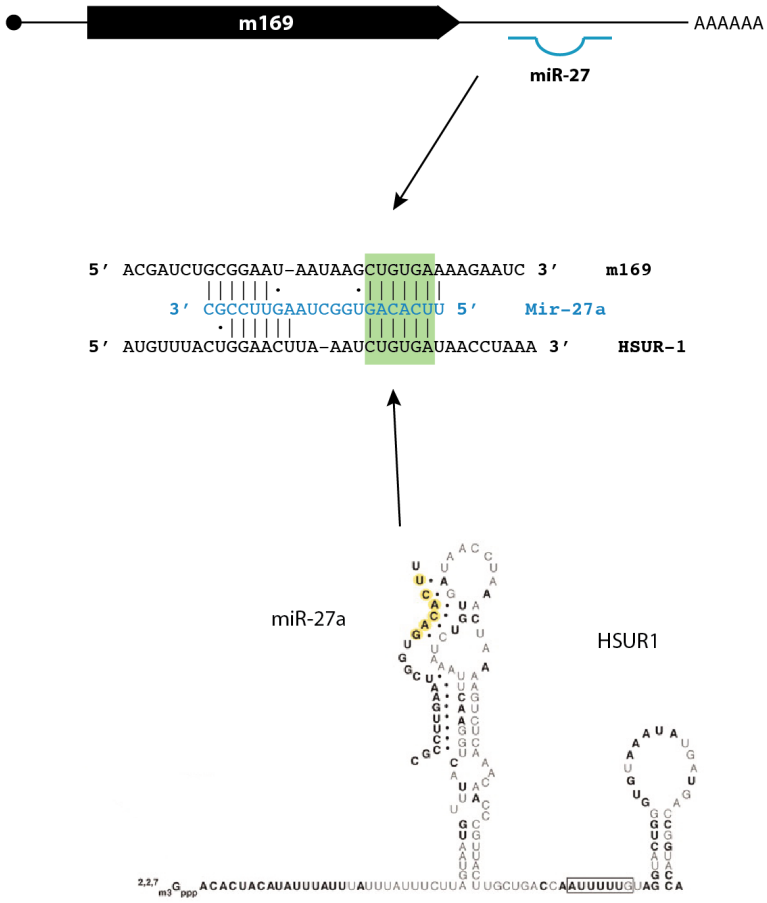

Figure 17: miR-27 interaction HSUR1 and m169 during HVS and MCMV infection
miR-27a sequence is represented in blue, it binds to the 3' UTR of MCMV m169 and to a stem-loop structure on HVS HSUR1. The extent of the interaction between miR-27 (blue) and these viral RNAs (black) is shown where the seed region (green) and the 3' end of the miRNA engage in interaction creating a bulge in the middle of the miRNA. G:U wobbles are indicated with a " · " and Watson-Crick interactions with " | ".

The first published example of a virus-induced miRNA degradation came from the infection of primate T-cells with *Herpesvirus saimiri* (HVS), during which virally expressed small non-coding HSUR RNAs (*Herpesvirus saimiri* U-rich RNAs) binds with partial complementarity to miR-142, miR-27 (miR-27a and miR-27b) and miR-16. However, only miR-27 is destabilized by its interaction with HSUR1, which is most probably due to the more extensive

interaction between these RNAs (Cazalla et al., 2010) (Figure 17). This binding site is found in a flexible region that makes it available for miR-27 binding and induction of degradation (Pawlica et al., 2016). The transfection of constructs expressing HSUR-1 can recapitulate destabilization of miR-27 and shows that it is sequence and binding dependent, moreover another cellular miRNA can be targeted by mutating the binding site on HSUR1 (Cazalla et al., 2010). However, experiments did not address whether the destabilization of miR-27 is accompanied by its tailing and trimming or that it affects the viral replication in any way.

The second reported example comes from the infection by mouse cytomegalovirus (MCMV), which induces the rapid destabilization of the same cellular miRNA, miR-27. During MCMV infection, the cellular miRNA miR-27 (a and b) is destabilized while miR-23a and b and miR-24, which derive from the same primary transcripts, are not affected. The pre-miRNAs are not affected either, showing that the destabilization happens at the mature miR-27 level. Transcription arrest by Actinomycin D treatment demonstrated that the destabilization of miR-27 is dependent of a RNA that is transcribed during infection (Buck et al., 2010). A couple years later, a viral messenger RNA called m169 was found to induce the degradation of miR-27; it possesses a single binding site for this miRNA in its 3'UTR (Libri et al., 2012; Marcinowski et al., 2012). m169 is the sole RNA responsible for the induction of miR-27 destabilization as transient expression of this transcript in uninfected NIH-3T3 cells is sufficient to destabilize miR-27 showing that no other viral factors are necessary (Marcinowski et al., 2012). This viral transcript is the most abundant transcript expressed in MCMV-infected cell (Juranic Lisnic et al., 2013) and its interaction with miR-27 comprises a full match of the seed region and of the 3' end, leaving only a bulge in the middle of the miRNA (Libri et al., 2012; Marcinowski et al., 2012) (Figure 17). The destabilization of miR-27 during MCMV infection is accompanied by its tailing and trimming similar to what has been shown in *Drosophila* and human cells (Ameres et al., 2010), with the tails composed of As and Us and trimming happening in 3' to 5' direction (Marcinowski et al., 2012). Furthermore, m169 can be mutated to target other viral or host encoded miRNAs and induce their degradation. An infection by a mutant MCMV that cannot destabilize miR-27 shows a decrease in viral replication in mice, indicating that the regulation of this miRNA is important during the virus infection cycle (Buck et al., 2010; Marcinowski et al., 2012).

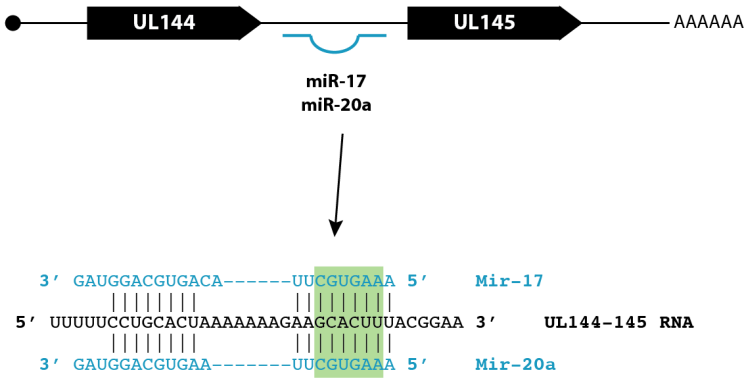

Figure 18: miR-17 and miR-20a interaction with UL144-145 during HCMV infection
miR-17 and miR-20a sequences are represented in blue, they bind to the intergenic region between UL144 and UL145. The extent of the interaction of miR-17 and miR-20a (blue) with the viral UL144-145 (black) is shown where the seed region (green) and the 3' end of the miRNA engage in interaction creating a bulge in the middle of the miRNA.

Another example of cellular miRNA degradation by a virus occurs during human cytomegalovirus (HCMV) infection. Several laboratory strains of this virus up-regulate the miRNA cluster miR-17~92, but only virulent strains down-regulate specifically specifically miR-17 and miR-20a from this cluster, whereas attenuated strains do not. The difference between these strains turns out to be a 15kb segment that is missing in the attenuated strains. This genomic sequence codes for a viral transcript called UL144-145 RNA containing two open reading frames separated by an intergenic region. This transcript carries a region called miRNA decay element (miRDE) by the authors. It specifically induces the destabilization of miR-17 and miR-20a. Similar to previous examples, the miRNAs and miRDE are engaging in extensive but incomplete interaction with a bulge in the middle of the miRNA (Figure 18) and again miRDE can be mutated to target other cellular miRNAs. Counteracting the destabilization of miR-17 results in the down-regulation of HCMV replication, making miR-17 an anti-viral miRNA (Lee et al., 2013).

In these examples of viral infections inducing host miRNA destabilization several common aspects appear. The miRNA decay is sequence specific and induced by binding of the miRNA to a coding or non-coding viral RNA. The interaction between the two RNAs is extensive but incomplete usually creating a bulge in the middle of the miRNA and only minimal mismatches at its 3' end. The only viral factor necessary for the induction of the

destabilization is the transcript, as its heterologous expression without infection is sufficient to induce decay of the miRNA. This suggests that miRNA degradation machineries exist in the host cell and viruses take advantage of this to destabilize anti-viral host miRNA at least in the case of HCMV and MCMV. By mutating the sequence of the target RNA binding sites, other miRNA can be targeted, demonstrating the sequence specificity and versatility of this mechanism. Only in the case of MCMV infection, was it reported that miR-27 destabilization was accompanied by tailing and trimming of the miRNA, whereas it was not verified in HVS and HCMV infection. Further investigation is necessary to verify if tailing and trimming is a necessary step during the degradation of a mature miRNA and its implications concerning the unloading of the miRNA from AGO.

RESULTS

1. Discovery of factors involved in Target RNA mediated miRNA degradation (TDMD)

Regulation of gene expression is crucial for survival. miRNA pathway discovered in the last decade, have been shown to handle one of the levels of gene expression regulation. miRNAs are ubiquitous in higher eukaryotes and a functioning miRNA pathway is indispensable for life. The miRNA pathway has been subject of extensive research and how their biogenesis, function and their regulation work has been addressed in several organisms. Our knowledge is quite broad on their biogenesis, their mechanism of action and our understanding of miRNA function is expanded more and more every day. Although some miRNAs can work as molecular switches for example during development, most miRNA function to ensure the robustness of biological processes. Depending on the needs of the cell however, gene expression has to be adjusted accordingly and this can be achieved by means modulation of miRNA activity. The activity of a miRNA is dependent on its expression level, though the regulation of miRNA expression has received attention more recently. Research uncovered examples of regulatory layers at every step of the miRNA pathway whether they are at steps of biogenesis, at the target recognition and repression steps or at the level of their stability. Even though miRNAs have been considered as stable molecules, in some specific contexts some miRNAs show shorter half-lives. Some of these examples of miRNAs have been shown to be inherently unstable and their level can be adjusted with transcriptional control but other examples display targeted destabilization of miRNAs. Such an example has been discovered in our laboratory during MCMV infection where a cellular mature miRNA is specifically destabilized through an interaction with a viral mRNA called m169.

MCMV belongs to the family of *Herpesviridae* which are large enveloped viruses with linear double-stranded DNA (dsDNA) genomes ranging between 145-241 kbp. All *Herpesviridae* package their genomes in an icosahedral capsid which sits in a proteinaceous matrix called tegument that is in turn contained in the envelope enriched in viral glycoproteins (Davison and Bhella, 2007). *Herpesviridae* family is separated into three sub-families *Alphaherpesviridae*, *Betaherpesviridae* and *Gammaherpesviridae* on the basis of their genomic organization and they infect mostly mammalians and birds however some species of

Herpesviridae can infect lower vertebrates like reptiles, amphibian or invertebrates. In natural context, herpesviruses can probably only infect only one species, however in experimental settings transfer to other species can occur. Herpesviruses are highly adapted to their host and the co-evolution of the virus and the host results in the restriction of severe symptoms of infection to the immunocompromised individuals or the very young (Davison, 2007). The expression of viral genes in herpesviruses follows a pattern that divides genes into three categories, immediate early (IE genes), early (E genes) and late genes. IE gene expression does not necessitate any viral protein synthesis by contrast early gene transcription needs IE proteins and thus can be blocked by protein synthesis inhibitors and late gene expression happens only after DNA replication has occured (White and Spector, 2007).

The most studied virus among *Betaherpesviridae* is HCMV, its seroprevalence in human populations range between 45 to 100% and congenital HCMV infection can cause permanent hearing loss and neurological impairment (Cannon et al., 2010) and CMV retinitis in individuals with acquired immunodeficiency syndrome (Pass et al., 2006). One close relative of HCMV is MCMV and it is used as an *in vivo* model for studying cytomegalovirus infections as both share the same characteristics with respect to their genome organization (although not sequence), gene expression pattern, tissue tropism and infection dynamics (Krmpotic et al., 2003). Moreover, most of miRNA of viral origin identified are expressed by Herpesviruses, HCMV and MCMV both encode miRNAs that are distributed similarly through the genome from single loci or small clusters and show early kinetics. Cytomegalovirus miRNAs offer not only a way to regulate viral gene expression but also the host's, creating another level of complexity between the host and virus interaction. For broader information about the roles of miRNAs of herpesviruses or cytomegaloviruses please refer to (Piedade and Azevedo-Pereira, 2016; Tuddenham and Pfeffer, 2011).

MCMV has been shown to alter the cellular miRNA pathway in different ways, after only 24 hours post-infection, more than the third of miRNA sequencing reads from infected cells are of viral origin and this ratio increases as the infection progresses to further time points (Dölken et al., 2007). The functional relevance of two of these viral miRNAs, miR-m23-2 and miR-m21-1, has been demonstrated *in vivo*; infection of mice with the deletion mutant MCMV for these miRNAs compared to wildtype MCMV showed 100 fold reduced viral titers at 14 days post-infection in salivary glands but showed no difference in lungs (Dölken et al., 2010a). This indicates that MCMV can use its miRNAs for tissue specific persistence.

Moreover, MCMV infection has been shown to affect cellular miRNA levels, one study showed the decrease of cellular miR-199 and miR-214 levels during infection (Santhakumar et al., 2010). The same study also demonstrated that these miRNAs had anti-viral functions during MCMV and HCMV infection (Santhakumar et al., 2010), illustrating that viruses have developed ways to counteract effects of some cellular miRNAs through the modulation of their accumulation. However, in this study one of the most potent anti-viral cellular miRNA against MCMV infection was found to be miR-27 (Santhakumar et al., 2010) and it was shown that during infection miR-27 was quickly destabilized (Buck et al., 2010). Further studies demonstrated the sequence specific destabilization of miR-27 that was dependent on binding to a viral mRNA called m169 bearing a single binding site for miR-27. m169 accumulation correlates with the destabilization of miR-27, the two RNAs interact extensively only with a bulge in the middle region of the miRNA (Libri et al., 2012; Marcinowski et al., 2012). Interestingly, the same cellular miRNA is targeted for destabilization during HVS infection by another type of viral RNA called HSUR1 (Cazalla et al., 2010). Moreover, small RNA sequencing in infected cells revealed that miR-27 destabilization coincides with miR-27 acquiring a tail by non-templated nucleotide additions and its shortening by trimming (Marcinowski et al., 2012). This is similar to what has been observed in Drosophila after a miRNA encounters a mRNA bearing perfectly matching target site (Ameres et al., 2010). The tails of miR-27 species are composed of As and Us and these modified species have been shown associate less with AGO2, suggesting that the modified miRNAs are unloaded from AGO (Marcinowski et al., 2012).

In this chapter, we have used MCMV infection and the interaction between m169 and miR-27 as models to get insights to how target mediated degradation of miRNA (TDMD) works. We set out to discover which are the molecular requirements of the interaction between miR-27 and m169 for the miRNA degradation to occur, to that end we made use of antagomiR transfections that have been shown to induce TDMD in mammalian cells (Ameres et al., 2010; Krutzfeldt et al., 2005). AntagomiRs allowed us to simulate different extents of interaction between the two RNA and follow the degree of destabilization of miR-27. Moreover, by inducing the tailing and trimming of miR-27 with the help of luciferase reporters bearing the 3' UTR of m169, we followed how miR-27 degradation and translational inhibition of the reporter behaved by multiplying the number target sites for miR-27. Finally, by using antagomiRs that carry a biotin molecule, we set up a proteomic approach in which the antagomiR would induce tailing and trimming and its biotin would

enable the pulldown of the complexes that take part in talling and trimming of the miRNA. This approach allowed us to obtain several candidate factors, for two most promising of which we have proceeded to validate them for their function in TDMD. The results that we obtained were published in *Nucleic acids research* in an article that is attached here.

Published online 24 January 2016

Nucleic Acids Research, 2016, Vol. 44, No. 6 ***2873–2887***
doi: 10.1093/nar/gkw040

Identification of factors involved in target RNA-directed microRNA degradation

Gabrielle Haas†, Semih Cetin†, Mélanie Messmer, Béatrice Chane-Woon-Ming, Olivier Terenzi, Johana Chicher, Lauriane Kuhn, Philippe Hammann and Sébastien Pfeffer*

Architecture and Reactivity of RNA, Institut de biologie moléculaire et cellulaire du CNRS, Université de Strasbourg, 15 rue René Descartes, 67084 Strasbourg, France

Received March 09, 2015; Revised January 12, 2016; Accepted January 13, 2016

ABSTRACT

The mechanism by which micro (mi)RNAs control their target gene expression is now well understood. It is however less clear how the level of miRNAs themselves is regulated. Under specific conditions, abundant and highly complementary target RNA can trigger miRNA degradation by a mechanism involving nucleotide addition and exonucleolytic degradation. One such mechanism has been previously observed to occur naturally during viral infection. To date, the molecular details of this phenomenon are not known. We report here that both the degree of complementarity and the ratio of miRNA/target abundance are crucial for the efficient decay of the small RNA. Using a proteomic approach based on the transfection of biotinylated antimiRNA oligonucleotides, we set to identify the factors involved in target-mediated miRNA degradation. Among the retrieved proteins, we identified members of the RNA-induced silencing complex, but also RNA modifying and degradation enzymes. We further validate and characterize the importance of one of these, the Perlman Syndrome 3′-5′ exonuclease DIS3L2. We show that this protein interacts with Argonaute 2 and functionally validate its role in target-directed miRNA degradation both by artificial targets and in the context of mouse cytomegalovirus infection.

INTRODUCTION

Among the various classes of small regulatory RNAs, miRNAs represent one of the most studied in mammals. They act as guides to recruit Argonaute proteins (Ago) to target mRNAs, resulting in translation inhibition and reduced stability (1). These tiny regulators are involved in a wide variety of biological processes (2,3), and their aberrant expression can be the cause of genetic diseases and/or cancers (4,5). Consequently, their synthesis and turnover must be tightly controlled. Briefly, miRNAs are transcribed in the nucleus as a primary transcript (pri-miRNA) containing a hairpin structure, which is recognized and cleaved by the RNase III Drosha. This cleavage generates a precursor miRNA (pre-miRNA) which will be exported to the cytoplasm, where a second cleavage by the RNase III Dicer gives rise to a ≈22 nucleotides (nt) miRNA duplex (1). One strand of the duplex (guide strand) is loaded in the RISC (RNA-Induced Silencing Complex) and becomes the active miRNA, while the second strand (passenger strand) is often degraded.

miRNA biogenesis is regulated both transcriptionally and post-transcriptionally by different mechanisms controlling the level of pri-miRNA transcription, the activity or the accessibility of Drosha and/or Dicer or the stability of the pre-miRNA (1). One of the best described example of miRNA biogenesis regulation involves the LIN28 protein, which negatively impacts the synthesis of Let-7 miRNA (6–11). LIN28 reduces the cleavage activity of both Drosha and Dicer, at respectively the pri-Let-7 and the pre-Let-7 levels (6–8). LIN28 also recruits the Terminal-Uridylyl-Transferases TUT4/TUT7 (9,10), which uridylate pre-Let-7 leading to its subsequent degradation by the exonuclease DIS3L2 (11). More recently, TUT4 and TUT7 were also described to have a more widespread role in the control of pre-miRNA degradation via a mechanism involving the RNA exosome (12).

Mature miRNAs, which represent the active end products of this biogenesis were long thought to be very stable molecules with half-lives ranging from hours to days (13,14). But recently, several examples showed that they are also subjected to active regulation. In this case, modifications of the small RNA play essential roles to influence its stability or function. For example, miR-122 monoadenylation by GLD-2 (TUT2) stabilizes this miRNA in mammals (15). At the opposite, miR-26a is no longer functional as a consequence of its uridylation by ZCCHC11 (TUT4) (16). In addition, accelerated miRNA turnover has been reported. This is especially true for biological situ-

*To whom correspondence should be addressed. Tel: +33 3 88 41 70 60; Fax: +33 3 88 60 22 18; Email: s.pfeffer@ibmc-cnrs.unistra.fr
†These authors contributed equally to the paper as first authors.

ations that require rapid changes in gene expression (i.e. cell cycle, light-dark transitions) (17–19), or during viral infections (20–22). Moreover, the presence of a highly complementary target can induce miRNA degradation via a mechanism involving tailing (3′ addition of non-templated nucleotides) followed by trimming of the miRNA (13,23). From now on, we will refer to this phenomenon as target RNA-directed miRNA degradation (TDMD) according to a recent report from the Grosshans laboratory (24).

In several organisms, small RNA species are usually protected from degradation by addition of a 2'O-methyl group at their 3′ extremity by the methyltransferase HEN1 (23,25). In *hen-1* mutant plants and flies, the lack of a 2'O-methylated 3′ terminal residue results in 3′ uridylation/adenylation and subsequent 3′ to 5′ degradation of small interfering (si)RNAs (and plant miRNAs) (23,26). As opposed to siRNAs or plant miRNAs, *Drosophila* and mammals miRNAs are not 3′ protected and usually present only a partial complementarity with their target RNAs. This explains why a near-perfect miRNA/target complementarity (involving an extensive pairing of the 3′ region of the miRNA) coupled to a high abundance of the target seems to trigger miRNA degradation rather than mRNA regulation (23). Therefore, TDMD could represent a potential and powerful spatiotemporal way to regulate mature miRNA accumulation. Accordingly, TDMD has been observed *in vivo* in the context of mouse cytomegalovirus (MCMV) infection. Indeed, MCMV expresses an abundant viral transcript (m169), which localizes to the cytoplasm and induces degradation of the cellular miR-27a and b (20,21). To date, the molecular details of the process and the cellular enzymes involved in this mechanism are unknown.

In this study, we developed a biochemical approach that allowed us to induce TDMD in cell lines and to uncover the identity of the cellular factors responsible for the target-induced degradation of mature miRNAs. We retrieved known components of the RISC as well as several putative candidates for the miRNA modification and degradation. Among those, we identified the Terminal-Uridylyl-Transferase TUT1 and the 3′-5′ exoribonuclease DIS3L2. We confirmed that these two proteins interact with Argonaute 2 and together in an RNA-dependent manner. Although we could not assign a direct role to TUT1 in the TDMD process, most likely because of the redundancy with other TUTases, we could observe that impairing DIS3L2 activity leads to a reduced degradation of miRNAs in human cells, but also in mouse cells infected with MCMV, a natural inductor of TDMD.

MATERIALS AND METHODS

Plasmids, cloning and mutagenesis

DIS3L2 was amplified from HeLa total cDNA whereas cDNA clones (Thermo Scientific) were used as template for TUT1 (Accession BC128263), mouse mTUT1 (Accession BC025499), mouse mDIS3L2 (Accession BC036177) and mouse mAGO2 (Accession BC129922). TUT2, TUT4 and TUT7 were amplified from the plasmids Flag-TEVAP-TUT2, -TUT4 and -TUT7 provided by Narry Kim. Human AGO2 was re-amplified from the pIRESneo-FLAG/HA-AGO2 vector (Addgene). The vector expressing GFP-MBP was a gift from E. Izaurralde. To generate GFP fusion proteins, TUT1 (*Bgl*II/*Eco*RI), DIS3L2 (*Bgl*II/*Bam*HI), mTUT1 (*Bgl*II/*Eco*RI), mDIS3L2 (*Eco*RI/*Kpn*I), TUT2 (*Eco*RI/*Bam*HI), TUT4 (*Xho*I/*Sma*I) and TUT7 (*Xho*I/*Bam*HI) were each cloned in the pEGFP-C2 expression vector (Clontech) using the restriction sites indicated in parentheses. For HA-tagged proteins, the pcDNA3.1(+) vector (Invitrogen) was first modified by mutagenesis to insert the coding sequence of the HA-tag 5′ of the MCS cassette. Then, AGO2 (*Eco*RI/*Not*I), mAGO2 (*Eco*RI/*Not*I), TUT1 (*Eco*RI/*Not*I), mTUT1 (*Eco*RI/*Not*I), DIS3L2 (*Bam*HI/*Not*I) and mDIS3L2 (*Eco*RI/*Not*I) were inserted between the indicated restriction sites. The catalytic mutants of DIS3L2 (D391N, D392N) and mDIS3L2 (D389N) were generated by mutagenesis. For the luciferase reporters, m169–3′ UTR or SH fragment was cloned in the pcDNA3.1 vector using *Eco*RV restriction site. Mutation in the seed region was then done by mutagenesis. To concatamerize the SH region, SH fragments were amplified with the insertion of different cloning sites, then treated for multiple ligation before being re-amplified and cloned as described above. Finally, the F-Luc coding sequence was inserted in pcDNA-m169 versions using *Nhe*I/*Kpn*I. All the sequences of the cloning and mutagenesis primers are available in Supplementary Table S2.

Cell culture and transfection

HeLa cells, Hepa 1.6 cells and HEK293 cells were cultured in Dulbecco's modified Eagle's medium (DMEM) supplemented with 10% (v/v) fetal calf serum at 37°C in a humidified 5% CO_2 atmosphere. For co-immunoprecipitation, HeLa and Hepa cells were transfected with a mixture containing plasmids expressing HA-tagged and GFP-tagged protein using the Turbofect reagent (Thermo Scientific). For RNA-immunoprecipitation, HeLa cells (15×10^6 cells in 15-cm plates) were transfected with 60 μg of plasmid expressing GFP-tagged protein. The day after, cells were divided and re-seeded in two 15-cm plates. After 10 h, cells were retransfected with either control antimiRNA directed against the *Caenorhabditis elegans* specific miR-67 (antimiR-67) or antimiR-27 (or -16) at a final concentration of 10 nM using lipofectamine 2000 (Invitrogen). The immunoprecipitation was performed 16 h after the last transfection. For RNAi (DIS3L2 and TUT1), HeLa cells were transfected twice (at day 1 and day 2) with 100 nM siRNA using Dharmafect-3 (Dharmacon) (siRNA sequences are listed in Supplementary Table S2) or 50 nM each when co-knocked-down. On day 3, cells were re-seeded to be at 50% confluence and allowed to adhere. Then, HeLa cells were transfected with 5 nM antimiRNAs using lipofectamine 2000. Samples were collected 16 h after the antimiRNA transfection. For overexpression experiment, HEK293 cells were first transfected with 5 μg of the indicated plasmid using Lipofectamine 2000. The day after, cells are re-seeded, retransfected with the antimiRNA oligoribonucleotides and collected as described above. For luciferase assay, HeLa cells were seeded in 48-well plates and transfected with a mixture containing 25 ng of both

R-Luc and F-Luc reporters using Lipofectamine 2000. To overexpress the luciferase reporters, cells were seeded in 12-well plates, and transfected with mixtures containing 100 ng of the R-Luc transfection control, 0.375, 0.750 or 1.5 μg of the F-Luc reporters and empty plasmid to have equal amounts of DNA. Samples were analyzed 24 hours post-transfection.

Streptavidin affinity chromatography

For the mass spectrometry analysis, HeLa cells were grown in 500 cm^2 plates to reach 50–60% confluence and then biotinylated antisense 2'O methylated oligoribonucleotides were transfected using the calcium-phosphate method at the indicated concentrations. Up to five independent experiments were performed using 4 plates per samples. 48 hpi, cells were collected and resuspended in lysis buffer (50 mM Tris HCl [pH 7.4], 150 mM NaCl, 0.02% sodium azide, 100 μg/ml PMSF, 1% NP40), supplemented with Complete-EDTA-free Protease Inhibitor Cocktail (Roche). After lysis, the samples were cleared by 15 min centrifugation at 4000 g and 4°C. Then, 200 μl of streptavidin-beads (Dynabeads MyOne Streptavidin C1, Invitrogen) were prepared in RNase-free conditions according to the manufacturer's protocol and added to each sample. Samples were incubated for 30 min at 4°C under rotation and then, beads were washed 5 times in 0.1× SSC. Finally, 1/5 of the sample was treated with phenol-chloroform to extract total RNA, 1/5 was used for western blot and 3/5 served for mass spectrometry analysis by nanoLC-MS/MS.

For smaller scale experiments, the protocol remained the same except that HeLa cells were seeded in two 15-cm plates, lysed in 1 ml lysis buffer and incubated with 40 μl of streptavidin beads. 50% of the sample were dedicated to RNA analysis whereas the second half served for western blotting.

Immunoprecipitation

HeLa cells were harvested, washed twice with ice-cold phosphate-buffered saline (1× PBS), and resuspended in 1 ml of NET buffer (50 mM Tris HCl [pH 7.4], 150 mM NaCl, 1 mM EDTA, 0.1% Triton), supplemented with Complete-EDTA-free Protease Inhibitor Cocktail (Roche). Cells are lysed by three 15 s sonication followed by 30 min incubation on ice and debris are removed by 15 min centrifugation at 16 000 g and 4°C. If required, lysates are treated 30 min with 100 μg/ml of RNase A and then re-cleared by centrifugation. An aliquot of the cleared lysates (50 μl) is kept aside as protein Input and 50 μl additional aliquot for RNA Input when needed. Polyclonal anti-GFP antibodies (a kind gift from E. Izaurralde) or AGO2 monoclonal antibodies (kindly provided by G. Meister) are added and samples are incubated for 1 h at 4°C under rotation (18 rpm). Then, 50 μl of Protein-G-Agarose beads (Roche) were added and the samples were rotated similarly for 1 h. After three washes in NET buffer and a fourth wash in NET buffer without Triton, bound proteins are eluted with 100 μl of protein sample buffer (100 mM Tris HCl [pH 6.8], 4% SDS, 20% glycerol, 0.2 M DTT, 0.5% bromophenol blue), and/or bound RNA by phenol/chloroform extraction.

Nucleocytoplasmic fractionation and subsequent immunoprecipitation

The cytoplasmic and nuclear fractions were separated following the protocol established by Lim and collaborators (27). Briefly, 10×10^6 HeLa cells were harvested, washed twice with ice-cold 1× PBS, resuspended in 500 μl of lysis buffer (50 mM Tris HCl [pH 7.4], 140 mM NaCl, 1.5 mM $MgCl_2$, 0.1% Igepal CA-630) and incubated for 5 min on ice. After 10 min of centrifugation at 2000 g and 4°C, the supernatant (cytoplasmic fraction) was collected and put aside. The pellet was then washed twice with wash buffer (50 mM Tris HCl [pH 7.4], 140 mM NaCl, 1.5 mM $MgCl_2$) at 2200 g for 5 min at 4°C. After resuspension in 300 μl of lysis buffer followed by sonication, the samples were spun at 16 000 g for 15 min at 4°C. The supernatant (nuclear fraction) was then collected. The concentration of each sample was measured using the DC protein assay kit (Bio-rad).

When the cytoplasmic fraction was followed by immunoprecipitation, an aliquot was kept aside as input and the volume of the fraction was increased to 1 ml. Then the samples were rotated with 25 μl of GFP-Trap-A beads (Chromotek) during 45 min at 4°C. After three washes with the lysis buffer and one additional with the wash buffer, bound proteins were eluted with 100 μl of protein sample buffer.

Luciferase assay

HeLa cells, tranfected with Luciferase reporters 24 h before, were washed in PBS, lysed with passive lysis buffer (Promega) and assayed for firefly and *Renilla* luciferase activities, using the dual-luciferase reporter assay system (Promega) and a luminescence module (Glomax, Promega) according to the manufacturer's instructions. The relative F-Luc reporter activity was obtained by first normalizing to the transfection control (*Renilla* activity), and then, to the firefly activity obtained for the reporter without m169-UTR, which was arbitrarily set to 100.

RNA extraction and northern blot

Total RNA was extracted using Tri-Reagent Solution (MRC, Inc) according to the manufacturer's instructions except the precipitation step, which was done in presence of 3 volumes absolute ethanol and 0.05 volumes 3 M NaAc [pH 5].

Northern blotting was performed on 10 to 15 μg of total RNA. RNA was resolved on a 17.5% urea-acrylamide gel of 20 cm in length, transferred onto Hybond-NX membrane (GE Healthcare). RNAs were then chemically cross-linked to the membrane during 90 min at 65°C using 1-ethyl-3-[3-dimethylaminopropyl]carbodiimide hydrochloride (EDC) (Sigma). Membranes were prehybridized for 1 h in PerfectHyb™ plus (Sigma) at 50°C. Probes consisting of oligodeoxyribonucleotides (containing Locked Nucleic Acids for the detection of miR-27 and miR-16 tailed/trimmed isoforms) (see Supplementary Table S2) were 5′-end labeled using T4 polynucleotide kinase (Fermentas) with 25 μCi of [γ-32P]dATP. The labeled probe was hybridized to the blot overnight at 50°C. The blot was then washed twice at 50°C for 20 min (5× SSC/0.1% SDS), followed by an additional wash (1× SSC/0.1% SDS) for 5 min.

Northern blots were exposed to phosphorimager plates and scanned using a Bioimager FLA-5100 (Fuji).

Antibodies for western blot analysis

Antibodies were used at the following dilutions: mouse anti-GFP antibodies (1:2000) and anti-HA-Peroxidase (1:5000) were purchased from Roche. Rat anti-AGO2 monoclonal antibody (1:200), rat anti-AGO1 monoclonal antibody (1:10) and rat anti-TNRC6B antibody (1:20) were kindly provided by G. Meister. Rabbit anti-DIS3L2 (1:1000) is a gift from A. Dziembowski and rabbit anti-STARPAP (TUT1) was kindly provided by R.A. Anderson and used at 1:3300. Rabbit anti-DIS3 (1:1000), rabbit anti-TUT7 (1:500), mouse anti-tubulin (1:5000), anti-mouse, anti-rat and anti-rabbit secondary antibodies (1:10000) were purchased from Sigma-Aldrich. Rabbit anti-XRN2 (1:500), anti-EXOSC3 (1:500), anti-RRP6 (1:3000) and mouse anti-Histone H3 (1:5000) were purchased from Abcam. Rabbit anti-XRN1 (1:2000) is from Bethyl laboratories.

MCMV infection of Hepa 1.6 cells

Hepa 1.6 cells were seeded in 6-well plates (5×10^5 cells/well) at day 0, and then transfected at day 1 with 4 μg of indicated plasmids using lipofectamine 2000. On day 2, cells were counted and infected accordingly with MCMV at MOI 1 after centrifugal enhancement at 18°C and 800 g for 30 min. Media was replaced after 1 h of infection. RNA samples were then collected at the indicated time points.

Real time RT-PCR analysis

The quantitative real-time PCR analysis was performed using Roche LightCycler 480 II. Prior to reverse transcription reaction, 1 μg of total RNA was treated with DNase I (Fermentas) according to the provider's instructions. Reverse transcription reaction was performed using miScript reverse transcription II kit (Qiagen) according to the manufacturer's instructions. The resulting cDNA was PCR amplified with Maxima SYBR green kit (Fermentas) in 10 μl reaction volume. For the analysis of miRNA expression, the mature sequence of each miRNA was used to design the forward primer and the miScript universal primer (Qiagen) was used as reverse primer. Forward and reverse primers were used respectively at 0.5 μM and 0.7×. For mRNA analysis 0.25 μM of each forward and reverse primers were used. The PCR program was composed of an initial denaturation step at 95°C for 10 min followed by 44 cycles at 95°C for 15 s, 55°C for 30 s and 72°C for 30 s including melting curve analysis. Data were analyzed as described previously (28).

RESULTS

Target RNA induces miRNA decay in a non-cooperative manner

The ectopic expression of the m169 transcript using an adenoviral vector is sufficient to induce degradation of both miR-27a and miR-27b (20), thus indicating that no other MCMV-encoded factor is needed to tail and trim these miRNAs. Because it appears that both miRNAs are targeted indifferently, and since we will extensively refer to these miRNAs in the manuscript, we will refer to both miR-27a and b using the generic term miR-27.

It was clearly shown that the two main features required to induce TDMD of a miRNA are an extensive pairing and an abundant target (23). To gain understanding in the sensitivity of the balance between a classical miRNA response and the triggering of TDMD, we built luciferase reporters carrying the m169 transcript full 3′ UTR, a shorter version of it (termed SH and comprising ≈200 nucleotides surrounding miR-27 binding site), or repetitions of the SH sequence to increase the number of target sites (Figure 1A). All versions of the luciferase reporter displayed translation inhibition (Figure 1B, Supplementary Figure S1A). Furthermore, the level of repression increased with the number of repetitions of the SH sequence and thus with the number of miR-27 binding sites, due to a cooperative effect of miRNAs as previously reported (29–31). This effect could be slightly but significantly reverted by inserting mutations in the miR-27 seed-match as shown previously (20) and reflects the contribution of miR-27 in the repression of the reporters. Indeed, the m169 transcript possesses several putative binding sites for other miRNAs, which could explain that the reporters bearing mutation in the miR-27 binding site are never completely derepressed. Transfecting increasing amounts of reporters did not alter the efficiency of miRNA-mediated repression (Supplementary Figure S1B), while overexpression of the reporter constructs allows the induction of miR-27 tailing as assessed by the detection of bands migrating slower than the four majors isoforms of miR-27 (Figure 1C, Supplementary Figure S1C). Nevertheless, increasing the number of miRNA binding sites did not cause a greater impact on miR-27 tailing than the single binding site contained in m169 (Figure 1C). Thus, as opposed to miRNA-mediated repression, which exhibits a cooperative effect, TDMD appears to be a non-cumulative phenomenon.

A high complementarity between the miRNA and its target is a prerequisite to induce TDMD and it was previously shown in *Drosophila* that only little bulges (≈3 nt) can be tolerated (23). To understand how a m169-like binding site can trigger tailing-trimming with a 6-nt bulge, we transfected HeLa cells with increasing amounts of 2'O-methylated antisense oligoribonucleotides (antimiRNAs) presenting either a perfect complementarity with miR-27 (antimiR-27) or mimicking the interaction with m169 (m169-like, Figure 1D) since it was described that antimiRNAs are sufficient to recapitulate TDMD in cells (23). Northern blot analysis of miR-27 expression showed that a 100-fold more of the m169-like compared to antimiR-27 oligoribonucleotide was needed to induce TDMD (Figure 1E).

In addition, we confirmed the importance of a strong pairing in the 3′ of the miRNA by inserting mismatches in the antimiRNA oligoribonucleotide (Figure 1D). A single mismatch in the position exactly opposite the 3′ proximal nucleotide in the miRNA was sufficient to abrogate TDMD (Figure 1F). In addition, increasing the pairing strength 3′ of the bulge (position 15) by replacing a G-U by a G-C pair is enough to increase TDMD efficiency (Figure 1G). Thus,

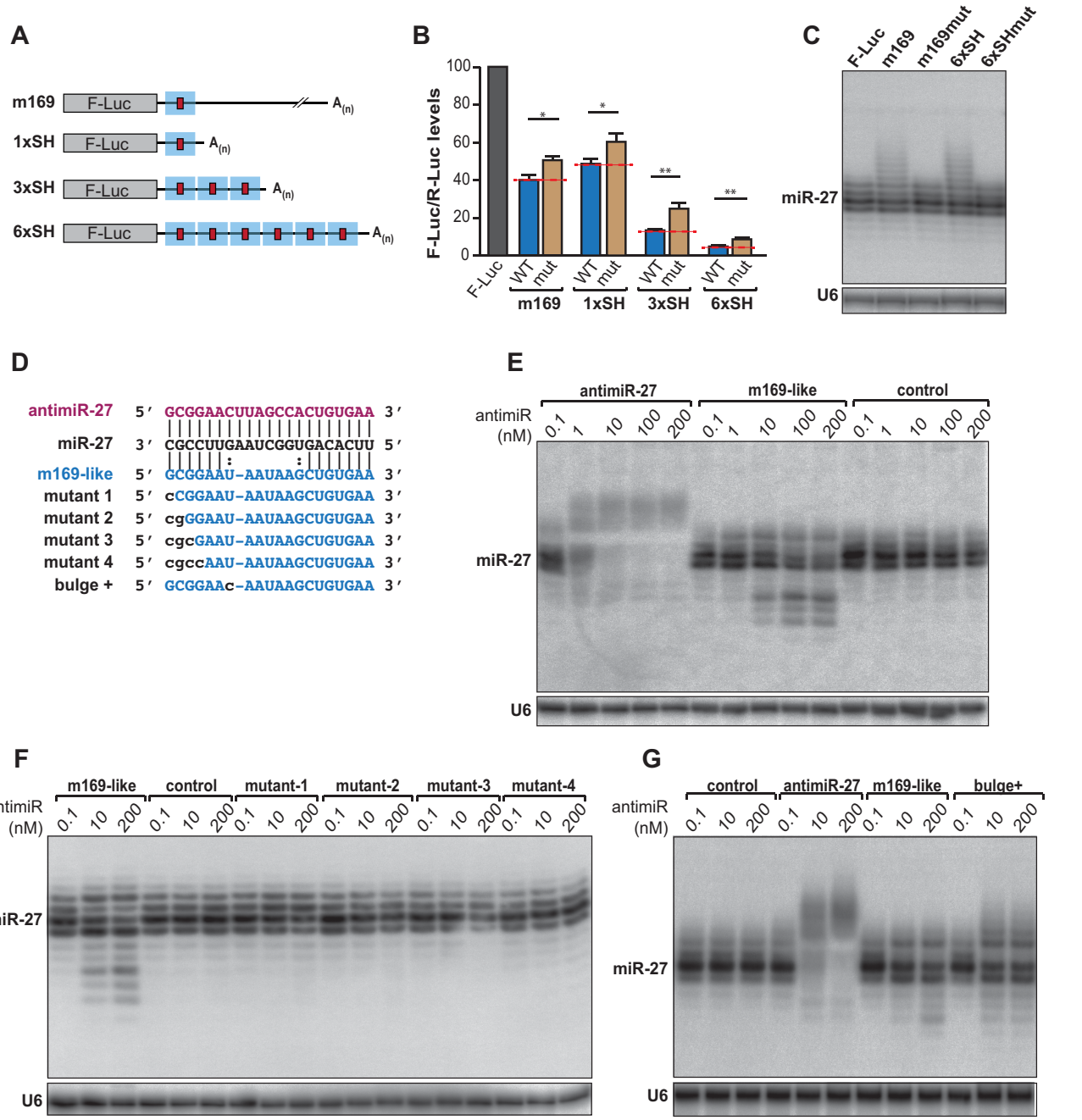

Figure 1. Characterization of m169-miR27 features triggering TDMD. (**A**) Reporters containing the 3′ UTR of m169 transcript or single/multiple shorter (SH) region (blue square) containing miR-27 binding site (red square). (**B**) Relative expression of the reporters described in (A) and containing either an intact miR-27 binding site (WT) or mutations in the seed (mut) by luciferase assay. Each F-Luc coding reporter was transfected into HeLa cells together with a plasmid coding for the *Renilla* luciferase (R-Luc) as transfection control. The F-Luc activities were normalized to those of *Renilla* and arbitrarily set at 100 in absence of 3′ UTR (F-Luc). Mean values +/- standard deviations from three independent experiments are shown. (Student *t*-test $*P < 0.05$, $**P < 0.01$, $n = 3$ biological replicates). (**C**) Analysis of miR-27 expression by northern blot when the reporters are overexpressed. U6 serves as loading control. (**D**) Sequences and pairing between miR-27 and the antimiRNAs used in this study. AntimiR-27 is in purple and m169-like is in blue. Modifications introduced in the pairing are in lowercase. (**E**–**G**) Northern blots analyzing miR-27 accumulation profil upon antimiRNA transfection in HeLa cells. Control: antimiR-67. U6 serves as loading control.

TDMD in mammals requires an extensive 3′ pairing between the miRNA and its target. However, the ratio between the miRNA and its target is important and this probably restrains the number of naturally occurring targets triggering miRNA tailing-trimming. Indeed, even if an m169-like interaction can trigger TDMD, the size of the central bulge limits its efficacy and only its expression at high levels such as during viral infection probably renders such interactions functional.

Isolation of protein complexes involved in TDMD induction

Since it is possible to purify RISC complexes from crude extract using biotinylated 2'O-methylated oligoribonucleotides (32), we used a similar approach to capture the TDMD nucleoprotein complexes by transfecting antimiRNAs in HeLa cells (Figure 2A). To this end, we used antimiR-27, m169-like and antimiR-16 2'O-methylated oligoribonucleotides carrying a triethylene glycol spacer with a biotin group on the 3′ terminal residue. We first determined the optimal concentration required to induce tailing-trimming without extensive degradation of the targeted miRNA, and found that 7.5, 250 and 3 nM were optimal for biotinylated antimiR-27, m169-like and antimiR-16 respectively. After collection of total cell lysates from transfected cells and incubation with paramagnetic-streptavidin beads, the analysis of retrieved RNAs revealed specific binding of miR-27 with both antimiR-27 and m169-like (Figure 2B,C) as well as miR-16 with its corresponding antimiRNA (Figure 2D). No signal was detected in non-transfected cells (beads) or cells transfected with a control oligoribonucleotide (control = antimiR-67). More importantly, we could also detect tailed and trimmed miRNA isoforms with this method.

We then increased the scale of the experiment and analyzed the bound proteins by nanoLC-MS/MS. The data were filtered to consider only proteins specifically bound to the antimiRNAs and not to the control oligoribonucleotide or to the beads (Supplementary Figure S2A–C). Among the factors identified, we could retrieve known components of RISC complexes such as AGO1, 2 and 3, TNRC6B, and RBM4 (Figure 2E). We also identified exoribonucleases such as XRN2 or the 3′-5′ exonuclease DIS3L2, recently shown to be involved in mRNA and let-7 precursor decay (11,33) with the three capture-oligoribonucleotides. Finally, the Terminal-Uridylyl-Transferase (TUT)-1 (Star-PAP/RBM21) was pulled-down specifically with antimiR-27 in our two replicates, albeit at relatively low levels.

To increase the confidence in our mass spectrometry analysis, we performed additional replicate experiments (up to five with the antimiR-27) and decided to focus on proteins that were present in at least three of the replicates, while being absent in their respective negative control experiments (control oligoribonucleotide or beads alone) (Supplementary Table S1). This allowed us to significantly reduce the number of false positives and to narrow down the list of putative candidates. With this approach, we found that DIS3L2 was reproducibly pulled-down both with antimiR-27 and antimiR-16. This enzyme belongs to the Dis3 family together with two other homologs, DIS3 and DIS3L but with the difference that it is not associated with the RNA exosome. It is a highly processive enzyme, also capable of degrading dsRNA with little (2 nt) or no 3′ overhangs (33,34). More interestingly, DIS3L2 was also detectable with m169-like oligoribonucleotide only when it was transfected at 250 nM (Figure 2E, R1), a concentration that triggers TDMD. This re-enforces the idea that DIS3L2 is specifically recruited for miRNA trimming.

The replicate experiments also confirmed that TUT1 was only retrieved with the antimiR-27 oligonucleotide. However, it was the only of the seven human TUTases to be identified in our mass spectrometry analysis. This enzyme belongs to the family of ribonucleotidyl transferases known among others to contribute to miRNA 3′ heterogeneity (35) and it possesses both a non canonical poly(A) polymerase and a terminal uridylyl transferase activities (36–38).

We then confirmed that DIS3L2 and TUT1 could indeed be detected in our pull-down experiments. Western blot analysis of proteins bound to antimiR-27 revealed a specific binding of both proteins, as well as of AGO2 (Figure 3A). Similarly, both DIS3L2 and AGO2 could also be detected by western blot associated to m169-like or antimiR-16 oligoribonucleotides (Figure 3B,C). The comparative analysis of proteins and RNA bound to antimiR-27 and m169-like oligoribonucleotides, when the two biotinylated-oligoribonucleotides are transfected at similar amounts, shows they both associate with similar amounts of miR-27 and are equally bound by RISC as assessed by the presence of AGO2 (Figure 3D). On the contrary, TUT1 and DIS3L2 are only associated with antimiR-27, the sole target capable to trigger TDMD at this concentration. Similarly, even though TUT1 was not found associated to antimiR-16 in the mass spectrometry data, we managed to detect it by western blot analysis when we increased the concentration of the oligoribonucleotide (Figure 3E). Under these conditions, we could also pull-down with both antimiR-27 and antimiR-16 oligonucleotides the AGO1 protein and TNRC6B, a GW182 family member essential for miRNA-mediated gene silencing (39) (Figure 3F).

We also tested the possibility of retrieving other related enzymes with antimiR-27 or antimiR-16 oligonucleotides even if we never or rarely detected them in our MS analysis. For this purpose, we tested the 5′-3′ exoribonucleases XRN1 and XRN2 (40), the exosome components EXOSC3 (RRP40), RRP6 and DIS3 (41), and finally TUT7 (ZCCHC6), which was recently shown to participate to mature miRNA mono-uridylation (42). None of these proteins were found specifically associated with antimiR-27 and antimiR-16 after TDMD induction (Supplementary Figure S3). Only XRN2 and DIS3 were detectable but without any specificity for TDMD since they both co-purified equally well with our control oligoribonucleotide.

Altogether, these results indicate that DIS3L2 and TUT1 are good candidates for TDMD. We thus decided to proceed with their functional characterization.

TDMD is induced in the RISC complex and occurs in the cytoplasm

We first sought to answer the question of how the mechanism is initiated. TDMD depends on a high degree of complementarity between the miRNA and its target, rais-

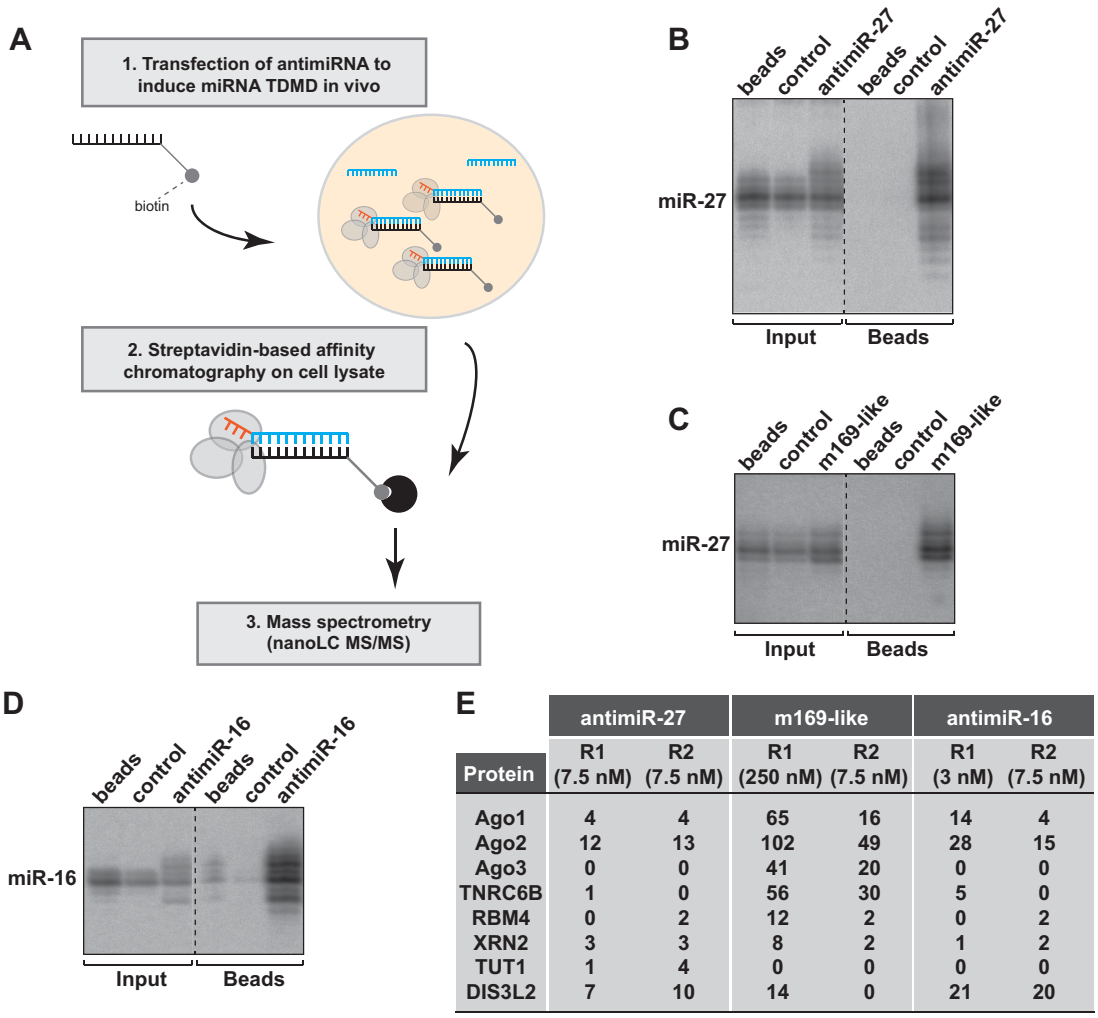

E

Protein	antimiR-27 R1 (7.5 nM)	antimiR-27 R2 (7.5 nM)	m169-like R1 (250 nM)	m169-like R2 (7.5 nM)	antimiR-16 R1 (3 nM)	antimiR-16 R2 (7.5 nM)
Ago1	4	4	65	16	14	4
Ago2	12	13	102	49	28	15
Ago3	0	0	41	20	0	0
TNRC6B	1	0	56	30	5	0
RBM4	0	2	12	2	0	2
XRN2	3	3	8	2	1	2
TUT1	1	4	0	0	0	0
DIS3L2	7	10	14	0	21	20

Figure 2. Identification of the cellular factors involved in TDMD. (**A**) Schematic representation of the biochemical approach to induce and capture the factors involved in TDMD. (**B**–**D**) HeLa cells were transfected with antimiRNA at a concentration inducing miR-27 or miR-16 TDMD. The complexes bound to antimiRNA were pulled-down using streptavidin-beads. The specific pull-down of miR-27 and miR-16 using antimiR-27 (replicate R1) (B), m169-like (C) and antimiR-16 (D) was verified by northern blot. A dashed line indicates discontinuous lanes but Input and IP fractions were systematically analyzed on a same gel. (**E**) Table showing the number of spectral counts detected by nanoLC-MS/MS for the indicated proteins found specifically associated with each antimiRNA. The concentration of antimiRNA used in each replicate is indicated in parentheses. Control: antimiR-67.

ing the possibility that the miRNA tailing and trimming is induced within the RISC. Alternatively, the miRNA could also be marked for degradation after its release from the AGO protein. We therefore analyzed small RNAs by northern blot after AGO2 immunoprecipitation, which allowed us to show that the RISC effector interacted not only with the major isoforms, but also with tailed and trimmed isoforms of miR-27 when TDMD is induced (Figure 4A). The tailed and trimmed isoforms detectable by northern blot were comprised between 16 and 26 nucleotides in length (Supplementary Figure S4A). Similar results were obtained with miR-16 (Supplementary Figure S4B) or when miR-27 TDMD was induced by transient expression of a piece of the m169 transcript (Supplementary Figure S4C). Thus, although it is unclear whether the miRNA undergoing TDMD is eventually ejected from RISC, both tailing and trimming of miRNA seem to occur, at least partially, within AGO2.

More importantly, these observations suggest that both TUT1 and DIS3L2 might be recruited to the RISC. To test this hypothesis, we performed co-immunoprecipitation of DIS3L2, TUT1 and AGO2 after transfection of HeLa cells with plasmids expressing tagged-versions of the proteins. We observed that both TUT1 and DIS3L2 interact with AGO2 (Figure 4B,C) but also together (Figure 4D). These interactions are RNA-mediated (putatively miRNA-mediated), since they were sensitive to RNaseA treatment (Figure 4B–D). So, TUT1, DIS3L2 and AGO2 seem to be part of the same complex even if it is probably transient since target-induced miRNA decay is not a predominant mechanism.

The previous results raise the question of the formation of a complex comprising AGO2, DIS3L2 and TUT1, since

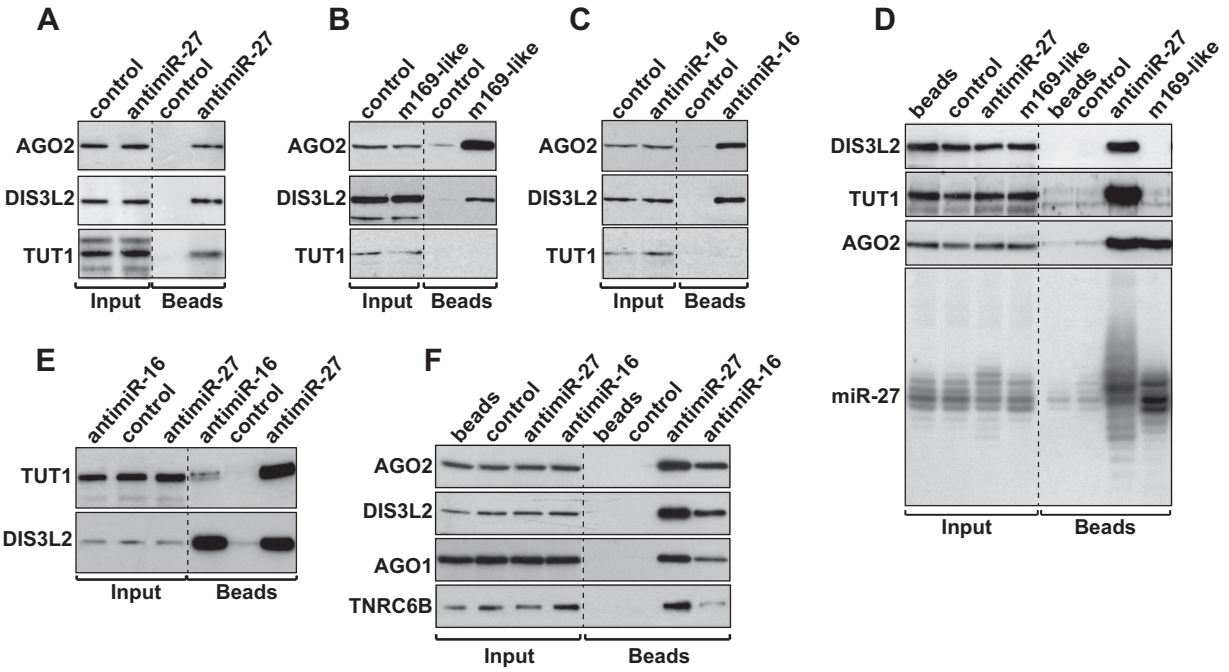

Figure 3. AntimiRNAs associate with DIS3L2, TUT1 and RISC components. (**A**–**C**) The presence of AGO2, DIS3L2 and TUT1 with antimiR-27 (A), m169-like (B) or antimiR-16 (C) was confirmed by western blot. (**D**) Comparative analysis of DIS3L2, TUT1, AGO2 and miR-27 pulled-down with antimiR-27 or m169-like oligonucleotides at 10 nM. (**E**) TUT1 and DIS3L2 detection after pull-down of antimiR-27 and antimiR-16 both transfected at 10 nM to induce TDMD. (**F**) AGO1 and TNRC6B are also associated with antimiR-27 and antimiR-16 both transfected at 10 nM. A dashed line indicates discontinuous lanes but Input and IP fractions were systematically analyzed on a same gel (A-F). Control: antimiR-67.

TDMD is most likely to occur in the cytoplasm and earlier reports showed that TUT1 was a nuclear protein (37). However, recent work indicates that this might not be its sole localization, as it could be observed both in the nucleus and the cytoplasm (43). We thus wanted to verify the relative amount of TUT1 in the cytoplasm and in the nucleus in our experimental setup, and to confirm that the cytoplasmic TUT1 interacts with DIS3L2 and AGO2. We therefore performed a subcellular fractionation and analyzed the distribution of the different proteins (Figure 4E). Using tubulin as a cytoplasmic marker and histone H3 as a nuclear marker, we found that DIS3L2 was only present in the cytoplasm as expected (33,34), similar to TUT7 (27), AGO2 could be observed in both compartments, as previously reported (44), and we also found TUT1 both in the cytoplasm and the nucleus (Figure 4E) confirming that this TUTase is indeed a nucleo-cytoplasmic protein. We then immunoprecipitated TUT1 from a cytoplasmic extract and could observe that it interacted with endogenous DIS3L2 and AGO2, thereby confirming that these interactions naturally occur in the cytoplasm (Figure 4F).

We showed earlier that DIS3L2 and TUT1 could be pulled-down with the antimiRNA oligoribonucleotide only under conditions where TDMD was induced (Figure 3D). We therefore looked whether we could confirm the interaction by immunoprecipitating the proteins and detecting the miRNA. For DIS3L2, we used the catalytic mutant because the wild type protein association with the targeted RNA would be too transient. The immunoprecipitation of DIS3L2mut shows that the exonuclease seems to interact weakly with miR-27 but independently of TDMD (Figure 4G). DIS3L2 might therefore have additional roles in miRNA decay that are independent of TDMD. Nonetheless, the mutant protein interacted more strongly than the wild-type exonuclease with tailed/trimmed isoforms of miR-27 (Supplementary Figure S4D) confirming its role in miRNA trimming.

Finally, we analyzed small RNAs after immunoprecipitation of TUT1. We confirmed that the pull-down was efficient, since we could retrieve its known substrate U6 (38). The northern blot analysis also revealed that it exclusively interacted with miR-27 isoforms when TDMD was induced with antimiR-27 oligonucleotide (Figure 4H). In addition, we also performed northern blot analysis of miR-27 after immunoprecipitation of other TUTases (TUT4, TUT7 and TUT2), but could not detect the miRNA coming down with any of these, be it in the presence or not of the antimiRNA oligonucleotide (Supplementary Figure S4E).

DIS3L2 is implicated in miRNA trimming

We then aimed at validating the involvement of TUT1 and DIS3L2 in TDMD by performing knockdown experiments of either each factor separately or both of them together and we monitored the level of TDMD induced by antimiRNA transfection. We observed an efficient depletion of these two factors at the protein level in HeLa cells (Figure 5A). Nonetheless, the efficiency of TDMD was not altered as assessed by northern blot analysis of miR-27 (Supplementary Figure S5A) and miR-16 (Supplementary Figure S5B) com-

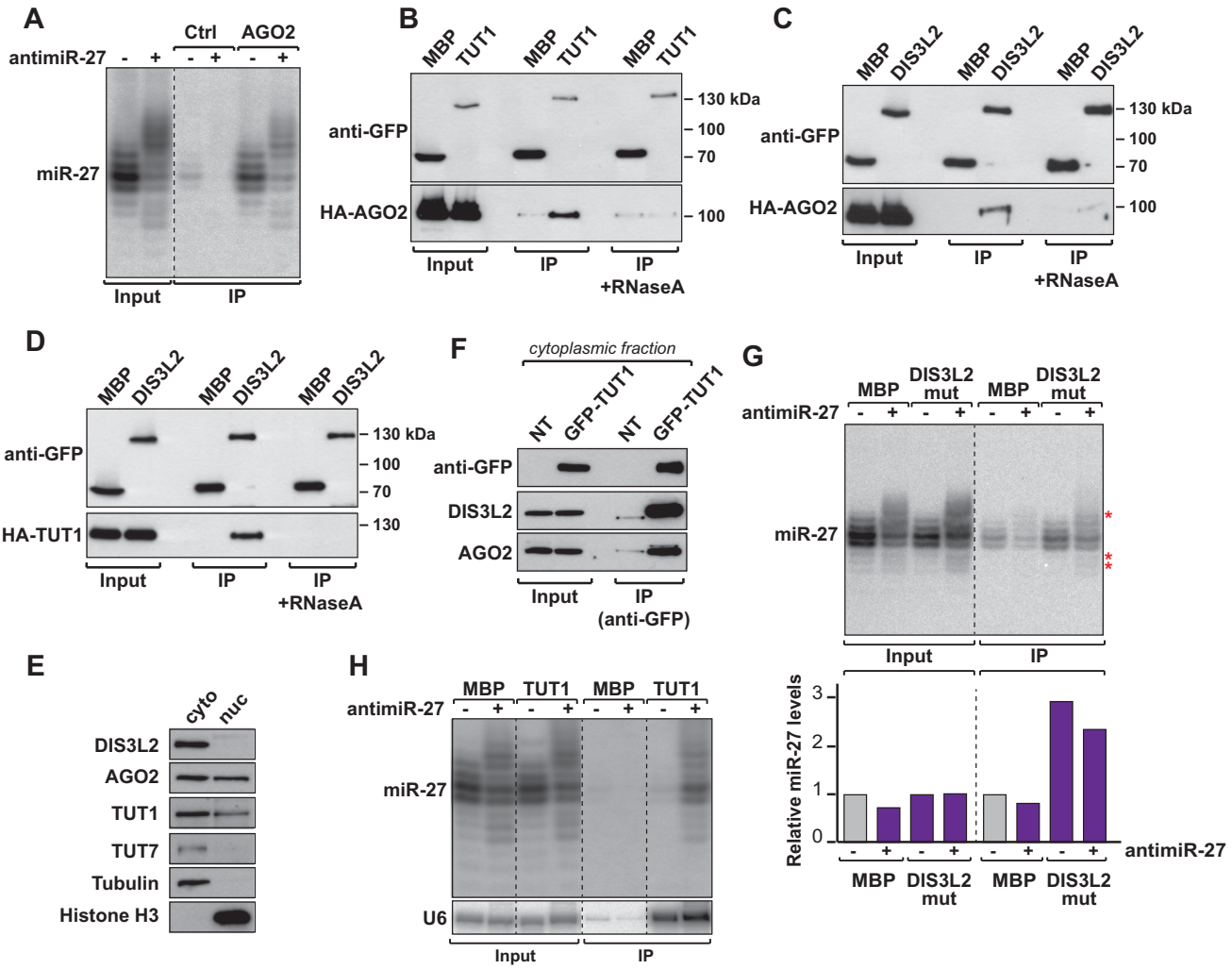

Figure 4. TDMD is induced in the RISC complex by recruitment of TUT1 and DIS3L2. (**A**) AGO2-associated tailed and trimmed isoforms of miR-27 were analyzed by northern blot. A space indicates discontinuous lanes from the same gel (also applicable to panels E and F). (**B**–**D**) Co-immunoprecipitation (anti-GFP) experiments show interaction between GFP-TUT1 and HA-AGO2 (B), GFP-DIS3L2 and HA-AGO2 (C) and GFP-DIS3L2 and HA-TUT1 (D). GFP-MBP serves as negative control. (**E**) Subcellular location of TUT1, DIS3L2 and AGO2 in cells. The relative amount of TUT1, DIS3L2 and AGO2 proteins in the nucleus (nuc) and the cytoplasm (cyto) were analyzed by western blot. TUT7 and Tubulin serve as cytoplasmic markers while Histone H3 is used as nuclear marker. (**F**) GFP-TUT1 interaction with endogenous DIS3L2 and AGO2 was assayed by co-immunoprecipitation (anti-GFP) performed on the cytoplasmic fraction. Non-transfected cells (NT) serve as negative control. (**G**) miR-27 isoforms co-precipitate together with GFP-DIS3L2 mutant. miR-27 enrichment was measured using miR-27 signal (normalized to tRNA in the input fraction) arbitrarily set at 1 for GFP-MBP in absence of antimiR-27. Asterisks highlight tailed and trimmed isoforms. (**H**) Northern blot showing TUT1 interacts with miR-27 isoforms only when TDMD is induced. U6, a known substrate of TUT1, serves as positive control. A dashed line indicates discontinuous lanes from the same gel (A, E, G, H).

pared to the cells transfected with the control siRNA (siCtrl).

This result could be explained by the tendency of TUTases to complement each other *in vivo* (45) and/or the high processivity of DIS3L2 (34). To evaluate the contribution of the other TUTases, we performed multiple knockdowns in HeLa cells and again tested the efficiency of the TDMD. To this end, we separated the TUTases in two groups. In addition to TUT1, the first group (TUT1+2+4+7) comprises TUT2 (also called GLD2 and PAPD4), TUT4 (ZCCHC11) and TUT7 (ZCCHC6) as they are known to act redundantly in the pre-let-7 mono-uridylation (45). The second group (TUT1+3+5+6) is composed of TUT1, TUT3 (PAPD5), TUT5 (PAPD7) and TUT6 (MTPAP). However, we did not manage to rescue miRNA stability with any of the two siRNA mixes (data not shown). So, we cannot exclude that other combinations of TUTases, or more than four of them might act redundantly in this process. Similarly, we also tried to knockdown other exoribonucleases such as XRN1 and XRN2 alone or in combination with DIS3L2, but again could not observe an effect on miR-27 degradation induced by antimiRNA oligonucleotides (data not shown).

It could also be that the northern blot analysis approach we used to measure the effect of TUT1 and DIS3L2 knockdowns on miRNA levels presents limitations when it comes to assess subtle differences. We thus decided to perform small RNA cloning and sequencing in order to verify if

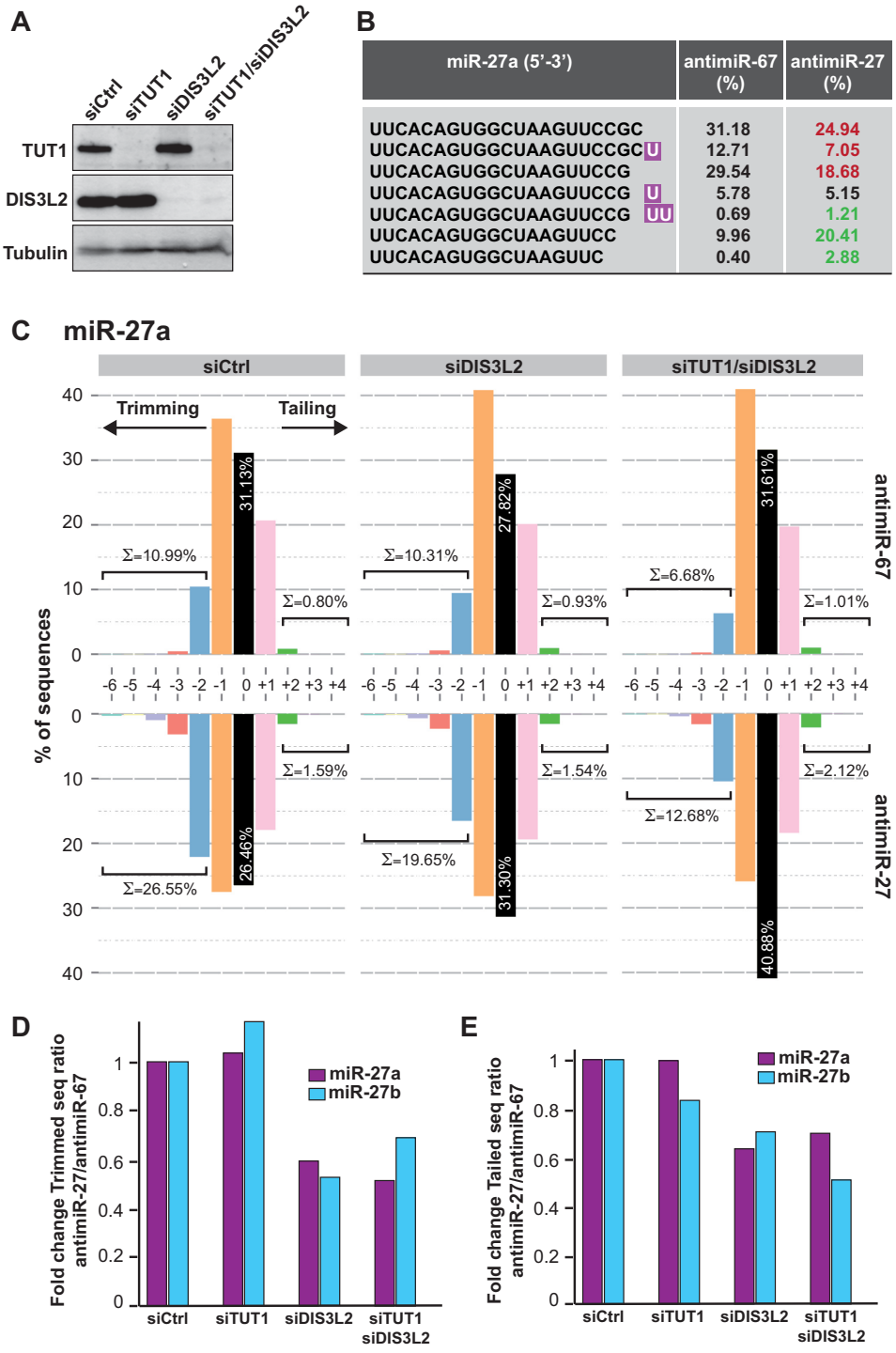

miR-27a (5'-3')	antimiR-67 (%)	antimiR-27 (%)
UUCACAGUGGCUAAGUUCCGC	31.18	24.94
UUCACAGUGGCUAAGUUCCGCU	12.71	7.05
UUCACAGUGGCUAAGUUCCG	29.54	18.68
UUCACAGUGGCUAAGUUCCGU	5.78	5.15
UUCACAGUGGCUAAGUUCCGUU	0.69	1.21
UUCACAGUGGCUAAGUUCC	9.96	20.41
UUCACAGUGGCUAAGUUC	0.40	2.88

Figure 5. Functional implication of DIS3L2 in miRNA degradation. (**A**) Efficiency of TUT1 and DIS3L2 knockdowns by western blot. The control siRNA (siCtrl) is targeting the *Renilla* luciferase. Tubulin serves as loading control. (**B**) Representative examples of the most abundant miR-27a isoforms detected in one of the libraries treated with the control siRNA and control antimiRNA (antimiR-67) or antimiR-27. Tailed nucleotides are highlighted in purple. The relative abundance of each isoform (%) is given before (antimiR-67) or after (antimiR-27) TDMD induction by the transfection of the corresponding antimiRNAs. The red color indicates a decrease and the green an increase in abundance of the respective sequence. (**C**) Distribution in percentage of miR-27a tailed and trimmed isoforms as assessed by small RNAs deep-sequencing of cells treated with the indicated siRNA and antimiRNA oligonucleotides. The '0' indicates the wild-type (WT) isoform of 21 nt. The sum of all trimmed (≤-2) or tailed (≥+2) sequences is indicated. (**D**) The efficiency of the trimming was evaluated in each knockdown condition and antimiRNA treatment. The graph represents the ratio of miR-27a (purple) or miR-27b (blue) trimmed *versus* WT ('0' or mature sequence) reads after TDMD induction (antimiR-27) normalized to those observed without TDMD (antimiR-67) using the values shown in C. The values were arbitrarily set at 1 in cells transfected with the control siRNA (siCtrl). (**E**) The efficiency of the tailing in each knockdown condition was analyzed as explained in D, except that the graph represents the ratio of tailed isoforms versus WT ('0') reads.

some changes that could not be observed by other means occur after TUT1 and/or DIS3L2 depletion. We first monitored the impact of antimiR-27 transfection on miR-27 isoforms, which allowed us to see that the most abundant tailed isoforms of miR-27a present an addition of one or two U residues at their 3′ end (Figure 5B). We could also detect a low number of miR-27 sequences presenting additional A residues, or a mix of A and U residues (data not shown). We calculated the respective abundance of the most abundant isoforms of miR-27a (in percentage relative to the total number of miR-27a in each sample) in presence or absence of TDMD induction by antimiR-27 and we observed an increase in the abundance of tailed and trimmed isoforms and a decrease of the major isoforms of miR-27a or b in presence of the antimiR-27 (respectively in green and in red in Figure 5B).

We then determined more precisely the distribution of miR-27a isoforms in libraries generated from cells treated with a control siRNA or siRNAs directed against TUT1, DIS3L2 or both and transfected with an antimiR-27 or control (antimiR-67) oligonucleotide. For each library, we calculated the number of wild-type (after miRBase) sequences of miR-27a that we set as the '0' modification, as well as the number of sequences tailed or trimmed by 1, 2 or more nucleotides (respectively +1, +2… and −1, −2…). The deep-sequencing analysis confirmed that miR-27a exists mainly as three isoforms of 21 (0), 20 (−1) and 22 (+1) nucleotides. We therefore considered as trimmed and tailed sequences, all isoforms presenting with an addition or deletion of more than 2 nucleotides. As shown in Figure 5C for miR-27a, in cells treated with the control siRNA the percentage of trimmed sequences indeed increased in the presence of antimiR-27 (bottom graph) compared to antimiR-67 (top graph). We also observed a modest increase in tailing upon transfection of the specific antimiRNA. This increase in trimming seems to be less pronounced when DIS3L2, TUT1 or both DIS3L2 and TUT1 were knocked-down (Figure 5C and Supplementary Figure S5C). We did the same calculation for miR-27b and roughly observed the same effects, although less pronounced, which might be due to the fact that the antimiRNA oligonucleotide we transfected was directed against miR-27a (Supplementary Figure S6).

To quantify these differences, we then calculated the efficiency of trimming (Figure 5D) and tailing (Figure 5E) in each knockdown condition and for both miR-27a and miR-27b. To this end, we first determined the ratio of trimmed (or tailed) to wild-type (mature) sequences in antimiR-27 versus antimiR-67 in each condition, and then normalized it to the ratio found in the control cells, which was arbitrarily set to 1. TUT1 depletion did not seem to affect the efficiency of trimming of both miR-27a and b (Figure 5D and Supplementary Figure S5C). However, we observed a 40–50% reduction in trimming of miR-27a and b in cells where DIS3L2 or DIS3L2 and TUT1 were knocked-down (Figure 5D). The effect on tailing was more difficult to assess given the weaker induction of tailing measured by deep-sequencing. The extent of tailing appeared to be quite limited and did not expend much further than 2 nt at most. This might be due to the timing at which the RNA was isolated after TDMD induction, and that was a bit too late to fully capture tailed miRNAs. Alternatively, it might also be explained by the experimental procedure used for the small RNA library preparation and by a sub-optimal size selection of the PCR products prior to their sequencing. Nevertheless, it seems that TUT1 knock-down had no effect on tailing, while DIS3L2 or DIS3L2 and TUT1 knock-down had a mild negative impact (Figure 5E).

Overexpression of a catalytic mutant of DIS3L2 impairs TDMD

To further prove the involvement of DIS3L2 in the mechanism, we also used another strategy consisting in the expression of a catalytically inactive mutant protein. Indeed, knockdown by siRNA will never achieve a complete removal of the targeted protein, and the remaining DIS3L2 might still be capable of degrading its substrate RNA. The mutant DIS3L2 (DIS3L2mut) was therefore generated by replacing two residues from the catalytic site (D391N, D392N), a mutation known to affect DIS3L2 activity without impairing its ability to bind RNA (34,46). We then overexpressed HA-DIS3L2, HA-DIS3L3mut or an empty plasmid (pcDNA) in HEK293 cells and induced TDMD by transfection of antimiRNA oligonucleotides.

We first verified that the mutation in DIS3L2 did not affect its expression (Figure 6A). The RNA samples were then analyzed by northern blot and we measured the fold change accumulation of the targeted miRNAs. If we were expecting that the over-accumulation of HA-DIS3L2 would either stimulate TDMD or induces a dominant negative effect, its overexpression did not alter the efficiency of the TDMD of miR-27 compared to the control (Figure 6B). This might be due to the fact that the activity of the endogenous DIS3L2 was already at saturating level. On the contrary, the overexpression of DIS3L2mut led to a stabilization of miR-27 isoforms most likely due to a dominant negative effect (Figure 6B). This effect was reproducibly observed and resulted on average in a mild but significant 1.5-fold increase in miR-27 level (Figure 6B). A similar stabilization was observed for miR-16, as transfection of DIS3L2mut impaired TDMD on this miRNA as well (Figure 6C). Thus, this result confirms the involvement of DIS3L2 in TDMD.

We have shown previously that MCMV degrades endogenous miR-27 via the viral transcript m169 (20). We therefore wanted to test whether DIS3L2 could also be involved in TDMD naturally induced by this virus. We infected cells transiently overexpressing the mouse (m)DIS3L2 or its catalytic mutant with MCMV and investigated the impact on miR-27 accumulation. Both HA-mDIS3L2 and HA-mDIS3L2mut were expressed at similar levels (Figure 6D). The levels of miR-27 (Figure 6E) and of the viral transcript m169 (Figure 6F) were monitored by qRT-PCR at different time points of infection and in three independent experiments. We first observed that the overexpression of mDIS3L2 does not globally impact miR-27 degradation compared to the control cells expressing the empty vector (Figure 6E, HA-mDIS3L2 versus pcDNA) as observed in human cells. We have only a slight enhancement of miR-27 degradation at 8 hpi, but this effect seems to disappear over time. On the contrary, we could observe a mild but significant stabilization of miR-27 in

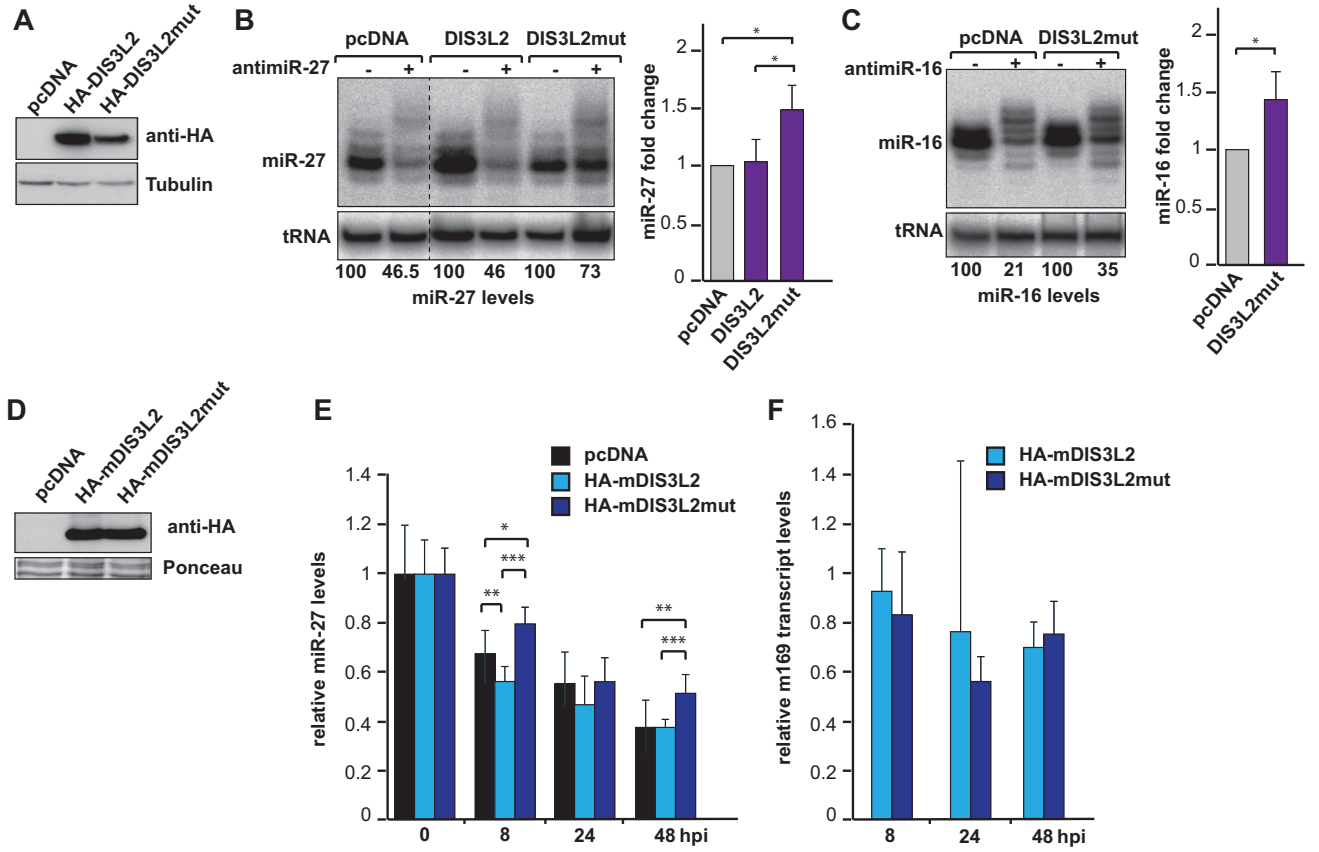

Figure 6. Overexpression of a catalytic mutant DIS3L2 inhibits TDMD. (**A**) Expression levels of HA-DIS3L2 and HA-DIS3L2mut in HEK293 cells by western blot. Tubulin serves as loading control. (**B**) miR-27 degradation is inhibited in HEK293 cells overexpressing the catalytically inactive version of DIS3L2 (DIS3L2mut) as shown by northern blot and after quantification. A dashed line indicates discontinuous lanes from the same gel. The bar graph shows the quantification of miR-27 fold change normalized to the empty vector (pcDNA), which was arbitrarily set to 1. Error bars indicate SDs (Student *t*-test: $*P < 0.05$, $n = 4$ biological replicates). (**C**) Same analysis as in (B), but for miR-16 degradation. (**D**) Expression levels of HA-mDIS3L2 and HA-mDIS3L2mut by western blot at 48 hpi. Ponceau S staining serves as loading control. (**E**) MiR-27 accumulation was monitored in mouse Hepa 1.6 cells during a time course of infection by the MCMV. Prior to infection, Hepa 1.6 cells were transfected with an empty plasmid (black), a plasmid coding for HA-mDIS3L2 (light blue) or HA-mDIS3L2mut (dark blue). The graph represents the relative miR-27 levels measured by qRT-PCR at 0, 8, 24 and 48 hpi. MiR-27 levels were normalized to those of miR-24 which serves as reference and arbitrarily set at 1 at 0 hpi for each condition. Error bars indicate SDs performed on three independent experiments. (Student *t*-test $*P < 0.05$, $**P < 0.01$, $***P < 0.001$; $n = 3$ biological replicates). (**F**) The level of the viral m169 transcript was measured by qRT-PCR in the samples used in (E) at 8, 24 and 48 hpi. The transcript coding for PPIA (Peptidylprolyl isomerase A) was used as reference. For each time point, the expression of m169 transcript in HA-mDIS3L2 and HA-mDIS3L2mut expressing cells was normalized to the samples containing the empty vector (pcDNA) which was set at 1.

cells expressing mDIS3L2mut compared to cells transfected with mDIS3L2 or empty pcDNA at 8 and 48 hpi (Figure 6E; HA-mDIS3L2mut versus HA-mDIS3L2 and HA-mDIS3L2mut versus pcDNA).

This stabilization was confirmed by northern blot (Supplementary Figure S7), which allowed us to visualize the different isomiRs, when the qRT-PCR only measures the abundance of the whole population of a given miRNA. Indeed, we could observe a stronger accumulation of the major isoforms of miR-27 in the presence of mDIS3L2mut at 48 hpi. To verify that this difference was not solely due to a defect in the infection efficiency, or in the production of the m169 transcript, we measured its accumulation by qRT-PCR in the experiments described above. This transcript starts to be expressed 2–3 h after infection (20), we thus arbitrarily decided to normalize its relative expression to the 8 hpi time point (and not 0 hpi) as we are sure that the signal detected is due to *de novo* synthesis of the m169 transcript. As shown in Figure 6F, we could appreciate that m169 transcript accumulates at similar level in cells expressing mDIS3L2 and mDIS3L2mut, no significant differences were observed. Thus, the differential accumulation of miR-27 in those cells are only due to the overexpression or not, of the inactive form of mDIS3L2. Taken together, these results indicate that DIS3L2 is also involved in TDMD when this mechanism is naturally induced by MCMV.

DISCUSSION

The stability and function of a miRNA is tightly linked to its interaction with other RNA molecules. Thus, it has been demonstrated that it was possible to prevent miRNA loading into the RISC by the use of artificial decoy or sponge RNAs (47). This observation was later confirmed to naturally exist with the discovery of circular RNAs that can titer

miRNAs such as miR-7 (48). Pairing with its RNA target will usually result in the stabilization of the miRNA (49), a mechanism that has been referred to as target-mediated miRNA protection. However, in other cases, the miRNA-target pairing can have the opposite effect and lead to the miRNA decay via the TDMD mechanism we studied here. In addition to the MCMV m169 transcript, the herpesvirus saimiri HSUR RNA can also target miR-27 for degradation (22). Similarly, the human cytomegalovirus encodes a bicistronic mRNA that triggers degradation of the cellular miRNA family miR-17/miR-20a (50). The molecular mechanisms at play in this particular mode of regulation have not been elucidated to date.

We confirmed here previous observations (23,24) that showed that TDMD is governed by the miRNA/target ratio as well as the degree of complementarity. Nevertheless, we also observed that TDMD operates in a non-cooperative manner in contrast to the classical miRNA-mediated target regulation. The cellular factors implicated in this particular miRNA decay mechanism were not known. Using a powerful proteomic approach, we characterized the protein complexes involved in miRNA tailing and trimming. Among the proteins we identified, we focused our analysis on two promising candidates: TUT1 and DIS3L2. As opposed to other TUTases, TUT1 had never been implicated in miRNA biogenesis. In addition, the most studied nucleotidyl transferases TUT4 and TUT7 act at the pri- or pre-miRNA level and never on the mature miRNA (51). In plants, the HESO1 protein has been implicated in uridylation of unmethylated miRNAs (52), but multiple terminal nucleotidyl transferases are required for this process to be fully active, including uncharacterized ones (53).

We did not manage to functionally implicate TUT1 in TDMD in our conditions, which might also indicate that this is a complicated synergistic process. Nonetheless, we could confirm the interaction between TUT1 and AGO2. We also show here that TUT1 interacts with tailed and trimmed isoforms of miR-27 only when TDMD is induced. In addition we also retrieved peptides for the SART3 protein in our mass spectrometry analysis (Supplementary Table S1). SART3, also known as Tip110, associates with U6 snRNP (54) and has been recently confirmed to interact directly with the *C. elegans* homolog of TUT1, USIP1, to participate in U6 snRNA recycling (55). Most importantly, it has been identified as a direct interactor of both AGO1 and AGO2 in HEK293 cells (56). Therefore, we have a link explaining how TUT1 could be recruited to AGO2 when TDMD is induced. This also confirms that both TUT1 and SART3 must interact with AGO proteins in the cytoplasm, as we could show for TUT1 and AGO2. Our results also indicate that TUT1 might not bind with the same efficiency to all miRNAs, since we could only retrieve it by mass spectrometry with antimiR-27 oligonucleotides, and its association with miR-16 seemed to be much weaker. Recently, it was demonstrated that TUT4 (ZCCHC11) and TUT7 (ZCCHC6) selectively mono-uridylate a subset of miRNAs harboring a specific motif (42). This observation strongly suggests that similar specificity for given miRNAs will govern the choice of TUTases recruited for the TDMD of other miRNAs. More work will be needed to definitely know which of the seven TUTases are involved in TDMD.

Our results are more conclusive when it comes to the other factor involved in TDMD. Indeed, we could functionally implicate DIS3L2 in this process both using knockdown followed by small RNA sequencing analysis and overexpression of a catalytic mutant showing a dominant negative effect. We did not manage to fully restore miRNA stability, which might either indicate that other enzymes could be implicated or that the high processivity of DIS3L2 makes it difficult to fully inactivate it be it by RNAi or overexpression of a dominant negative mutant.

It could also be that DIS3L2 would only be involved in the degradation of miR-27 presenting with additional U residues, as it was shown to preferentially target U-tailed substrates (46). The recently obtained crystal structure of DIS3L2 revealed that it could accommodate an artificial 12-mer oligonucleotides solely composed of Us (57), but our sequencing analysis revealed that the vast majority of miR-27 sequences appear to present with only few additional U residues at their 3′ extremity. In addition, a few sequences also had A residues. So, DIS3L2 might also be active on short RNAs presenting as little as two Us and/or As. This is in agreement with characterization of its *in vitro* activity, which indicates that the enzyme can target sequences with overhanging As (34).

Alternatively, miRNAs presenting A additions might be degraded by another enzyme. In that respect, miR-27a was shown to be adenylated by PAPD4 (TUT2), but this did not seem to affect its stability (58). Similarly, PAPD5 (TUT3) was also implicated in the adenylation of other miRNAs, such as miR-21, and in this case this resulted in its degradation by PARN (59). To verify that the enzymes that were studied in these two reports had no impact on miR-27a and b, we reanalyzed the small RNA libraries that were generated in these manuscripts, but did not find evidence of differential accumulation, or of an impact on the tailed and trimmed forms of these miRNAs (data not shown). Altogether our results therefore allowed us to identify DIS3L2 as the exoribonuclease involved in one specific mature miRNA degradation pathway.

ACCESSION NUMBERS

The sequencing data discussed in this publication have been deposited in NCBI's Gene Expression Omnibus (60) and are accessible through GEO Series accession number GSE73210 (http://www.ncbi.nlm.nih.gov/geo/query/acc.cgi?acc=GSE73210).

SUPPLEMENTARY DATA

Supplementary Data are available at NAR Online.

ACKNOWLEDGEMENTS

We are grateful to E. Izaurralde, N. Kim, G. Meister, A. Dziembowski and R. A Anderson for the gift of plasmids and antibodies. We also thank the IGBMC Microarray and Sequencing platform, member of the France Genomique program, for the sequencing of our libraries. We thank all members of the Pfeffer laboratory for discussion, and Sophie Cooke for technical assistance.

Author contributions: G.H., S.C., M.M. and O.T. performed the experiments. J.C., L.K. and P.H. performed the MS procedure, B.C.W.M. and J.C. analyzed the MS data and B.C.W.M. compiled all MS results. B.C.W.M. performed the deep sequencing analysis. G.H., S.C. and S.P. analyzed the data. G.H. and S.P. designed the experiments and wrote the paper. S.P. supervised the project.

FUNDING

This work was funded by the European Research Council [ERC starting grant ncRNAVIR 260767] and has been published under the framework of the LABEX: ANR-10-LABX-0036_NETRNA and benefits from a funding from the state managed by the French National Research Agency as part of the Investments for the future program. Funding for open access charge: European Research Council [ERC starting grant ncRNAVIR 260767].
Conflict of interest statement. None declared.

REFERENCES

1. Krol,J., Loedige,I. and Filipowicz,W. (2010) The widespread regulation of microRNA biogenesis, function and decay. *Nat. Rev. Genet.*, **11**, 597–610.
2. Ambros,V. (2003) MicroRNA pathways in flies and worms: growth, death, fat, stress, and timing. *Cell*, **113**, 673–676.
3. Zhang,B., Wang,Q. and Pan,X. (2007) MicroRNAs and their regulatory roles in animals and plants. *J. Cell. Physiol.*, **210**, 279–289.
4. Farazi,T.A., Hoell,J.I., Morozov,P. and Tuschl,T. (2013) MicroRNAs in human cancer. *Adv. Exp. Med. Biol.*, **774**, 1–20.
5. Chang,T.-C. and Mendell,J.T. (2007) microRNAs in vertebrate physiology and human disease. *Annu. Rev. Genomics Hum. Genet.*, **8**, 215–239.
6. Rybak,A., Fuchs,H., Smirnova,L., Brandt,C., Pohl,E.E., Nitsch,R. and Wulczyn,F.G. (2008) A feedback loop comprising lin-28 and let-7 controls pre-let-7 maturation during neural stem-cell commitment. *Nat. Cell Biol.*, **10**, 987–993.
7. Newman,M.A., Thomson,J.M. and Hammond,S.M. (2008) Lin-28 interaction with the Let-7 precursor loop mediates regulated microRNA processing. *RNA*, **14**, 1539–1549.
8. Viswanathan,S.R., Daley,G.Q. and Gregory,R.I. (2008) Selective blockade of microRNA processing by Lin28. *Science*, **320**, 97–100.
9. Heo,I., Joo,C., Kim,Y.-K., Ha,M., Yoon,M.-J., Cho,J., Yeom,K.-H., Han,J. and Kim,V.N. (2009) TUT4 in concert with Lin28 suppresses microRNA biogenesis through pre-microRNA uridylation. *Cell*, **138**, 696–708.
10. Heo,I., Joo,C., Cho,J., Ha,M., Han,J. and Kim,V.N. (2008) Lin28 mediates the terminal uridylation of let-7 precursor MicroRNA. *Mol. Cell*, **32**, 276–84.
11. Chang,H.-M., Triboulet,R., Thornton,J.E. and Gregory,R.I. (2013) A role for the Perlman syndrome exonuclease Dis3l2 in the Lin28-let-7 pathway. *Nature*, **497**, 244–248.
12. Liu,X., Zheng,Q., Vrettos,N., Maragkakis,M., Alexiou,P., Gregory,B.D. and Mourelatos,Z. (2014) A MicroRNA precursor surveillance system in quality control of MicroRNA synthesis. *Mol. Cell*, **55**, 868–879.
13. Baccarini,A., Chauhan,H., Gardner,T.J., Jayaprakash,A.D., Sachidanandam,R. and Brown,B.D. (2011) Kinetic analysis reveals the fate of a microRNA following target regulation in mammalian cells. *Curr. Biol.*, **21**, 369–376.
14. Gantier,M.P., McCoy,C.E., Rusinova,I., Saulep,D., Wang,D., Xu,D., Irving,A.T., Behlke,M.A., Hertzog,P.J., Mackay,F. *et al.* (2011) Analysis of microRNA turnover in mammalian cells following Dicer1 ablation. *Nucleic Acids Res.*, **39**, 5692–5703.
15. D'Ambrogio,A., Gu,W., Udagawa,T., Mello,C.C. and Richter,J.D. (2012) Specific miRNA stabilization by Gld2-catalyzed monoadenylation. *Cell Rep.*, **2**, 1537–1545.
16. Jones,M.R., Quinton,L.J., Blahna,M.T., Neilson,J.R., Fu,S., Ivanov,A.R., Wolf,D.A. and Mizgerd,J.P. (2009) Zcchc11-dependent uridylation of microRNA directs cytokine expression. *Nat. Cell Biol.*, **11**, 1157–1163.
17. Rüegger,S. and Großhans,H. (2012) MicroRNA turnover: when, how, and why. *Trends Biochem. Sci.*, **37**, 436–446.
18. Krol,J., Busskamp,V., Markiewicz,I., Stadler,M.B., Ribi,S., Richter,J., Duebel,J., Bicker,S., Fehling,H.J., Schubeler,D. *et al.* (2010) Characterizing light-regulated retinal microRNAs reveals rapid turnover as a common property of neuronal microRNAs. *Cell*, **141**, 618–631.
19. Rissland,O.S., Hong,S.-J. and Bartel,D.P. (2011) MicroRNA destabilization enables dynamic regulation of the miR-16 family in response to cell-cycle changes. *Mol. Cell*, **43**, 993–1004.
20. Marcinowski,L., Tanguy,M., Krmpotic,A., Rädle,B., Lisnić,V.J., Tuddenham,L., Chane-Woon-Ming,B., Ruzsics,Z., Erhard,F., Benkartek,C. *et al.* (2012) Degradation of cellular mir-27 by a novel, highly abundant viral transcript is important for efficient virus replication in vivo. *PLoS Pathog.*, **8**, e1002510.
21. Libri,V., Helwak,A., Miesen,P., Santhakumar,D., Borger,J.G., Kudla,G., Grey,F., Tollervey,D. and Buck,A.H. (2012) Murine cytomegalovirus encodes a miR-27 inhibitor disguised as a target. *Proc. Natl. Acad. Sci. U. S. A.*, **109**, 279–284.
22. Cazalla,D., Yario,T., Steitz,J.A. and Steitz,J. (2010) Down-regulation of a host microRNA by a Herpesvirus saimiri noncoding RNA. *Science*, **328**, 1563–1566.
23. Ameres,S.L., Horwich,M.D., Hung,J.H., Xu,J., Ghildiyal,M., Weng,Z. and Zamore,P.D. (2010) Target RNA-directed trimming and tailing of small silencing RNAs. *Science*, **328**, 1534–1539.
24. de la Mata,M., Gaidatzis,D., Vitanescu,M., Stadler,M.B., Wentzel,C., Scheiffele,P., Filipowicz,W. and Großhans,H. (2015) Potent degradation of neuronal miRNAs induced by highly complementary targets. *EMBO Rep.*, **16**, 500–511.
25. Ji,L. and Chen,X. (2012) Regulation of small RNA stability: methylation and beyond. *Cell Res.*, **22**, 624–636.
26. Li,J., Yang,Z., Yu,B., Liu,J. and Chen,X. (2005) Methylation Protects miRNAs and siRNAs from a 3′-End Uridylation Activity in Arabidopsis. *Curr Biol*, **15**, 1501–1507.
27. Lim,J., Ha,M., Chang,H., Kwon,S.C., Simanshu,D.K., Patel,D.J. and Kim,V.N. (2014) Uridylation by TUT4 and TUT7 Marks mRNA for Degradation. *Cell*, **159**, 1365–1376.
28. Buck,A.H., Perot,J., Chisholm,M.A., Kumar,D.S., Tuddenham,L., Cognat,V., Marcinowski,L., Dolken,L. and Pfeffer,S. (2010) Post-transcriptional regulation of miR-27 in murine cytomegalovirus infection. *RNA*, **16**, 307–315.
29. Broderick,J.A., Salomon,W.E., Ryder,S.P., Aronin,N. and Zamore,P.D. (2011) Argonaute protein identity and pairing geometry determine cooperativity in mammalian RNA silencing. *RNA*, **17**, 1858–1869.
30. Saetrom,P., Heale,B.S.E., Snøve,O., Aagaard,L., Alluin,J. and Rossi,J.J. (2007) Distance constraints between microRNA target sites dictate efficacy and cooperativity. *Nucleic Acids Res.*, **35**, 2333–2342.
31. Grimson,A., Farh,K.K.-H., Johnston,W.K., Garrett-Engele,P., Lim,L.P. and Bartel,D.P. (2007) MicroRNA targeting specificity in mammals: determinants beyond seed pairing. *Mol. Cell*, **27**, 91–105.
32. Flores-Jasso,C.F., Salomon,W.E. and Zamore,P.D. (2013) Rapid and specific purification of Argonaute-small RNA complexes from crude cell lysates. *RNA*, **19**, 271–279.
33. Malecki,M., Viegas,S.C., Carneiro,T., Golik,P., Dressaire,C., Ferreira,M.G. and Arraiano,C.M. (2013) The exoribonuclease Dis3L2 defines a novel eukaryotic RNA degradation pathway. *EMBO J.*, **32**, 1842–1854.
34. Lubas,M., Damgaard,C.K., Tomecki,R., Cysewski,D., Jensen,T.H. and Dziembowski,A. (2013) Exonuclease hDIS3L2 specifies an exosome-independent 3′-5′ degradation pathway of human cytoplasmic mRNA. *EMBO J.*, **32**, 1855–1868.
35. Wyman,S.K., Knouf,E.C., Parkin,R.K., Fritz,B.R., Lin,D.W., Dennis,L.M., Krouse,M.A., Webster,P.J. and Tewari,M. (2011) Post-transcriptional generation of miRNA variants by multiple nucleotidyl transferases contributes to miRNA transcriptome complexity. *Genome Res.*, **21**, 1450–1461.
36. Mellman,D.L. and Anderson,R.A. (2009) A novel gene expression pathway regulated by nuclear phosphoinositides. *Adv. Enzyme Regul.*, **49**, 11–28.
37. Mellman,D.L., Gonzales,M.L., Song,C., Barlow,C.A., Wang,P., Kendziorski,C. and Anderson,R.A. (2008) A PtdIns4, 5P2-regulated

nuclear poly(A) polymerase controls expression of select mRNAs. *Nature*, **451**, 1013–1017.
38. Trippe,R., Guschina,E., Hossbach,M., Urlaub,H., Lührmann,R. and Benecke,B.-J. (2006) Identification, cloning, and functional analysis of the human U6 snRNA-specific terminal uridylyl transferase. *RNA*, **12**, 1494–1504.
39. Pfaff,J. and Meister,G. (2013) Argonaute and GW182 proteins: an effective alliance in gene silencing. *Biochem. Soc. Trans.*, **41**, 855–860.
40. Nagarajan,V.K., Jones,C.I., Newbury,S.F. and Green,P.J. (2013) XRN 5′→3′ exoribonucleases: structure, mechanisms and functions. *Biochim. Biophys. Acta*, **1829**, 590–603.
41. Chlebowski,A., Lubas,M., Jensen,T.H. and Dziembowski,A. (2013) RNA decay machines: the exosome. *Biochim. Biophys. Acta*, **1829**, 552–560.
42. Thornton,J.E., Du,P., Jing,L., Sjekloca,L., Lin,S., Grossi,E., Sliz,P., Zon,L.I. and Gregory,R.I. (2015) Selective microRNA uridylation by Zcchc6 (TUT7) and Zcchc11 (TUT4). *Nucleic Acids Res.*, **42**, 11777–11791.
43. Mohan,N., Ap,S., Francis,N., Anderson,R. and Laishram,R.S. (2015) Phosphorylation regulates the Star-PAP-PIPKIα interaction and directs specificity toward mRNA targets. *Nucleic Acids Res.*, **43**, 7005–7020.
44. Ameyar-Zazoua,M., Rachez,C., Souidi,M., Robin,P., Fritsch,L., Young,R., Morozova,N., Fenouil,R., Descostes,N., Andrau,J.-C. *et al.* (2012) Argonaute proteins couple chromatin silencing to alternative splicing. *Nat. Struct. Mol. Biol.*, **19**, 998–1004.
45. Heo,I., Ha,M., Lim,J., Yoon,M.-J., Park,J.-E., Kwon,S.C., Chang,H. and Kim,V.N. (2012) Mono-uridylation of pre-microRNA as a key step in the biogenesis of group II let-7 microRNAs. *Cell*, **151**, 521–532.
46. Ustianenko,D., Hrossova,D., Potesil,D., Chalupnikova,K., Hrazdilova,K., Pachernik,J., Cetkovska,K., Uldrijan,S., Zdrahal,Z. and Vanacova,S. (2013) Mammalian DIS3L2 exoribonuclease targets the uridylated precursors of let-7 miRNAs. *RNA*, **19**, 1632–1638.
47. Ebert,M.S. and Sharp,P.A. (2010) Emerging roles for natural microRNA sponges. *Curr. Biol.*, **20**, R858–R861.
48. Hansen,T.B., Jensen,T.I., Clausen,B.H., Bramsen,J.B., Finsen,B., Damgaard,C.K. and Kjems,J. (2013) Natural RNA circles function as efficient microRNA sponges. *Nature*, **495**, 384–388.
49. Chatterjee,S., Fasler,M., Büssing,I. and Grosshans,H. (2011) Target-mediated protection of endogenous microRNAs in C. elegans. *Dev. Cell*, **20**, 388–396.
50. Lee,S., Song,J., Kim,S., Kim,J., Hong,Y., Kim,Y., Kim,D., Baek,D. and Ahn,K. (2013) Selective degradation of host MicroRNAs by an intergenic HCMV noncoding RNA accelerates virus production. *Cell Host Microbe*, **13**, 678–690.
51. Ha,M. and Kim,V.N. (2014) Regulation of microRNA biogenesis. *Nat. Rev. Mol. Cell Biol.*, **15**, 509–524.
52. Zhao,Y., Yu,Y., Zhai,J., Ramachandran,V., Dinh,T.T., Meyers,B.C., Mo,B. and Chen,X. (2012) The Arabidopsis nucleotidyl transferase HESO1 uridylates unmethylated small RNAs to trigger their degradation. *Curr. Biol.*, **22**, 689–694.
53. Wang,X., Zhang,S., Dou,Y., Zhang,C., Chen,X., Yu,B. and Ren,G. (2015) Synergistic and independent actions of multiple terminal nucleotidyl transferases in the 3′ tailing of small RNAs in Arabidopsis. *PLoS Genet.*, **11**, e1005091.
54. Licht,K., Medenbach,J., Luhrmann,R., Kambach,C. and Bindereif,A. (2008) 3′-cyclic phosphorylation of U6 snRNA leads to recruitment of recycling factor p110 through LSm proteins. *RNA*, **14**, 1532–1538.
55. Ruegger,S., Miki,T.S., Hess,D. and Grosshans,H. (2015) The ribonucleotidyl transferase USIP-1 acts with SART3 to promote U6 snRNA recycling. *Nucleic Acids Res.*, **43**, 3344–3357.
56. Hock,J., Weinmann,L., Ender,C., Rudel,S., Kremmer,E., Raabe,M., Urlaub,H. and Meister,G. (2007) Proteomic and functional analysis of Argonaute-containing mRNA-protein complexes in human cells. *EMBO Rep.*, **8**, 1052–1060.
57. Faehnle,C.R., Walleshauser,J. and Joshua-Tor,L. (2014) Mechanism of Dis3l2 substrate recognition in the Lin28-let-7 pathway. *Nature*, **514**, 252–256.
58. Burroughs,A.M., Ando,Y., de Hoon,M.J.L., Tomaru,Y., Nishibu,T., Ukekawa,R., Funakoshi,T., Kurokawa,T., Suzuki,H., Hayashizaki,Y. *et al.* (2010) A comprehensive survey of 3′ animal miRNA modification events and a possible role for 3′ adenylation in modulating miRNA targeting effectiveness. *Genome Res.*, **20**, 1398–1410.
59. Boele,J., Persson,H., Shin,J.W., Ishizu,Y., Newie,I.S., Søkilde,R., Hawkins,S.M., Coarfa,C., Ikeda,K., Takayama,K. *et al.* (2014) PAPD5-mediated 3′ adenylation and subsequent degradation of miR-21 is disrupted in proliferative disease. *Proc. Natl. Acad. Sci. U. S. A.*, **111**, 11467–11472.
60. Edgar,R., Domrachev,M. and Lash,A.E. (2002) Gene Expression Omnibus: NCBI gene expression and hybridization array data repository. *Nucleic Acids Res.*, **30**, 207–210.

Supplementary material for

Identification of factors involved in target RNA-directed microRNA degradation

Gabrielle Haas[#], Semih Cetin[#], Mélanie Messmer, Béatrice Chane-Woon-Ming, Olivier Terenzi, Johana Chicher, Lauriane Kuhn, Philippe Hammann and Sébastien Pfeffer*

Correspondence: s.pfeffer@ibmc-cnrs.unistra.fr

SUPPLEMENTARY FIGURE LEGENDS

Figure S1. Characterization of m169-miR-27 features triggering TDMD, related to Figure 1.

(A) Representation of m169 pairing with miR-27. Three mismatches were introduced in the seed region and are represented in red. (B) HeLa cells were transfected with increasing amounts of F-Luc, F-Luc-m169 or F-Luc-6xSH reporters and together with a plasmid coding for the *Renilla* luciferase (R-Luc) as transfection control, and subjected to luciferase assay. The F-Luc values were normalized to those of *Renilla* and arbitrarily set at 100 in cells expressing the F-Luc reporter. The graph represents mean values +/- standard deviations from three independent experiments. (C) Description of the miRNA isoforms. miR-27 and miR-16 serve as examples. The major isoforms (red) correspond to the isomiRs always detectable in absence of specific antimiRNAs. When TDMD is induced by transfection of antimiRNAs, tailed isoforms correspond to the bands of higher sizes than the major isoforms (purple) and the trimmed isomiRs to the shorter bands (blue).

Figure S2. Identification of the cellular factors involved in TDMD, related to Figure 2.

(A-C) Proteins identified by mass spectrometry using antimiR-27 (A), m169-like (B) and antimiR-16 (C) are represented in Venn diagrams including proteins found with the control-oligoribonucleotide or bound to the beads alone. For each section, the corresponding number of proteins validated with FDR<1% and the percentage (in parentheses) are mentioned.

Figure S3. Identification of the cellular factors involved in TDMD, related to Figure 3F.

AntimiR-27 and antimiR-16 were tested for their ability to pull-down several known exonucleases or the Terminal-Uridylyl-transferase (TUT)-7 by western blot. AntimiRNAs were transfected at 10 nM. A dashed line indicates discontinuous lanes but Input and IP fractions were systematically analyzed on a same gel.

Figure S4. TDMD is induced in the RISC complex by recruitment of TUT1 and DIS3L2, related to Figure 4.

(A) AGO2-associated tailed and trimmed isoforms of miR-27 were analyzed by northern blot. The Ctrl IP (with IgG) serves as negative control. A ladder made of 4 RNA oligos with sizes

of 16, 18, 21 and 24 nucleotides in length was loaded to evaluate the sizes of miR-27 isoforms.
(B) AGO2-associated tailed and trimmed isoforms of miR-16 by RNA-immunoprecipitation. (C) AGO2-associated tailed and trimmed isoforms of miR-27 after induction of TDMD by the F-Luc-3xSH reporter. The 3xSH m169mut version serves as negative control for tailing-trimming. Asterisks highlight tailed isoforms. (D) Comparative immunoprecipitation of miR-27 isoforms bound to DIS3L2mut and DIS3L2. MBP serves as negative control. A dashed line indicates discontinuous lanes but Input and IP fractions were systematically analyzed on a same gel (B, C). (E) Immunoprecipitation (anti-GFP) of miR-27 from cells expressing GFP-TUT2, GFP-TUT4 or GFP-TUT7 in presence or absence of antimiR-27. tRNA is used as loading control.

Figure S5. Effect of TUT1 and DIS3L2 knockdowns on TDMD, related to Figure 5.
(A) The efficiency of miR-27 TDMD in cells depleted from TUT1 (siTUT1), DIS3L2 (siDIS3L2) or both was quantified by northern blot analysis. A representative experiment is depicted on the left, while the right panel depicts the quantification of miR-27 accumulation after normalization to tRNA. It was arbitrarily set at 100 in absence of antimiR-27 for each condition. Error bars indicate SDs (n = 3 independent experiments). (B) Left: Analysis of miR-16 TDMD by northern blot as described in (A). Right: the graph represents miR-16 levels from three independent experiments. miR-16 accumulation is represented normalized to tRNA and set at 100 in absence of antimiR-16 for each condition. Error bars indicate SDs. (C) Distribution in percentage of miR-27a tailed and trimmed isoforms as assessed by small RNA deep-sequencing of cells treated with the indicated siRNA and antimiRNA oligonucleotides. The "0" indicates the wild-type (WT) isoform of 21 nt. The sum of all trimmed (≤-2) or tailed (≥+2) sequences is indicated.

Figure S6. Functional implication of DIS3L2 in miRNA degradation, related to Figure 5.
(A) Representative examples of the most abundant miR-27b isoforms detected in one of the libraries treated with the control siRNA and antimiR-67 or antimiR-27. Tailed nucleotides are highlighted in purple. The relative abundance of each isoform (%) is given before (antimiR-67) or after (antimiR-27) TDMD induction by the transfection of the corresponding antimiRNAs. The red color indicates a decrease and the green an increase in abundance of the respective sequence. (B) and (C) Distribution in percentage of miR-27b tailed and trimmed

isoforms as assessed by small RNAs deep-sequencing of cells treated with the indicated siRNA and antimiRNA oligonucleotides. The “0” indicates the wild-type (WT) isoform of 21 nt. The sum of all trimmed (≤-2) or tailed (≥+2) sequences is indicated.

Figure S7. DIS3L2 is involved in TDMD induced during MCMV infection, related to Figure 6.

(A) Representative northern blot of miR-27 levels in Hepa 1.6 cells overexpressing HA-mDIS3L2, HA-mDIS3L2mut or an empty plasmid (pcDNA) during a time course of MCVM infection. Samples are the same as in Figure 6D and 6E. tRNA serves as loading control. Time points are indicated in hours post-infection (hpi).

Table S1. Short list of the most frequent proteins associated with antimiRNAs and identified by nanoLC-MS/MS, related to Figure 2.

This table summarizes the proteins found in at least 3 independent experiments for antimiR-27 (5 experiments in total), antimiR-16 (4 experiments) and the m169-like oligoribonucleotides (4 experiments) and absent in all their respective negative controls (beads alone and antimiR-67). For each protein, both their gene name and accession number are mentioned.

* An exception is made for DIS3L2 in the m169 samples as only 3 of the 4 experiments allowed to trigger TDMD and the protein was found twice in these 3 samples.

Gene names	Accession number	antimiR-27	antimiR-16	m169-like
AGO1	Q9UL18	***yes***	*no*	***yes***
AGO2	Q9UKV8	***yes***	***yes***	***yes***
AGO3	Q9H9G7	*no*	*no*	***yes***
DIS3L2	Q8IYB7	***yes***	***yes***	***yes****
FUBP3	Q96I24	***yes***	***yes***	***yes***
SSB	P05455	***yes***	*no*	*no*
MEPCE	Q7L2J0	***yes***	*no*	*no*
MYH10	P35580	***yes***	*no*	*no*
NONO	Q15233	***yes***	*no*	*no*
RBM4	Q9BWF3	***yes***	*no*	***yes***
SART3	Q15020	***yes***	*no*	*no*
SND1	Q7KZF4	*no*	*no*	***yes***
TUT1	Q9H6E5	***yes***	*no*	*no*
ZFP36L2	P47974	*no*	*no*	***yes***
TNRC6B	Q9UPQ9	*no*	*no*	***yes***
XRN2	Q9H0D6	*no*	*no*	***yes***
U2AF1	Q01081	***yes***	*no*	*no*
U2AF2	P26368	***yes***	*no*	*no*

Table S2. List of the oligonucleotides used in this study.

Nucleotides generating a mutation or modifying a pairing are in bold; Locked Nucleic Acids are underlined; 2'O-methyl nucleotides are preceded by a "m". F, forward; R, reverse.

Cloning primers (provided by Sigma-Aldrich)

Name	Type	Sequence (5' to 3')
HA-TUT1-F	DNA	GGAATTCAATGGCGGCGGTGGATTCGGATG
HA-TUT1-R	DNA	GAAAAAAGCGGCCGCTCACTTGAGATGTCGAATTGCTTG
HA-DIS3L2-F	DNA	CGGGATCCATGAGCCATCCTGACTACAGAATG
HA-DIS3L2-R	DNA	GAAAAAAGCGGCCGCTCAGCTGGTGCTTGAGTCCTCG
HA-AGO2-F	DNA	GGAATTCAATGTACTCGGGAGCCGGCC
HA-AGO2-R	DNA	GAAAAAAGCGGCCGCTCAAGCAAAGTACATGGTGCG
GFP-TUT1-F	DNA	GAAGATCTTAATGGCGGCGGTGGATTCGGATG
GFP-TUT1-R	DNA	GGAATTCTCACTTGAGATGTCGAATTGCTTG
GFP-DIS3L2-F	DNA	GAAGATCTTAATGAGCCATCCTGACTACAGAATG
GFP-DIS3L2-R	DNA	CGGGATCCTCAGCTGGTGCTTGAGTCCTCG
HA-mTUT1-F	DNA	GGAATTCAATGGCGGCGGTGGATTCGG
HA-mTUT1-R	DNA	GAAAAAAGCGGCCGCTCACTTGAGGAGATTTTTAAGTG
HA-mDIS3L2-F	DNA	GGAATTCAATGAACCATCCTGACTACAAGC
HA-mDIS3L2-R	DNA	GAAAAAAGCGGCCGCTCAGTCCTCAGGCTCCTCATC
GFP-mTUT1-F	DNA	GAAGATCTTAATGGCGGCGGTGGATTCGG
GFP-mTUT1-R	DNA	GGAATTCTCACTTGAGGAGATTTTTAAGTG
GFP-mDIS3L2-F	DNA	GGAATTCATGAACCATCCTGACTACAAGC
GFP-mDIS3L2-R	DNA	CGGGGTACCTCAGTCCTCAGGCTCCTCATC
HA-mAGO2-F	DNA	GGAATTCAATGTACTCGGGAGCCGGCCC
HA-mAGO2-R	DNA	GAAAAAAGCGGCCGCTCAAGCAAAGTACATGGTGC
GFP-TUT2-F	DNA	GGAATTCATGTTCCCAAACTCAATTTTGG
GFP-TUT2-R	DNA	CGGGATCCTTATCTTTTCAGGACAGCAGC
GFP-TUT4-F	DNA	GCGTCGACCATGGAAGAGTCTAAAACCTTAAAAAG
GFP-TUT4-R	DNA	CCATTTAAATTTACTCCGACACGTTTCCTCTTG

GFP-TUT7-F	DNA	GCTCGAGAATGGGAGATACAGCAAAACC
GFP-TUT7-R	DNA	CGGGATCCTCATGATTCCTGCTGGGTCC

Mutagenesis primers (provided by Sigma-Aldrich)

Name	Type	Sequence (5' to 3')
DIS3L2mut-F	DNA	ACCCATCAACCGCCCGAGACCTC**A**AT**A**ATGCCCTCTCCTGCAAG CCAC
DIS3L2mut-R	DNA	GTGGCTTGCAGGAGAGGGCAT**T**AT**T**GAGGTCTCGGGCGGTTGA TGGGT
mDIS3L2mut-F	DNA	GTAAATAGCTTTGATGTTCATGGCTGT**GCC**CTC**GCC**CTCTTCTT GGACATGGGTGATATGG
mDIS3L2mut-R	DNA	CCATATCACCCATGTCCAAGAAGAG**GGC**GAG**GGC**ACAGCCAT GAACATCAAAGCTATTTAC
pcDNA3.1-HA-F	DNA	GTTTAAACTTAAGCTTGGTACCGAG**GCCACCATGTACCCATAC GATGTTCCAGATTACGCT**CTCGGATCCACTAGTCCAGTGTG
pcDNA3.1-HA-R	DNA	CACACTGGACTAGTGGATCCGAGAGCGTAATCTGGAACATCGT ATGGGTACATGGTGGCCTCGGTACCAAGCTTAAGTTTAAAC

Northern probes (provided by Eurogentec)

Name	Type	Sequence (5' to 3')
miR-27	DNA (LNA)	GCGGAACTTAGCCACTGTGAA
miR-16	DNA (LNA)	CGCCAATATTTACGTGCTGCTA
tRNA Asp	DNA	CCGGTCTCCCGCGTGACAGGCGGGGATACTA
U6	DNA	GCAGGGGCCATGCTAATCTTCTCTGTATCG

Biotinylated oligoribonucleotides (provided by IDT)

Name	Type	Sequence (5' to 3')
ASmir27-space3Bio	RNA	mGmCmGmGmAmAmCmUmUmAmGmCmCmAmCmUmGmUmGmA mA/iSp9/3Bio
ASmir67Ce-space3Bio	RNA	mUmCmAmCmAmAmCmCmUmCmCmUmAmGmAmAmAmGmAmG mUmAmGmA/iSp9/3Bio/
m169-space3Bio	RNA	mGmCmGmGmAmAmUmAmAmUmAmAmGmCmUmGmUmGmAmA /iSp9/3Bio/
ASmir16-space3Bio	RNA	mCmGmCmCmAmAmUmAmUmUmUmAmCmGmUmGmCmUmGmC mUmA/iSp9/3Bio/

AntimiRNAs (provided by IDT)

Name	Type	Sequence (5' to 3')
antimiR-27	RNA	mGmCmGmGmAmAmCmUmUmAmGmCmCmAmCmUmGmUmGmA mA
antimiR-16	RNA	mCmGmCmCmAmAmUmAmUmUmUmAmCmGmUmGmCmUmGmC mUmA
antimiR-67Ce	RNA	mUmCmAmCmAmAmCmCmUmCmCmUmAmGmAmAmAmGmAmG mUmAmGmA
m169-like	RNA	mGmCmGmGmAmAmUmAmAmUmAmAmGmCmUmGmUmGmAmA
Mutant 1	RNA	**mU**mCmGmGmAmAmUmAmAmUmAmAmGmCmUmGmUmGmAm A

Mutant 2	RNA	**mUmA**mGmGmAmAmUmAmAmUmAmAmGmCmUmGmUmGmAmA
Mutant 3	RNA	**mUmAmU**mGmAmAmUmAmAmUmAmAmGmCmUmGmUmGmAmA
Mutant 4	RNA	**mUmAmUmU**mAmAmUmAmAmUmAmAmGmCmUmGmUmGmAmA
Bulge +	RNA	mGmCmGmGmAmAmU**mU**mAmUmAmAmGmCmUmGmUmGmAmA

siRNA sequences (provided by Sigma-Aldrich)

Name	Type	Sequence (5' to 3') sense strand
siRLuc (siCtrl)	siRNA	CACAUCGAGCCCGUGGCUA
siTUT1-1	siRNA	GUGUGUUUGUCAGUGGCUU
siDIS3L2-1	siRNA	GGGGAUCUGGUGGUCGUGAA

qRT-PCR primers (provided by Sigma-Aldrich)

Name	Type	Sequence (5' to 3')
miR-27	DNA	TTCACAGTGGCTAAGTTCCGC
miR-24	DNA	TGGCTCAGTTCAGCAGGAACAG
PPIA-F	DNA	GCGGCAGGTCCATCTACG
PPIA-R	DNA	GCCATCCAGCCATTCAGTC
m169-F	DNA	ATCTTCTTCGGCGTTAGCGA
m169-R	DNA	TGAGGTCCAGGTCGTGTGA

SUPPLEMENTAL EXPERIMENTAL PROCEDURES

Mass spectrometry procedure and analysis

In-solution digestion was carried out directly on the magnetic beads. Straight before digestion, the beads were washed twice in 25 mM ammonium bicarbonate using a magnetic stand to retain the beads. Out of the stand, proteins were reduced with 5 mM DTT for 6 min at 95°C, alkylated with 10 mM iodoacetamide for 30 min in the dark and digested overnight with 100 ng of modified sequencing-grade trypsin in 25 mM ammonium bicarbonate.

Dried tryptic peptides were re-suspended in 15 μL of water containing 0.1% FA (solvent A) before analysis on a NanoLC-2DPlus system (with nanoFlex ChiP module; Eksigent, ABSciex, Concord, Ontario, Canada) coupled to a TripleTOF 5600 mass spectrometer (ABSciex) operating in high-sensitivity positive mode. Sample acquisitions were performed using a "trap and elute" configuration on the nanoFlex System using C-18 precolumn (300 μm ID x 5 mm ChromXP; Eksigent) and column (75 μm ID x 15 cm ChromXP; Eksigent) Peptides were eluted with a 60 min 5%-40% gradient of solvent B (0.1% formic acid in ACN). The TripleTOF 5600 was operated with Analyst software (version 1.5, ABSciex) in data-dependent acquisition mode with survey MS scans acquired in the 400-1250 m/z range and up to 20 of the most intense multiply charged ions (2+ to 5+) selected for CID fragmentation. To prevent carry-over due to stationary phase memory, 2 consecutive washing runs were performed after each sample injection. Data were searched against the complete Human proteome set from the UniProt database (released 2013/01/09; 141168 sequences) with an added decoy database. Mascot algorithm (version 2.2, Matrix Science, London, UK) was used through the ProteinScape package (Bruker, v3.1) which validated protein identifications with a FDR < 1%.

Small RNA libraries and sequencing

RNA quality was assessed by Agilent 2100 Bioanalyzer (Agilent), and samples with an RNA integrity number (a measure of RNA quality) higher than 8 were used for the study. We followed Illumina's protocol (Truseq small RNA, # 15004197 Rev. C) to generate small RNA libraries directly from total RNAs, suitable for subsequent high throughput sequencing. The protocol takes advantage of the natural structure common to most microRNA molecules that have a 3′ hydroxyl group resulting from enzymatic cleavage by Dicer or other RNA processing enzymes. Briefly, in the first step, RNA adapters were sequentially ligated to each

end of the RNA, first the 3′ RNA adapter that is specifically modified to target microRNAs and other small RNAs, then the 5′ RNA adapter. Small RNA ligated with 3′ and 5′ adapters were reverse transcribed and PCR amplified (30 sec at 98°C; [10 sec at 98°C, 30 sec at 60°C, 15 sec at 72°C] x 13 cycles; 10 min at 72°C) to create cDNA constructs. This process selectively enriched those fragments that have adapter molecules on both ends. The last step was an acrylamide gel purification of the 140-150 nt amplified cDNA constructs (corresponding to cDNA inserts from small RNA + 120 nt from the adapters). Small RNA libraries were checked for quality and quantified using 2100 Bioanalyzer (Agilent). The libraries were loaded in the flowcell at 8 pM concentration and clusters were generated using the Cbot and sequenced on Hiseq 2500 as single-end 50 bases reads following Illumina's instructions.

Bioinformatics analysis of deep sequencing data

Short sequences generated by the Illumina instrument were first preprocessed using the Dustmasker program (1) and FASTX-Toolkit (http://hannonlab.cshl.edu/fastx_toolkit) to filter out low complexity reads and remove instances of the 3' adapter, respectively. Before further analysis, reads corresponding to the exogenous siRNA and antimiR sequences were also excluded. Remaining reads of at least 15 nt in length were then mapped to the human genome (assembly version hg19 – UCSC repository), using Bowtie 1.0.0 (2), by permitting up to 1 mismatch in the first 15 nucleotides of each read. Only alignments from the lowest mismatch-stratum were recorded provided they didn't exceed a total number of 9 mismatches and reads that could map to more than 50 loci were discarded. From there, all known human miRNAs (miRBase v.20 (3)) were annotated using BEDTools 2.16.2 (4) by comparing their genomic coordinates to those of the aligned reads, and by keeping reads with at least 80 % of their length inside the genomic feature. By doing so, we were able to inventory and quantify all miRNA isoforms. During the quantification process, multiple mapped reads were weighted by the number of mapping sites in miRNAs and the annotations of miR-27a-3p and miR-27b-3p were manually curated to redistribute the few sequences that were initially mis-attributed between the two (most probably due to the loose constraints applied on the 3' read ends during the mapping step).

To further characterize the TDMD mechanism of miR-27a and b, only isoforms corresponding to the wild-type (WT) mature sequence (as defined in miRBase) of these miRNAs, as well as the ones presenting with shifted 3' extremities were taken into account,

providing that they showed a 5' genome matched component and an optional 3' tail (addition of non-templated nucleotides). These sequences were classified as: WT, trimming, tailing, trimming+tailing, cleavageshift, and cleavageshift+tailing. For the representation of histograms shown in Figure 5C and S5C, we determined the number of sequences presenting with a tail of +1, …, +4 nucleotides as well as the sequences presenting with a trimming of -1, -2, …, -6 nucleotides. We then calculated the percentage of each category. This allowed us to see that the predominant isoforms in all libraries were the WT (i.e. 0), and the -1, and +1 sequences. We therefore took into account for our further calculation only sequences that were tailed or trimmed by more than 2 nucleotides. We then computed a tailing ratio by dividing all tailed sequences (tailing, trimming+tailing, cleavageshift+tailing) by the number of WT sequences, and a trimming ratio by dividing all trimmed sequences (trimming and trimming+tailing) by the number of WT sequences for each isoform. We then calculated the fold change of the tailing ratio of cells transfected with the antimiR-27 to the one of cells transfected with the control antimiR-67. This fold change was then normalized to the control siRNA (against R-Luc) condition, which was set to 1. The same was done for the trimming ratio.

Supplementary references

1. Morgulis,A., Gertz,E.M., Schäffer,A.A. and Agarwala,R. (2006) A fast and symmetric DUST implementation to mask low-complexity DNA sequences. *J. Comput. Biol. J. Comput. Mol. Cell Biol.*, 13, 1028–1040.

2. Langmead,B., Trapnell,C., Pop,M. and Salzberg,S.L. (2009) Ultrafast and memory-efficient alignment of short DNA sequences to the human genome. *Genome Biol.*, 10, R25.

3. Kozomara,A. and Griffiths-Jones,S. (2014) miRBase: annotating high confidence microRNAs using deep sequencing data. *Nucleic Acids Res.*, 42, D68–73.

4. Quinlan,A.R. and Hall,I.M. (2010) BEDTools: a flexible suite of utilities for comparing genomic features. *Bioinforma. Oxf. Engl.*, 26, 841–842.

Figure S1

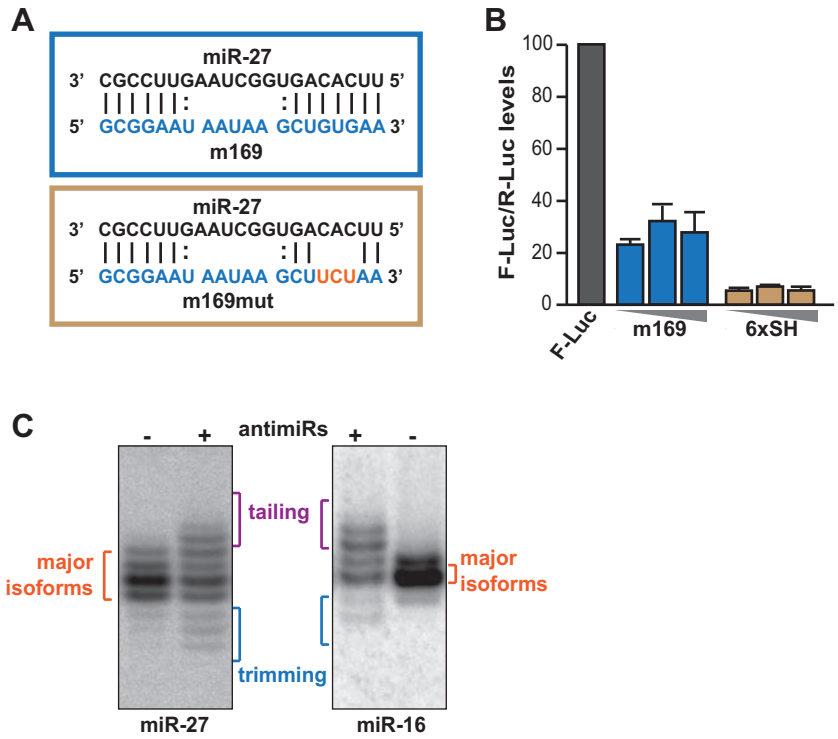
A
miR-27
3' CGCCUUGAAUCGGUGACACUU 5'
5' GCGGAAU AAUAA GCUGUGAA 3'
m169
miR-27
3' CGCCUUGAAUCGGUGACACUU 5'
5' GCGGAAU AAUAA GCUUCUAA 3'
m169mut
B
F-Luc/R-Luc levels
100
80
60
40
20
0
F-Luc
m169
6xSH
C
antimiRs
-
+
+
-
tailing
major isoforms
trimming
major isoforms
miR-27
miR-16

Figure S2


A
antimiR-27 (R1 [7.5 nM])
antimiR-27
73 (9.72%)
27 (3.6%)
56 (7.46%)
398 (53%)
64 (8.52%)
85 (11.32%)
48 (6.39%)
beads
control
antimiR-27 (R2 [7.5 nM])
antimiR-27
60 (13.48%)
80 (17.98%)
15 (3.37%)
179 (40.22%)
20 (4.49%)
11 (2.47%)
80 (17.98%)
beads
control
B
m169-like (R1 [250 nM])
m169-like
75 (9.96%)
27 (3.59%)
49 (6.51%)
381 (50.6%)
64 (8.5%)
92 (12.22%)
65 (8.63%)
beads
control
m169-like (R2 [7.5 nM])
m169-like
42 (9.84%)
79 (18.5%)
10 (2.34%)
165 (38.64%)
25 (5.85%)
81 (18.97%)
25 (5.85%)
beads
control
C
antimiR-16 (R1 [3 nM])
antimiR-16
50 (6.87%)
33 (4.53%)
59 (8.1%)
405 (55.63%)
58 (7.97%)
82 (11.26%)
41 (5.63%)
beads
control
antimiR-16 (R2 [7.5 nM])
antimiR-16
60 (13.48%)
92 (20.67%)
14 (3.15%)
175 (39.33%)
21 (4.72%)
68 (15.28%)
15 (3.37%)
beads
control

Figure S3

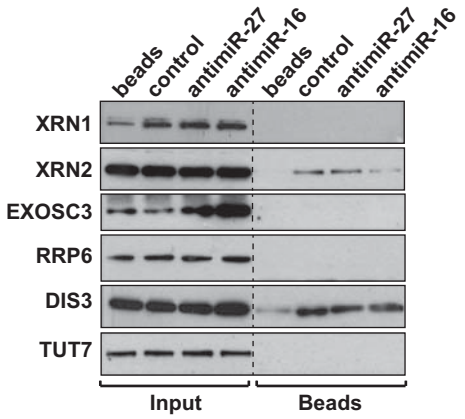
beads
control
antimiR-27
antimiR-16
beads
control
antimiR-27
antimiR-16
XRN1
XRN2
EXOSC3
RRP6
DIS3
TUT7
Input
Beads

Figure S4

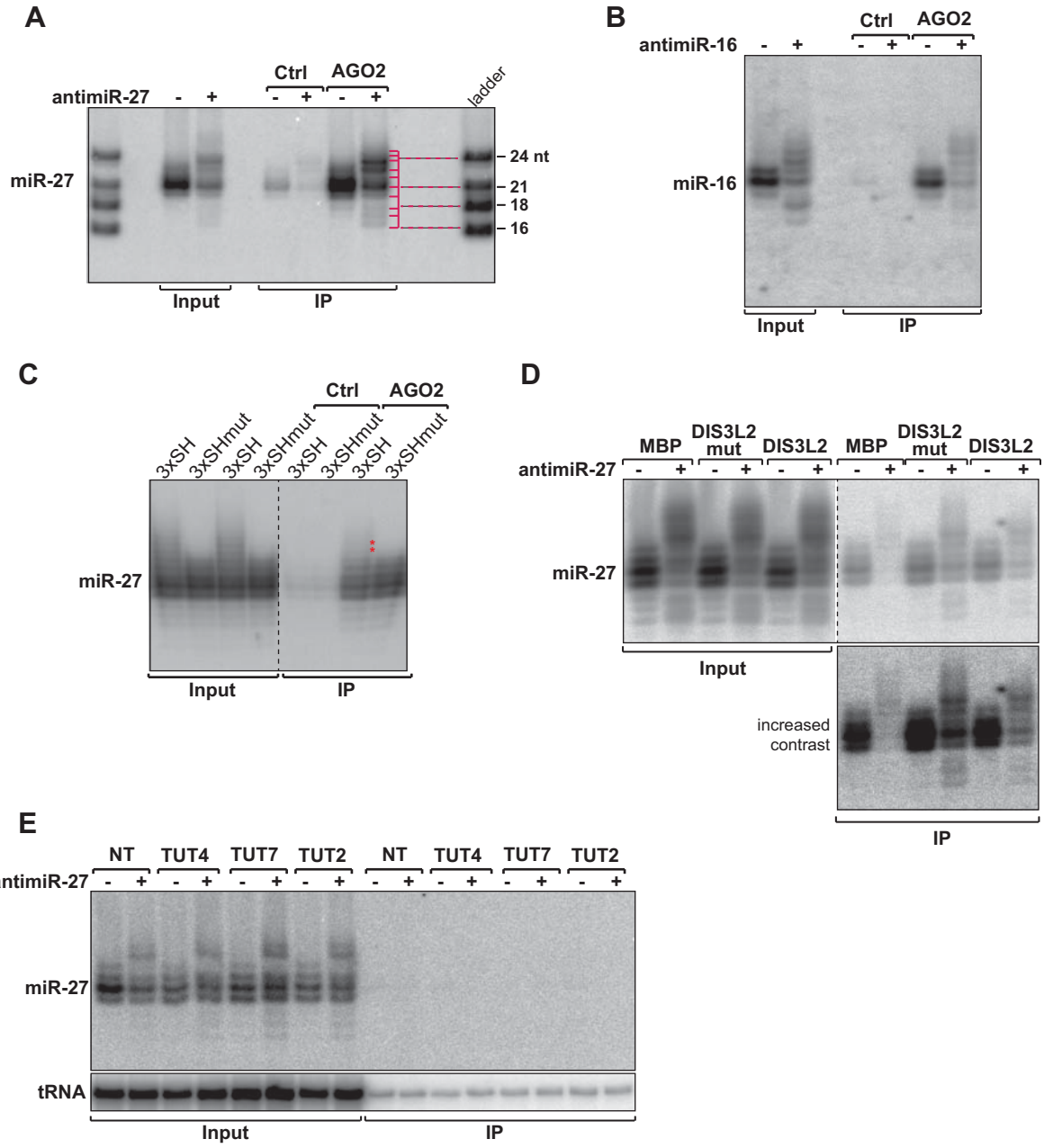
A
antimiR-27
Ctrl
AGO2
ladder
miR-27
24 nt
21
18
16
Input
IP
B
antimiR-16
Ctrl
AGO2
miR-16
Input
IP
C
Ctrl
AGO2
3xSH
3xSHmut
miR-27
Input
IP
D
MBP
DIS3L2 mut
DIS3L2
antimiR-27
miR-27
Input
increased contrast
IP
E
NT
TUT4
TUT7
TUT2
antimiR-27
miR-27
tRNA
Input
IP

Figure S5

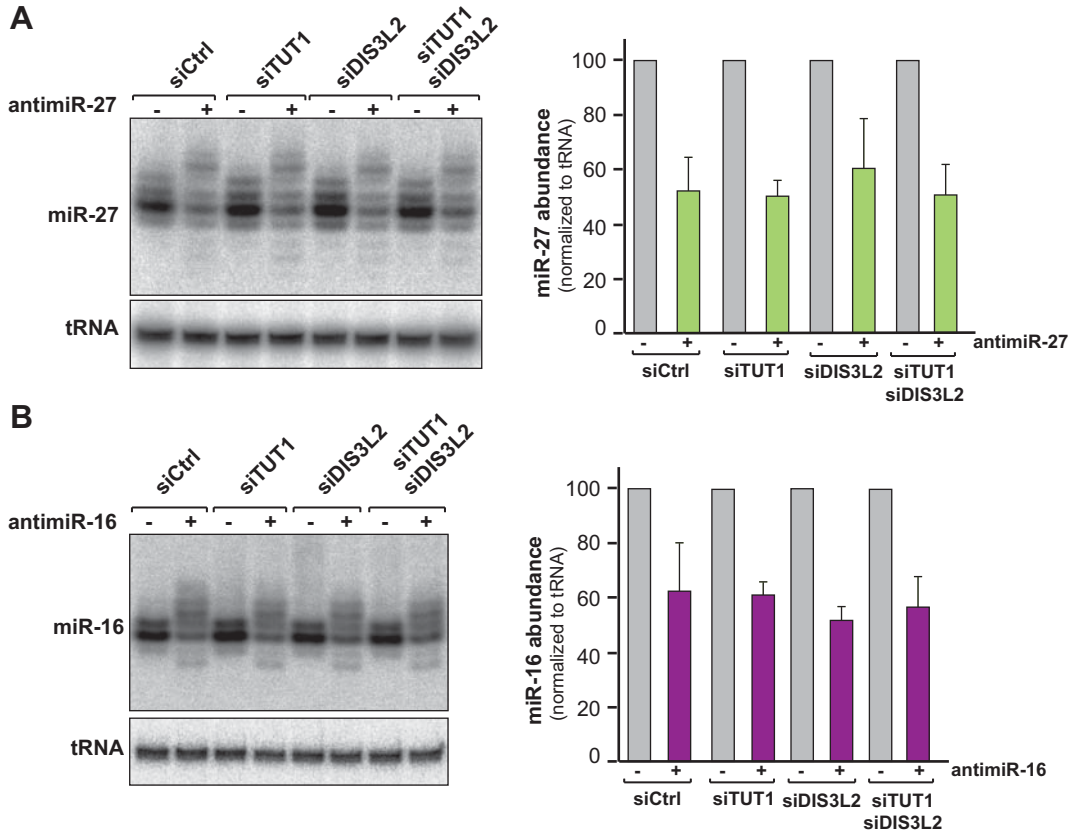
A
siCtrl
siTUT1
siDIS3L2
siTUT1 siDIS3L2
antimiR-27
miR-27
tRNA
miR-27 abundance (normalized to tRNA)
antimiR-27
B
antimiR-16
miR-16
miR-16 abundance (normalized to tRNA)
antimiR-16

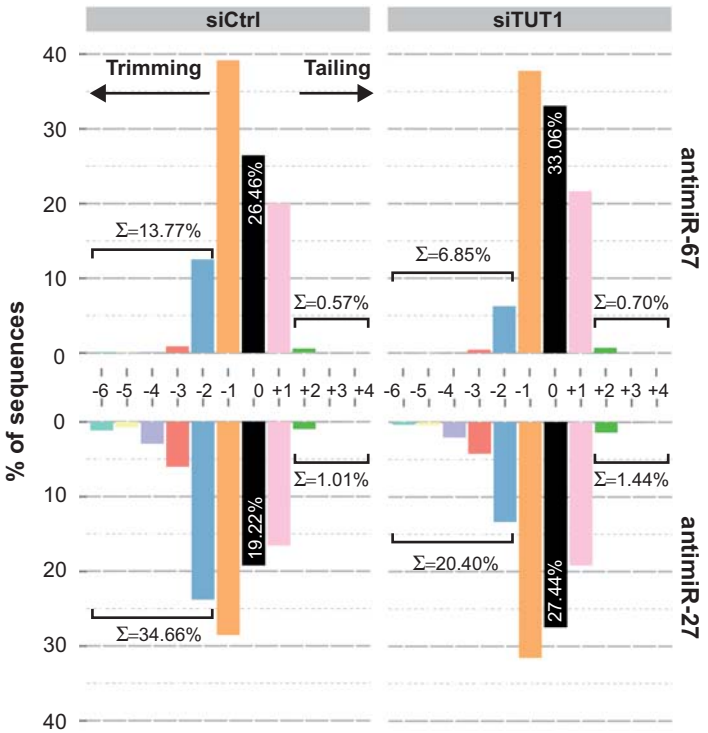
C miR-27a
siCtrl
siTUT1
Trimming
Tailing
% of sequences
Σ=13.77%
26.46%
Σ=0.57%
Σ=34.66%
19.22%
Σ=1.01%
Σ=6.85%
33.06%
Σ=0.70%
Σ=20.40%
27.44%
Σ=1.44%
antimiR-67
antimiR-27

Figure S6

A

miR-27b (5'-3')	antimiR-67 (%)	antimiR-27 (%)
UUCACAGUGGCUAAGUUCUGCA	1.68	0.96
UUCACAGUGGCUAAGUUCUGC	46.18	44.18
UUCACAGUGGCUAAGUUCUGC U	8.09	6.56
UUCACAGUGGCUAAGUUCUG	34.49	33.38
UUCACAGUGGCUAAGUUCUG U	0.64	0.54
UUCACAGUGGCUAAGUUC	0.21	1.43
UUCACAGUGGCUAAGUUC U	0.60	1.14

B miR-27b

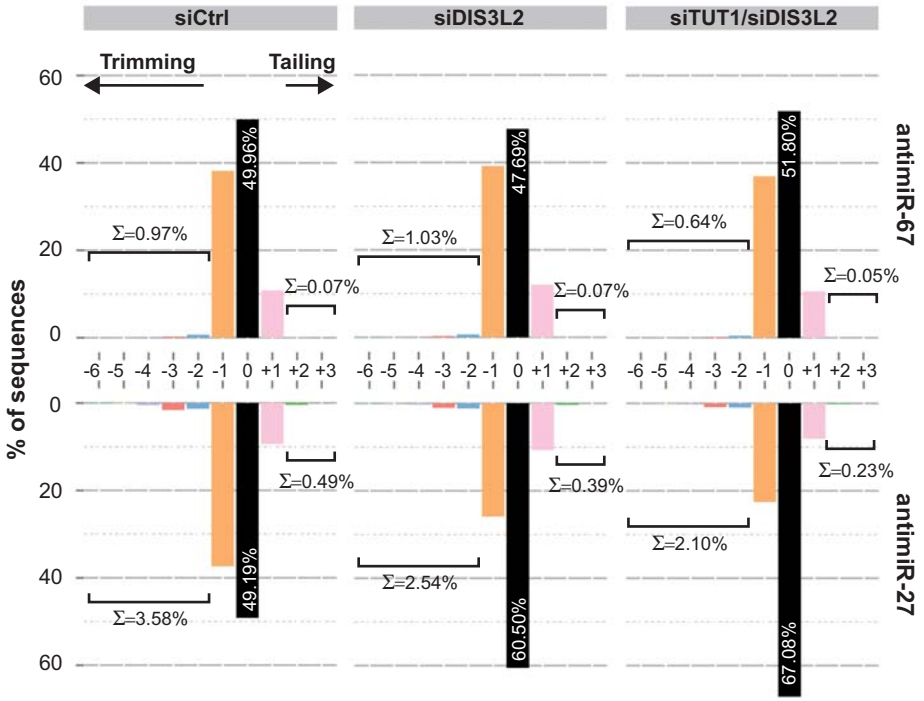

C miR-27b

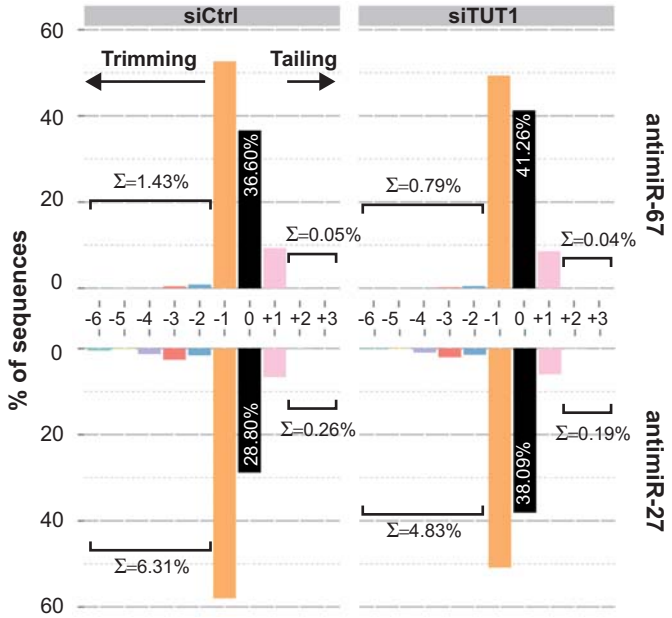

Figure S7

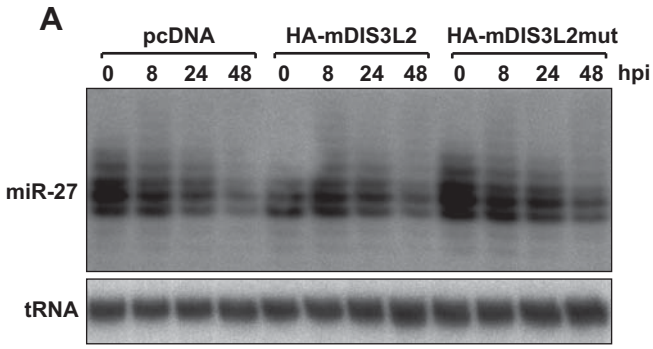
A
pcDNA
HA-mDIS3L2
HA-mDIS3L2mut
0 8 24 48 0 8 24 48 0 8 24 48 hpi
miR-27
tRNA

2. Identification of Argonaute 2 partners by proximity dependent labeling

2.1 Aim

In this chapter, the main goal is to find whether the interactome of the AGO2 protein changes during viral infection, more specifically, we looked at the impact of MCMV infection in fibroblasts. Understanding the networks of molecular interactions of a given molecule, in our case AGO2, can broaden our view of host-pathogen interactions at the level of miRNA function. In order to do so, I have used proximity labelling by a promiscuous biotin ligase called BirA, which allows direct labelling of interacting proteins with biotin followed by affinity capture of labelled proteins and mass spectrometry analysis. Three major interaction networks implicating proteins exist; protein-protein, protein-DNA and protein-RNA. As here, we are interested by protein partners of AGO2, I will briefly present other methods of identification of protein-protein interactions that can be used for this kind of study and discuss their respective advantages and disadvantages.

2.2 Large scale protein interaction mapping techniques

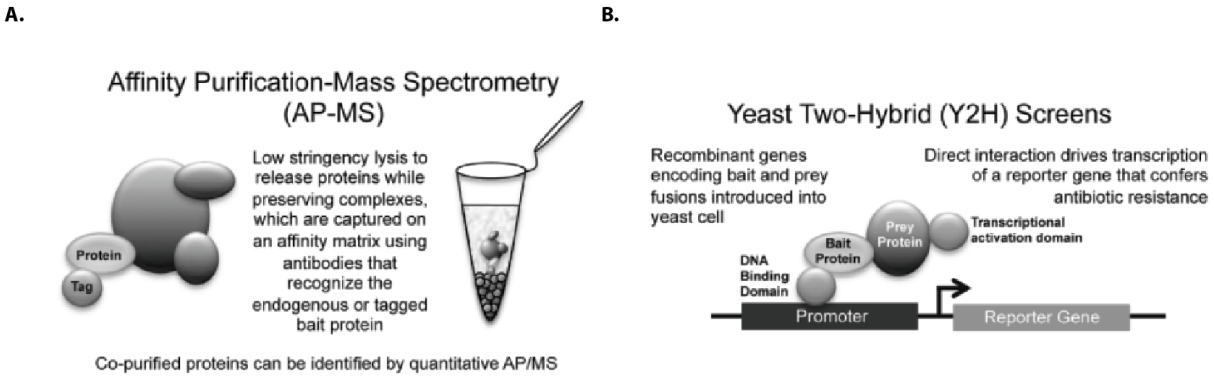

Figure 19: Examples of approaches to map protein-protein interactions
A. Affinity purification followed by mass spectrometry used to identify proteins in association with the bait. **B.** Yeast two-hybrid, strategy behind the first described method used for screening direct protein interactions. Taken from (Mehta and Trinkle-Mulcahy, 2016).

2.2.1 Affinity purification coupled to mass spectrometry

Currently the most popular technique for high-throughput interactome mapping is affinity purification followed by mass spectrometry identification (AP-MS). Usually the protein of interest is expressed ectopically with a tag (Flag, HA, GFP, Myc) as a bait, the complexes in which this protein is involved are recovered by affinity reagents such as antibodies recognizing the bait's tag coupled to beads (Figure 19-A). This approach has been used on a large scale in two recent studies, in which the interactome of over a thousand proteins in human cell lines has been identified (Hein et al., 2015; Huttlin et al., 2015). Although this strategy of overexpressing the protein of interest allows for the enrichment of complexes that might otherwise be lowly abundant, this also opens the possibility for false positives due to potential artefacts from overexpression, as well as non-specific binding to tag or affinity matrix (Mellacheruvu et al., 2013). To control for non-specific protein-protein interactions, optimization of the stringency conditions of purification is necessary, while at the same time preserving protein complexes.

2.2.2 Tandem Affinity Purification

Another technique that can be used to resolve issues of stringency is tandem affinity purification (TAP) (Rigaut et al., 1999). This method relies on the expression of a TAP-tagged bait protein. The TAP tag consists of two different tags separated by a protease cleavage site. This allows for sequential affinity purification of the bait protein with the complexes that it might engage in. After purification with the first tag and washes, the bound bait is eluted by protease cleavage, the eluate is then purified with the use of the second tag (Puig et al., 2001). This method allows for a higher specificity and stringency, resulting in a low level of background interactions, although like AP-MS approach, artefacts induced by overexpression of the bait can still be an issue.

To circumvent artefacts arising from the overexpression of the bait for the affinity purification approaches, BAC (bacterial artificial chromosome) have been used to express baits in more physiological conditions, as BACs are large enough to contain the genomic context of the bait (Hubner et al., 2010; Poser et al., 2008). More recently, with the use of CRISPR/Cas9 (Clustered regulatory interspaced short palindromic repeat/Cas9) gene editing, affinity tag insertion on endogenous proteins is possible, allowing to preserve physiological expression level of the bait (Cong et al., 2013; Lackner et al., 2015; Mali et al., 2013).

2.2.3 Yeast two-hybrid system

Another approach used for identification of protein interactions or proximity is the yeast two-hybrid system (Y2H) (Fields and Song, 1989) (Figure 19-B). In the original approach, one needs to express two fusion proteins in yeast, a bait in fusion with a DNA binding domain and a prey fused to a transcription activation domain. If these two recombinant proteins are directly interacting with each other, the transcription activation domain will be functional, inducing the expression of a reporter gene. This method, although quite robust, has several drawbacks as there is a bias for strong interactions happening in the nucleus, and it is limited by interactions on cellular membrane or involving more than two partners. These drawbacks have been addressed over the years by creating variations on the original Y2H approach, opening it to proteins in the cytosol, membrane or extracellular and transmembrane proteins (reviewed in (Brückner et al., 2009)).

2.2.4 Proximity labelling strategies

Recently, new methods have been described that overcome some of the disadvantages of AP-MS approach. Notably, in affinity purification strategies, optimized stringency conditions for purification are necessary to limit nonspecific protein interactions, while at the same time preserving formed protein complexes, resulting in the potential loss of weak and/or transient protein interactions. In these methods, protein proximity is analysed based on covalent labelling of proteins dependent on their proximity to each other *in vivo*. This eliminates the need for low-stringency purification conditions to keep proteins in the complexes together. Most commonly, biotinylation is used as a labelling reaction, giving the possibility to perform stringent purification conditions by taking advantage of the high affinity of streptavidin for biotin. Moreover, biotinylation is a relatively rare modification as only a handful of proteins are biotinylated endogenously in mammalian cells; PC (Pyruvate carboxylase), ACACA (Acetyl-CoA carboxylase 1), MCCA (Methylcrotonoyl-CoA carboxylase subunit alpha), PCCA (Propionyl-CoA carboxylase alpha chain) (Roux et al., 2013). Two particular proximity labeling techniques have been recently described: APEX (ascorbate peroxidase) and BioID (biotin identification). These two techniques will be introduced in the following part.

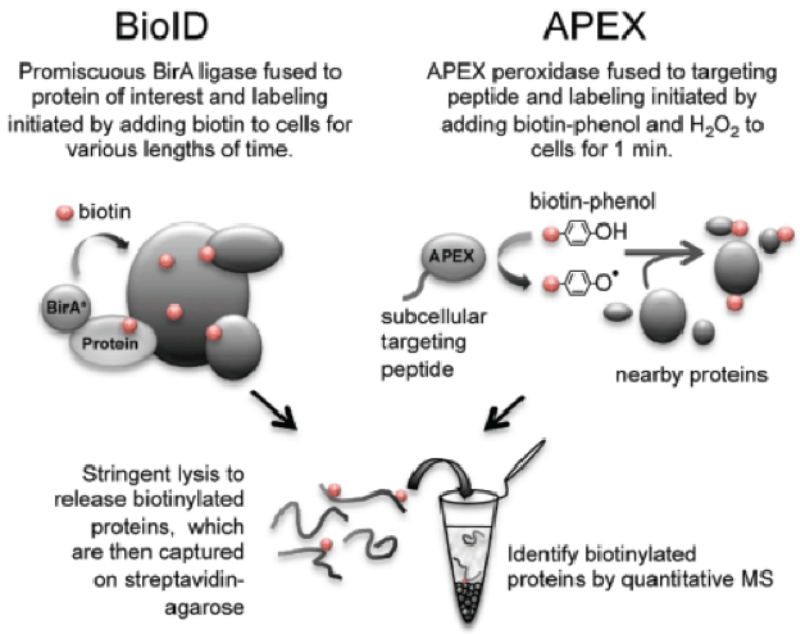

Figure 20: Proximity based labelling techniques
Two spatially restricted enzymatic-labelling approaches. Proximal proteins to a bait protein are tagged with biotin and enriched with streptavidin beads for subsequent identification. Taken from (Mehta and Trinkle-Mulcahy, 2016).

2.2.4.1 APEX approach

APEX has been developed by Rhee and colleagues to identify protein in the mitochondrial matrix (Rhee et al., 2013). In this method, ascorbate peroxidase (28 kDa) has been expressed with a mitochondrial targeting sequence, and the addition of phenol-biotin and H_2O_2 for one minute allowed biotin labelling of proximal proteins in the mitochondria matrix. Ascorbate peroxidase oxidizes phenol-biotin to phenoxyl-biotin radical able to react with the electron rich aminoacids Tyr, Trp, His, and Cys. The radical has a small labelling radius (<20nm) and is short lived (<1ms). Subsequent purification of biotinylated proteins and mass spectrometry analysis identified several hundred proteins most of which are annotated as mitochondrial (Rhee et al., 2013). This same approach has also been used for the identification of proteins in cilia in mammalian cells (Mick et al., 2015), in mitochondria of *Drosophila* muscle (Chen et al., 2015), in mitochondrial intermembrane space in human cells (Hung et al., 2014). APEX has so far only been targeted to closed cellular compartments to analyse the proteome of said compartments, which was previously unfeasible with other techniques. APEX is also quite amenable to quantitative mass spectrometry approaches like SILAC (stable isotope labelling

with aminoacids in cell culture) (Hung et al., 2014). It has yet to be tested for proximity labelling in fusion to a bait protein of interest, although for another application of APEX, it has already been expressed in fusion to a protein of interest where it catalyzed the polymerization of diaminobenzidine to improve contrast for imaging in electron microscopy experiments (Lam et al., 2015; Martell et al., 2012). It would be interesting to see whether it is feasible to determine the interactome of an APEX fused bait by proximity labelling, as short times of labelling would provide snapshots of a bait's proximity, which can give insights to how the dynamics of the bait's interactome can evolve in response to different stimuli.

2.2.4.2 BioID approach

Another iteration of proximity labelling approach is BioID, which relies on the biotin ligation activity of a prokaryotic biotin ligase. A bait fused to the biotin ligase is expressed in cells, with the addition of excess biotin to the culture medium, proximal proteins to the bait are biotinylated. This approach exploits the ability of a mutant 35 kDa Escherichia coli biotin ligase (R118G) to promiscuously biotinylate any protein found in a ~10nm diameter range (Roux et al., 2012). The biotin ligase called BirA, in its wild type form is only capable of biotinylating a specific set of proteins that have a particular sequence in bacteria, the minimal sequence requirements for biotinylation has been defined as a 14-mer peptide (Beckett et al., 1999). This minimal sequence called BAT (biotin acceptor tag) has been used for several applications from high affinity purification of tagged proteins to hypothesis based proximity labeling where one can test the proximity of a bait to a potential prey (reviewed in (Roux, 2013)).

For screening purposes, where one wants to identify unknown prey proteins for a specific bait, a mutant BirA enzyme is used, it is the mutant R118G, hereafter called BirA*. Biotinylation happens in two steps where in the first step biotin and ATP are combined to form highly reactive Biotin-AMP, BirA then holds on to biotin-AMP until it reacts with a lysine residue in the BAT sequence. BirA* however, has much lower affinity for biotin-AMP and it results in promiscuous biotinylation in the presence of excess biotin in mammalian cells (Kwon and Beckett, 2000; Roux et al., 2012). Labelling times are quite longer compared to APEX approach, although biotinylation is noticeable after an hour, its saturation happens before 24H of labelling (Roux et al., 2012). However this might be an advantage, as a long period of labelling will result in the accumulation of weak or transient partners of the bait. Another difference over APEX is that the half-life of activated biotin, biotin-AMP has a

longer half-life (minutes) meaning that labelling radius is probably larger (Hung et al., 2014). Although less than 20nm labeling has been proposed for BirA*, it might change depending on the bait and cellular environment (Roux, 2013). BirA* labels predominantly lysine residues on proximal proteins, meaning there is bias for the identification of lysine containing proteins. Moreover, the presence of biotin on lysine residues can interfere with other modifications that could be present on the same residues, potentially affecting the activity and behaviour of a particular partner and/or of a complex. BioID first was applied in 2012 to identify Lamin A partner proteins (Roux et al., 2012), and was then utilized by several groups to identify partners of various baits. Some of which include c-MYC (Dingar et al., 2015), HIV-Gag (Le Sage et al., 2015), SCF E3 ligases (Coyaud et al., 2015), NMD factors (Schweingruber et al., 2016) and proteins localized in specific cellular complexes or organelles like nuclear pore complex (Kim et al., 2014a) and centrosome components (Firat-Karalar et al., 2014). Recently a new and improved version of BioID was described; the new biotin ligase is from *Aquifex aeolicus* and is substantially smaller than BirA (28kDa versus 35kDa). The smaller size improves localization of fusion proteins, all the while requiring less biotin (Kim et al., 2016a). Unfortunately, BioID approach has yet to be performed in a quantitative setting for example using SILAC, this would allow for precise quantification of detected partner proteins. Recently, the affinity purification was compared to the BioID approach for chromatin associated proteins complexes. As expected BioID produced a larger dataset, containing lower abundance partners with only a partial overlap in identified proteins between the two approaches (Lambert et al., 2015).

2.3 Objective of the experiment

The objective in this chapter is to find cellular or viral protein partners of AGO2 during MCMV infection. Identification of proteins after proximity labelling of AGO2 in infected samples versus mock-infected samples would allow us to determine how the interactome of AGO2 changes during infection. MCMV infection induces several changes concerning miRNAs, firstly it induces quite a big change in the cellular miRNA profile, as 35 % of miRNA reads are of viral origin after only 24 hours of infection (Dölken et al., 2007) and secondly it induces the rapid degradation of the cellular miR-27 (Buck et al., 2010). So, with this approach, we hope to identify protein factors that would be implicated in the miRNA and/or RISC turnover. To that end, we will use the comparison between mock and MCMV infected cells, moreover we have at our disposition in the laboratory a mutant version of

MCMV which does not induce the degradation of miR-27 (Marcinowski et al., 2012). This would therefore help us with the identification of proteins implicated in mature miRNA degradation. Here, I will present the creation of the material and optimization of conditions necessary for setting up this approach along with some preliminary results that I obtained.

2.4 BioID of Argonaute 2

2.4.1 Cloning, expression and biotin labelling

For the setting up of BioID approach, I took as a guide the protocol of Roux and colleagues (Roux et al., 2013). The first step is the cloning of the expression vector coding for the fusion BirA*-AGO2. To this end, I inserted myc-tagged BirA* cDNA on the N-terminus of mouse AGO2 (hereafter called BirA*-mAGO2). This clone was tested for its expression in Hepa 1.6 cells along with BirA* alone without mAGO2 and biotinylation levels was measured upon addition of biotin to the culture media (Figure 21).

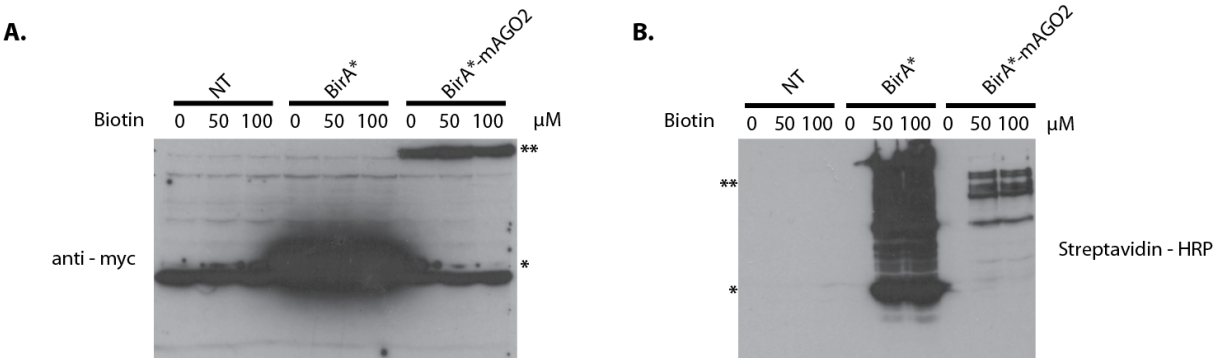

Figure 21: Expression and biotin labelling of BirA* constructs in Hepa1.6 cells
BirA* and BirA*- mAGO2 constructs were transfected into Hepa1.6 cells, biotin was added at the moment of the transfection to the culture media. 24 hours post transfection, cells were lysed and total protein extracts were separated on a SDS-PAGE gel. **A**. Western blot revealed with an anti-myc antibody. **B**. Western blot analysis of biotin labeled proteins revealed by hybridization of streptavidin coupled to HRP. (*) designates BirA* (35kDa) protein and (**) designates BirA*-mAGO2 (135 kDa).

Transient transfection of BirA* constructs worked as expected as the expression of BirA* proteins are easily detectable with anti-myc antibody 24 hours after transfection, although BirA* seems to be expressed at a much higher level than BirA*-mAGO2 probably due to its smaller size (Figure 21-A). When it comes to biotinylation levels of these two proteins, they are both capable of biotinylating proteins when biotin is added in the culture media. 50µM of

biotin is enough to get saturated levels of biotinylation after 24 hours as doubling the amount of biotin does not change the levels of biotinylated proteins (Figure 21-B). In addition, too much biotin would be detrimental for the affinity capture step, as free biotin will decrease the binding capacity of beads. In the samples without any addition of biotin as well as non-transfected samples, three bands corresponding to four different naturally biotinylated endogenous proteins should have been detected (Roux et al., 2012), meaning that in this experiment probably other biotinylated proteins especially in the BirA*-mAGO2 sample escape visualization on the western blot.

2.4.2 Pull-down of labelled proteins and mass spectrometry analysis

As BirA*-mAGO2 is expressed and functional for biotinylation, the next step is to set up the conditions for streptavidin enrichment of biotinylated proteins. There are two things to control for, first the non-specific binding of proteins to the streptavidin beads and second the non-specific biotinylation of BirA*-mAGO2 fusion. The latter would be a control to do if we wanted to identify steady-state partners of AGO2, but as we want to see specific partners of AGO2 during infection, the non-infected sample can be used as our negative control. So, we wanted to test if the streptavidin beads are binding non-specific proteins, for that we have two choices, either we can use BirA*-mAGO2 protein but without the addition of any biotin or mAGO2 fused to another protein which does not have any biotinylation activity. The former would not be very clean as the serum in culture media brings some biotin into the cell, potentially causing low level labeling of AGO2 proximal proteins, so we decided to use GFP-mAGO2 as control, as GFP is a tag about the same size as BirA* (25 kDa versus 35 kDa).
To test the protocol of affinity capture of biotinylated proteins, we transfected Hepa1.6 cells with either GFP-mAGO2 or BirA*-mAGO2, and biotin was added at the moment of transfection. 24 hours later cells were lysed and streptavidin pull-down was performed. Overexpression of mAGO2 fusion proteins showed that compared to endogenous mAGO2, the levels at which they are expressed are quite high (Figure 22-A). The overexpression of mAGO2 might affect its localization or turnover, changing in turn the identity of its proximal partners. Nonetheless, we continued with the pull-down. The silver nitrate staining (Figure 22-B) showed that for the GFP-mAGO2 sample, three high molecular weight bands are detected, these probably are the four endogenously biotinylated proteins; ACACA at 265 kDa, PC at 130 kDa, MCCA and PCCA at 79 kDa. For BirA*-mAGO2, several proteins in addition to the four endogenous proteins are detectable. Most of these pulled-down proteins seem to be

revealed by streptavidin-HRP meaning that they were indeed biotin labelled and are not non-specific proteins bound to the beads (Figure 22-B and 22-C).

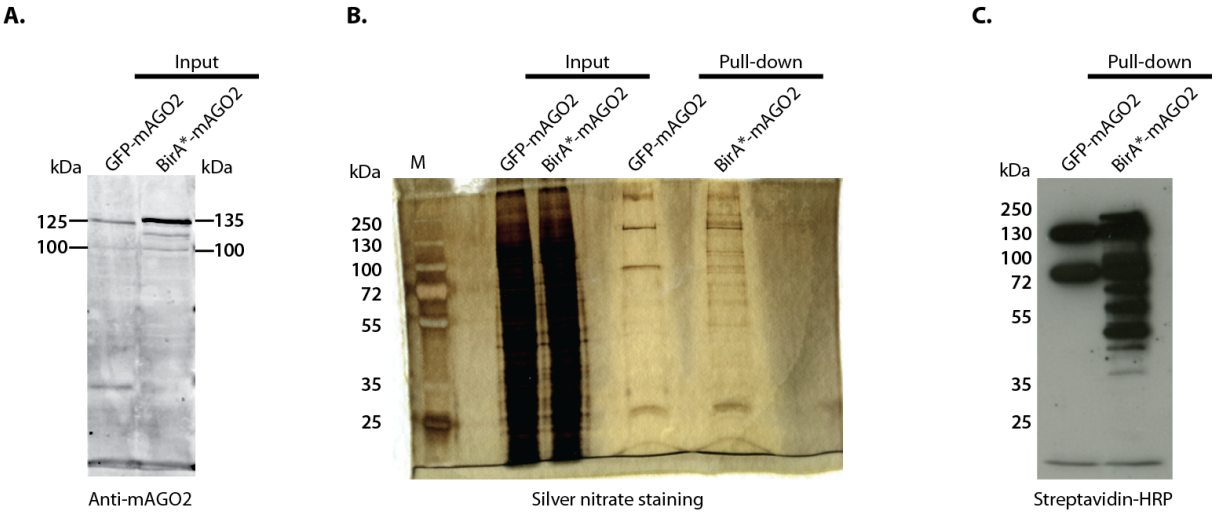

Figure 22: Pull-down of biotin labeled proteins in Hepa cells.
A. Expression level of endogenous mAGO2 and overexpressed mAGO2 in fusion with GFP or BirA*. **B.** Silver nitrate staining after pull-down of biotin labeled proteins. **C.** Streptavidin-HRP revelation of proteins after pull-down.

In order to reveal the identities of these pulled-down proteins, we analyzed these two samples by mass spectrometry. There were only 20 proteins identified in the control sample, whereas 200 proteins were identified in the BirA*-mAGO2 sample (Annex-1 and 2).

Common proteins identified with high spectral counts in the GFP-mAGO2 and BirA*-mAGO2 sample are listed in Table 1. The identification of these proteins is expected, as they are indeed the endogenously biotinylated proteins detected in BioID experiments (Roux et al., 2013). There are also other proteins commonly identified in this sample with very limited spectral counts listed in Annex-1.

The spectral counts obtained for the endogenously biotinylated proteins between the two samples, are quite different. This probably occurred because of the difference between the total number of proteins biotinylated in each sample, meaning that the quantity of streptavidin beads used is not saturating over biotinylated proteins at least in the BirA*-mAGO2 sample. This also might be due to the low complexity of the GFP-mAGO2 sample, where the number of different proteins is low, allocating more identification time during mass spectrometry analysis.

Table 1: Common proteins identified in both GFP-mAGO2 and BirA*-mAGO2 samples

Protein identity	Protein description	Molecular weight (kDa)	Spectral count (GFP/BirA*)	Sequence coverage (%)
ACACA	Acetyl-CoA carboxylase 1	265.1	1636/714	75.7
PYC	Pyruvate carboxylase, mitochondrial 1	129.6	1202/1037	77.2
MCCA	Methylcrotonoyl-CoA carboxylase subunit alpha, mitochondrial	79.3	578/241	73.8
PCCA	Propionyl-CoA carboxylase alpha chain, mitochondrial	79.9	313/217	66.9

For the BirA*-mAGO2 sample, 200 different proteins were identified (Annex-2). As in this experiment, we did not control for non-specific labeling of BirA*, this list most certainly contains non-specifically labelled proteins. Nonetheless, we made an enrichment analysis on gene ontology (GO) consortium's website (www.geneontology.com), which compares the number of proteins identified in the sample for a given biological process or molecular function to the expected number of proteins that would fall in this same process or function by chance. For the 179 proteins differentially identified in BirA*-mAGO2, the resulting significant biological processes and molecular functions have been sorted from the most significant to less significant in Table 2 and 3 and the cellular component for the most fold enrichment in the Table 4. We find enrichment for posttranscriptional regulation of gene expression and regulation of translation as well as enrichment for stress granules and P-bodies.

Table 2: Top 4 GO biological processes enriched for proteins identified in BirA*-mAGO2.

GO Biological process	Reference mus musculus #	Obtained #	Expected #	Fold enrichment	P-value ▼
Regulation of cellular amide metabolic process	309	22	2.41	9.13	5.84E-11
Posttranscriptional regulation of gene expression	337	22	2.63	8.37	3.27E-10
Macromolecular complex assembly	1143	37	8.91	4.15	1.20E-09
Regulation of translation	285	20	2.22	9	1.37E-09

Table 3: Top 4 GO molecular functions enriched for proteins identified in BirA*-mAGO2.

GO Molecular function	Reference mus musculus #	Obtained #	Expected #	Fold enrichment	P-value ▼
Poly(A) RNA binding	1841	63	8.71	7.23	2.39E-33
RNA binding	1117	69	11.92	5.79	3.22E-31
Protein binding	1529	121	60.86	1.99	5.79E-17
Nucleic acid binding	7807	73	26.47	2.76	7.11E-14

Table 4: Top 4 GO cellular component enriched for proteins identified in BirA*-mAGO2.

GO Cellular component	Reference mus musculus #	Obtained #	Expected #	Fold enrichment ▼	P-value
Cytoplasmic stress granule	33	8	1.09	31.10	5.84E-11
Ribonucleoprotein granule	140	15	1.03	13.74	3.27E-10
Cytoplasmic ribonucleoprotein granule	132	14	0.48	13.61	1.20E-09
Cytoplasmic mRNA processing body	62	6	1.01	12.41	1.37E-09

Looking at the list of identified proteins, we find known cofactors of AGO2 among others HSP90/HSC70 (Iwasaki et al., 2010; Johnston et al., 2010), TNRC6B (Lian et al., 2009; Pfaff et al., 2013), EDC4 and PATL1 (Jonas and Izaurralde, 2013), PABP (Jinek et al., 2010; Zekri et al., 2009) as well as several mRNA binding proteins like PUM2 (Galgano et al., 2008), FXR1 (Vasudevan and Steitz, 2007; Vasudevan et al., 2007), IGF2BP1(Elcheva et al., 2009), UPF1 (Jin et al., 2009) and ribosomal proteins. Some of these proteins were found by other affinity purification and mass spectrometry analysis performed by others (Frohn et al., 2012; Höck et al., 2007; Landthaler et al., 2008; Meister et al., 2005). Some of the identified proteins are represented in the Figure 23 where they are regrouped depending on their function. Although we cannot guarantee that none of these identified proteins are originating from non-specific tagging of BirA* enzyme, the enrichment analysis gives encouraging results, as they are related to AGO2 function.

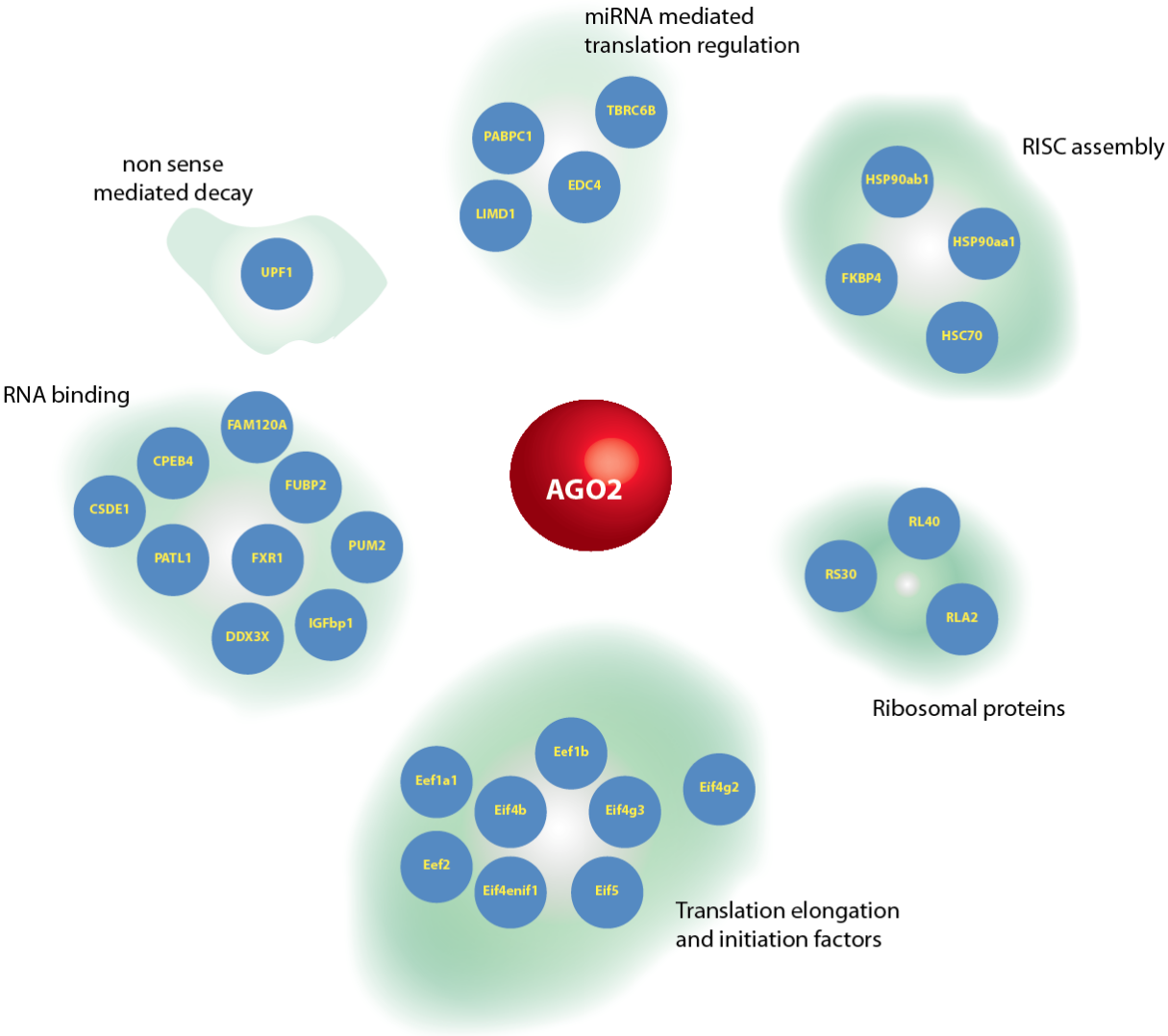

Figure 23: Schematic representation of identified proteins proximal to mAGO2.
A subset of proteins identified in the mass spectrometry analysis were included in this representation depending on their known interaction with AGO2 or according to their biological function in RNA metabolism or translation.

2.5 BioID of Argonaute 2 during MCMV infection

2.5.1 Generation of a stable cell line expressing BirA*-mAGO2

A major criticism that can be made for the previous experiment is that the level of expression of BirA*-mAGO2 is several times higher than the endogenous expression level of AGO2 (Figure 22-A). Moreover, it would be preferable to have a stable cell-line expressing BirA*-

mAGO2 in an AGO2 knockout context, as the stable expression would prevent the inertia of *de novo* miRNA loading, and the absence of endogenous AGO2 expression would mean that every AGO2 molecule would be biotinylation proficient. For this reason we decided to use MEF AGO2 -/- (mouse embryonic fibroblasts) cells, obtained from AGO2 knockout mice (Liu et al., 2004), and created a stable cell-line expressing BirA*-mAGO2.

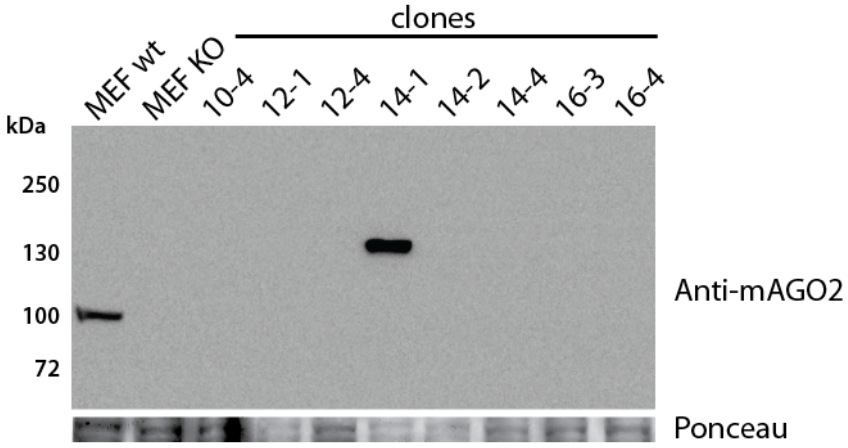

Figure 24: Verification of BirA*-mAGO2 expression in MEF AGO2 -/- clones.
Western blot analysis of clones selected for BirA*-mAGO2 expression, MEF wild type sample serves as a control for the endogenous expression level of mAGO2. MEF knockout sample comes from parental cells that served for the generation of the clones. Ponceau staining serves as loading control.

For the generation of the stable cell line, we chose to clone BirA*-mAGO2 under the control of the EF-1α promoter as the CMV promoter is known to be prone to silencing (Gill et al., 2001). After successful cloning of the expression vector and verification of its expression (not shown), it was linearized and transfected into MEF AGO2 -/- cells after blasticidin selection and amplification of selected clones, the expression of BirA*-mAGO2 was verified. Out of the 8 clones tested, subjected to different concentrations of blasticidin, only one clone was positive, which was named 14-1 (Figure 24). This clone still expresses higher levels of mAGO2 compared to wild type MEF cells, but it is closer to the endogenous level of AGO2 when compared to the previous transient overexpression (Figure 24, Figure 22-A).

2.5.2 Verification of the 14-1 clone for miRNA loading and biotinylation

We then wanted to verify if BirA*-mAGO2 expressed in this clone was capable of loading miRNAs. To this end we performed an immunoprecipitation of mAGO2 in MEF wt cells and 14-1 clone. We first analysed the immunoprecipitated RNA by Northern blot (Figure 25-A)

and by RT-qPCR (Figure 25-B). The Northern blot is not very clear, miR-27 signal in the immunoprecipitated fraction is not very high, although it shows that the immunoprecipitation has worked as in anti-BrdU samples no signal is detected (Figure 25-A). We also analysed the same samples by RT-qPCR, we are able to enrich miR-27 in AGO2 IP sample compared to the negative control BrdU IP 16 and 27 times (Figure 25-B). The same enrichment is also true for another cellular miRNA miR-24 (not shown). These fold change figures obtained are quite low, as in the literature for AGO2 immunoprecipitation in human cell-lines although it is a different antibody for hAGO2, enrichments of 1000 fold are standardly obtained (Dölken et al., 2010b).

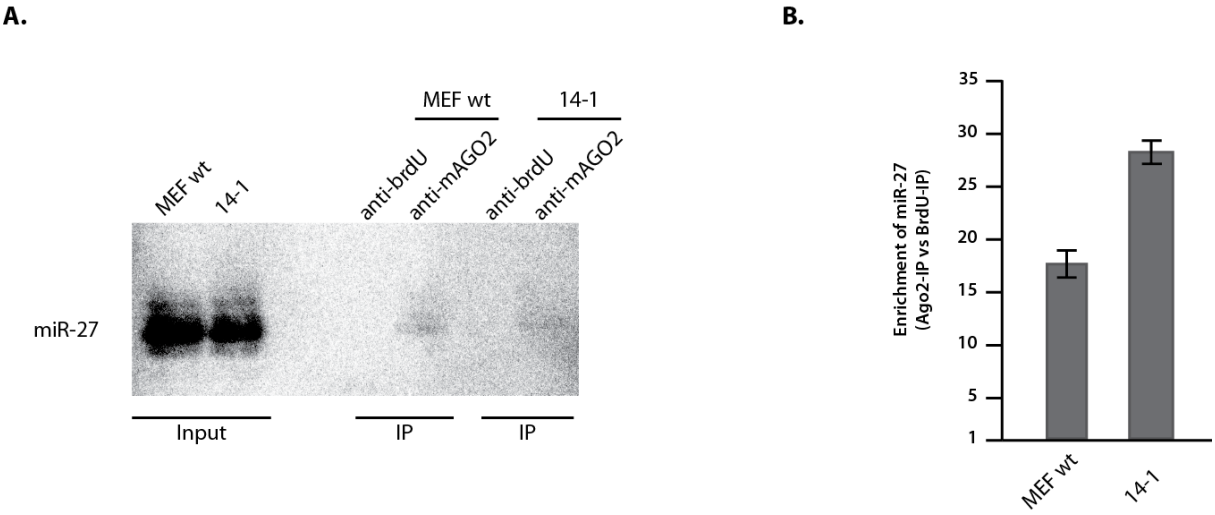

Figure 25: Immunoprecipitation of mAGO2 in MEF wild type and 14-1 cells.
Anti-BrdU antibody was used as negative control. **A.** Northern blot analysis using a probe for endogenous miR-27. **B.** RT-qPCR analysis of endogenous miR-27 levels, fold enrichment was calculated by comparing the level of miR-27 in AGO2 IP versus BrdU IP. Error bars represent standard deviation from technical triplicates.

We also wanted to be sure of the biotinylation capability of the 14-1 clone, so we performed biotin labelling for 24 hours with or without the addition of excess biotin to the culture media. We then performed pull-down of biotinylated proteins. Although normal culture media contains low levels of biotin and should permit biotinylation to some extent, we want to observe a difference in the quantity of biotinylated proteins. In the sample without any addition of biotin, we see several bands including the ones corresponding to endogenously biotinylated proteins, as expected with the addition of biotin to the culture media we can detect additional biotinylated bands (Figure 26-A). This is also visible on the silver nitrate staining that was performed on these same samples (Figure 26-B, left two lanes).

One of the critical steps of streptavidin pull-down, is the elution of biotinylated proteins before sending the sample for mass spectrometry analysis. We previously opted for the elution by boiling the beads in 0.1% SDS solution, as per the streptavidin beads manufacturer's instructions. In the literature however, two other ways of proceeding to the mass spectrometry analysis after pull-down exist; one where tryptic digestion is performed directly on the beads and the other where biotinylated proteins are eluted by denaturation in SDS sample buffer followed by electrophoretic separation and mass spectrometry on protein bands (Roux et al., 2012). We suspected that these two other treatments might cause the contamination of the sample to be analyzed by a lot of streptavidin. In these control experiment, we performed a second elution step with SDS-sample buffer following the first elution to verify the efficiency of elution as well as the contamination levels of streptavidin (Figure 26-B).

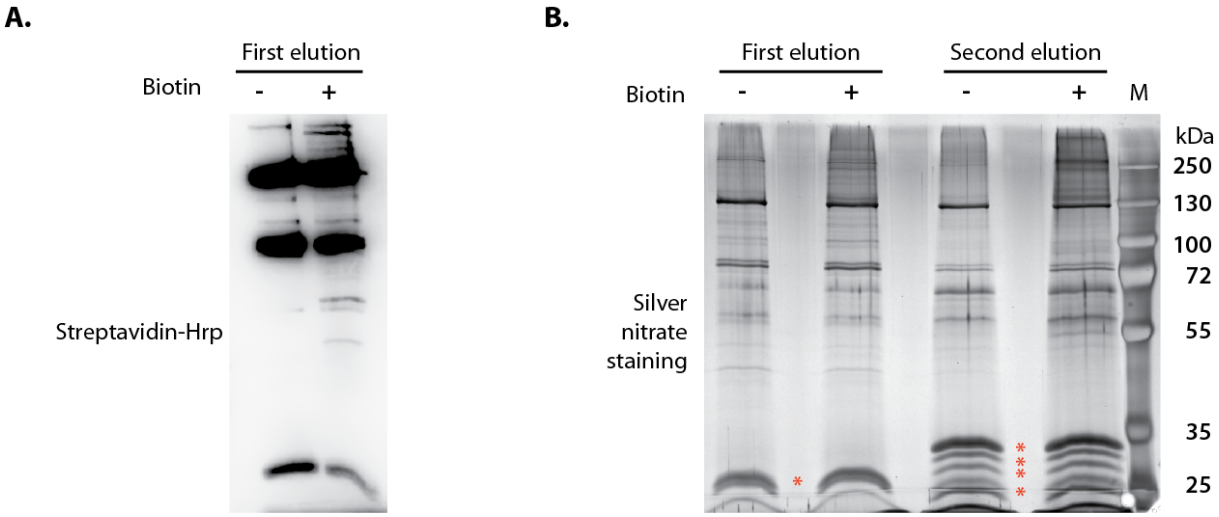

Figure 26: Biotinylation property of the clone 14-1.
14-1 cells were incubated with or without excess biotin for 24 hours, followed by streptavidin pull-down. The first elution was performed by boiling the beads in 0.1% SDS, after which the beads were resuspended in SDS sample buffer for the second elution. **A.** Western blot analysis of pulled-down proteins with streptavidin-HRP hybridization after the first elution. **B.** Silver nitrate staining of samples after each step of elution. *: show the bands corresponding to streptavidin monomer and polymers.

First of all, quite a big percentage of the total biotinylated proteins bound by streptavidin beads stay attached after the first elution step as evidenced by the proteins coming off with the second elution step. Also, this second elution step causes a lot more streptavidin molecules (red asterisks) and possibly polymers to be detached and to mix with the sample (Figure 26-B).

2.5.3 Identification of AGO2 partners during MCMV infection

After verifying that 14-1 is functional for loading miRNAs and biotinylation, we finally went on to perform our proximity labelling in infection and non-infection conditions. For the elution step of bound proteins, we decided to go with the elution by boiling with 0.1% SDS, but after this first elution, we kept the beads and also performed trypsic digestion on them. As introduced earlier, we used two different MCMV strains in this experiment, the wild type and a mutant strain that carries three point mutations in its m169 transcript 3'UTR called (hereafter called MCMV mut168). This mutant is not capable of inducing the degradation of miR-27 as previously described by our laboratory (Marcinowski et al., 2012). The objective of this experiment is firstly, to identify AGO2 partner proteins by proximity labelling during MCMV infection compared to mock infection, secondly to compare MCMV wild-type and mut168 infection conditions to identify partners of AGO2 which would be involved in target-directed miRNA decay. As biotin labelling is saturated around 24 hours of labelling and BirA*-mAGO2 is constitutively expressed, habitual partners of AGO2 would cause high background. So, to augment our chances of identifying proteins partnering with AGO2 during infection, we used a high multiplicity of infection (MOI) as it correlates with the rapidity of miR-27 degradation (Buck et al., 2010).

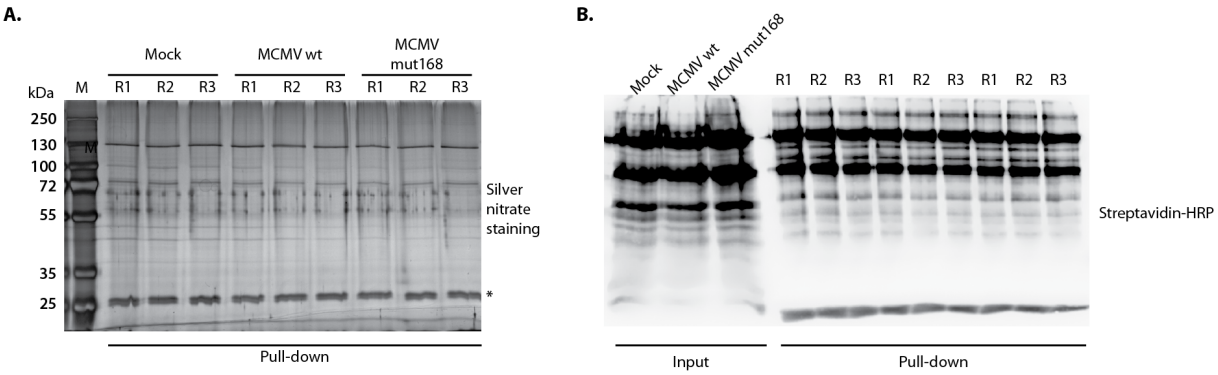

Figure 27: Analysis of pulled-down biotinylated proteins after MCMV infection
Cells were mock, MCMV wild type and MCMV mut168 infected for 24 hours and biotinylation was carried on for a total of 20 hours. After lysis each of the three samples were separated into three, to perform streptavidin pull-down and mass spectrometry analysis in technical triplicates. **A.** Silver nitrate staining of pulled-down proteins. **B.** Western Blot analysis of input and pull-down samples with streptavidin-hrp hybridization. M: Protein size marker. R: replicate number. *: Streptavidin monomer

The three conditions were therefore mock-infected cells, MCMV wt and MCMV mut168 infected cells at MOI 10 for 24 hours, and biotin was added after 4 hours of infection (20 hours of biotinylation). After lysis, each sample was separated into three technical replicates to test eventual differences in streptavidin pulldown and mass spectrometry analysis. Before sending samples to mass spectrometry analysis, samples were verified with silver nitrate staining, as well as western blotting revealed with streptavidin HRP (Figure 27).

One thing that can be observed in the silver staining, is that the quantity of total proteins in every condition relative to the free streptavidin quantity is not very high, at least not as high as in previous experiments (Figure 27-A, 26-B, bands marked with asterisk). We are also not able to visualize any differential bands between samples (Figure 27-A and 27-B), however this does not necessarily mean that we would not be able to identify differences with the mass spectrometry analysis. The low level of biotinylated proteins is probably due to the more physiological expression level of BirA*-mAGO2, which is an issue as the quantity of endogenously biotinylated proteins can prevent the detection of the biotin tagged proteins that we want to identify.

We first began by analysing proteins detached by the first elution step. As suspected, the analysis produced a low number of identified proteins, i.e. in between all the samples a total of 80 different proteins. Most of the identified proteins have very low spectral counts (complete list in Annex-3). The number of identified spectra for the four endogenously biotinylated proteins and streptavidin are presented in the Table 5.

Table 5: Spectra identified for endogenously biotin tagged proteins and streptavidin.

		Mock			**MCMV WT**			**MCMV mut168**		
Protein identity	**Protein description**	**R1**	**R2**	**R3**	**R1**	**R2**	**R3**	**R1**	**R2**	**R3**
SAV	Streptavidin	1307	1262	1339	1343	1316	1359	1371	1361	1356
PYC	Pyruvate carboxylase, mitochondrial 1	1009	1055	1057	1030	1018	1085	1062	1063	1084
PCCA	Propionyl-CoA carboxylase alpha chain, mitochondrial	378	377	392	333	315	342	341	363	353
MCCA	Methylcrotonoyl-CoA carboxylase subunit alpha, mitochondrial	141	143	130	127	87	88	96	116	100
ACACA	Acetyl-CoA carboxylase 1	48	43	44	38	34	41	36	32	39

The number of spectra identified for these proteins are quite similar in each sample and replicate, meaning that the total quantity of biotinylated proteins was roughly the same. This is also true for spectra coming from streptavidin showing that the same amount of streptavidin beads has been utilized. All in all, this demonstrates the good reproducibility of the streptavidin enrichment and mass spectrometry analysis steps.

Table 6: Spectra identified for AGO2 and its known direct and indirect partners

		Mock			MCMV WT			MCMV mut168		
Protein identity	**Protein description**	**R1**	**R2**	**R3**	**R1**	**R2**	**R3**	**R1**	**R2**	**R3**
Ago2	Protein argonaute-2 (BirA* fusion)	112	121	121	101	89	103	103	106	107
Hsp90ab1	Heat shock protein HSP 90-beta	19	20	22	17	20	24	24	21	23
Hsp90aa1	Heat shock protein HSP 90-alpha	5	4	5	5	5	8	8	7	6
Hspa8	Heat shock cognate 71 kDa protein	4	5	6	5	6	10	6	7	8
Tnrc6b	Trinucleotide repeat-containing gene 6B	9	8	13	6	7	8	5	7	6
Tnrc6c	Trinucleotide repeat-containing gene 6C	17	19	17	14	9	11	13	13	13
Edc4	Enhancer of mRNA-decapping protein 4	18	20	24	27	28	20	32	27	28
Cnot1	CCR4-NOT transcription complex subunit 1	4	2	4	1					1

Concerning the other identified proteins, as expected, mAGO2 itself is a top hit, with around a hundred spectral counts identified. We also can detect HSP90 and HSC70 (also known as Hspa8) involved in the loading of miRNA into AGO2, TNRC6 proteins recruited by RISC to silence target mRNAs along with EDC4 and CNOT1 involved respectively in decapping and deadenylation of targets (Table 6). As this experiment was only performed once and we do not have high spectral counts for these AGO2 partners, we cannot consider this analysis as quantitative. As such, we can speculate only speculate at this point about the tendencies of these proteins in different conditions. To do that, we generated another table where we calculated the ratio of spectral counts of these proteins comparing wt or mut168 MCMV infection to mock by averaging the spectral counts in all three technical replicates (Table 7). We see a tendency for TNRC6B and C to go down with the infection. However, we cannot rule out at this stage that this might be due to the slight decrease in AGO2 counts. Nonetheless, this tendency is followed by CNOT1, although, this should be taken with caution as it is not identified in all the replicates. For EDC4, spectral counts go up with the infection. Different peptides of HSP90/HSC70 also increase in spectral counts with the infection, this might be explained by the need to load the viral encoded miRNAs into AGO2 (Table 6 and 7).

Table 7: Ratios of the spectral of counts of AGO2 partners between WT and mut168 compared to mock infection

		Ratio	
Protein identity	**Protein description**	**WT/Mock**	**Mut168/mock**
Ago2	Protein argonaute-2 (BirA* fusion)	0.83	0.89
Hsp90ab1	Heat shock protein HSP 90-beta	1.00	1.11
Hsp90aa1	Heat shock protein HSP 90-alpha	1.29	1.50
Hspa8	Heat shock cognate 71 kDa protein	1.40	1.40
Tnrc6b	Trinucleotide repeat-containing gene 6B	0.70	0.60
Tnrc6c	Trinucleotide repeat-containing gene 6C	0.64	0.74
Edc4	Enhancer of mRNA-decapping protein 4	1.21	1.40
Cnot1	CCR4-NOT transcription complex subunit 1	0.3	0.3

Concerning viral encoded proteins, we have only two proteins identified and only in MCMV wt infection condition. These are m142 and m86 proteins from MCMV (Annex 3). As they are only identified in 2 out three technical replicates with very few spectral counts, we cannot rely upon these results to make any conclusions. The fact that we did not identify viral proteins might be due a low level of infection or that viral proteins do not interact with AGO2. MCMV might choose to use its RNAs instead of its proteins to interact with the miRNA pathway, like in the case of miR-27 and m169 as it might be a quicker and more efficient means compared to using proteins.

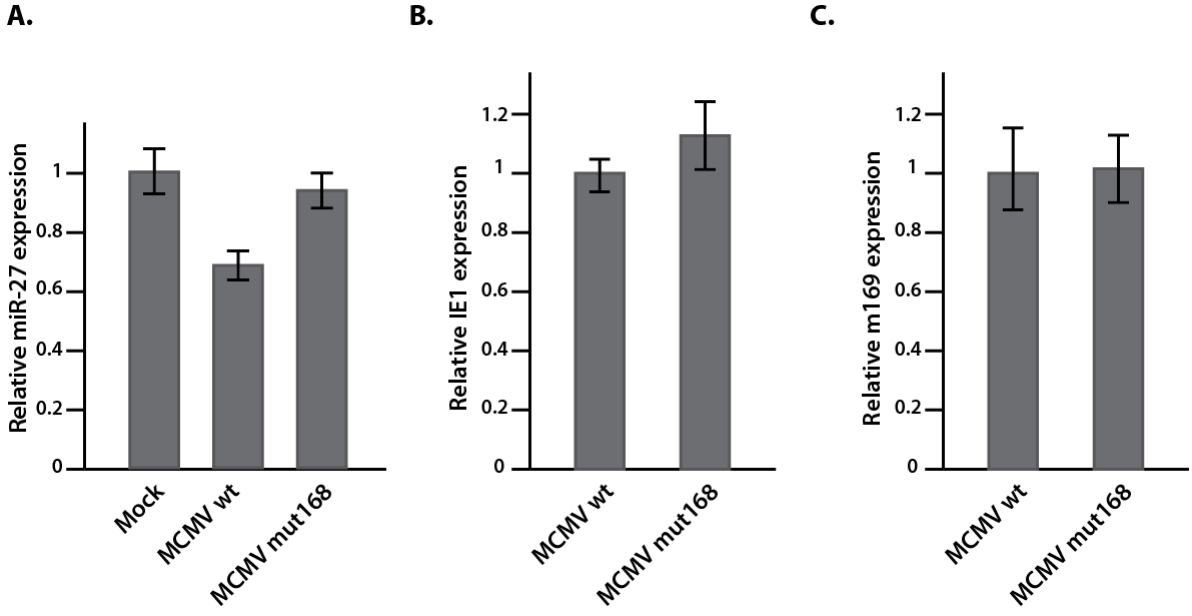

Figure 28: Analysis of miR-27 expression and MCMV transcripts by RT-qPCR
A. miR-27 expression levels, mock infection is normalized to 1. **B** and **C**. Relative expression of IE1 and m169, MCMV wt is normalized to 1.

We measured the level of infection and the level of miR-27 degradation by qPCR (Figure 28). The levels of m169 in MCMV wt and mut168 is very similar (Figure 28-C), this is also true for another viral transcript IE1 (immediate early 1) (Figure 28-B). Concerning miR-27 level, we see that after 24h of infection, its levels drop to 70% compared to it levels in mock or mut168 infected conditions (Figure 28-A). This is not a very high level of degradation compared to Hepa 1.6 cells that we were infecting with an equivalent MOI with centrifugal enhancement, which had %50 of miR-27 degradation after (Haas et al., 2016). This can be due to our infection protocol that does not include centrifugal enhancement for cell culture format reasons. On the other hand, different cell-lines can demonstrate different efficacies of TDMD for example in neuronal cells TDMD is more efficient than in fibroblasts (de la Mata et al., 2015). It might be interesting to measure TDMD efficiencies in different cell lines, in order to choose one that has high efficiency if we want to identify factors implicated in TDMD.

This mass spectrometry analysis was performed with the first elution off the streptavidin beads, since previously we saw that a lot of material stays on the beads (Figure 26-B), we decided to carry out on bead tryptic digestion to perform another mass spectrometry run with the same samples. We wanted to compare the two elutions, to see if there would be a difference in the identification of peptides, especially concerning streptavidin contamination. Unfortunately, the second elution produced very low quality results, due to a strong polymer contamination coming from the beads. Future optimisation efforts should be focused on finding the appropriate solution for elution of peptides from streptavidin beads.

2.6 Materials and methods

2.6.1 Plasmids and cloning

Mouse mAGO2 (Accession BC129922) was cloned in the pEGFP-C2 expression vector (ClonTech) using the restriction sites EcoRI/BamHI. Mouse mAGO2 (Accession BC129922) was cloned in the pcDNA3.1(+) vector (Invitrogen) with sites EcoRI/NotI, this plasmid was modified with the addition of myc-BirA* (addgene #35700) coding sequence by the use of NheI/HindIII sites. For the creation of stable cell line, first the pcDNA3.1(+) vector (Invitrogen) was modified, SV40 promoter and neomycin resistance was taken out by NaeI digestion and this fragment was replaced with a fragment containing SV40 promoter, an EM7 promoter and blasticidin resistance obtained from plenti6-DEST plasmid (Invitrogen) with a digestion by XmnI/DraI. On the other hand, CMV promoter on pcDNA3.1(+) expressing myc-BirA*-mAgo2 vector was taken out by MluI/NheI and replaced by EF1-α promoter taken with digestion by MluI/XbaI from pEF5/FRT/V5/gw-cat (Invitrogen) plasmid after excision of gateway cassette with EcoRV sites. The final plasmid used eventually for stable cell line called pEF5-mycbirA*-mAGO2 from the ligation of; the backbone of modified pcdna3.1(+) blasticidin resistance plasmid produce by MluI and XbaI digestion and the insert fragment coming from last plasmid taken out with MluI and XbaI.

2.6.2 Oligonucleotide sequences

Cloning

pcDNA3.1-mAGO2-F	DNA	GGAATTCAATGTACTCGGGAGCCGGCCC
pcDNA3.1-mAGO2-R	DNA	GAAAAAAGCGGCCGCTCAAGCAAAGTACATGGTGC
pEGFP-mAGO2-F	DNA	GGAATTCATGTACTCGGGAGCCGGCCC
pEGFP-mAGO2-R	DNA	CGGGATCCTCAAGCAAAGTACATGGTGC
pcDNA3.1-mycBirA*-F	DNA	CTAGCTAGCATGGAACAAAAACTCATCTCAG
pcDNA3.1-mycBirA*-R	DNA	CCCAAGCTTATGGAACAAAAACTCATCTCAG

Northern blot

Anti-miR-27	LNA	GCGGAACTTAGCCACTGTGAA

RT-qPCR

miR-27 (qPCR)	DNA	TTCACAGTGGCTAAGTTCCGC
miR-24 (qPCR)	DNA	TGGCTCAGTTCAGCAGGAACAG
PPIA-F (qPCR)	DNA	GCGGCAGGTCCATCTACG
PPIA-R (qPCR)	DNA	GCCATCCAGCCATTCAGTC
IE1-F (qPCR)	DNA	GTTACACCAAGCCTTTCCTGGAT
IE1-R (qPCR)	DNA	TGTGTGGATACGCTCTCACCTCTAT
m169-F (qPCR)	DNA	ATCTTCTTCGGCGTTAGCGA
m169-R (qPCR)	DNA	TGAGGTCCAGGTCGTGTGA

2.6.3 Cell culture and transfection

Hepa 1.6 cells, MEF and MEF Ago2 -/- (Liu et al., 2004) cells were cultured in Dulbecco's modified Eagle's medium (DMEM) supplemented with 10% (v/v) fetal calf serum at 37°C in a humidified 5% CO_2 atmosphere. Hepa 1.6 cells were transfected with Turbofect reagent (Thermo Scientific), and MEF cells with lipofectamine 2000 (Invitrogen) according to manufacturer's instructions, at the moment of transfection, biotin (sigma Aldrich) (dilution from 25mM Biotin stock in 100mM sodium phosphate buffer or directly dissolved in DMEM) was added to the desired concentration.

2.6.4 Stable cell line generation

The plasmid pEF5-mycbirA*-mAGO2 was first linearized by AatII digestion, followed by phenol/chloroform purification, ethanol precipitation. MEF Ago2 -/- cells were transfected in 6 well plates with lipofectamine 2000. 48 hours after transfection, cells were detached and $5x10^5$ cells were reseeded to 10 cm plates with blasticidin selection at 10, 12, 14 and 16 µg/ml. Blasticidin was refreshed every 3 days, after a week colonies appeared and they were picked into 24 well plates. After colonies were amplified into 25 cm^2 flasks, they were analysed by Western blot for BirA*-mAGO2.

2.6.5 Immunoprecipitation

Approximately 10^7 MEF WT and MEF Ago2 -/- 14-1 cells were harvested, washed twice with ice-cold phosphate-buffered saline (1× PBS), and resuspended in 2 mL of NET buffer (50 mM Tris HCl [pH 7.4], 150 mM NaCl, 1 mM EDTA, 0.1% triton), supplemented with

Complete-EDTA-free Protease Inhibitor Cocktail (Roche). Cells were lysed for a totalof 30 min by incubation on ice including three 30 seconds sonications. Debris were removed by 15 min centrifugation at 16,000 g at 4°C. An aliquot of the cleared lysates (100 µL) is kept aside as RNA Input. The rest of the lysate was divided into two and mono clonal anti-BrdU antibody (Abcam) or anti-mAGO2 6F4 monoclonal antibody (kindly provided by G. Meister) are added and samples are incubated for 1 hour at 4°C under tumble-over rotation (18 rpm). Then, 50 µL of Protein-G-Agarose beads (Roche) was added and the samples were rotated similarly for another hour. After three washes in NET buffer and a fourth wash in NET buffer without Triton. The 100µl of input aliquot and the beads are taken into 1ml of Tri-Reagent Solution (MRC, Inc) for further RNA extraction.

2.6.6 RNA extraction and northern blot

RNA was extracted using Tri-Reagent Solution (MRC, Inc) according to the manufacturer's instructions, with IP fraction having an addition of 1µl of glycogen at the precipitation step.
Northern blotting was performed with 80% of input fraction and 80% of IP fraction RNA. RNA samples were resolved on a 17.5% urea-acrylamide gel of 20 cm in length, transferred onto Hybond-NX membrane (GE Healthcare). RNAs were then chemically cross-linked to the membrane during 90 min at 65°C using 1-ethyl-3-[3-dimethylaminopropyl]carbodiimide hydrochloride (EDC) (Sigma). Membranes were pre-hybridized for 1 h in PerfectHyb™ Plus (Sigma) at 50°C. Probes consisted of oligodeoxyribonucleotides (Locked Nucleic Acids) which were 5′ end labelled using T4 polynucleotide kinase (Fermentas) with 25 µCi of [γ-32P] ATP. The labelled probe was hybridized to the blot overnight at 50°C. The blot was then washed twice at 50°C for 20 min (5× SSC/0.1% SDS), followed by an additional wash (1× SSC/0.1% SDS) for 5 min. Northern blots were exposed to phosphorimager plates and scanned using a Bioimager FLA-5100 (Fuji).

2.6.7 Western blot and antibodies

Western blot analysis in this chapter were performed under the following conditions: anti-mouse and anti-rabbit HRP secondary antibodies purchased from Sigma-Aldrich hybridized at 1/10000 dilution. The secondary anti-rabbit-Cy5 antibody was used at 1/2500 dilution (Amersham) Streptavidin-Hrp was used at 1/10000 dilution (Pierce, Sulfo-Bed kit). Anti-myc

antibody used at 1/2000 dilution (Abcam). Anti-mAGO2 was used at 1/1000 dilution (Cell-signaling). All the primary and secondary antibody incubation were performed in 5% non-fat milk in 1X PBS-0,3 % Tween buffer. Washes were performed in 1X PBS-0,3 % Tween buffer.

2.6.8 Real time RT-PCR analysis

The quantitative real-time PCR analysis was performed using Biorad CFX96. Prior to reverse transcription reaction, 1 µg of total RNA was treated with DNase I (Fermentas) according to the provider's instructions for controlling MCMV infection level. After the Dnase treatment, samples were divided into two for RT and noRT control. Dnase treatment was not performed for immunoprecipitation of AGO2. Reverse transcription reaction was performed using miScript reverse transcription II kit (Qiagen) according to the manufacturer's instructions. The resulting cDNA was PCR amplified with Maxima SYBR green kit (Fermentas) in 10 µL reaction volume. For the analysis of miRNA expression, the mature sequence of each miRNA was used to design the forward primer and (Qiagen) was used as reverse primer. Forward primers were used at 0.5 µM and reverse primers were used at and the miScript universal primer at 0.7x. For mRNA analysis forward and reverse primers were used at 0.25 µM each. The PCR program was composed of an initial denaturation step at 95°C for 10 min followed by 44 cycles at 95°C for 15 sec, 55°C for 30 sec and 72°C for 30 sec including melting curve analysis. Data were analyzed as described previously (Buck et al., 2010).

2.6.9 Enrichment of biotinylated proteins by streptavidin pull down

After biotin labeling cells ($4x10^7$ cells per condition) were washed with PBS and were lysed at 25°C in 2 ml lysis buffer (50 mM Tris, pH 7.5, 500 mM NaCl, 0.2% SDS, 1 mM DTT, and 1x Complete protease inhibitor (Roche)) and 200µl of 20% Triton X-100 was added. Lysates were sonicated 5 times 30sec on/30sec off. 1.8ml of 4°C 50 mM Tris (pH 7.5) was added before additional sonication (3 times 30sec on/30 sec off), followed by centrifugation at 16,000 relative centrifugal force for 15 minutes. Supernatants were separated into three replicates and incubated with 200µl of magnetic streptavidin beads (MyOne Steptavadin C1; Invitrogen) overnight at 4°C on a rotator. Beads were collected and washed twice for 8 min on the rotator at 25°C (all subsequent steps at 25°C) in 1 ml wash buffer 1 (2% SDS in

dH_2O). Subsequent washes are with wash buffer 2 (0.1% deoxycholic acid, 1% Triton X-100, 500 mM NaCl, 1 mM EDTA, and 50 mM Hepes, pH 7.5), once with wash buffer 3 (250 mM LiCl, 0.5% NP-40, 0.5% deoxycholate, 1 mM EDTA, and 10 mM Tris, pH 7.5) for 8 min each. Lastly, beads were washed once more with 50mM Tris pH 7.5 to remove any remaining detergents. Finally to elute bound proteins, the wash solution is discarded and beads are resuspended in 150µl of 0.1% SDS and heated at 95°C for 5 min. After the elution beads were magnetized and the elution is transferred to a clean tube, ready to be sent to mass spectrometry analysis. For small scale experiments, the protocol stays the same except that a quarter of the amount of cells is used per condition to obtain on fourth of lysate volume along with 150µl of magnetic streptavidin beads is used.

2.6.10 Mass spectrometry analysis

2.6.10.1 Liquid Samples & In-Solution Approach

2.6.10.1.1 Sample Preparation: in-solution trypsine digestion

Samples were prepared as described in Romilly *et al* and Chicher *et al* (Chicher et al., 2015; Romilly et al., 2014). Each sample was precipitated with 0.1M ammonium acetate in 100% methanol, and proteins were resuspended in 50 mM ammonium bicarbonate. After a reduction-alkylation step (Dithiothreitol 5 mM - Iodoacetamide 10 mM), proteins were digested overnight with 1/25 (W/W) of sequencing-grade porcin trypsin.

2.6.10.1.2 Mass Spectrometry: nanoLC-MS/MS analysis

After digestion, the resulting vacuum-dried peptides were resuspended in 25µL of water containing 0.1% FA (solvent A). The peptide mixtures were analyzed on a nano HPLC Easy nLC 1000 system (Thermo Scientific) coupled to a Q exactive Plus mass spectrometer (Thermo Scientific) operating in positive mode. 5µL of each sample was loaded on a C-18 precolumn (75 µm ID x 2 cm Acclaim Pepmap100; Thermo Scientific) at 2 µL/min in solvent A. After 10 min of desalting and concentration, the pre-column was switched online with the analytical C-18 analytical column (75 µm ID x 15 cm Pepmap100; Thermo Scientific) equilibrated in 95% solvent A and 5% solvent B (0.1% formic acid in acetonitrile). Peptides were eluted by using a 5%-40% gradient of solvent B at a flow rate of 300 nL/min. The duration of the analysis was 120min. The Q exactive Plus was operated in data-dependant

acquisition mode (DDA) with Excalibur. Survey MS scans were acquired in the 350-1500 m/z range. Up to 10 of the most intense multiply charged ions (2+ to 5+) were selected for CID fragmentation. After the conversion of the raw .psd files into a mascot generic file format (.mgf), experimental data were further processed to identify the peptides and proteins related to these spectra.

2.6.10.2 Protein Identification & Relative Quantification

2.6.10.2.1 Database search

Data were searched against the UniProt database (release from 2013-01-09), Mus musculus taxonomy, using a fasta file consisting of a forward database (proteins from N- to C-terminal part) and a decoy database (reversed sequences from C- to N-terminal part, obtained by a Perl script, makeDecoyDB.pl from Bruker). We used Mascot as the database search algorithm (version 2.2, Matrix Science, London, UK) through the ProteinScape 3.1 package (Bruker). Peptide modifications allowed during the search were: N-acetyl (protein), carbamidomethylation (C), oxidation (M), biotine (K) and phophorylation (S) (T). Mass tolerances in MS and MS/MS were set to 10 ppm and 0.02 Da, respectively. Three trypsin missed cleavages sites were allowed. Peptide identifications obtained from Mascot were validated with p-value<0.05 and proteins were validated respecting FDR<1% (False-Discovery Rate)

2.6.10.2.2 Mass Spectrometry - based Quantification: Spectral Count approach

A Spectral Counting (SpC) quantitative strategy was carried on using the Mascot identification results and Proteinscape 3.1 package (Thiele et al., 2010): a spectral count value was first attributed to each protein by counting the number of spectra matching to a given protein (all peptides, all charge states). As Spectral Counting is affected by the size of the protein, a normalization step was performed by dividing the SpC value by the molecular weight (MW) of the protein. Proteins identified in the same sample were then sorted according to their SpC/MW ratio, reflecting their relative abundance.

DISCUSSION

A miRNA, once loaded into RISC, will negatively regulate target mRNAs through sequence specific interactions by the recruitment of several factors through protein-protein interactions. For a longtime, miRNAs have been considered stable molecules, suggesting that the control of miRNA abundance would only act at the level of their biogenesis. Indeed, several examples of miRNA expression regulation at different levels of miRNA biogenesis have been uncovered. However, as other molecules in the cell, the abundance of a miRNA will depend on the balance between its biogenesis and stability. During certain conditions like environmental changes/stresses, development or the cell cycle, the expression level of certain miRNAs have been observed to rapidly change. This is not surprising as the cell has to adapt its genetic program to the ever-changing conditions and the miRNA pathway represents one of the ways to undertake this adaptation. In recent years, RNA sequence modification by non-templated nucleotide additions has emerged as a new way to modulate miRNA action or stability. These modifications can affect miRNA by two different mechanisms either by modulating their activity towards target mRNAs or by modulating their stability.

Target RNA-mediated miRNA degradation (TDMD) happens when a miRNA encounters a perfect or extensively matching target RNA which induces its modification by non-templated nucleotide additions (tailing) and subsequent degradation by trimming (Ameres et al., 2010; Baccarini et al., 2011). This is reminiscent of what happens to unprotected plant miRNAs and fly siRNAs since they function similarly by recognizing their targets with perfect match interactions. As mammalian and fly miRNAs do not have this protective modification, they are sensitive to TDMD in case of extensive pairing. One might speculate that animal miRNAs have evolved to engage in partially complementary interactions with their targets (Bartel, 2009) to avoid degradation through TDMD, making extensive or perfect pairing of an animal miRNA to its target is a very rare occurrence (Yekta et al., 2004).

So far, natural examples of TDMD have only been discovered during herpesvirus infections, where host miRNAs are targeted for degradation after pairing with viral RNAs (Cazalla et al., 2010; Lee et al., 2013; Libri et al., 2012; Marcinowski et al., 2012). This demonstrates that viruses evolved to take advantage of TDMD, in order to modulate the cellular environment for their own benefit. This hypothesis is supported by the fact that the cellular miRNAs

targeted during HCMV and MCMV infection have anti-viral roles (Lee et al., 2013; Marcinowski et al., 2012).

During my thesis, we have used MCMV infection and the interaction between m169 and miR-27 as a model to study several aspects of TDMD mechanism. Moreover, I set up conditions to perform proximity labeling of AGO2 during MCMV infection, in order to discover viral or host protein partners that might be differentially engaging in interactions with AGO2 during infection to modulate its activity.

TDMD is a process that is triggered following extensive pairing of the miRNA to its target and relative abundance between the miRNA and the target is an essential component of this mechanism. In the case of miR-27/m169, the viral transcript is the most abundant one in infected cell (Juranic Lisnic et al., 2013). The bulge formed in the middle of miR-27 interacting with m169 seems to be a common feature of other natural examples of TDMD, such as the ones occurring during HVS and HCMV infections (Cazalla et al., 2010; Lee et al., 2013). The fact that viruses have evolved to maintain a bulge in the middle of the paired RNAs makes sense as otherwise the target would be subjected to slicing by AGO2. This is consistent with bulge targets being less efficiently suppressed by a miRNA than perfectly matching targets (Doench et al., 2003). Moreover, expression of a bulge target as a miRNA sponge can saturate a miRNA at a lower concentration than a perfectly matching target (Ebert et al., 2007). However, the bulge formed in the interaction between miR-27 and m169 is particularly large with 5 mismatches and 2 G:U wobbles, whereas a previous account in *Drosophila* only showed tolerance of a 3 nucleotide bulges for TDMD to occur (Ameres et al., 2010). The fact that in our experimental settings TDMD of miR-27 is abrogated when only the matching of the most 3' proximal nucleotide of miR-27 is abolished, shows that the bulge is too large to accommodate any additional mismatch. In fact, we showed that the bulged interaction of miR-27/m169 is approximately 100-fold less efficient than perfectly matching anti-miR-27 for the induction of miR-27 tailing and trimming. The fact that TDMD can still be induced during infection is probably due to the fact that m169 is replacing what it lacks in efficacy with its high abundance, assuming that this bulged interaction is preferable to having a perfectly matching target site. The importance of the relative abundance between miRNA and the target in TDMD is backed up by findings of a recent TDMD study in neuronal cells, where TDMD was found to be more efficient for low compared to high

abundance miRNAs, and where the authors also showed that increasing the levels of a miRNA exogenously resulted in less efficient TDMD (de la Mata et al., 2015).

TDMD of miR-27 is accompanied by its tailing and trimming during MCMV infection. Although it was not verified for HVS and HCMV infection, in other reports where TDMD is induced through expression of artificial highly complementary targets, the modification of the miRNA by nucleotide additions was shown to occur (Ameres et al., 2010; Baccarini et al., 2011; de la Mata et al., 2015; Xie et al., 2012). Whether tailing and trimming occurs while the miRNA is still in AGO or if is first unloaded and then modified is an important question. *In vitro*, extensive binding of a miRNA to its target results in the unloading of the miRNA from AGO2 (De et al., 2013). This suggests that AGO is capable of ejecting the miRNA without the need for miRNA tailing. Initially, our laboratory had shown that extensively tailed miR-27 species were less represented in AGO2-IP fractions compared to total RNA (Marcinowski et al., 2012). We later showed that the modification of the miR-27 by tailing was at least initiated while it is in AGO2 with some of the modified species still present inside AGO2. It therefore seems like the tailing of miR-27 would ultimately induce its unloading from AGO, which is similar to what others have observed where AGO2 immuno-precipitated fraction compared to total RNA is quite similar for the tailed miRNA (de la Mata et al., 2015). AGO proteins can carry a miRNA that is longer than a classical length miRNA, the most striking example is miR-451 which is accommodated in AGO2 in its a pre-miRNA form and can stay in AGO2 after its slicing with quite a long tail awaiting trimming (Cifuentes et al., 2010).

We and others have shown that compared to miRNA-mediated mRNA repression that have been shown to work cooperatively when several binding sites are present on the target mRNA (Broderick et al., 2011; Grimson et al., 2007; Saetrom et al., 2007), TDMD works in a non-cooperative manner, where multiple extensive binding sites do not appear to increase TDMD efficacy (de la Mata et al., 2015). This is probably why in none of the reported cases of TDMD during herpesvirus infections, target RNAs possess multiple binding sites for the miRNA (Cazalla et al., 2010; Lee et al., 2013; Libri et al., 2012; Marcinowski et al., 2012). This also makes sense, since multiple binding sites would increase the efficiency of miRNA-mediated repression of the target RNA, reducing in turn the efficacy of TDMD. This finding adds to the current understanding of miRNA sponges, showing that different constraints act on TDMD-inducing sponges and sponges that titrate miRNAs. Recently discovered circular RNAs (circRNAs) that titrate miR-7, possess several dozens of miR-7 binding sites (Hansen

et al., 2013; Memczak et al., 2013). These binding sites are seed match only sites that do not induce TDMD of miR-7, and since the circular nature of this RNA makes it refractory to any miRNA mediated degradation, it can get away with having that many sites. This is true as long as the binding sites are canonical sites that do not induce miRNA induced slicing. Interestingly, a perfectly matching binding site for miR-671 is found on this circRNA controlling the levels of this circular sponge (Hansen et al., 2013).

Our proteomic approach is based upon a previously described method that allows purification of AGO complexes programmed with a specific miRNA from cell lysates, through the use of biotinylated 2'O-methylated oligoribonucleotides that are partially complementary to the specific miRNA (Flores-Jasso et al., 2013). In our case, the biotinylated 2'O-methylated oligoribonucleotide has two functions: as an anti-miRNA it induces tailing and trimming of the miRNA, and the attached biotin allows the capture of TDMD nucleoprotein complexes whether the miRNA is loaded in AGO or not. This approach gave us among other factors, two really interesting candidates; one is TUT1 and the other is Dis3l2. TUT1 belongs to the family of TUTases which counts seven family members six of which has been shown to act on miRNA (Wyman et al., 2011). Since the tails of miR-27 during its destabilization are composed of A and U residues, TUT1 would make sense since it has been shown to have adenylyl and uridylyl-tranferase activities (Mellman et al., 2008; Trippe et al., 2003, 2006). Indeed, TUT1 action on miRNA has been tested by knockdown experiments which discovered that it adds 3' A and U residues on miRNAs (Wyman et al., 2011) and it was shown to affect some miRNAs directly by 3' nucleotide additions and broadly affect miRNA abundance independently of its nucleotidyl-transferase activity (Knouf et al., 2013).

Dis3l2 is a 3' to 5' exoribonuclease that is involved in the degradation of polyuridylated RNA substrates, such as pre-let-7 (Chang et al., 2013; Ustianenko et al., 2013). This suggests that Dis3l2 recognizes its substrates by their 3' uridine residues. To support this idea, in *S. pombe,* Dis3l2 has been shown to target mRNAs, and its depletion results in the accumulation of uridylated mRNAs, suggesting that it preferentially degrades uridylated RNA substrates (Malecki et al., 2013). Structural analysis of mouse Dis3l2 revealed its specificity toward U residues on which it acts the most effectively, with several U specific interactions made by the nuclease (Faehnle et al., 2014). Similarly to *S. pombe*, human Dis3l2 has been shown to be implicated in the degradation of a subset of mRNAs (Lubas et al., 2013), however *in vitro* experiments showed that Dis3l2 was capable of recognizing and degrading RNAs that have at

least a double adenine residues at their 3' ends (Lubas et al., 2013). Other than on pre-let-7, TUTases and Dis3l2 have been shown to act synergistically in different contexts not only on mRNA but also on several types of noncoding RNA (Pirouz et al., 2016; Łabno et al., 2016; Thomas et al., 2015; Lim et al., 2014). In light of these accounts, we continued with the validation of the role of Dis3l2 and TUT1 in TDMD.

Both m169 and miR-27 are localized in the cytoplasm therefore TDMD most likely occurs in the cytoplasm (Libri et al., 2012). Our two candidates should therefore be localized in the same cellular compartment as them. TUT1 was shown to be a nuclear protein in earlier reports (Mellman et al., 2008), but it was recently shown to be also cytoplasmic under specific conditions (Mohan et al., 2015). Our experiments confirm the cytoplasmic localization of TUT1 and Dis3l2 as well as the nuclear and cytoplasmic localization of AGO2 in agreement with previous reports (Ameyar-Zazoua et al., 2012; Lubas et al., 2013; Malecki et al., 2013). Although, TDMD most likely occurs in the cytoplasm, one might speculate that at least some steps could take place in the nucleus. A particularly interesting example is miR-29b that harbors a U rich motif in its middle region required for its fast turnover (Zhang et al., 2011) and also happens to be a miRNA mostly localized in the nucleus (Hwang et al., 2007). Similarly, HSUR1-induced miR-27 degradation might also in part happen in the nucleus as HSUR1 and miR-27 containing RISC might shuttle between the cytoplasm and the nucleus (Cazalla et al., 2010).

Our efforts in validating TUT1 function in TDMD failed, this might either mean that TUT1 is indeed not implicated in TDMD or that its implication might have been difficult to demonstrate due to several reasons. One reason might be due to the fact that TUTases are known to complement each other, as was already shown by the redundant action of TUT2, TUT4 and TUT7 on different RNA substrates (Heo et al., 2012; Kim et al., 2015; Lim et al., 2014). Moreover, knockdown of some TUTases has been reported to cause an elevation of the expression levels of other TUTases (Wyman et al., 2011). Indeed, following the knockdown of TUT1, several miRNAs have been shown to acquire new tails possibly due to the action of other enzymes (Knouf et al., 2013). Similarly in plants, *hen1* null mutants show miRNA polyuridylation by the action of HESO1 due to the loss of miRNA 2'O-methylation (Zhao et al., 2012), however in double *hen1 heso1* null mutants, some miRNAs still show polyuridylation and this has been shown to be catalyzed by the action of URT1 (Wang et al., 2015b). These results confirm that TDMD is a complicated process that might involve several

redundant actors not only in the tailing but also trimming process. Since with the advent of CRISPR/CAS9 (clustered regularly interspaced short palindromic repeats/CRISPR-associated protein) technology, creating a knock-out cell line is becoming more and more routine, it can be used to create knock-out cell-lines for single or multiple TUTases. However, failure to generate a double knockout of TUT4 and TUT7 has already been reported, suggesting their combined activity to be essential (Lim et al., 2014). Other TUTases might also be essential however either alone or in combination, and two recent studies reported a list of essential genes in human cell lines (Blomen et al., 2015; Wang et al., 2015a) which will be helpful to determine an experimental strategy for gene function studies. TUT1 was among these essential genes, indicating that it will prove difficult to study its involvement in TDMD by generating knock-out cell lines.

Dis3l2 knockdown did allow us to detect by small RNA sequencing a small reduction in the trimming of miR-27 after TDMD induction by anti-miR-27. However, we could more clearly observe a significant stabilization of miR-27 when we overexpressed a catalytic mutant of Dis3l2 and when TDMD was induced through transfection of anti-miR-27 or by MCMV infection. The catalytic mutant of Dis3l2 was previously defined to be unable to degrade its substrate but nonetheless keep its ability to bind its RNA substrates (Faehnle et al., 2014; Lubas et al., 2013; Ustianenko et al., 2013). This might be expected as Dis3l2 is a highly processive enzyme and its knockdown by siRNA will never result in its complete clearance at the protein level. However, in either condition the miRNA stabilization was not complete. As miR-27 tails are composed of a mix of A and U residues during infection and Dis3l2 has an affinity toward U stretches, we might only have been able to stabilize those that possess U tails but not A tails. To verify this, we should perform small RNA sequencing in the overexpressed Dis3l2 catalytic mutant condition and look at the identities of the tails of stabilized miR-27 species, a similar approach to (Pirouz et al., 2016). Ultimately, we should knock-out Dis3l2 with CRISPR/CAS9 and challenge these cells with MCMV infection to observe miR-27 tails. Although we observed the stabilization of miR-27 with the overexpression of the catalytic mutant, it may very well be due in part to this mutant binding to and remaining bound on an RNA in proximity of AGO, thereby preventing the action of other exoribonucleases on miR-27. Cross-linking immunoprecipitation of Dis3l2 catalytic mutant followed by RNA sequencing can give us the answer regarding the availability of miR-27 as a direct substrate. Furthermore, redundancy between exoribonucleases might again be at play here, as redundancy in miRNA degradation has been shown in other organisms: in

plants several SDNs have to be depleted together to give rise to an observable phenotype (Ramachandran and Chen, 2008); and XRN1 and XRN2 act redundantly on miRNAs in *C. elegans* during TMMP (Chatterjee et al., 2011).

Tailing of the miRNA by non-templated nucleotide additions during TDMD is thought to signal the miRNA for degradation by trimming, this same signal also occurs on unprotected plant miRNA and fly siRNAs. These tails mostly are composed of A and U residues and uridylation of RNAs have been associated with degradation in several organisms (Lim et al., 2014; Shen and Goodman, 2004; Wang et al., 2015b; Zhao et al., 2012). However, one could also imagine that other kinds of modifications could also work as signals to regulate miRNAs, like chemical changes on the RNA molecule that would be undetectable by most popular miRNA detection methods or be refractory to cloning applications for sequencing. One example of chemical modification involved in miRNA biogenesis is methylation. 5' monophosphate of pre-miR-145 and pre-miR-23b are O-methylated by a human RNA methyltransferase called BCDIN3D, that interferes negatively with the recognition of these pre-miRNA by Dicer, thereby regulating their biogenesis (Xhemalce et al., 2012). Global N^6-Methyladenosine (m6A) methylation of pri-miRNA by methyltransferase like 3 (METTL3) have recently been discovered, this modification helps DGCR8 recognition of pri-miRNAs (Alarcón et al., 2015). This modification is suggested to mark pri-miRNAs for recognition by the Microprocessor, helping it discriminate against other hairpin structures. Research on these kinds of modifications could reveal a new layer of complexity in miRNA regulation that remains for now obscure.

The study of host-virus interaction has helped to advance our understanding of many cellular processes. miRNA pathway is one of the levels of interaction that viruses and their hosts use to engage in with each other. Several viruses have evolved to use the host machinery to express their own set of miRNAs, as they represent a non-immunogenic tool to modulate the host gene expression program. Moreover, viruses have been shown to interact with the cellular miRNA pathway at different levels: acting at the level of miRNA turnover like in HVS, HCMV and MCMV infections that induce specific degradation of cellular miRNA; acting more globally on host miRNA, HIV-1 has been shown to downregulate Dicer (Coley et al., 2010), Exportin-5 blockade by noncoding RNA VA1 in adenovirus infected cells (Lu and Cullen, 2004) or VP55 expressed by vaccinia virus that induces the clearance of host miRNAs (Backes et al., 2012). Lastly, post translational modifications like poly-ADP-ribosylation of

Argonaute has been shown to occur during stress conditions (Leung et al., 2011), including infections by RNA viruses (Seo et al., 2013). It has been suggested that the reduction in the activity of RISC mediated silencing is advantageous to the host. This shows that viruses interact with the host miRNA pathway by employing several strategies either by acting on RNA or on protein level.

By using MCMV infection as a model we started to set up a protocol to identify AGO2 partners during infection to discover factors that would interact with AGO2 and modulate its activity. To this end, we have chosen a proximity labelling approach called BioID which presents several advantages over classical methods of purifying complexes of interest, as discussed previously. Although we were able to identify known partners of AGO2, we encountered several problems in the realization of this approach that has limited our analysis to the identification of a small number of proteins with few spectral counts. Some of these problems are due to drawbacks inherent to this technique.

BioID technique allows to pulldown and identify naturally biotinylated proteins found in the cell, when the labelling efficiency is low, the proportion of tagged proteins of interest will be smaller compared to those naturally biotinylated. Indeed, in our experiment we found that our samples contained a lot of naturally biotinylated proteins. Low levels of labelling can either result from low expression of BirA* tagged protein of interest or shorter than necessary times of labelling. In our case, we want to stay as close as possible to the expression level of endogenous AGO2 with the expression of our tagged BirA*-mAGO2. Overexpression of bait proteins can result in an interaction network or subcellular localization that might not be physiological. This can be observed for AGO2 in a recent study, where its partners identified following the immunoprecipitation of overexpressed tagged AGO2 or of endogenous AGO2 were quite different (Kalantari et al., 2016); or for GFP-tagged Dicer's localization that is strictly cytoplasmic when its expression is controlled by its endogenous promoter (Much et al., 2016) compared to previous studies that demonstrated that it can also be nuclear when overexpressed (White et al., 2014). For these reasons, we do not want to increase the expression level of our BirA*-mAGO2. Lengthening the time of labelling past 24h of infection would ameliorate this ratio, however the choice of time of labelling will also depend on the time window of infection we want to visualize. We chose 24h of infection to increase our chances to identify proteins involved in TDMD as well as proteins that might be involved

in RISC turnover as a strong expression of viral miRNAs happens during this time window (Dölken et al., 2007).

Streptavidin contamination is another source of problem when it comes to the identification of our biotinylated proteins. As we elute pulled-down proteins by heating, this treatment contaminates the sample to some degree with streptavidin molecules released from the beads. The contaminating streptavidin molecules will hamper the mass spectrometry analysis, by masking the identification of other peptides if they are over-represented by allocating unnecessary time during mass spectrometry. To minimize this problem, one should not use more streptavidin beads than necessary. A bead titration step must be performed to determine the minimal quantity of beads required for the experiment (Hung et al., 2016). Following the pull-down, we performed our analysis by eluting our pulled-down proteins by heating the beads at the end of the protocol, however other methods of elution exist in the literature. On-bead trypsic digestion can be used or alternatively proteins can be eluted by boiling in sample buffer followed by gel separation and band cutting. The latter might be a good solution to our problem as it can help getting rid of some of the low-molecular weight contaminants like streptavidin. This also gives the advantage to target specific parts of the gel to prioritize analysis of the areas of interest. However, gel separation and cutting bands during the sample preparation can increase the vulnerability of the sample to typical sources of contamination like keratins, and as such it might be better to try and avoid them. One method that has been proposed to minimize the detrimental effects of contaminant proteins for mass spectrometry analysis is to modify the run with an exclusion list. This list that contains the masses of typical contaminants is provided to the mass spectrometer and commands it to ignore those masses in order to allocate more time to identify peptides of interest. This list has been developed for the most classical contaminants like keratins and trypsin in mass spectrometry runs (Hodge et al., 2013). In our case, we can imagine to include in the exclusion list, the masses of peptides deriving from streptavidin and the naturally biotinylated proteins, this could potentially increase the efficiency of our analyses. As such, several steps of our labelling, pull-down and analysis are to be improved in order to be able to get the optimal conditions to identify proteins of interest.

With our approach we could identify known partners of Argonaute or proteins implicated in the miRNA pathway like TNRC6 (Lian et al., 2009; Pfaff et al., 2013), CNOTI (Chekulaeva et al., 2011), EDC4 (Jonas and Izaurralde, 2013) and HSP90 (Iwasaki et al., 2010; Johnston

et al., 2010). The spectral counts of these factors seem to have a tendency to go up or down slightly in infection conditions compared to the mock, although at this stage we can only speculate about these tendencies. We observed TNRC6 and CNOT1 to have lower spectral counts in infection conditions, which might indicate less miRNA mediated repression happening during infection. Alternatively, this decrease might be due to the fact that BirA*-mAGO2 counts also go down with infection. Decreasing mAGO2 spectral counts in infection might be due to cell death occuring in infection conditions, however this seems improbable since we virtually have the same spectral counts for naturally biotinylated proteins, meaning that we probably had the same number of cells for each conditions at the beginning of the pull-down. This hypothesis might be supported by the increase observed in HSP90/HSC70 spectra which would make sense as viral miRNAs are being synthesized, putting more AGO2 in the process of loading miRNAs. However, we did not identify Dicer or TRBP in any of our conditions, the levels of which would also need to go up if the latter were true, as they are the other members of the RISC loading complex (Chendrimada et al., 2005; Gregory et al., 2005; Maniataki and Mourelatos, 2005).

In order for our experiment to be quantitative, we first of all have to repeat it several times, to account for biological and technical variations. Analysis of the mass spectrometry data can be implemented by normalization methods that will allow for relative quantification between conditions. For a semi-quantitative proteomic analysis, we can use normalized spectral index (SINQ) method (Griffin et al., 2010). This label free quantitation method calculates a normalized spectral count that will depend on several parameters of all the peptides for the identified protein and first normalized to correct for protein loading differences in different datasets and normalized again with protein length as they can produce many more peptides than small proteins. This method was applied recently in a study that identified AGO2 partners in the cytoplasm as well as in the nucleus (Kalantari et al., 2016). We can also go with stable isotope labeling with amino acids in cell culture (SILAC) to label our different conditions with light and heavy amino acids that would allow us to relatively quantify the abundance of each protein in each condition. This method has been used to identify AGO2 partner proteins in the presence or absence of miRNAs (Frohn et al., 2012).

Finally, the proximity labelling approach offers us the possibility to identify not only the direct partners of AGO2 but also the proteins that are in its proximity like RBPs. They are involved in the modulation of the activity of RISC like it was demonstrated for HUR or PUM

(Kedde et al., 2010; Meisner and Filipowicz, 2011). As the miRNA modifying enzymes like TUTases or exoribonucleases act on a broad spectrum of RNA substrates, their specificity towards miRNA can be oriented by accessory proteins, for which RBPs would be candidates. However, these interactions could be detectable only under certain conditions or be too transient to be detected by classical immunoprecipitation approaches. BioID approach is a valuable technique that can overcome those limitations (Lambert et al., 2015). This method coupled to an infection model can allow us to broaden our understanding of the regulation of the miRNA pathway not only through the action of its protein partners but also by post translational modifications on its components.

Finally, this work allowed us to get some insights into how TDMD works. The fact that TDMD is a conserved cellular process that viruses take advantage of shows the importance of this mechanism. The importance of the homeostasis of the miRNA pathway is increasingly evident as at every level of the miRNA pathway there are examples of regulatory processes. TDMD is a rapid and efficient means of active regulation of miRNA activity through its stability. Highly abundant extensively complementary target RNAs whether they are coding or non-coding can potentially induce TDMD of a cognate miRNA. Neuronal cells have been shown to have highly effective TDMD, probably due to their needs that require highly dynamic and local regulation of gene expression. We showed the implication of Dis3l2 in the trimming step of TDMD. This enzyme has emerged as a regulator of mRNA but also non-coding RNAs like pre-miRNAs and snRNAs. As substrates of Dis3l2 are 3'end uridylated RNAs, it has a tight relationship with TUTases as their prior action is required. TDMD is an additional model to study how Dis3l2 and TUTases can synergistically act on RNAs. Redundancy of certain TUTases also hints to the robustness of RNA metabolism, which can be a barrier to assess the implication of one particular TUTase. It would anyway be surprising to think that only one enzyme would be responsible for the tailing or trimming of all miRNAs, considering the diversity of processes that miRNAs are engaged in, several enzymes and accessory proteins are likely involved. As such, our proteomic approach can be fruitful by allowing us to discover not only RNA modifying enzymes but also other factors that can modulate the activity of the RISC either by post-translational modifications or by association with RNA binding proteins.

REFERENCES

A

Alarcón, C.R., Lee, H., Goodarzi, H., Halberg, N., and Tavazoie, S.F. (2015). N6-methyl-adenosine (m6A) marks primary microRNAs for processing. Nature *519*, 482–485.

Ameres, S.L., Horwich, M.D., Hung, J.H., Xu, J., Ghildiyal, M., Weng, Z., and Zamore, P.D. (2010). Target RNA-directed trimming and tailing of small silencing RNAs. Science *328*, 1534–1539.

Ameyar-Zazoua, M., Rachez, C., Souidi, M., Robin, P., Fritsch, L., Young, R., Morozova, N., Fenouil, R., Descostes, N., Andrau, J.-C., et al. (2012). Argonaute proteins couple chromatin silencing to alternative splicing. Nat. Struct. Mol. Biol. *19*, 998–1004.

Auyeung, V.C., Ulitsky, I., McGeary, S.E., and Bartel, D.P. (2013). Beyond Secondary Structure: Primary-Sequence Determinants License Pri-miRNA Hairpins for Processing. Cell *152*, 844–858.

B

Babiarz, J.E., Ruby, J.G., Wang, Y., Bartel, D.P., and Blelloch, R. (2008). Mouse ES cells express endogenous shRNAs, siRNAs, and other Microprocessor-independent, Dicer-dependent small RNAs. Genes Dev *22*, 2773–2785.

Baccarini, A., Chauhan, H., Gardner, T.J., Jayaprakash, A.D., Sachidanandam, R., and Brown, B.D. (2011). Kinetic analysis reveals the fate of a microRNA following target regulation in mammalian cells. Curr. Biol. *21*, 369–376.

Backes, S., Shapiro, J.S., Sabin, L.R., Pham, A.M., Reyes, I., Moss, B., Cherry, S., and Tenoever, B.R. (2012). Degradation of Host MicroRNAs by Poxvirus Poly(A) Polymerase Reveals Terminal RNA Methylation as a Protective Antiviral Mechanism. Cell Host Microbe *12*, 200–210.

Baek, D., Villen, J., Shin, C., Camargo, F.D., Gygi, S.P., and Bartel, D.P. (2008). The impact of microRNAs on protein output. Nature *455*, 64–71.

Bail, S., Swerdel, M., Liu, H., Jiao, X., Goff, L.A., Hart, R.P., and Kiledjian, M. (2010). Differential regulation of microRNA stability. RNA N. Y. N *16*, 1032–1039.

Baran-Gale, J., Fannin, E.E., Kurtz, C.L., and Sethupathy, P. (2013). Beta Cell 5′-Shifted isomiRs Are Candidate Regulatory Hubs in Type 2 Diabetes. PLOS ONE *8*, e73240.

Bartel, D.P. (2009). MicroRNAs: target recognition and regulatory functions. Cell *136*, 215–233.

Bartel, D.P., and Chen, C.Z. (2004). Micromanagers of gene expression: the potentially widespread influence of metazoan microRNAs. Nat Rev Genet *5*, 396–400.

Baskerville, S., and Bartel, D.P. (2005). Microarray profiling of microRNAs reveals frequent coexpression with neighboring miRNAs and host genes. RNA *11*, 241–247.

Bazzini, A.A., Lee, M.T., and Giraldez, A.J. (2012). Ribosome profiling shows that miR-430 reduces translation before causing mRNA decay in zebrafish. Science *336*, 233–237.

Beckett, D., Kovaleva, E., and Schatz, P.J. (1999). A minimal peptide substrate in biotin holoenzyme synthetase-catalyzed biotinylation. Protein Sci. *8*, 921–929.

Bennasser, Y., Chable-Bessia, C., Triboulet, R., Gibbings, D., Gwizdek, C., Dargemont, C., Kremer, E.J., Voinnet, O., and Benkirane, M. (2011). Competition for XPO5 binding between Dicer mRNA, pre-miRNA and viral RNA regulates human Dicer levels. Nat. Struct. Mol. Biol. *18*, 323–327.

Berezikov, E., Chung, W.J., Willis, J., Cuppen, E., and Lai, E.C. (2007). Mammalian mirtron genes. Mol Cell *28*, 328–336.

Berndt, H., Harnisch, C., Rammelt, C., Stöhr, N., Zirkel, A., Dohm, J.C., Himmelbauer, H., Tavanez, J.-P., Hüttelmaier, S., and Wahle, E. (2012). Maturation of mammalian H/ACA box snoRNAs: PAPD5-dependent adenylation and PARN-dependent trimming. RNA *18*, 958–972.

Bernstein, E., Kim, S.Y., Carmell, M.A., Murchison, E.P., Alcorn, H., Li, M.Z., Mills, A.A., Elledge, S.J., Anderson, K.V., and Hannon, G.J. (2003). Dicer is essential for mouse development. Nat Genet *35*, 215–217.

Betancur, J.G., and Tomari, Y. (2012). Dicer is dispensable for asymmetric RISC loading in mammals. RNA N. Y. N *18*, 24–30.

Bhattacharyya, S.N., Habermacher, R., Martine, U., Closs, E.I., and Filipowicz, W. (2006). Relief of microRNA-mediated translational repression in human cells subjected to stress. Cell *125*, 1111–1124.

Blomen, V.A., Májek, P., Jae, L.T., Bigenzahn, J.W., Nieuwenhuis, J., Staring, J., Sacco, R., Diemen, F.R. van, Olk, N., Stukalov, A., et al. (2015). Gene essentiality and synthetic lethality in haploid human cells. Science *350*, 1092–1096.

Blow, M.J., Grocock, R.J., van Dongen, S., Enright, A.J., Dicks, E., Futreal, P.A., Wooster, R., and Stratton, M.R. (2006). RNA editing of human microRNAs. Genome Biol *7*, R27.

Boele, J., Persson, H., Shin, J.W., Ishizu, Y., Newie, I.S., Søkilde, R., Hawkins, S.M., Coarfa, C., Ikeda, K., Takayama, K., et al. (2014). PAPD5-mediated 3' adenylation and subsequent degradation of miR-21 is disrupted in proliferative disease. Proc. Natl. Acad. Sci. U. S. A. *111*, 11467–11472.

Bogerd, H.P., Karnowski, H.W., Cai, X., Shin, J., Pohlers, M., and Cullen, B.R. (2010). A mammalian herpesvirus uses noncanonical expression and processing mechanisms to generate viral MicroRNAs. Mol. Cell *37*, 135–142.

Bohnsack, M.T., Czaplinski, K., and Gorlich, D. (2004). Exportin 5 is a RanGTP-dependent dsRNA-binding protein that mediates nuclear export of pre-miRNAs. RNA *10*, 185–191.

Bortolamiol-Becet, D., Hu, F., Jee, D., Wen, J., Okamura, K., Lin, C.-J., Ameres, S.L., and Lai, E.C. (2015). Selective Suppression of the Splicing-Mediated MicroRNA Pathway by the Terminal Uridyltransferase Tailor. Mol. Cell *59*, 217–228.

Braun, J.E., Huntzinger, E., Fauser, M., and Izaurralde, E. (2011). GW182 proteins directly recruit cytoplasmic deadenylase complexes to miRNA targets. Mol. Cell *44*, 120–133.

Braun, J.E., Truffault, V., Boland, A., Huntzinger, E., Chang, C.-T., Haas, G., Weichenrieder, O., Coles, M., and Izaurralde, E. (2012). A direct interaction between DCP1 and XRN1 couples mRNA decapping to 5' exonucleolytic degradation. Nat. Struct. Mol. Biol. *19*, 1324–1331.

Brennecke, J., Stark, A., Russell, R.B., and Cohen, S.M. (2005). Principles of microRNA-target recognition. PLoS Biol *3*, e85.

Brenner, J.L., Jasiewicz, K.L., Fahley, A.F., Kemp, B.J., and Abbott, A.L. (2010). Loss of Individual MicroRNAs Causes Mutant Phenotypes in Sensitized Genetic Backgrounds in C. elegans. Curr. Biol. *20*, 1321–1325.

Broderick, J.A., Salomon, W.E., Ryder, S.P., Aronin, N., and Zamore, P.D. (2011). Argonaute protein identity and pairing geometry determine cooperativity in mammalian RNA silencing. RNA *17*, 1858–1869.

Brückner, A., Polge, C., Lentze, N., Auerbach, D., and Schlattner, U. (2009). Yeast Two-Hybrid, a Powerful Tool for Systems Biology. Int. J. Mol. Sci. *10*, 2763–2788.

Buck, A.H., Perot, J., Chisholm, M.A., Kumar, D.S., Tuddenham, L., Cognat, V., Marcinowski, L., Dolken, L., and Pfeffer, S. (2010). Post-transcriptional regulation of miR-27 in murine cytomegalovirus infection. RNA *16*, 307–315.

Burroughs, A.M., Ando, Y., de Hoon, M.J.L., Tomaru, Y., Nishibu, T., Ukekawa, R., Funakoshi, T., Kurokawa, T., Suzuki, H., Hayashizaki, Y., et al. (2010). A comprehensive survey of 3' animal miRNA modification events and a possible role for 3' adenylation in modulating miRNA targeting effectiveness. Genome Res. *20*, 1398–1410.

C

Cai, X., Hagedorn, C.H., and Cullen, B.R. (2004). Human microRNAs are processed from capped, polyadenylated transcripts that can also function as mRNAs. RNA *10*, 1957–1966.

Calin, G.A., Ferracin, M., Cimmino, A., Di Leva, G., Shimizu, M., Wojcik, S.E., Iorio, M.V., Visone, R., Sever, N.I., Fabbri, M., et al. (2005). A MicroRNA Signature Associated with Prognosis and Progression in Chronic Lymphocytic Leukemia. N. Engl. J. Med. *353*, 1793–1801.

Cannon, M.J., Schmid, D.S., and Hyde, T.B. (2010). Review of cytomegalovirus seroprevalence and demographic characteristics associated with infection. Rev. Med. Virol. *20*, 202–213.

Carmell, M.A., Xuan, Z., Zhang, M.Q., and Hannon, G.J. (2002). The Argonaute family: tentacles that reach into RNAi, developmental control, stem cell maintenance, and tumorigenesis. Genes Dev *16*, 2733–2742.

Cazalla, D., Yario, T., Steitz, J.A., and Steitz, J. (2010). Down-regulation of a host microRNA by a Herpesvirus saimiri noncoding RNA. Science *328*, 1563–1566.

Cazalla, D., Xie, M., and Steitz, J.A. (2011). A primate herpesvirus uses the integrator complex to generate viral microRNAs. Mol. Cell *43*, 982–992.

Chan, Y.-T., Lin, Y.-C., Lin, R.-J., Kuo, H.-H., Thang, W.-C., Chiu, K.-P., and Yu, A.L. (2013). Concordant and Discordant Regulation of Target Genes by miR-31 and Its Isoforms. PLOS ONE *8*, e58169.

Chang, H.-M., Triboulet, R., Thornton, J.E., and Gregory, R.I. (2013). A role for the Perlman syndrome exonuclease Dis3l2 in the Lin28-let-7 pathway. Nature *497*, 244–248.

Chang, T.-C., Yu, D., Lee, Y.-S., Wentzel, E.A., Arking, D.E., West, K.M., Dang, C.V., Thomas-Tikhonenko, A., and Mendell, J.T. (2008). Widespread microRNA repression by Myc contributes to tumorigenesis. Nat. Genet. *40*, 43–50.

Chatterjee, S., and Grosshans, H. (2009). Active turnover modulates mature microRNA activity in Caenorhabditis elegans. Nature *461*, 546–549.

Chatterjee, S., Fasler, M., Büssing, I., and Grosshans, H. (2011). Target-mediated protection of endogenous microRNAs in C. elegans. Dev. Cell *20*, 388–396.

Chekulaeva, M., Mathys, H., Zipprich, J.T., Attig, J., Colic, M., Parker, R., and Filipowicz, W. (2011). miRNA repression involves GW182-mediated recruitment of CCR4–NOT through conserved W-containing motifs. Nat. Struct. Mol. Biol. *18*, 1218–1226.

Cheloufi, S., Dos Santos, C.O., Chong, M.M.W., and Hannon, G.J. (2010). A dicer-independent miRNA biogenesis pathway that requires Ago catalysis. Nature *465*, 584–589.

Chen, C.-L., Hu, Y., Udeshi, N.D., Lau, T.Y., Wirtz-Peitz, F., He, L., Ting, A.Y., Carr, S.A., and Perrimon, N. (2015). Proteomic mapping in live Drosophila tissues using an engineered ascorbate peroxidase. Proc. Natl. Acad. Sci. U. S. A. *112*, 12093–12098.

Chen, Y., Boland, A., Kuzuoğlu-Öztürk, D., Bawankar, P., Loh, B., Chang, C.-T., Weichenrieder, O., and Izaurralde, E. (2014). A DDX6-CNOT1 complex and W-binding pockets in CNOT9 reveal direct links between miRNA target recognition and silencing. Mol. Cell *54*, 737–750.

Chendrimada, T.P., Gregory, R.I., Kumaraswamy, E., Norman, J., Cooch, N., Nishikura, K., and Shiekhattar, R. (2005). TRBP recruits the Dicer complex to Ago2 for microRNA processing and gene silencing. Nature *436*, 740–744.

Chi, S.W., Zang, J.B., Mele, A., and Darnell, R.B. (2009). Argonaute HITS-CLIP decodes microRNA–mRNA interaction maps. Nature *460*, 479–486.

Chiang, H.R., Schoenfeld, L.W., Ruby, J.G., Auyeung, V.C., Spies, N., Baek, D., Johnston, W.K., Russ, C., Luo, S., Babiarz, J.E., et al. (2010). Mammalian microRNAs: experimental evaluation of novel and previously annotated genes. Genes Dev. *24*, 992–1009.

Chicher, J., Simonetti, A., Kuhn, L., Schaeffer, L., Hammann, P., Eriani, G., and Martin, F. (2015). Purification of mRNA-programmed translation initiation complexes suitable for mass spectrometry analysis. Proteomics *15*, 2417–2425.

Cifuentes, D., Xue, H., Taylor, D.W., Patnode, H., Mishima, Y., Cheloufi, S., Ma, E., Mane, S., Hannon, G.J., Lawson, N.D., et al. (2010). A novel miRNA processing pathway independent of Dicer requires Argonaute2 catalytic activity. Science *328*, 1694–1698.

Cloonan, N., Wani, S., Xu, Q., Gu, J., Lea, K., Heater, S., Barbacioru, C., Steptoe, A.L., Martin, H.C., Nourbakhsh, E., et al. (2011). MicroRNAs and their isomiRs function cooperatively to target common biological pathways. Genome Biol. *12*, R126.

Coley, W., Van Duyne, R., Carpio, L., Guendel, I., Kehn-Hall, K., Chevalier, S., Narayanan, A., Luu, T., Lee, N., Klase, Z., et al. (2010). Absence of DICER in monocytes and its regulation by HIV-1. J. Biol. Chem. *285*, 31930–31943.

Cong, L., Ran, F.A., Cox, D., Lin, S., Barretto, R., Habib, N., Hsu, P.D., Wu, X., Jiang, W., Marraffini, L.A., et al. (2013). Multiplex genome engineering using CRISPR/Cas systems. Science *339*, 819–823.

Coyaud, E., Mis, M., Laurent, E.M.N., Dunham, W.H., Couzens, A.L., Robitaille, M., Gingras, A.-C., Angers, S., and Raught, B. (2015). BioID-based Identification of Skp Cullin F-box (SCF)β-TrCP1/2 E3 Ligase Substrates. Mol. Cell. Proteomics MCP *14*, 1781–1795.

D

Das, S.K., Sokhi, U.K., Bhutia, S.K., Azab, B., Su, Z., Sarkar, D., and Fisher, P.B. (2010). Human polynucleotide phosphorylase selectively and preferentially degrades microRNA-221 in human melanoma cells. Proc. Natl. Acad. Sci. *107*, 11948–11953.

Davis, B.N., Hilyard, A.C., Lagna, G., and Hata, A. (2008). SMAD proteins control DROSHA-mediated microRNA maturation. Nature *454*, 56–61.

Davis, B.N., Hilyard, A.C., Nguyen, P.H., Lagna, G., and Hata, A. (2010). Smad Proteins Bind a Conserved RNA Sequence to Promote MicroRNA Maturation by Drosha. Mol. Cell *39*, 373–384.

Davison, A.J. (2007). Overview of classification. In Human Herpesviruses: Biology, Therapy, and Immunoprophylaxis, A. Arvin, G. Campadelli-Fiume, E. Mocarski, P.S. Moore, B. Roizman, R. Whitley, and K. Yamanishi, eds. (Cambridge: Cambridge University Press),.

Davison, A.J., and Bhella, D. (2007). Comparative genome and virion structure. In Human Herpesviruses: Biology, Therapy, and Immunoprophylaxis, A. Arvin, G. Campadelli-Fiume, E. Mocarski, P.S. Moore, B. Roizman, R. Whitley, and K. Yamanishi, eds. (Cambridge: Cambridge University Press),.

De, N., Young, L., Lau, P.-W., Meisner, N.-C., Morrissey, D.V., and MacRae, I.J. (2013). Highly complementary target RNAs promote release of guide RNAs from human Argonaute2. Mol. Cell *50*, 344–355.

Denli, A.M., Tops, B.B., Plasterk, R.H., Ketting, R.F., and Hannon, G.J. (2004). Processing of primary microRNAs by the microprocessor complex. Nature *432*, 231–235.

Didiano, D., and Hobert, O. (2008). Molecular architecture of a miRNA-regulated 3′ UTR. RNA *14*, 1297–1317.

Diederichs, S., and Haber, D.A. (2007). Dual role for argonautes in microRNA processing and posttranscriptional regulation of microRNA expression. Cell *131*, 1097–1108.

Dingar, D., Kalkat, M., Chan, P.-K., Srikumar, T., Bailey, S.D., Tu, W.B., Coyaud, E., Ponzielli, R., Kolyar, M., Jurisica, I., et al. (2015). BioID identifies novel c-MYC interacting partners in cultured cells and xenograft tumors. J. Proteomics *118*, 95–111.

Doench, J.G., and Sharp, P.A. (2004). Specificity of microRNA target selection in translational repression. Genes Dev *18*, 504–511.

Doench, J.G., Petersen, C.P., and Sharp, P.A. (2003). siRNAs can function as miRNAs. Genes Dev *17*, 438–442.

Dölken, L., Perot, J., Cognat, V., Alioua, A., John, M., Soutschek, J., Ruzsics, Z., Koszinowski, U., Voinnet, O., and Pfeffer, S. (2007). Mouse cytomegalovirus microRNAs dominate the cellular small RNA profile during lytic infection and show features of posttranscriptional regulation. J. Virol. *81*, 13771–13782.

Dölken, L., Krmpotic, A., Kothe, S., Tuddenham, L., Tanguy, M., Marcinowski, L., Ruzsics, Z., Elefant, N., Altuvia, Y., Margalit, H., et al. (2010a). Cytomegalovirus microRNAs Facilitate Persistent Virus Infection in Salivary Glands. PLoS Pathog *6*, e1001150.

Dölken, L., Malterer, G., Erhard, F., Kothe, S., Friedel, C.C., Suffert, G., Marcinowski, L., Motsch, N., Barth, S., Beitzinger, M., et al. (2010b). Systematic analysis of viral and cellular microRNA targets in cells latently infected with human gamma-herpesviruses by RISC immunoprecipitation assay. Cell Host Microbe *7*, 324–334.

E

Ebert, M.S., and Sharp, P.A. (2012). Roles for microRNAs in conferring robustness to biological processes. Cell *149*, 515–524.

Ebert, M.S., Neilson, J.R., and Sharp, P.A. (2007). MicroRNA sponges: competitive inhibitors of small RNAs in mammalian cells. Nat. Methods *4*, 721–726.

Eichhorn, S.W., Guo, H., McGeary, S.E., Rodriguez-Mias, R.A., Shin, C., Baek, D., Hsu, S., Ghoshal, K., Villén, J., and Bartel, D.P. (2014). mRNA Destabilization Is the Dominant Effect of Mammalian MicroRNAs by the Time Substantial Repression Ensues. Mol. Cell *56*, 104–115.

Elcheva, I., Goswami, S., Noubissi, F.K., and Spiegelman, V.S. (2009). CRD-BP protects the coding region of betaTrCP1 mRNA from miR-183-mediated degradation. Mol. Cell *35*, 240–246.

Elkayam, E., Kuhn, C.-D., Tocilj, A., Haase, A.D., Greene, E.M., Hannon, G.J., and Joshua-Tor, L. (2012). The Structure of Human Argonaute-2 in Complex with miR-20a. Cell *150*, 100–110.

Ender, C., Krek, A., Friedlander, M.R., Beitzinger, M., Weinmann, L., Chen, W., Pfeffer, S., Rajewsky, N., and Meister, G. (2008). A human snoRNA with microRNA-like functions. Mol Cell *32*, 519–528.

Esquela-Kerscher, A., and Slack, F.J. (2006). Oncomirs — microRNAs with a role in cancer. Nat. Rev. Cancer *6*, 259–269.

Eulalio, A., Behm-Ansmant, I., Schweizer, D., and Izaurralde, E. (2007). P-body formation is a consequence, not the cause, of RNA-mediated gene silencing. Mol Cell Biol *27*, 3970–3981.

Eulalio, A., Huntzinger, E., and Izaurralde, E. (2008). Getting to the root of miRNA-mediated gene silencing. Cell *132*, 9–14.

F

Fabian, M.R., and Sonenberg, N. (2012). The mechanics of miRNA-mediated gene silencing: a look under the hood of miRISC. Nat. Struct. Mol. Biol. *19*, 586–593.

Fabian, M.R., Cieplak, M.K., Frank, F., Morita, M., Green, J., Srikumar, T., Nagar, B., Yamamoto, T., Raught, B., Duchaine, T.F., et al. (2011). miRNA-mediated deadenylation is orchestrated by GW182 through two conserved motifs that interact with CCR4-NOT. Nat. Struct. Mol. Biol. *18*, 1211–1217.

Faehnle, C.R., Walleshauser, J., and Joshua-Tor, L. (2014). Mechanism of Dis3l2 substrate recognition in the Lin28-let-7 pathway. Nature *514*, 252–256.

Fang, W., and Bartel, D.P. (2015). The Menu of Features that Define Primary MicroRNAs and Enable De Novo Design of MicroRNA Genes. Mol. Cell *60*, 131–145.

Farh, K.K., Grimson, A., Jan, C., Lewis, B.P., Johnston, W.K., Lim, L.P., Burge, C.B., and Bartel, D.P. (2005). The Widespread Impact of Mammalian MicroRNAs on mRNA Repression and Evolution. Science.

Fields, S., and Song, O. (1989). A novel genetic system to detect protein-protein interactions. Nature *340*, 245–246.

Firat-Karalar, E.N., Rauniyar, N., Yates, J.R., and Stearns, T. (2014). Proximity interactions among centrosome components identify regulators of centriole duplication. Curr. Biol. CB *24*, 664–670.

Flores-Jasso, C.F., Salomon, W.E., and Zamore, P.D. (2013). Rapid and specific purification of Argonaute-small RNA complexes from crude cell lysates. RNA *19*, 271–279.

Forman, J.J., Legesse-Miller, A., and Coller, H.A. (2008). A search for conserved sequences in coding regions reveals that the let-7 microRNA targets Dicer within its coding sequence. Proc. Natl. Acad. Sci. U. S. A. *105*, 14879–14884.

Friedman, R.C., Farh, K.K., Burge, C.B., and Bartel, D.P. (2009). Most mammalian mRNAs are conserved targets of microRNAs. Genome Res *19*, 92–105.

Frohn, A., Eberl, H.C., Stöhr, J., Glasmacher, E., Rüdel, S., Heissmeyer, V., Mann, M., and Meister, G. (2012). Dicer-dependent and -independent Argonaute2 Protein Interaction Networks in Mammalian Cells. Mol. Cell. Proteomics *11*, 1442–1456.

Fukuda, T., Yamagata, K., Fujiyama, S., Matsumoto, T., Koshida, I., Yoshimura, K., Mihara, M., Naitou, M., Endoh, H., Nakamura, T., et al. (2007). DEAD-box RNA helicase subunits of

the Drosha complex are required for processing of rRNA and a subset of microRNAs. Nat. Cell Biol. *9*, 604–611.

G

Gaidatzis, D., van Nimwegen, E., Hausser, J., and Zavolan, M. (2007). Inference of miRNA targets using evolutionary conservation and pathway analysis. BMC Bioinformatics *8*, 69.

Galgano, A., Forrer, M., Jaskiewicz, L., Kanitz, A., Zavolan, M., and Gerber, A.P. (2008). Comparative Analysis of mRNA Targets for Human PUF-Family Proteins Suggests Extensive Interaction with the miRNA Regulatory System. PLOS ONE *3*, e3164.

Gantier, M.P., McCoy, C.E., Rusinova, I., Saulep, D., Wang, D., Xu, D., Irving, A.T., Behlke, M.A., Hertzog, P.J., Mackay, F., et al. (2011). Analysis of microRNA turnover in mammalian cells following Dicer1 ablation. Nucleic Acids Res. *39*, 5692–5703.

Geiss, G.K., Bumgarner, R.E., Birditt, B., Dahl, T., Dowidar, N., Dunaway, D.L., Fell, H.P., Ferree, S., George, R.D., Grogan, T., et al. (2008). Direct multiplexed measurement of gene expression with color-coded probe pairs. Nat. Biotechnol. *26*, 317–325.

Gibbings, D., Mostowy, S., Jay, F., Schwab, Y., Cossart, P., and Voinnet, O. (2012). Selective autophagy degrades DICER and AGO2 and regulates miRNA activity. Nat. Cell Biol. *14*, 1314–1321.

Gill, D.R., Smyth, S.E., Goddard, C.A., Pringle, I.A., Higgins, C.F., Colledge, W.H., and Hyde, S.C. (2001). Increased persistence of lung gene expression using plasmids containing the ubiquitin C or elongation factor 1alpha promoter. Gene Ther. *8*, 1539–1546.

Gonzales, M.L., Mellman, D.L., and Anderson, R.A. (2008). CKIalpha is associated with and phosphorylates star-PAP and is also required for expression of select star-PAP target messenger RNAs. J. Biol. Chem. *283*, 12665–12673.

Gregory, R.I., Yan, K.P., Amuthan, G., Chendrimada, T., Doratotaj, B., Cooch, N., and Shiekhattar, R. (2004). The Microprocessor complex mediates the genesis of microRNAs. Nature *432*, 235–240.

Gregory, R.I., Chendrimada, T.P., Cooch, N., and Shiekhattar, R. (2005). Human RISC couples microRNA biogenesis and posttranscriptional gene silencing. Cell *123*, 631–640.

Griffin, N.M., Yu, J., Long, F., Oh, P., Shore, S., Li, Y., Koziol, J.A., and Schnitzer, J.E. (2010). Label-free, normalized quantification of complex mass spectrometry data for proteomic analysis. Nat. Biotechnol. *28*, 83–89.

Grimson, A., Farh, K.K.-H., Johnston, W.K., Garrett-Engele, P., Lim, L.P., and Bartel, D.P. (2007). MicroRNA targeting specificity in mammals: determinants beyond seed pairing. Mol. Cell *27*, 91–105.

Guil, S., and Caceres, J.F. (2007). The multifunctional RNA-binding protein hnRNP A1 is required for processing of miR-18a. Nat Struct Mol Biol *14*, 591–596.

Guo, L., and Chen, F. (2014). A challenge for miRNA: multiple isomiRs in miRNAomics. Gene *544*, 1–7.

Guo, H., Ingolia, N.T., Weissman, J.S., and Bartel, D.P. (2010). Mammalian microRNAs predominantly act to decrease target mRNA levels. Nature *466*, 835–840.

H

Ha, M., and Kim, V.N. (2014). Regulation of microRNA biogenesis. Nat. Rev. Mol. Cell Biol. *15*, 509–524.

Haas, G., Cetin, S., Messmer, M., Chane-Woon-Ming, B., Terenzi, O., Chicher, J., Kuhn, L., Hammann, P., and Pfeffer, S. (2016). Identification of factors involved in target RNA-directed microRNA degradation. Nucleic Acids Res. *44*, 2873–2887.

Haase, A.D., Jaskiewicz, L., Zhang, H., Laine, S., Sack, R., Gatignol, A., and Filipowicz, W. (2005). TRBP, a regulator of cellular PKR and HIV-1 virus expression, interacts with Dicer and functions in RNA silencing. EMBO Rep *6*, 961–967.

Hafner, M., Landthaler, M., Burger, L., Khorshid, M., Hausser, J., Berninger, P., Rothballer, A., Ascano, M., Jr, Jungkamp, A.-C., Munschauer, M., et al. (2010). Transcriptome-wide identification of RNA-binding protein and microRNA target sites by PAR-CLIP. Cell *141*, 129–141.

Hagan, J.P., Piskounova, E., and Gregory, R.I. (2009). Lin28 recruits the TUTase Zcchc11 to inhibit let-7 maturation in mouse embryonic stem cells. Nat. Struct. Mol. Biol. *16*, 1021–1025.

Hammond, S.M. (2007). MicroRNAs as tumor suppressors. Nat. Genet. *39*, 582–583.

Han, B.W., Hung, J.-H., Weng, Z., Zamore, P.D., and Ameres, S.L. (2011). The 3′-to-5′ Exoribonuclease Nibbler Shapes the 3′ Ends of MicroRNAs Bound to Drosophila Argonaute1. Curr. Biol. *21*, 1878–1887.

Han, J., Lee, Y., Yeom, K.-H., Kim, Y.-K., Jin, H., and Kim, V.N. (2004). The Drosha-DGCR8 complex in primary microRNA processing. Genes Dev. *18*, 3016–3027.

Han, J., Lee, Y., Yeom, K.H., Nam, J.W., Heo, I., Rhee, J.K., Sohn, S.Y., Cho, Y., Zhang, B.T., and Kim, V.N. (2006). Molecular basis for the recognition of primary microRNAs by the Drosha-DGCR8 complex. Cell *125*, 887–901.

Han, J., Pedersen, J.S., Kwon, S.C., Belair, C.D., Kim, Y.-K., Yeom, K.-H., Yang, W.-Y., Haussler, D., Blelloch, R., and Kim, V.N. (2009). Posttranscriptional crossregulation between Drosha and DGCR8. Cell *136*, 75–84.

Hansen, T.B., Jensen, T.I., Clausen, B.H., Bramsen, J.B., Finsen, B., Damgaard, C.K., and Kjems, J. (2013). Natural RNA circles function as efficient microRNA sponges. Nature *495*, 384–388.

He, L., He, X., Lowe, S.W., and Hannon, G.J. (2007). microRNAs join the p53 network--another piece in the tumour-suppression puzzle. Nat Rev Cancer *7*, 819–822.

Hein, M.Y., Hubner, N.C., Poser, I., Cox, J., Nagaraj, N., Toyoda, Y., Gak, I.A., Weisswange, I., Mansfeld, J., Buchholz, F., et al. (2015). A human interactome in three quantitative dimensions organized by stoichiometries and abundances. Cell *163*, 712–723.

Heo, I., Joo, C., Cho, J., Ha, M., Han, J., and Kim, V.N. (2008). Lin28 mediates the terminal uridylation of let-7 precursor MicroRNA. Mol Cell *32*, 276–284.

Heo, I., Joo, C., Kim, Y.-K., Ha, M., Yoon, M.-J., Cho, J., Yeom, K.-H., Han, J., and Kim, V.N. (2009). TUT4 in concert with Lin28 suppresses microRNA biogenesis through pre-microRNA uridylation. Cell *138*, 696–708.

Heo, I., Ha, M., Lim, J., Yoon, M.-J., Park, J.-E., Kwon, S.C., Chang, H., and Kim, V.N. (2012). Mono-uridylation of pre-microRNA as a key step in the biogenesis of group II let-7 microRNAs. Cell *151*, 521–532.

Herbert, K.M., Pimienta, G., DeGregorio, S.J., Alexandrov, A., and Steitz, J.A. (2013). Phosphorylation of DGCR8 Increases Its Intracellular Stability and Induces a Progrowth miRNA Profile. Cell Rep. *5*, 1070–1081.

Heyam, A., Lagos, D., and Plevin, M. (2015). Dissecting the roles of TRBP and PACT in double-stranded RNA recognition and processing of noncoding RNAs. Wiley Interdiscip. Rev. RNA *6*, 271–289.

Höck, J., Weinmann, L., Ender, C., Rüdel, S., Kremmer, E., Raabe, M., Urlaub, H., and Meister, G. (2007). Proteomic and functional analysis of Argonaute-containing mRNA-protein complexes in human cells. EMBO Rep. *8*, 1052–1060.

Hodge, K., Have, S.T., Hutton, L., and Lamond, A.I. (2013). Cleaning up the masses: exclusion lists to reduce contamination with HPLC-MS/MS. J. Proteomics *88*, 92–103.

Hoon, M.J.L. de, Taft, R.J., Hashimoto, T., Kanamori-Katayama, M., Kawaji, H., Kawano, M., Kishima, M., Lassmann, T., Faulkner, G.J., Mattick, J.S., et al. (2010). Cross-mapping and the identification of editing sites in mature microRNAs in high-throughput sequencing libraries. Genome Res. *20*, 257–264.

Horman, S.R., Janas, M.M., Litterst, C., Wang, B., MacRae, I.J., Sever, M.J., Morrissey, D.V., Graves, P., Luo, B., Umesalma, S., et al. (2013). Akt-Mediated Phosphorylation of Argonaute 2 Downregulates Cleavage and Upregulates Translational Repression of MicroRNA Targets. Mol. Cell *50*, 356–367.

Horwich, M.D., Li, C., Matranga, C., Vagin, V., Farley, G., Wang, P., and Zamore, P.D. (2007). The Drosophila RNA Methyltransferase, DmHen1, Modifies Germline piRNAs and Single-Stranded siRNAs in RISC. Curr. Biol. *17*, 1265–1272.

Hubner, N.C., Bird, A.W., Cox, J., Splettstoesser, B., Bandilla, P., Poser, I., Hyman, A., and Mann, M. (2010). Quantitative proteomics combined with BAC TransgeneOmics reveals in vivo protein interactions. J. Cell Biol. *189*, 739–754.

Humphreys, D.T., Hynes, C.J., Patel, H.R., Wei, G.H., Cannon, L., Fatkin, D., Suter, C.M., Clancy, J.L., and Preiss, T. (2012). Complexity of Murine Cardiomyocyte miRNA Biogenesis, Sequence Variant Expression and Function. PLOS ONE *7*, e30933.

Hung, V., Zou, P., Rhee, H.-W., Udeshi, N.D., Cracan, V., Svinkina, T., Carr, S.A., Mootha, V.K., and Ting, A.Y. (2014). Proteomic mapping of the human mitochondrial intermembrane space in live cells via ratiometric APEX tagging. Mol. Cell *55*, 332–341.

Hung, V., Udeshi, N.D., Lam, S.S., Loh, K.H., Cox, K.J., Pedram, K., Carr, S.A., and Ting, A.Y. (2016). Spatially resolved proteomic mapping in living cells with the engineered peroxidase APEX2. Nat. Protoc. *11*, 456–475.

Huntzinger, E., and Izaurralde, E. (2011). Gene silencing by microRNAs: contributions of translational repression and mRNA decay. Nat. Rev. Genet. *12*, 99–110.

Huntzinger, E., Braun, J.E., Heimstädt, S., Zekri, L., and Izaurralde, E. (2010). Two PABPC1-binding sites in GW182 proteins promote miRNA-mediated gene silencing. EMBO J. *29*, 4146–4160.

Huttlin, E.L., Ting, L., Bruckner, R.J., Gebreab, F., Gygi, M.P., Szpyt, J., Tam, S., Zarraga, G., Colby, G., Baltier, K., et al. (2015). The BioPlex Network: A Systematic Exploration of the Human Interactome. Cell *162*, 425–440.

Hutvágner, G., McLachlan, J., Pasquinelli, A.E., Balint, E., Tuschl, T., and Zamore, P.D. (2001). A cellular function for the RNA-interference enzyme Dicer in the maturation of the let-7 small temporal RNA. Science *293*, 834–838.

Hutvagner, G., Simard, M.J., Mello, C.C., and Zamore, P.D. (2004). Sequence-specific inhibition of small RNA function. PLoS Biol *2*, E98.

Hwang, H.-W., Wentzel, E.A., and Mendell, J.T. (2007). A hexanucleotide element directs microRNA nuclear import. Science *315*, 97–100.

I

Ibrahim, F., Rymarquis, L.A., Kim, E.-J., Becker, J., Balassa, E., Green, P.J., and Cerutti, H. (2010). Uridylation of mature miRNAs and siRNAs by the MUT68 nucleotidyltransferase promotes their degradation in Chlamydomonas. Proc. Natl. Acad. Sci. U. S. A. *107*, 3906–3911.

Iwasaki, S., Kobayashi, M., Yoda, M., Sakaguchi, Y., Katsuma, S., Suzuki, T., and Tomari, Y. (2010). Hsc70/Hsp90 chaperone machinery mediates ATP-dependent RISC loading of small RNA duplexes. Mol. Cell *39*, 292–299.

Iwasaki, Y.W., Kiga, K., Kayo, H., Fukuda-Yuzawa, Y., Weise, J., Inada, T., Tomita, M., Ishihama, Y., and Fukao, T. (2013). Global microRNA elevation by inducible Exportin 5 regulates cell cycle entry. RNA *19*, 490–497.

J

Jakymiw, A., Lian, S., Eystathioy, T., Li, S., Satoh, M., Hamel, J.C., Fritzler, M.J., and Chan, E.K.L. (2005). Disruption of GW bodies impairs mammalian RNA interference. Nat. Cell Biol. *7*, 1267–1274.

Jazdzewski, K., Murray, E.L., Franssila, K., Jarzab, B., Schoenberg, D.R., and Chapelle, A. de la (2008). Common SNP in pre-miR-146a decreases mature miR expression and predisposes to papillary thyroid carcinoma. Proc. Natl. Acad. Sci. *105*, 7269–7274.

Jazdzewski, K., Liyanarachchi, S., Swierniak, M., Pachucki, J., Ringel, M.D., Jarzab, B., and Chapelle, A. de la (2009). Polymorphic mature microRNAs from passenger strand of pre-miR-146a contribute to thyroid cancer. Proc. Natl. Acad. Sci. *106*, 1502–1505.

Jiang, P., and Coller, H. (2012). Functional interactions between microRNAs and RNA binding proteins. MicroRNA *1*, 70–79.

Jin, H., Suh, M.R., Han, J., Yeom, K.-H., Lee, Y., Heo, I., Ha, M., Hyun, S., and Kim, V.N. (2009). Human UPF1 participates in small RNA-induced mRNA downregulation. Mol. Cell. Biol. *29*, 5789–5799.

Jinek, M., Fabian, M.R., Coyle, S.M., Sonenberg, N., and Doudna, J.A. (2010). Structural insights into the human GW182-PABC interaction in microRNA-mediated deadenylation. Nat. Struct. Mol. Biol. *17*, 238–240.

Johnston, M., Geoffroy, M.-C., Sobala, A., Hay, R., and Hutvagner, G. (2010). HSP90 protein stabilizes unloaded argonaute complexes and microscopic P-bodies in human cells. Mol. Biol. Cell *21*, 1462–1469.

Jonas, S., and Izaurralde, E. (2013). The role of disordered protein regions in the assembly of decapping complexes and RNP granules. Genes Dev. *27*, 2628–2641.

Jonas, S., and Izaurralde, E. (2015). Towards a molecular understanding of microRNA-mediated gene silencing. Nat. Rev. Genet. *16*, 421–433.

Jones, M.R., Quinton, L.J., Blahna, M.T., Neilson, J.R., Fu, S., Ivanov, A.R., Wolf, D.A., and Mizgerd, J.P. (2009). Zcchc11-dependent uridylation of microRNA directs cytokine expression. Nat. Cell Biol. *11*, 1157–1163.

Jones, M.R., Blahna, M.T., Kozlowski, E., Matsuura, K.Y., Ferrari, J.D., Morris, S.A., Powers, J.T., Daley, G.Q., Quinton, L.J., and Mizgerd, J.P. (2012). Zcchc11 uridylates mature miRNAs to enhance neonatal IGF-1 expression, growth, and survival. PLoS Genet. *8*, e1003105.

Jones-Rhoades, M.W., Bartel, D.P., and Bartel, B. (2006). MicroRNAs AND THEIR REGULATORY ROLES IN PLANTS. Annu. Rev. Plant Biol. *57*, 19–53.

Juranic Lisnic, V., Babic Cac, M., Lisnic, B., Trsan, T., Mefferd, A., Das Mukhopadhyay, C., Cook, C.H., Jonjic, S., and Trgovcich, J. (2013). Dual Analysis of the Murine Cytomegalovirus and Host Cell Transcriptomes Reveal New Aspects of the Virus-Host Cell Interface. PLoS Pathog. *9*.

K

Kalantari, R., Hicks, J.A., Li, L., Gagnon, K.T., Viswanadham Sridhara, Lemoff, A., Mirzaei, H., and Corey, D.R. (2016). Stable association of RNAi machinery is conserved between the cytoplasm and nucleus of human cells. RNA N. Y. N *22*, 1085–1098.

Katoh, T., Sakaguchi, Y., Miyauchi, K., Suzuki, T., Kashiwabara, S., Baba, T., and Suzuki, T. (2009). Selective stabilization of mammalian microRNAs by 3′ adenylation mediated by the cytoplasmic poly(A) polymerase GLD-2. Genes Dev. *23*, 433–438.

Kawahara, Y., Zinshteyn, B., Chendrimada, T.P., Shiekhattar, R., and Nishikura, K. (2007a). RNA editing of the microRNA-151 precursor blocks cleavage by the Dicer-TRBP complex. EMBO Rep. *8*, 763–769.

Kawahara, Y., Zinshteyn, B., Sethupathy, P., Iizasa, H., Hatzigeorgiou, A.G., and Nishikura, K. (2007b). Redirection of silencing targets by adenosine-to-inosine editing of miRNAs. Science *315*, 1137–1140.

Kawamata, T., Seitz, H., and Tomari, Y. (2009). Structural determinants of miRNAs for RISC loading and slicer-independent unwinding. Nat. Struct. Mol. Biol. *16*, 953–960.

Kedde, M., Strasser, M.J., Boldajipour, B., Vrielink, J.A.F.O., Slanchev, K., le Sage, C., Nagel, R., Voorhoeve, P.M., van Duijse, J., Ørom, U.A., et al. (2007). RNA-Binding Protein Dnd1 Inhibits MicroRNA Access to Target mRNA. Cell *131*, 1273–1286.

Kedde, M., van Kouwenhove, M., Zwart, W., Oude Vrielink, J.A.F., Elkon, R., and Agami, R. (2010). A Pumilio-induced RNA structure switch in p27-3′ UTR controls miR-221 and miR-222 accessibility. Nat. Cell Biol. *12*, 1014–1020.

Khvorova, A., Reynolds, A., and Jayasena, S.D. (2003). Functional siRNAs and miRNAs exhibit strand bias. Cell *115*, 209–216.

Kim, Y.-K., and Kim, V.N. (2007). Processing of intronic microRNAs. EMBO J. *26*, 775–783.

Kim, B., Ha, M., Loeff, L., Chang, H., Simanshu, D.K., Li, S., Fareh, M., Patel, D.J., Joo, C., and Kim, V.N. (2015). TUT7 controls the fate of precursor microRNAs by using three different uridylation mechanisms. EMBO J. *34*, 1801–1815.

Kim, D.I., Birendra, K.C., Zhu, W., Motamedchaboki, K., Doye, V., and Roux, K.J. (2014a). Probing nuclear pore complex architecture with proximity-dependent biotinylation. Proc. Natl. Acad. Sci. U. S. A. *111*, E2453–E2461.

Kim, D.I., Jensen, S.C., Noble, K.A., Kc, B., Roux, K.H., Motamedchaboki, K., and Roux, K.J. (2016a). An improved smaller biotin ligase for BioID proximity labeling. Mol. Biol. Cell *27*, 1188–1196.

Kim, H.H., Kuwano, Y., Srikantan, S., Lee, E.K., Martindale, J.L., and Gorospe, M. (2009). HuR recruits let-7/RISC to repress c-Myc expression. Genes Dev. *23*, 1743–1748.

Kim, Y., Yeo, J., Lee, J.H., Cho, J., Seo, D., Kim, J.-S., and Kim, V.N. (2014b). Deletion of Human tarbp2 Reveals Cellular MicroRNA Targets and Cell-Cycle Function of TRBP. Cell Rep. *9*, 1061–1074.

Kim, Y.-K., Kim, B., and Kim, V.N. (2016b). Re-evaluation of the roles of DROSHA, Exportin 5, and DICER in microRNA biogenesis. Proc. Natl. Acad. Sci. U. S. A. *113*, E1881–E1889.

Knouf, E.C., Wyman, S.K., and Tewari, M. (2013). The human TUT1 nucleotidyl transferase as a global regulator of microRNA abundance. PloS One *8*, e69630.

Kobayashi, H., and Tomari, Y. (2016). RISC assembly: Coordination between small RNAs and Argonaute proteins. Biochim. Biophys. Acta BBA - Gene Regul. Mech. *1859*, 71–81.

van Kouwenhove, M., Kedde, M., and Agami, R. (2011). MicroRNA regulation by RNA-binding proteins and its implications for cancer. Nat. Rev. Cancer *11*, 644–656.

Krek, A., Grun, D., Poy, M.N., Wolf, R., Rosenberg, L., Epstein, E.J., Macmenamin, P., da Piedade, I., Gunsalus, K.C., Stoffel, M., et al. (2005). Combinatorial microRNA target predictions. Nat Genet *37*, 495–500.

Krmpotic, A., Bubic, I., Polic, B., Lucin, P., and Jonjic, S. (2003). Pathogenesis of murine cytomegalovirus infection. Microbes Infect *5*, 1263–1277.

Krol, J., Busskamp, V., Markiewicz, I., Stadler, M.B., Ribi, S., Richter, J., Duebel, J., Bicker, S., Fehling, H.J., Schubeler, D., et al. (2010). Characterizing light-regulated retinal microRNAs reveals rapid turnover as a common property of neuronal microRNAs. Cell *141*, 618–631.

Krutzfeldt, J., Rajewsky, N., Braich, R., Rajeev, K.G., Tuschl, T., Manoharan, M., and Stoffel, M. (2005). Silencing of microRNAs in vivo with "antagomirs." Nature *438*, 685–689.

Kundu, P., Fabian, M.R., Sonenberg, N., Bhattacharyya, S.N., and Filipowicz, W. (2012). HuR protein attenuates miRNA-mediated repression by promoting miRISC dissociation from the target RNA. Nucleic Acids Res. *40*, 5088–5100.

Kwak, J.E., and Wickens, M. (2007). A family of poly(U) polymerases. RNA *13*, 860–867.

Kwak, P.B., and Tomari, Y. (2012). The N domain of Argonaute drives duplex unwinding during RISC assembly. Nat. Struct. Mol. Biol. *19*, 145–151.

Kwon, K., and Beckett, D. (2000). Function of a conserved sequence motif in biotin holoenzyme synthetases. Protein Sci. Publ. Protein Soc. *9*, 1530–1539.

Kwon, S.C., Nguyen, T.A., Choi, Y.-G., Jo, M.H., Hohng, S., Kim, V.N., and Woo, J.-S. (2016). Structure of Human DROSHA. Cell *164*, 81–90.

L

Łabno, A., Warkocki, Z., Kuliński, T., Krawczyk, P.S., Bijata, K., Tomecki, R., and Dziembowski, A. (2016). Perlman syndrome nuclease DIS3L2 controls cytoplasmic non-coding RNAs and provides surveillance pathway for maturing snRNAs. Nucleic Acids Res.

Lackner, D.H., Carré, A., Guzzardo, P.M., Banning, C., Mangena, R., Henley, T., Oberndorfer, S., Gapp, B.V., Nijman, S.M.B., Brummelkamp, T.R., et al. (2015). A generic strategy for CRISPR-Cas9-mediated gene tagging. Nat. Commun. *6*.

Laishram, R.S., and Anderson, R.A. (2010). The poly A polymerase Star-PAP controls 3'-end cleavage by promoting CPSF interaction and specificity toward the pre-mRNA. EMBO J. *29*, 4132–4145.

Lam, S.S., Martell, J.D., Kamer, K.J., Deerinck, T.J., Ellisman, M.H., Mootha, V.K., and Ting, A.Y. (2015). Directed evolution of APEX2 for electron microscopy and proximity labeling. Nat. Methods *12*, 51–54.

Lambert, J.-P., Tucholska, M., Go, C., Knight, J.D.R., and Gingras, A.-C. (2015). Proximity biotinylation and affinity purification are complementary approaches for the interactome mapping of chromatin-associated protein complexes. J. Proteomics *118*, 81–94.

Landgraf, P., Rusu, M., Sheridan, R., Sewer, A., Iovino, N., Aravin, A., Pfeffer, S., Rice, A., Kamphorst, A.O., Landthaler, M., et al. (2007). A mammalian microRNA expression atlas based on small RNA library sequencing. Cell *129*, 1401–1414.

Landthaler, M., Yalcin, A., and Tuschl, T. (2004). The human DiGeorge syndrome critical region gene 8 and Its D. melanogaster homolog are required for miRNA biogenesis. Curr Biol *14*, 2162–2167.

Landthaler, M., Gaidatzis, D., Rothballer, A., Chen, P.Y., Soll, S.J., Dinic, L., Ojo, T., Hafner, M., Zavolan, M., and Tuschl, T. (2008). Molecular characterization of human Argonaute-containing ribonucleoprotein complexes and their bound target mRNAs. Rna *14*, 2580–2596.

Lazzaretti, D., Tournier, I., and Izaurralde, E. (2009). The C-terminal domains of human TNRC6A, TNRC6B, and TNRC6C silence bound transcripts independently of Argonaute proteins. RNA N. Y. N *15*, 1059–1066.

Lee, M., Choi, Y., Kim, K., Jin, H., Lim, J., Nguyen, T.A., Yang, J., Jeong, M., Giraldez, A.J., Yang, H., et al. (2014). Adenylation of Maternally Inherited MicroRNAs by Wispy. Mol. Cell *56*, 696–707.

Lee, S., Song, J., Kim, S., Kim, J., Hong, Y., Kim, Y., Kim, D., Baek, D., and Ahn, K. (2013). Selective degradation of host MicroRNAs by an intergenic HCMV noncoding RNA accelerates virus production. Cell Host Microbe *13*, 678–690.

Lee, Y., Jeon, K., Lee, J.T., Kim, S., and Kim, V.N. (2002). MicroRNA maturation: stepwise processing and subcellular localization. Embo J *21*, 4663–4670.

Lee, Y., Ahn, C., Han, J., Choi, H., Kim, J., Yim, J., Lee, J., Provost, P., Radmark, O., Kim, S., et al. (2003). The nuclear RNase III Drosha initiates microRNA processing. Nature *425*, 415–419.

Lee, Y., Kim, M., Han, J., Yeom, K.H., Lee, S., Baek, S.H., and Kim, V.N. (2004). MicroRNA genes are transcribed by RNA polymerase II. Embo J *23*, 4051–4060.

Lee, Y., Hur, I., Park, S.Y., Kim, Y.K., Suh, M.R., and Kim, V.N. (2006). The role of PACT in the RNA silencing pathway. Embo J *25*, 522–532.

Le Sage, V., Cinti, A., Valiente-Echeverría, F., and Mouland, A.J. (2015). Proteomic analysis of HIV-1 Gag interacting partners using proximity-dependent biotinylation. Virol. J. *12*, 138.

Leung, A.K.L., Young, A.G., Bhutkar, A., Zheng, G.X., Bosson, A.D., Nielsen, C.B., and Sharp, P.A. (2011a). Genome-wide identification of Ago2 binding sites from mouse

embryonic stem cells with and without mature microRNAs. Nat. Struct. Mol. Biol. *18*, 237–244.

Leung, A.K.L., Vyas, S., Rood, J.E., Bhutkar, A., Sharp, P.A., and Chang, P. (2011b). Poly(ADP-Ribose) Regulates Stress Responses and MicroRNA Activity in the Cytoplasm. Mol. Cell *42*, 489–499.

Lewis, B.P., Shih, I., Jones-Rhoades, M.W., Bartel, D.P., and Burge, C.B. (2003). Prediction of mammalian microRNA targets. Cell *115*, 787–798.

Lewis, B.P., Burge, C.B., and Bartel, D.P. (2005). Conserved Seed Pairing, Often Flanked by Adenosines, Indicates that Thousands of Human Genes are MicroRNA Targets. Cell *120*, 15–20.

Li, J., Yang, Z., Yu, B., Liu, J., and Chen, X. (2005). Methylation Protects miRNAs and siRNAs from a 3'-End Uridylation Activity in Arabidopsis. Curr Biol *15*, 1501–1507.

Li, W., Laishram, R.S., Ji, Z., Barlow, C.A., Tian, B., and Anderson, R.A. (2012). Star-PAP control of BIK expression and apoptosis is regulated by nuclear PIPKIα and PKCδ signaling. Mol. Cell *45*, 25–37.

Lian, S.L., Li, S., Abadal, G.X., Pauley, B.A., Fritzler, M.J., and Chan, E.K.L. (2009). The C-terminal half of human Ago2 binds to multiple GW-rich regions of GW182 and requires GW182 to mediate silencing. RNA *15*, 804–813.

Libri, V., Helwak, A., Miesen, P., Santhakumar, D., Borger, J.G., Kudla, G., Grey, F., Tollervey, D., and Buck, A.H. (2012). Murine cytomegalovirus encodes a miR-27 inhibitor disguised as a target. Proc. Natl. Acad. Sci. U. S. A. *109*, 279–284.

Lim, J., Ha, M., Chang, H., Kwon, S.C., Simanshu, D.K., Patel, D.J., and Kim, V.N. (2014). Uridylation by TUT4 and TUT7 Marks mRNA for Degradation. Cell *159*, 1365–1376.

Lingel, A., Simon, B., Izaurralde, E., and Sattler, M. (2004). Nucleic acid 3'-end recognition by the Argonaute2 PAZ domain. Nat Struct Mol Biol *11*, 576–577.

Liu, J., Carmell, M.A., Rivas, F.V., Marsden, C.G., Thomson, J.M., Song, J.J., Hammond, S.M., Joshua-Tor, L., and Hannon, G.J. (2004). Argonaute2 is the catalytic engine of mammalian RNAi. Science *305*, 1437–1441.

Liu, J., Valencia-Sanchez, M.A., Hannon, G.J., and Parker, R. (2005a). MicroRNA-dependent localization of targeted mRNAs to mammalian P-bodies. Nat Cell Biol.

Liu, J., Rivas, F.V., Wohlschlegel, J., Yates, J.R., Parker, R., and Hannon, G.J. (2005b). A role for the P-body component GW182 in microRNA function. Nat Cell Biol *7*, 1261–1266.

Liu, N., Abe, M., Sabin, L.R., Hendriks, G.-J., Naqvi, A.S., Yu, Z., Cherry, S., and Bonini, N.M. (2011). The exoribonuclease Nibbler controls 3' end processing of microRNAs in Drosophila. Curr. Biol. CB *21*, 1888–1893.

Liu, X., Jin, D.-Y., McManus, M.T., and Mourelatos, Z. (2012). Precursor MicroRNA-Programmed Silencing Complex Assembly Pathways in Mammals. Mol. Cell *46*, 507–517.

Liu, X., Zheng, Q., Vrettos, N., Maragkakis, M., Alexiou, P., Gregory, B.D., and Mourelatos, Z. (2014). A MicroRNA precursor surveillance system in quality control of MicroRNA synthesis. Mol. Cell *55*, 868–879.

Loffreda, A., Rigamonti, A., Barabino, S.M.L., and Lenzken, S.C. (2015). RNA-Binding Proteins in the Regulation of miRNA Activity: A Focus on Neuronal Functions. Biomolecules *5*, 2363–2387.

Lu, S., and Cullen, B.R. (2004). Adenovirus VA1 noncoding RNA can inhibit small interfering RNA and MicroRNA biogenesis. J. Virol. *78*, 12868–12876.

Lu, J., Getz, G., Miska, E.A., Alvarez-Saavedra, E., Lamb, J., Peck, D., Sweet-Cordero, A., Ebert, B.L., Mak, R.H., Ferrando, A.A., et al. (2005). MicroRNA expression profiles classify human cancers. Nature *435*, 834–838.

Lubas, M., Damgaard, C.K., Tomecki, R., Cysewski, D., Jensen, T.H., and Dziembowski, A. (2013). Exonuclease hDIS3L2 specifies an exosome-independent 3'-5' degradation pathway of human cytoplasmic mRNA. EMBO J. *32*, 1855–1868.

Luciano, D.J., Mirsky, H., Vendetti, N.J., and Maas, S. (2004). RNA editing of a miRNA precursor. RNA *10*, 1174–1177.

Lund, E., Guttinger, S., Calado, A., Dahlberg, J.E., and Kutay, U. (2004). Nuclear export of microRNA precursors. Science *303*, 95–98.

M

Ma, J.B., Ye, K., and Patel, D.J. (2004). Structural basis for overhang-specific small interfering RNA recognition by the PAZ domain. Nature *429*, 318–322.

Ma, L., Young, J., Prabhala, H., Pan, E., Mestdagh, P., Muth, D., Teruya-Feldstein, J., Reinhardt, F., Onder, T.T., Valastyan, S., et al. (2010). miR-9, a MYC/MYCN-activated microRNA, regulates E-cadherin and cancer metastasis. Nat. Cell Biol. *12*, 247–256.

Macrae, I.J., Zhou, K., Li, F., Repic, A., Brooks, A.N., Cande, W.Z., Adams, P.D., and Doudna, J.A. (2006). Structural basis for double-stranded RNA processing by Dicer. Science *311*, 195–198.

Malecki, M., Viegas, S.C., Carneiro, T., Golik, P., Dressaire, C., Ferreira, M.G., and Arraiano, C.M. (2013). The exoribonuclease Dis3L2 defines a novel eukaryotic RNA degradation pathway. EMBO J. *32*, 1842–1854.

Mali, P., Yang, L., Esvelt, K.M., Aach, J., Guell, M., DiCarlo, J.E., Norville, J.E., and Church, G.M. (2013). RNA-Guided Human Genome Engineering via Cas9. Science *339*, 823–826.

Maniataki, E., and Mourelatos, Z. (2005). A human, ATP-independent, RISC assembly machine fueled by pre-miRNA. Genes Dev *19*, 2979–2990.

Marcinowski, L., Tanguy, M., Krmpotic, A., Rädle, B., Lisnić, V.J., Tuddenham, L., Chane-Woon-Ming, B., Ruzsics, Z., Erhard, F., Benkartek, C., et al. (2012). Degradation of cellular

mir-27 by a novel, highly abundant viral transcript is important for efficient virus replication in vivo. PLoS Pathog. *8*, e1002510.

Martell, J.D., Deerinck, T.J., Sancak, Y., Poulos, T.L., Mootha, V.K., Sosinsky, G.E., Ellisman, M.H., and Ting, A.Y. (2012). Engineered ascorbate peroxidase as a genetically encoded reporter for electron microscopy. Nat. Biotechnol. *30*, 1143–1148.

Martin, G., and Keller, W. (2007). RNA-specific ribonucleotidyl transferases. RNA *13*, 1834–1849.

Martinez, N.J., and Gregory, R.I. (2013). Argonaute2 expression is post-transcriptionally coupled to microRNA abundance. RNA *19*, 605–612.

de la Mata, M., Gaidatzis, D., Vitanescu, M., Stadler, M.B., Wentzel, C., Scheiffele, P., Filipowicz, W., and Großhans, H. (2015). Potent degradation of neuronal miRNAs induced by highly complementary targets. EMBO Rep. *16*, 500–511.

Mathys, H., Basquin, J., Ozgur, S., Czarnocki-Cieciura, M., Bonneau, F., Aartse, A., Dziembowski, A., Nowotny, M., Conti, E., and Filipowicz, W. (2014). Structural and biochemical insights to the role of the CCR4-NOT complex and DDX6 ATPase in microRNA repression. Mol. Cell *54*, 751–765.

Mazumder, A., Bose, M., Chakraborty, A., Chakrabarti, S., and Bhattacharyya, S.N. (2013). A transient reversal of miRNA-mediated repression controls macrophage activation. EMBO Rep. *14*, 1008–1016.

Mehta, V., and Trinkle-Mulcahy, L. (2016). Recent advances in large-scale protein interactome mapping. F1000Research *5*.

Meisner, N.-C., and Filipowicz, W. (2011). Properties of the Regulatory RNA-Binding Protein HuR and its Role in Controlling miRNA Repression. Adv. Exp. Med. Biol. *700*, 106–123.

Meister, G., Landthaler, M., Patkaniowska, A., Dorsett, Y., Teng, G., and Tuschl, T. (2004). Human Argonaute2 mediates RNA cleavage targeted by miRNAs and siRNAs. Mol Cell *15*, 185–197.

Meister, G., Landthaler, M., Peters, L., Chen, P.Y., Urlaub, H., Lührmann, R., and Tuschl, T. (2005). Identification of novel argonaute-associated proteins. Curr. Biol. CB *15*, 2149–2155.

Mellacheruvu, D., Wright, Z., Couzens, A.L., Lambert, J.-P., St-Denis, N.A., Li, T., Miteva, Y.V., Hauri, S., Sardiu, M.E., Low, T.Y., et al. (2013). The CRAPome: a contaminant repository for affinity purification-mass spectrometry data. Nat. Methods *10*, 730–736.

Mellman, D.L., Gonzales, M.L., Song, C., Barlow, C.A., Wang, P., Kendziorski, C., and Anderson, R.A. (2008). A PtdIns4,5P2-regulated nuclear poly(A) polymerase controls expression of select mRNAs. Nature *451*, 1013–1017.

Melo, S.A., Ropero, S., Moutinho, C., Aaltonen, L.A., Yamamoto, H., Calin, G.A., Rossi, S., Fernandez, A.F., Carneiro, F., Oliveira, C., et al. (2009). A TARBP2 mutation in human cancer impairs microRNA processing and DICER1 function. Nat. Genet. *41*, 365–370.

Melo, S.A., Moutinho, C., Ropero, S., Calin, G.A., Rossi, S., Spizzo, R., Fernandez, A.F., Davalos, V., Villanueva, A., Montoya, G., et al. (2010). A Genetic Defect in Exportin-5 Traps Precursor MicroRNAs in the Nucleus of Cancer Cells. Cancer Cell *18*, 303–315.

Memczak, S., Jens, M., Elefsinioti, A., Torti, F., Krueger, J., Rybak, A., Maier, L., Mackowiak, S.D., Gregersen, L.H., Munschauer, M., et al. (2013). Circular RNAs are a large class of animal RNAs with regulatory potency. Nature *495*, 333–338.

Mencia, A., Modamio-Hoybjor, S., Redshaw, N., Morin, M., Mayo-Merino, F., Olavarrieta, L., Aguirre, L.A., del Castillo, I., Steel, K.P., Dalmay, T., et al. (2009). Mutations in the seed region of human miR-96 are responsible for nonsyndromic progressive hearing loss. Nat Genet *41*, 609–613.

Merritt, W.M., Lin, Y.G., Han, L.Y., Kamat, A.A., Spannuth, W.A., Schmandt, R., Urbauer, D., Pennacchio, L.A., Cheng, J.-F., Nick, A.M., et al. (2008). Dicer, Drosha, and outcomes in patients with ovarian cancer. N. Engl. J. Med. *359*, 2641–2650.

Michlewski, G., Guil, S., Semple, C.A., and Cáceres, J.F. (2008). Posttranscriptional regulation of miRNAs harboring conserved terminal loops. Mol. Cell *32*, 383–393.

Mick, D.U., Rodrigues, R.B., Leib, R.D., Adams, C.M., Chien, A.S., Gygi, S.P., and Nachury, M.V. (2015). Proteomics of Primary Cilia by Proximity Labeling. Dev. Cell *35*, 497–512.

Min, H., and Yoon, S. (2010). Got target?: computational methods for microRNA target prediction and their extension. Exp. Mol. Med. *42*, 233–244.

Miska, E.A., Alvarez-Saavedra, E., Abbott, A.L., Lau, N.C., Hellman, A.B., McGonagle, S.M., Bartel, D.P., Ambros, V.R., and Horvitz, H.R. (2007). Most Caenorhabditis elegans microRNAs Are Individually Not Essential for Development or Viability. PLOS Genet *3*, e215.

Mohan, N., Ap, S., Francis, N., Anderson, R., and Laishram, R.S. (2015). Phosphorylation regulates the Star-PAP-PIPKIα interaction and directs specificity toward mRNA targets. Nucleic Acids Res. *43*, 7005–7020.

Monteys, A.M., Spengler, R.M., Wan, J., Tecedor, L., Lennox, K.A., Xing, Y., and Davidson, B.L. (2010). Structure and activity of putative intronic miRNA promoters. RNA *16*, 495–505.

Morin, R.D., O'Connor, M.D., Griffith, M., Kuchenbauer, F., Delaney, A., Prabhu, A.-L., Zhao, Y., McDonald, H., Zeng, T., Hirst, M., et al. (2008). Application of massively parallel sequencing to microRNA profiling and discovery in human embryonic stem cells. Genome Res. *18*, 610–621.

Much, C., Auchynnikava, T., Pavlinic, D., Buness, A., Rappsilber, J., Benes, V., Allshire, R., and O'Carroll, D. (2016). Endogenous Mouse Dicer Is an Exclusively Cytoplasmic Protein. PLOS Genet *12*, e1006095.

Mukherjee, N., Corcoran, D.L., Nusbaum, J.D., Reid, D.W., Georgiev, S., Hafner, M., Ascano Jr., M., Tuschl, T., Ohler, U., and Keene, J.D. (2011). Integrative Regulatory Mapping Indicates that the RNA-Binding Protein HuR Couples Pre-mRNA Processing and mRNA Stability. Mol. Cell *43*, 327–339.

N

Nakanishi, T., Kubota, H., Ishibashi, N., Kumagai, S., Watanabe, H., Yamashita, M., Kashiwabara, S., Miyado, K., and Baba, T. (2006). Possible role of mouse poly(A) polymerase mGLD-2 during oocyte maturation. Dev. Biol. *289*, 115–126.

Neilsen, C.T., Goodall, G.J., and Bracken, C.P. (2012). IsomiRs – the overlooked repertoire in the dynamic microRNAome. Trends Genet. *28*, 544–549.

Newman, M.A., Thomson, J.M., and Hammond, S.M. (2008). Lin-28 interaction with the Let-7 precursor loop mediates regulated microRNA processing. RNA *14*, 1539–1549.

Newman, M.A., Mani, V., and Hammond, S.M. (2011). Deep sequencing of microRNA precursors reveals extensive 3′ end modification. RNA *17*, 1795–1803.

Nguyen, T.A., Jo, M.H., Choi, Y.-G., Park, J., Kwon, S.C., Hohng, S., Kim, V.N., and Woo, J.-S. (2015). Functional Anatomy of the Human Microprocessor. Cell *161*, 1374–1387.

Nishikura, K. (2010). Functions and regulation of RNA editing by ADAR deaminases. Annu. Rev. Biochem. *79*, 321–349.

Nishikura, K. (2016). A-to-I editing of coding and non-coding RNAs by ADARs. Nat. Rev. Mol. Cell Biol. *17*, 83–96.

O

O'Donnell, K.A., Wentzel, E.A., Zeller, K.I., Dang, C.V., and Mendell, J.T. (2005). c-Myc-regulated microRNAs modulate E2F1 expression. Nature *435*, 839–843.

Okada, C., Yamashita, E., Lee, S.J., Shibata, S., Katahira, J., Nakagawa, A., Yoneda, Y., and Tsukihara, T. (2009). A high-resolution structure of the pre-microRNA nuclear export machinery. Science *326*, 1275–1279.

Okamura, K., Ishizuka, A., Siomi, H., and Siomi, M.C. (2004). Distinct roles for Argonaute proteins in small RNA-directed RNA cleavage pathways. Genes Dev *18*, 1655–1666.

Okamura, K., Hagen, J.W., Duan, H., Tyler, D.M., and Lai, E.C. (2007). The mirtron pathway generates microRNA-class regulatory RNAs in Drosophila. Cell *130*, 89–100.

Olsen, P.H., and Ambros, V. (1999). The lin-4 regulatory RNA controls developmental timing in Caenorhabditis elegans by blocking LIN-14 protein synthesis after the initiation of translation. Dev Biol *216*, 671–680.

Ozsolak, F., Poling, L.L., Wang, Z., Liu, H., Liu, X.S., Roeder, R.G., Zhang, X., Song, J.S., and Fisher, D.E. (2008). Chromatin structure analyses identify miRNA promoters. Genes Dev. *22*, 3172–3183.

P

Park, C.Y., Jeker, L.T., Carver-Moore, K., Oh, A., Liu, H.J., Cameron, R., Richards, H., Li, Z., Adler, D., Yoshinaga, Y., et al. (2012). A Resource for the Conditional Ablation of microRNAs in the Mouse. Cell Rep. *1*, 385–391.

Park, J.-E., Heo, I., Tian, Y., Simanshu, D.K., Chang, H., Jee, D., Patel, D.J., and Kim, V.N. (2011). Dicer recognizes the 5′ end of RNA for efficient and accurate processing. Nature *475*, 201–205.

Parker, J.S., Roe, S.M., and Barford, D. (2005). Structural insights into mRNA recognition from a PIWI domain-siRNA guide complex. Nature *434*, 663–666.

Paroo, Z., Ye, X., Chen, S., and Liu, Q. (2009). Phosphorylation of the Human MicroRNA-Generating Complex Mediates MAPK/Erk Signaling. Cell *139*, 112–122.

Pasquinelli, A.E. (2012). MicroRNAs and their targets: recognition, regulation and an emerging reciprocal relationship. Nat. Rev. Genet. *13*, 271–282.

Pass, R.F., Fowler, K.B., Boppana, S.B., Britt, W.J., and Stagno, S. (2006). Congenital cytomegalovirus infection following first trimester maternal infection: symptoms at birth and outcome. J. Clin. Virol. Off. Publ. Pan Am. Soc. Clin. Virol. *35*, 216–220.

Pawlica, P., Moss, W.N., and Steitz, J.A. (2016). Host miRNA degradation by Herpesvirus saimiri small nuclear RNA requires an unstructured interacting region. RNA *22*, 1181–1189.

Peng, Z., Cheng, Y., Tan, B.C.-M., Kang, L., Tian, Z., Zhu, Y., Zhang, W., Liang, Y., Hu, X., Tan, X., et al. (2012). Comprehensive analysis of RNA-Seq data reveals extensive RNA editing in a human transcriptome. Nat. Biotechnol. *30*, 253–260.

Pfaff, J., Hennig, J., Herzog, F., Aebersold, R., Sattler, M., Niessing, D., and Meister, G. (2013). Structural features of Argonaute-GW182 protein interactions. Proc. Natl. Acad. Sci. U. S. A. *110*, E3770–E3779.

Pfeffer, S., Sewer, A., Lagos-Quintana, M., Sheridan, R., Sander, C., Grässer, F.A., van Dyk, L.F., Ho, C.K., Shuman, S., Chien, M., et al. (2005). Identification of microRNAs of the herpesvirus family. Nat. Methods *2*, 269–276.

Piedade, D., and Azevedo-Pereira, J.M. (2016). The Role of microRNAs in the Pathogenesis of Herpesvirus Infection. Viruses *8*.

Pillai, R.S., Bhattacharyya, S.N., Artus, C.G., Zoller, T., Cougot, N., Basyuk, E., Bertrand, E., and Filipowicz, W. (2005). Inhibition of translational initiation by Let-7 MicroRNA in human cells. Science *309*, 1573–1576.

Pillai, R.S., Bhattacharyya, S.N., and Filipowicz, W. (2007). Repression of protein synthesis by miRNAs: how many mechanisms? Trends Cell Biol *17*, 118–126.

Pirouz, M., Du, P., Munafò, M., and Gregory, R.I. (2016). Dis3l2-Mediated Decay Is a Quality Control Pathway for Noncoding RNAs. Cell Rep.

de Pontual, L., Yao, E., Callier, P., Faivre, L., Drouin, V., Cariou, S., Van Haeringen, A., Geneviève, D., Goldenberg, A., Oufadem, M., et al. (2011). Germline deletion of the miR-17[sim]92 cluster causes skeletal and growth defects in humans. Nat. Genet. *43*, 1026–1030.

Poser, I., Sarov, M., Hutchins, J.R.A., Hériché, J.-K., Toyoda, Y., Pozniakovsky, A., Weigl, D., Nitzsche, A., Hegemann, B., Bird, A.W., et al. (2008). BAC TransgeneOmics: a high-throughput method for exploration of protein function in mammals. Nat. Methods *5*, 409–415.

Puig, O., Caspary, F., Rigaut, G., Rutz, B., Bouveret, E., Bragado-Nilsson, E., Wilm, M., and Seraphin, B. (2001). The tandem affinity purification (TAP) method: a general procedure of protein complex purification. Methods *24*, 218–229.

Q

Qi, H.H., Ongusaha, P.P., Myllyharju, J., Cheng, D., Pakkanen, O., Shi, Y., Lee, S.W., Peng, J., and Shi, Y. (2008). Prolyl 4-hydroxylation regulates Argonaute 2 stability. Nature *455*, 421–424.

R

Rajasethupathy, P., Fiumara, F., Sheridan, R., Betel, D., Puthanveettil, S.V., Russo, J.J., Sander, C., Tuschl, T., and Kandel, E. (2009). Characterization of small RNAs in Aplysia reveals a role for miR-124 in constraining synaptic plasticity through CREB. Neuron *63*, 803–817.

Ramachandran, V., and Chen, X. (2008). Degradation of microRNAs by a family of exoribonucleases in Arabidopsis. Science *321*, 1490–1492.

Reese, T.A., Xia, J., Johnson, L.S., Zhou, X., Zhang, W., and Virgin, H.W. (2010). Identification of novel microRNA-like molecules generated from herpesvirus and host tRNA transcripts. J. Virol. *84*, 10344–10353.

Reimão-Pinto, M.M., Ignatova, V., Burkard, T.R., Hung, J.-H., Manzenreither, R.A., Sowemimo, I., Herzog, V.A., Reichholf, B., Fariña-Lopez, S., and Ameres, S.L. (2015). Uridylation of RNA Hairpins by Tailor Confines the Emergence of MicroRNAs in Drosophila. Mol. Cell *59*, 203–216.

Reinhart, B.J., Slack, F.J., Basson, M., Pasquinelli, A.E., Bettinger, J.C., Rougvie, A.E., Horvitz, H.R., and Ruvkun, G. (2000). The 21-nucleotide let-7 RNA regulates developmental timing in Caenorhabditis elegans. Nature *403*, 901–906.

Ren, G., Chen, X., and Yu, B. (2012). Uridylation of miRNAs by hen1 suppressor1 in Arabidopsis. Curr. Biol. CB *22*, 695–700.

Rhee, H.-W., Zou, P., Udeshi, N.D., Martell, J.D., Mootha, V.K., Carr, S.A., and Ting, A.Y. (2013). Proteomic Mapping of Mitochondria in Living Cells via Spatially Restricted Enzymatic Tagging. Science *339*, 1328–1331.

Rigaut, G., Shevchenko, A., Rutz, B., Wilm, M., Mann, M., and Seraphin, B. (1999). A generic protein purification method for protein complex characterization and proteome exploration. Nat Biotechnol *17*, 1030–1032.

Rissland, O.S., Mikulasova, A., and Norbury, C.J. (2007). Efficient RNA Polyuridylation by Noncanonical Poly(A) Polymerases. Mol. Cell. Biol. *27*, 3612–3624.

Rissland, O.S., Hong, S.-J., and Bartel, D.P. (2011). MicroRNA destabilization enables dynamic regulation of the miR-16 family in response to cell-cycle changes. Mol. Cell *43*, 993–1004.

Rodriguez, A., Griffiths-Jones, S., Ashurst, J.L., and Bradley, A. (2004). Identification of mammalian microRNA host genes and transcription units. Genome Res *14*, 1902–1910.

Romilly, C., Lays, C., Tomasini, A., Caldelari, I., Benito, Y., Hammann, P., Geissmann, T., Boisset, S., Romby, P., and Vandenesch, F. (2014). A non-coding RNA promotes bacterial persistence and decreases virulence by regulating a regulator in Staphylococcus aureus. PLoS Pathog. *10*, e1003979.

Rooij, E. van, Sutherland, L.B., Qi, X., Richardson, J.A., Hill, J., and Olson, E.N. (2007). Control of Stress-Dependent Cardiac Growth and Gene Expression by a MicroRNA. Science *316*, 575–579.

Roux, K.J. (2013). Marked by association: techniques for proximity-dependent labeling of proteins in eukaryotic cells. Cell. Mol. Life Sci. CMLS *70*, 3657–3664.

Roux, K.J., Kim, D.I., Raida, M., and Burke, B. (2012). A promiscuous biotin ligase fusion protein identifies proximal and interacting proteins in mammalian cells. J. Cell Biol. *196*, 801–810.

Roux, K.J., Kim, D.I., and Burke, B. (2013). BioID: a screen for protein-protein interactions. Curr. Protoc. Protein Sci. Editor. Board John E Coligan Al *74*, Unit 19.23.

Ruby, J.G., Jan, C.H., and Bartel, D.P. (2007). Intronic microRNA precursors that bypass Drosha processing. Nature *448*, 83–86.

Rüdel, S., Wang, Y., Lenobel, R., Körner, R., Hsiao, H.-H., Urlaub, H., Patel, D., and Meister, G. (2011). Phosphorylation of human Argonaute proteins affects small RNA binding. Nucleic Acids Res. *39*, 2330–2343.

Rüegger, S., and Großhans, H. (2012). MicroRNA turnover: when, how, and why. Trends Biochem. Sci. *37*, 436–446.

Ruegger, S., Miki, T.S., Hess, D., and Grosshans, H. (2015). The ribonucleotidyl transferase USIP-1 acts with SART3 to promote U6 snRNA recycling. Nucleic Acids Res. *43*, 3344–3357.

Ruggiero, T., Trabucchi, M., De Santa, F., Zupo, S., Harfe, B.D., McManus, M.T., Rosenfeld, M.G., Briata, P., and Gherzi, R. (2009). LPS induces KH-type splicing regulatory protein-dependent processing of microRNA-155 precursors in macrophages. FASEB J. Off. Publ. Fed. Am. Soc. Exp. Biol. *23*, 2898–2908.

Ryan, B.M., Robles, A.I., and Harris, C.C. (2010). Genetic variation in microRNA networks: the implications for cancer research. Nat. Rev. Cancer *10*, 389–402.

Rybak, A., Fuchs, H., Smirnova, L., Brandt, C., Pohl, E.E., Nitsch, R., and Wulczyn, F.G. (2008). A feedback loop comprising lin-28 and let-7 controls pre-let-7 maturation during neural stem-cell commitment. Nat Cell Biol *10*, 987–993.

Rybak, A., Fuchs, H., Hadian, K., Smirnova, L., Wulczyn, E.A., Michel, G., Nitsch, R., Krappmann, D., and Wulczyn, F.G. (2009). The let-7 target gene mouse lin-41 is a stem cell specific E3 ubiquitin ligase for the miRNA pathway protein Ago2. Nat. Cell Biol. *11*, 1411–1420.

S

Saetrom, P., Heale, B.S.E., Snøve, O., Aagaard, L., Alluin, J., and Rossi, J.J. (2007). Distance constraints between microRNA target sites dictate efficacy and cooperativity. Nucleic Acids Res. *35*, 2333–2342.

Santhakumar, D., Forster, T., Laqtom, N.N., Fragkoudis, R., Dickinson, P., Abreu-Goodger, C., Manakov, S.A., Choudhury, N.R., Griffiths, S.J., Vermeulen, A., et al. (2010). Combined agonist-antagonist genome-wide functional screening identifies broadly active antiviral microRNAs. Proc. Natl. Acad. Sci. U. S. A. *107*, 13830–13835.

Schirle, N.T., and MacRae, I.J. (2012). The Crystal Structure of Human Argonaute2. Science *336*, 1037–1040.

Schmidt, M.-J., West, S., and Norbury, C.J. (2011). The human cytoplasmic RNA terminal U-transferase ZCCHC11 targets histone mRNAs for degradation. RNA *17*, 39–44.

Schwarz, D.S., Hutvágner, G., Du, T., Xu, Z., Aronin, N., and Zamore, P.D. (2003). Asymmetry in the assembly of the RNAi enzyme complex. Cell *115*, 199–208.

Schwarz, D.S., Tomari, Y., and Zamore, P.D. (2004). The RNA-induced silencing complex Is a Mg(2+)-dependent endonuclease. Curr Biol *14*, 787–791.

Schweingruber, C., Soffientini, P., Ruepp, M.-D., Bachi, A., and Mühlemann, O. (2016). Identification of Interactions in the NMD Complex Using Proximity-Dependent Biotinylation (BioID). PLOS ONE *11*, e0150239.

Sen, G.L., and Blau, H.M. (2005). Argonaute 2/RISC resides in sites of mammalian mRNA decay known as cytoplasmic bodies. Nat. Cell Biol. *7*, 633–636.

Seo, G.J., Kincaid, R.P., Phanaksri, T., Burke, J.M., Pare, J.M., Cox, J.E., Hsiang, T.-Y., Krug, R.M., and Sullivan, C.S. (2013). Reciprocal inhibition between intracellular antiviral signaling and the RNAi machinery in mammalian cells. Cell Host Microbe *14*, 435–445.

Sethi, P., and Lukiw, W.J. (2009). Micro-RNA abundance and stability in human brain: specific alterations in Alzheimer's disease temporal lobe neocortex. Neurosci. Lett. *459*, 100–104.

Shen, B., and Goodman, H.M. (2004). Uridine addition after microRNA-directed cleavage. Science *306*, 997.

Shen, J., Xia, W., Khotskaya, Y.B., Huo, L., Nakanishi, K., Lim, S.-O., Du, Y., Wang, Y., Chang, W.-C., Chen, C.-H., et al. (2013). EGFR modulates microRNA maturation in response to hypoxia through phosphorylation of AGO2. Nature *497*, 383–387.

Shin, C. (2008). Cleavage of the star strand facilitates assembly of some microRNAs into Ago2-containing silencing complexes in mammals. Mol. Cells *26*, 308–313.

Smibert, P., Yang, J.-S., Azzam, G., Liu, J.-L., and Lai, E.C. (2013). Homeostatic control of Argonaute stability by microRNA availability. Nat. Struct. Mol. Biol. *20*, 789–795.

Song, J.J., Smith, S.K., Hannon, G.J., and Joshua-Tor, L. (2004). Crystal structure of Argonaute and its implications for RISC slicer activity. Science *305*, 1434–1437.

Stark, A., Brennecke, J., Bushati, N., Russell, R.B., and Cohen, S.M. (2005). Animal MicroRNAs confer robustness to gene expression and have a significant impact on 3'UTR evolution. Cell *123*, 1133–1146.

Stevenson, A.L., and Norbury, C.J. (2006). The Cid1 family of non-canonical poly(A) polymerases. Yeast *23*, 991–1000.

Su, W., Slepenkov, S.V., Slevin, M.K., Lyons, S.M., Ziemniak, M., Kowalska, J., Darzynkiewicz, E., Jemielity, J., Marzluff, W.F., and Rhoads, R.E. (2013). mRNAs containing the histone 3′ stem–loop are degraded primarily by decapping mediated by oligouridylation of the 3′ end. RNA *19*, 1–16.

Suh, M.R., Lee, Y., Kim, J.Y., Kim, S.K., Moon, S.H., Lee, J.Y., Cha, K.Y., Chung, H.M., Yoon, H.S., Moon, S.Y., et al. (2004). Human embryonic stem cells express a unique set of microRNAs. Dev Biol *270*, 488–498.

Suzuki, H.I., Yamagata, K., Sugimoto, K., Iwamoto, T., Kato, S., and Miyazono, K. (2009). Modulation of microRNA processing by p53. Nature *460*, 529–533.

Suzuki, H.I., Katsura, A., Yasuda, T., Ueno, T., Mano, H., Sugimoto, K., and Miyazono, K. (2015). Small-RNA asymmetry is directly driven by mammalian Argonautes. Nat. Struct. Mol. Biol. *22*, 512–521.

Svobodova, E., Kubikova, J., and Svoboda, P. (2016). Production of small RNAs by mammalian Dicer. Pflugers Arch.

T

Tang, X., Zhang, Y., Tucker, L., and Ramratnam, B. (2010). Phosphorylation of the RNase III enzyme Drosha at Serine300 or Serine302 is required for its nuclear localization. Nucleic Acids Res. *38*, 6610–6619.

Tang, X., Li, M., Tucker, L., and Ramratnam, B. (2011). Glycogen Synthase Kinase 3 Beta (GSK3β) Phosphorylates the RNAase III Enzyme Drosha at S300 and S302. PLOS ONE *6*, e20391.

Tang, X., Wen, S., Zheng, D., Tucker, L., Cao, L., Pantazatos, D., Moss, S.F., and Ramratnam, B. (2013). Acetylation of Drosha on the N-Terminus Inhibits Its Degradation by Ubiquitination. PLOS ONE *8*, e72503.

Thiele, H., Glandorf, J., and Hufnagel, P. (2010). Bioinformatics strategies in life sciences: from data processing and data warehousing to biological knowledge extraction. J. Integr. Bioinforma. *7*, 141.

Thomas, M.F., Abdul-Wajid, S., Panduro, M., Babiarz, J.E., Rajaram, M., Woodruff, P., Lanier, L.L., Heissmeyer, V., and Ansel, K.M. (2012). Eri1 regulates microRNA homeostasis and mouse lymphocyte development and antiviral function. Blood *120*, 130–142.

Thomas, M.P., Liu, X., Whangbo, J., McCrossan, G., Sanborn, K.B., Basar, E., Walch, M., and Lieberman, J. (2015). Apoptosis Triggers Specific, Rapid, and Global mRNA Decay with 3′ Uridylated Intermediates Degraded by DIS3L2. Cell Rep. *11*, 1079–1089.

Thomson, J.M., Newman, M., Parker, J.S., Morin-Kensicki, E.M., Wright, T., and Hammond, S.M. (2006). Extensive Post-Transcriptional Regulation of microRNAs and Its Implications for Cancer. Genes Dev. *20*, 2202–2207.

Thornton, J.E., Chang, H.-M., Piskounova, E., and Gregory, R.I. (2012). Lin28-mediated control of let-7 microRNA expression by alternative TUTases Zcchc11 (TUT4) and Zcchc6 (TUT7). RNA *18*, 1875–1885.

Till, S., Lejeune, E., Thermann, R., Bortfeld, M., Hothorn, M., Enderle, D., Heinrich, C., Hentze, M.W., and Ladurner, A.G. (2007). A conserved motif in Argonaute-interacting proteins mediates functional interactions through the Argonaute PIWI domain. Nat. Struct. Mol. Biol. *14*, 897–903.

Trabucchi, M., Briata, P., Garcia-Mayoral, M., Haase, A.D., Filipowicz, W., Ramos, A., Gherzi, R., and Rosenfeld, M.G. (2009). The RNA-binding protein KSRP promotes the biogenesis of a subset of microRNAs. Nature *459*, 1010–1014.

Triboulet, R., Chang, H.-M., Lapierre, R.J., and Gregory, R.I. (2009). Post-transcriptional control of DGCR8 expression by the Microprocessor. RNA N. Y. N *15*, 1005–1011.

Trippe, R., Richly, H., and Benecke, B.-J. (2003). Biochemical characterization of a U6 small nuclear RNA-specific terminal uridylyltransferase. Eur. J. Biochem. *270*, 971–980.

Trippe, R., Guschina, E., Hossbach, M., Urlaub, H., Lührmann, R., and Benecke, B.-J. (2006). Identification, cloning, and functional analysis of the human U6 snRNA-specific terminal uridylyl transferase. RNA *12*, 1494–1504.

Tuddenham, L., and Pfeffer, S. (2011). Roles and regulation of microRNAs in cytomegalovirus infection. Biochim. Biophys. Acta *1809*, 613–622.

U

Ustianenko, D., Hrossova, D., Potesil, D., Chalupnikova, K., Hrazdilova, K., Pachernik, J., Cetkovska, K., Uldrijan, S., Zdrahal, Z., and Vanacova, S. (2013). Mammalian DIS3L2 exoribonuclease targets the uridylated precursors of let-7 miRNAs. RNA *19*, 1632–1638.

V

Vasudevan, S., and Steitz, J.A. (2007). AU-Rich-Element-Mediated Upregulation of Translation by FXR1 and Argonaute 2. Cell *128*, 1105–1118.

Vasudevan, S., Tong, Y., and Steitz, J.A. (2007). Switching from repression to activation: microRNAs can up-regulate translation. Science *318*, 1931–1934.

Viswanathan, S.R., Daley, G.Q., and Gregory, R.I. (2008). Selective blockade of microRNA processing by Lin28. Science *320*, 97–100.

W

Wada, T., Kikuchi, J., and Furukawa, Y. (2012). Histone deacetylase 1 enhances microRNA processing via deacetylation of DGCR8. EMBO Rep. *13*, 142–149.

Wahle, E., and Winkler, G.S. (2013). RNA decay machines: Deadenylation by the Ccr4–Not and Pan2–Pan3 complexes. Biochim. Biophys. Acta BBA - Gene Regul. Mech. *1829*, 561–570.

Wan, G., Zhang, X., Langley, R.R., Liu, Y., Hu, X., Han, C., Peng, G., Ellis, L.M., Jones, S.N., and Lu, X. (2013). DNA-Damage-Induced Nuclear Export of Precursor MicroRNAs Is Regulated by the ATM-AKT Pathway. Cell Rep. *3*, 2100–2112.

Wang, S.-W., Toda, T., MacCallum, R., Harris, A.L., and Norbury, C. (2000). Cid1, a Fission Yeast Protein Required for S-M Checkpoint Control when DNA Polymerase δ or ε Is Inactivated. Mol. Cell. Biol. *20*, 3234–3244.

Wang, T., Birsoy, K., Hughes, N.W., Krupczak, K.M., Post, Y., Wei, J.J., Lander, E.S., and Sabatini, D.M. (2015a). Identification and characterization of essential genes in the human genome. Science *350*, 1096–1101.

Wang, X., Zhang, S., Dou, Y., Zhang, C., Chen, X., Yu, B., and Ren, G. (2015b). Synergistic and independent actions of multiple terminal nucleotidyl transferases in the 3' tailing of small RNAs in Arabidopsis. PLoS Genet. *11*, e1005091.

Wang, Y., Medvid, R., Melton, C., Jaenisch, R., and Blelloch, R. (2007). DGCR8 is essential for microRNA biogenesis and silencing of embryonic stem cell self-renewal. Nat. Genet. *39*, 380–385.

Wang, Y., Juranek, S., Li, H., Sheng, G., Wardle, G.S., Tuschl, T., and Patel, D.J. (2009). Nucleation, propagation and cleavage of target RNAs in Ago silencing complexes. Nature *461*, 754–761.

White, E.A., and Spector, D.H. (2007). Early viral gene expression and function. In Human Herpesviruses: Biology, Therapy, and Immunoprophylaxis, A. Arvin, G. Campadelli-Fiume, E. Mocarski, P.S. Moore, B. Roizman, R. Whitley, and K. Yamanishi, eds. (Cambridge: Cambridge University Press),.

White, E., Schlackow, M., Kamieniarz-Gdula, K., Proudfoot, N.J., and Gullerova, M. (2014). Human nuclear Dicer restricts the deleterious accumulation of endogenous double-stranded RNA. Nat. Struct. Mol. Biol. *21*, 552–559.

Wickens, M., and Kwak, J.E. (2008). A Tail Tale for U. Science *319*, 1344–1345.

Wilson, R.C., Tambe, A., Kidwell, M.A., Noland, C.L., Schneider, C.P., and Doudna, J.A. (2015). Dicer-TRBP complex formation ensures accurate mammalian microRNA biogenesis. Mol. Cell *57*, 397–407.

Wilusz, C.J., and Wilusz, J. (2008). New ways to meet your (3′) end—oligouridylation as a step on the path to destruction. Genes Dev. *22*, 1–7.

Wu, C., So, J., Davis-Dusenbery, B.N., Qi, H.H., Bloch, D.B., Shi, Y., Lagna, G., and Hata, A. (2011). Hypoxia Potentiates MicroRNA-Mediated Gene Silencing through Posttranslational Modification of Argonaute2. Mol. Cell. Biol. *31*, 4760–4774.

Wu, H., Ye, C., Ramirez, D., and Manjunath, N. (2009). Alternative Processing of Primary microRNA Transcripts by Drosha Generates 5′ End Variation of Mature microRNA. PLOS ONE *4*, e7566.

Wyman, S.K., Knouf, E.C., Parkin, R.K., Fritz, B.R., Lin, D.W., Dennis, L.M., Krouse, M.A., Webster, P.J., and Tewari, M. (2011). Post-transcriptional generation of miRNA variants by multiple nucleotidyl transferases contributes to miRNA transcriptome complexity. Genome Res. *21*, 1450–1461.

X

Xhemalce, B., Robson, S.C., and Kouzarides, T. (2012). Human RNA Methyltransferase BCDIN3D Regulates MicroRNA Processing. Cell *151*, 278–288.

Xie, J., Ameres, S.L., Friedline, R., Hung, J.-H., Zhang, Y., Xie, Q., Zhong, L., Su, Q., He, R., Li, M., et al. (2012). Long-term, efficient inhibition of microRNA function in mice using rAAV vectors. Nat. Methods *9*, 403–409.

Xie, M., Li, M., Vilborg, A., Lee, N., Shu, M.-D., Yartseva, V., Šestan, N., and Steitz, J.A. (2013). Mammalian 5′-Capped MicroRNA Precursors that Generate a Single MicroRNA. Cell *155*, 1568–1580.

Xue, Z., Yuan, H., Guo, J., and Liu, Y. (2012). Reconstitution of an Argonaute-dependent small RNA biogenesis pathway reveals a handover mechanism involving the RNA exosome and the exonuclease QIP. Mol. Cell *46*, 299–310.

Y

Yan, K.S., Yan, S., Farooq, A., Han, A., Zeng, L., and Zhou, M.M. (2003). Structure and conserved RNA binding of the PAZ domain. Nature *426*, 468–474.

Yang, J.-S., Maurin, T., Robine, N., Rasmussen, K.D., Jeffrey, K.L., Chandwani, R., Papapetrou, E.P., Sadelain, M., O'Carroll, D., and Lai, E.C. (2010). Conserved vertebrate mir-451 provides a platform for Dicer-independent, Ago2-mediated microRNA biogenesis. Proc. Natl. Acad. Sci. *107*, 15163–15168.

Yang, W., Chendrimada, T.P., Wang, Q., Higuchi, M., Seeburg, P.H., Shiekhattar, R., and Nishikura, K. (2006). Modulation of microRNA processing and expression through RNA editing by ADAR deaminases. Nat Struct Mol Biol *13*, 13–21.

Yekta, S., Shih, I.H., and Bartel, D.P. (2004). MicroRNA-directed cleavage of HOXB8 mRNA. Science *304*, 594–596.

Yeom, K.-H., Lee, Y., Han, J., Suh, M.R., and Kim, V.N. (2006). Characterization of DGCR8/Pasha, the essential cofactor for Drosha in primary miRNA processing. Nucleic Acids Res. *34*, 4622–4629.

Yi, R., Qin, Y., Macara, I.G., and Cullen, B.R. (2003). Exportin-5 mediates the nuclear export of pre-microRNAs and short hairpin RNAs. Genes Dev *17*, 3011–3016.

Yoda, M., Cifuentes, D., Izumi, N., Sakaguchi, Y., Suzuki, T., Giraldez, A.J., and Tomari, Y. (2013). Poly(A)-Specific Ribonuclease Mediates 3′-End Trimming of Argonaute2-Cleaved Precursor MicroRNAs. Cell Rep. *5*, 715–726.

Yu, B., Yang, Z., Li, J., Minakhina, S., Yang, M., Padgett, R.W., Steward, R., and Chen, X. (2005). Methylation as a crucial step in plant microRNA biogenesis. Science *307*, 932–935.

Z

Zekri, L., Huntzinger, E., Heimstädt, S., and Izaurralde, E. (2009). The Silencing Domain of GW182 Interacts with PABPC1 To Promote Translational Repression and Degradation of MicroRNA Targets and Is Required for Target Release. Mol. Cell. Biol. *29*, 6220–6231.

Zeng, Y., and Cullen, B.R. (2004). Structural requirements for pre-microRNA binding and nuclear export by Exportin 5. Nucleic Acids Res *32*, 4776–4785.

Zeng, Y., Sankala, H., Zhang, X., and Graves, P.R. (2008). Phosphorylation of Argonaute 2 at serine-387 facilitates its localization to processing bodies. Biochem. J. *413*, 429–436.

Zhang, P., and Zhang, H. (2013). Autophagy modulates miRNA-mediated gene silencing and selectively degrades AIN-1/GW182 in C. elegans. EMBO Rep. *14*, 568–576.

Zhang, H., Kolb, F.A., Jaskiewicz, L., Westhof, E., and Filipowicz, W. (2004). Single processing center models for human Dicer and bacterial RNase III. Cell in press.

Zhang, Z., Zou, J., Wang, G.-K., Zhang, J.-T., Huang, S., Qin, Y.-W., and Jing, Q. (2011). Uracils at nucleotide position 9-11 are required for the rapid turnover of miR-29 family. Nucleic Acids Res. *39*, 4387–4395.

Zhao, Y., Yu, Y., Zhai, J., Ramachandran, V., Dinh, T.T., Meyers, B.C., Mo, B., and Chen, X. (2012). The Arabidopsis nucleotidyl transferase HESO1 uridylates unmethylated small RNAs to trigger their degradation. Curr. Biol. *22*, 689–694.

Zhou, H., Arcila, M.L., Li, Z., Lee, E.J., Henzler, C., Liu, J., Rana, T.M., and Kosik, K.S. (2012). Deep annotation of mouse iso-miR and iso-moR variation. Nucleic Acids Res.

Zipprich, J.T., Bhattacharyya, S., Mathys, H., and Filipowicz, W. (2009). Importance of the C-terminal domain of the human GW182 protein TNRC6C for translational repression. RNA N. Y. N *15*, 781–793.

ANNEX

Annex 1: Complete list of identified proteins in the GFP-mAGO2 sample

Annex 2: Complete list of identified proteins in the BirA*-mAGO2 sample

Annex 3: Complete list of identified proteins in mock, MCMV wt and MCMV mut168 infection

Annex 4: MiR-30a-3p negatively regulates BAFF synthesis in systemic sclerosis and rheumatoid arthritis fibroblasts.
Alsaleh G, François A, Philippe L, Gong YZ, Bahram S, Cetin S, Pfeffer S, Gottenberg JE, Wachsmann D, Georgel P, Sibilia J.

PLos ONE PloS One *9*, e111266. (2014).

Annex 1: Complete list of identified proteins in the GFP-mAGO2 sample

Protein identity	Protein description	Spectra # ▼	SC [%]	MW [kDa]	pI	Mascot Score	RMS [ppm]
ACACA	Acetyl-CoA carboxylase 1 GN=Acaca	1636	75.7	265.1	5.9	1,5483.6	4.61
PYC	Pyruvate carboxylase, mitochondrial GN=Pc	1202	77.2	129.6	6.3	8329.4	4.63
MCCA	Methylcrotonoyl-CoA carboxylase subunit alpha, mitochondrial GN=Mccc1	578	73.8	79.3	8.5	4665.0	4.10
PCCA	Propionyl-CoA carboxylase alpha chain, mitochondrial GN=Pcca	313	66.9	79.9	6.9	3664.4	4.02
K1C10	Keratin, type I cytoskeletal 10 GN=Krt10	23	9.6	57.7	4.9	300.2	5.30
K2C1	Keratin, type II cytoskeletal 1 GN=Krt1	16	5.2	65.6	9.2	268.4	3.08
K2C6A	Keratin, type II cytoskeletal 6A GN=Krt6a	14	5.8	59.3	8.9	215.0	2.73
K2C73	Keratin, type II cytoskeletal 73 GN=Krt73	12	5.9	58.9	9.3	199.0	3.55
HSP72	Heat shock-related 70 kDa protein 2 GN=Hspa2	9	6.6	69.6	5.4	174.2	2.25
K2C8	Keratin, type II cytoskeletal 8 GN=Krt8	8	2.9	54.5	5.6	159.3	17.24
TBA1C	Tubulin alpha-1C chain GN=Tuba1c	8	8.0	49.9	4.8	170.3	6.62
ACTB	Actin, cytoplasmic 1 GN=Actb	8	13.3	41.7	5.2	178.4	5.91
CL023	UPF0444 transmembrane protein C12orf23 homolog	7	67.0	11.5	9.8	159.4	4.28
SRRM2	Serine/arginine repetitive matrix protein 2 GN=Srrm2	7	2.7	294.7	12.6	299.6	7.78
K1C15	Keratin, type I cytoskeletal 15 GN=Krt15	6	6.0	49.1	4.6	147.8	2.89
K2C79	Keratin, type II cytoskeletal 79 GN=Krt79	6	4.0	57.5	8.6	134.4	2.79
K22E	Keratin, type II cytoskeletal 2 epidermal GN=Krt2	5	5.0	70.9	9.1	203.2	11.98
SON	Protein SON GN=Son	4	1.4	265.5	5.4	158.2	2.75
HS90B	Heat shock protein HSP 90-beta GN=Hsp90ab1	4	3.2	83.2	4.8	150.6	3.38
G3P	Glyceraldehyde-3-phosphate dehydrogenase GN=Gapdh	2	7.2	35.8	9.2	75.1	2.91

Spectra **#:** Number of fragmentation MS/MS spectra observed for a given protein. SC%: Sequence coverage expressed in percentage. MW: molecular weight of the identified protein in kDa. pI: isoelectric pH. RMS: Mass error expressed in ppm.

Annex 2: Complete list of identified proteins in the BirA*-mAGO2 sample

Protein identity	Protein description	Spectra # ▼	SC [%]	MW [kDa]	pI	Mascot Score	RMS [ppm]
PYC	Pyruvate carboxylase, mitochondrial GN=Pc	1037	75,6	129,6	6,3	7291,5	4,68
ACACA	Acetyl-CoA carboxylase 1 GN=Acaca	714	66,2	265,1	5,9	9385,4	4,15
AGO2	Protein argonaute-2 GN=Eif2c2	600	78,1	97,2	10,1	5451,8	4,54
MCCA	Methylcrotonoyl-CoA carboxylase subunit alpha, mitochondrial GN=Mccc1	241	67,2	79,3	8,5	2959,2	5,28
PCCA	Propionyl-CoA carboxylase alpha chain, mitochondrial GN=Pcca	217	60,9	79,9	6,9	2879,2	4,18
HS90B	Heat shock protein HSP 90-beta GN=Hsp90ab1	185	57,2	83,2	4,8	2652	5,76
VIGLN	Vigilin GN=Hdlbp	182	39,5	141,7	6,4	2884,4	5,19
ES8L2	Epidermal growth factor receptor kinase substrate 8-like protein 2 GN=Eps8l2	126	45	82,2	6,8	1729,9	5,18
HNRPK	Heterogeneous nuclear ribonucleoprotein K GN=Hnrnpk	112	52,9	50,9	5,3	1319,2	4,68
HSP7C	Heat shock cognate 71 kDa protein GN=Hspa8	103	41,3	70,8	5,2	1738,5	6,03
NUCL	Nucleolin GN=Ncl	98	28,3	76,7	4,5	1461,4	5,36
TLN1	Talin-1 GN=Tln1	95	24,2	269,7	5,8	2163,2	5,07
CSDE1	Cold shock domain-containing protein E1 GN=Csde1	93	32,1	88,7	5,9	1495,1	6,83
IF4G1	Eukaryotic translation initiation factor 4 gamma 1 GN=Eif4g1	83	20	176	5,2	1561,4	4,37
IF5	Eukaryotic translation initiation factor 5 GN=Eif5	76	31	48,9	5,2	895,5	4,01
PRUNE	Protein prune homolog GN=Prune	75	51,5	50,2	4,8	1275,1	6,33
PCBP1	Poly(rC)-binding protein 1 GN=Pcbp1	73	70,8	37,5	6,8	1005	4,04
TCPQ	T-complex protein 1 subunit theta GN=Cct8	64	52	59,5	5,3	1277,7	4,06
NUDC	Nuclear migration protein nudC GN=Nudc	61	63	38,3	5	1040,5	3,61
HS90A	Heat shock protein HSP 90-alpha GN=Hsp90aa1	60	21,4	84,7	4,8	937,2	5,46
TAGL2	Transgelin-2 GN=Tagln2	59	77,9	22,4	9,3	915,7	4,77
TXNL1	Thioredoxin-like protein 1 GN=Txnl1	56	56,4	32,2	4,7	1008,3	5,35
COPG2	Coatomer subunit gamma-2 GN=Copg2	55	29,5	97,6	5,5	1026,3	5,86
UBP2L	Ubiquitin-associated protein 2-like GN=Ubap2l	51	22,7	116,7	6,6	1056,1	7,06
CRK	Adapter molecule crk GN=Crk	50	45,4	33,8	5,3	894	5,68

Annex 2: Complete list of identified proteins in the BirA*-mAGO2 sample

Protein identity	Protein description	Spectra # ▼	SC [%]	MW [kDa]	pI	Mascot Score	RMS [ppm]
RFIP5	Rab11 family-interacting protein 5 GN=Rab11fip5	48	34,9	69,5	9,8	899	3,87
FKBP4	Peptidyl-prolyl cis-trans isomerase FKBP4 GN=Fkbp4	44	36,2	51,5	5,4	879	5,2
ANXA2	Annexin A2 GN=Anxa2	43	46	38,7	8,5	773,7	7,07
TBA1B	Tubulin alpha-1B chain GN=Tuba1b	42	34,4	50,1	4,8	734	3,83
HS105	Heat shock protein 105 kDa GN=Hsph1	41	32,2	96,3	5,3	1125,6	7,31
COR1B	Coronin-1B GN=Coro1b	41	35,3	53,9	5,5	720,7	6,12
PCBP2	Poly(rC)-binding protein 2 GN=Pcbp2	38	34,8	38,2	6,4	531,7	3,76
RL40	Ubiquitin-60S ribosomal protein L40 GN=Uba52	34	41,4	14,7	10,7	341,9	2,9
K2C8	Keratin, type II cytoskeletal 8 GN=Krt8	33	21,4	54,5	5,6	816,6	13,41
SHQ1	Protein SHQ1 homolog GN=Shq1	33	29,9	63,4	4,6	639,4	9,25
CO038	UPF0552 protein C15orf38 homolog	31	42	25,2	4,9	512,1	5,97
TBA4A	Tubulin alpha-4A chain GN=Tuba4a	29	30,4	49,9	4,8	625,9	4,07
IF4B	Eukaryotic translation initiation factor 4B GN=Eif4b	28	14,4	68,8	5,3	467,2	6,96
DDX3X	ATP-dependent RNA helicase DDX3X GN=Ddx3x	27	14	73,1	6,8	564	5,44
SUGT1	Suppressor of G2 allele of SKP1 homolog GN=Sugt1	27	31,5	38,1	5,2	504,9	4,85
PSMD4	26S proteasome non-ATPase regulatory subunit 4 GN=Psmd4	26	28,7	40,7	4,5	483,7	7,18
F120A	Constitutive coactivator of PPAR-gamma-like protein 1 GN=FAM120A	26	13,8	121,6	9,8	850,8	3,7
TADBP	TAR DNA-binding protein 43 GN=Tardbp	26	28,3	44,5	6,3	454,3	7,56
CNN3	Calponin-3 GN=Cnn3	25	38,5	36,4	5,4	567,6	5,31
VCIP1	Deubiquitinating protein VCIP135 GN=Vcpip1	25	10,4	134,4	6,8	621,5	4,53
K2C5	Keratin, type II cytoskeletal 5 GN=Krt5	23	9	61,7	8,6	375,8	4,64
K1C10	Keratin, type I cytoskeletal 10 GN=Krt10	22	9,6	57,7	4,9	330,8	3,78
IF2B1	Insulin-like growth factor 2 mRNA-binding protein 1 GN=Igf2bp1	22	18,2	63,4	9,9	494,9	4,11
K2C1	Keratin, type II cytoskeletal 1 GN=Krt1	21	5,2	65,6	9,2	307,9	4
NP1L4	Nucleosome assembly protein 1-like 4 GN=Nap1l4	21	28,3	42,7	4,4	517,3	4,74
TIPRL	TIP41-like protein GN=Tiprl	19	37,6	31,2	5,3	438,9	6,2

Annex 2: Complete list of identified proteins in the BirA*-mAGO2 sample

Protein identity	Protein description	Spectra # ▼	SC [%]	MW [kDa]	pI	Mascot Score	RMS [ppm]
STAM2	Signal transducing adapter molecule 2 GN=Stam2	18	24,1	57,4	4,8	484	5,24
K2C73	Keratin, type II cytoskeletal 73 GN=Krt73	18	5,9	58,9	9,3	245,8	3,8
CTND1	Catenin delta-1 GN=Ctnnd1	17	13,3	104,9	6,4	464,3	5,8
UBAP2	Ubiquitin-associated protein 2 GN=Ubap2	16	7,6	117,9	7,9	326,3	12,31
EF2	Elongation factor 2 GN=Eef2	15	10,7	95,3	6,4	499,8	3,15
NASP	Nuclear autoantigenic sperm protein GN=Nasp	15	11,3	83,9	4,2	341,8	5,15
CPIN1	Anamorsin GN=Ciapin1	15	33,7	33,4	5	343,1	5,32
ARFG1	ADP-ribosylation factor GTPase-activating protein 1 GN=Arfgap1	14	16,7	45,3	5,3	329	11,18
EPN4	Clathrin interactor 1 GN=Clint1	13	7	68,5	5,8	202	5,71
LYPA2	Acyl-protein thioesterase 2 GN=Lypla2	13	19	24,8	6,9	152,1	6,93
CL023	UPF0444 transmembrane protein C12orf23 homolog	13	80,9	11,5	9,8	262,4	6,87
VILI	Villin-1 GN=Vil1	13	15,2	92,7	5,7	429,1	8,77
IF4G2	Eukaryotic translation initiation factor 4 gamma 2 GN=Eif4g2	13	8,9	102	6,8	445,4	4,11
K22E	Keratin, type II cytoskeletal 2 epidermal GN=Krt2	13	7,6	70,9	9,1	330,3	11,34
FUBP1	Far upstream element-binding protein 1 GN=Fubp1	12	9,4	68,5	8,5	276,2	6,46
ANR17	Ankyrin repeat domain-containing protein 17 GN=Ankrd17	12	2,1	274	6,1	262,8	3,45
IF4G3	Eukaryotic translation initiation factor 4 gamma 3 GN=Eif4g3	12	2,8	174,8	5,3	296,6	5,16
DBNL	Drebrin-like protein GN=Dbnl	12	14,9	48,7	4,7	313,5	2,64
UBP15	Ubiquitin carboxyl-terminal hydrolase 15 GN=Usp15	12	8,5	112,3	4,9	443,9	2,73
AVEN	Cell death regulator Aven GN=Aven	12	17,8	37,2	4,8	246,9	5,08
K2C79	Keratin, type II cytoskeletal 79 GN=Krt79	11	5,8	57,5	8,6	198,5	3,7
ACTB	Actin, cytoplasmic 1 GN=Actb	11	15,5	41,7	5,2	233,2	6
RTN4	Reticulon-4 GN=Rtn4	11	12,1	126,5	4,3	360,2	6,46
CYBP	Calcyclin-binding protein GN=Cacybp	11	31	26,5	8,7	271,2	2,3
FUBP2	Far upstream element-binding protein 2 GN=Khsrp	11	11,8	76,7	7,1	392,2	5,87
CDC37	Hsp90 co-chaperone Cdc37 GN=Cdc37	11	19,8	44,6	5,1	357,8	3,79

Annex 2: Complete list of identified proteins in the BirA*-mAGO2 sample

Protein identity	Protein description	Spectra # ▼	SC [%]	MW [kDa]	pI	Mascot Score	RMS [ppm]
GRP78	78 kDa glucose-regulated protein GN=Hspa5	10	9	72,4	4,9	405,4	9,68
ANXA1	Annexin A1 GN=Anxa1	10	15,3	38,7	7,7	212,1	5,74
NSF1C	NSFL1 cofactor p47 GN=Nsfl1c	10	19,2	40,7	4,9	263,9	3,99
PABP1	Polyadenylate-binding protein 1 GN=Pabpc1	9	12,3	70,6	10	366,2	11,74
BAG3	BAG family molecular chaperone regulator 3 GN=Bag3	9	8,3	61,8	6,9	206,3	7,35
NPM	Nucleophosmin GN=Npm1	9	12	32,5	4,5	168,8	5,7
HNRPF	Heterogeneous nuclear ribonucleoprotein F GN=Hnrnpf	9	9,4	45,7	5,2	155,5	3,83
NP1L1	Nucleosome assembly protein 1-like 1 GN=Nap1l1	9	10,2	45,3	4,2	168,7	5,12
STIP1	Stress-induced-phosphoprotein 1 GN=Stip1	9	15,1	62,5	6,4	392,6	8,78
KPYM	Pyruvate kinase isozymes M1/M2 GN=Pkm	8	16	57,8	7,9	311,5	6,46
NUDC3	NudC domain-containing protein 3 GN=Nudcd3	8	10,7	40,9	5	149,9	6,1
SH3G1	Endophilin-A2 GN=Sh3gl1	8	6	41,5	5,4	141,9	4,96
ZO1	Tight junction protein ZO-1 GN=Tjp1	8	4,1	194,6	6,2	228,1	5,36
AL1A1	Retinal dehydrogenase 1 GN=Aldh1a1	8	18	54,4	8,9	289,4	10,51
K22O	Keratin, type II cytoskeletal 2 oral GN=Krt76	8	5,1	62,8	9,5	244,2	5,59
SRRM2	Serine/arginine repetitive matrix protein 2 GN=Srrm2	7	2,7	294,7	12,6	322,2	3,71
E41L2	Band 4.1-like protein 2 GN=Epb41l2	7	4,4	109,9	5,3	186	10,93
PLIN3	Perilipin-3 GN=Plin3	7	16,2	47,2	5,3	204,5	1,19
K1C15	Keratin, type I cytoskeletal 15 GN=Krt15	7	6	49,1	4,6	211,8	1,42
TB182	182 kDa tankyrase-1-binding protein GN=Tnks1bp1	7	3,4	181,7	4,7	228,6	5,66
EF1A1	Elongation factor 1-alpha 1 GN=Eef1a1	7	13,6	50,1	9,7	139,5	4,77
FLNA	Filamin-A GN=Flna	7	1,7	281	5,6	151,8	6,09
RAI14	Ankycorbin GN=Rai14	7	4,1	108,8	5,8	160,3	4,79
SNX2	Sorting nexin-2 GN=Snx2	7	7,7	58,4	4,9	214,7	5,23
EDC4	Enhancer of mRNA-decapping protein 4 GN=Edc4	7	4,5	152,4	5,4	201,3	5,37
IPO7	Importin-7 GN=Ipo7	7	5,5	119,4	4,6	291,5	2,47
NACA	Nascent polypeptide-associated complex	7	19,5	23,4	4,4	175,8	3,42

Annex 2: Complete list of identified proteins in the BirA*-mAGO2 sample

Protein identity	Protein description	Spectra # ▼	SC [%]	MW [kDa]	pI	Mascot Score	RMS [ppm]
	subunit alpha GN=Naca						
MRE11	Double-strand break repair protein MRE11A GN=Mre11a	7	9,6	80,2	5,6	146,1	5,46
CAPR1	Caprin-1 GN=Caprin1	6	9,3	78,1	5	225,1	3,83
G3P	Glyceraldehyde-3-phosphate dehydrogenase GN=Gapdh	6	7,2	35,8	9,2	81,1	3,5
PRDX1	Peroxiredoxin-1 GN=Prdx1	6	28,6	22,2	9,2	193,1	6,9
K1C17	Keratin, type I cytoskeletal 17 GN=Krt17	6	7,2	48,1	4,9	182	1,68
SGT1	Protein SGT1 homolog GN=Ecd	6	8,9	71,7	4,7	185,6	6,84
LIMD1	LIM domain-containing protein 1 GN=Limd1	6	14,5	71,4	5,9	204,8	8,82
AFAD	Afadin GN=Mllt4	6	3,1	206,4	5,9	272,4	4,54
KANK2	KN motif and ankyrin repeat domain-containing protein 2 GN=Kank2	6	4,7	90,2	5,3	210,2	2,51
K1C18	Keratin, type I cytoskeletal 18 GN=Krt18	6	16,8	47,5	5,1	236,2	7,27
PRC2C	Protein PRRC2C GN=Prrc2c	6	1,1	310,7	9,1	181,7	2,85
RBM10	RNA-binding protein 10 GN=Rbm10	6	4,9	103,4	5,6	116,2	5,17
ATX2L	Ataxin-2-like protein GN=Atxn2l	5	3,9	110,6	9,4	194,9	3,99
PPID	Peptidyl-prolyl cis-trans isomerase D GN=Ppid	5	7,6	40,7	7,8	165,2	4,25
PATL1	Protein PAT1 homolog 1 GN=Patl1	5	8,7	86,7	5,9	222	8,82
PTBP1	Polypyrimidine tract-binding protein 1 GN=Ptbp1	5	4,4	56,4	9,2	120,7	4,97
DESP	Desmoplakin GN=Dsp PE=3	5	1,8	332,7	6,4	135,9	3,13
ANR49	Ankyrin repeat domain-containing protein 49 GN=Ankrd49	5	18,5	27,1	4,9	159,8	6,75
CNN2	Calponin-2 GN=Cnn2	5	8,9	33,1	8,7	80,5	13,17
S10AB	Protein S100-A11 GN=S100a11	5	16,3	11,1	5,1	79,6	3,96
AKAP1	A-kinase anchor protein 1, mitochondrial GN=Akap1	5	4,4	92,1	4,8	126,3	3,24
F10A1	Hsc70-interacting protein GN=St13	4	3,2	41,6	5	66,6	4,66
RPAP3	RNA polymerase II-associated protein 3 GN=Rpap3	4	4,4	74,1	8,7	56,3	1,97
SIPA1	Signal-induced proliferation-associated protein 1 GN=Sipa1	4	3,7	112	5,9	120,9	3,51
CD2AP	CD2-associated protein GN=Cd2ap	4	6,8	70,4	6	139,1	4,19
RAGP1	Ran GTPase-activating protein 1	4	3,7	63,5	4,4	108,2	2,98

Annex 2: Complete list of identified proteins in the BirA*-mAGO2 sample

Protein identity	Protein description	Spectra # ▼	SC [%]	MW [kDa]	pI	Mascot Score	RMS [ppm]
	GN=Rangap1						
RANB3	Ran-binding protein 3 GN=Ranbp3	4	2,4	52,5	4,9	114,4	2,57
LARP4	La-related protein 4 GN=Larp4	4	3,6	79,7	6	138	4,47
PYRG1	CTP synthase 1 GN=Ctps1	4	5,8	66,6	6,1	136,9	15,64
UBP10	Ubiquitin carboxyl-terminal hydrolase 10 GN=Usp10	3	3,2	87	4,9	80,9	7,1
TCPA	T-complex protein 1 subunit alpha GN=Tcp1	3	4,1	60,4	5,8	38,4	1,33
TTC4	Tetratricopeptide repeat protein 4 GN=Ttc4	3	7,3	44,3	5	106	4,44
SMAP	Small acidic protein GN=Smap	3	12,7	20	4,5	46,9	9,65
CIP2A	Protein CIP2A GN=Kiaa1524	3	1,1	102	5,9	39,3	3,87
PHAX	Phosphorylated adapter RNA export protein GN=Phax	3	7	43,2	5,1	80,1	4,54
TTC1	Tetratricopeptide repeat protein 1 GN=Ttc1	3	3,4	33,2	4,8	51,4	2,26
COBL1	Cordon-bleu protein-like 1 GN=Cobll1	3	1,5	137,3	9,1	63,4	0,53
PP6R1	Serine/threonine-protein phosphatase 6 regulatory subunit 1 GN=Ppp6r1	3	5	94,5	4,4	90,2	3,12
FXR1	Fragile X mental retardation syndrome-related protein 1 GN=Fxr1	3	4,7	76,2	6,6	105,5	7,27
SRC8	Src substrate cortactin GN=Cttn	3	7,9	61,2	5,1	186,6	12,49
TPD52	Tumor protein D52 GN=Tpd52	3	8,5	24,3	4,5	35,9	3,03
IDHC	Isocitrate dehydrogenase [NADP] cytoplasmic GN=Idh1	3	4,8	46,6	6,9	72,7	9,01
SODC	Superoxide dismutase [Cu-Zn] GN=Sod1	3	21,4	15,9	6	126,4	11,1
RBP2	E3 SUMO-protein ligase RanBP2 GN=Ranbp2	3	1,2	340,9	5,8	217,6	5,16
DLG1	Disks large homolog 1 GN=Dlg1	3	2,8	100,1	5,5	107,4	2,99
TBB4A	Tubulin beta-4A chain GN=Tubb4a	2	5,6	49,6	4,6	52,9	5,1
PICA	Phosphatidylinositol-binding clathrin assembly protein GN=Picalm	2	3	71,5	8,6	41,8	2,86
NUFP2	Nuclear fragile X mental retardation-interacting protein 2 GN=Nufip2	2	3,5	75,6	9,2	120,5	2,02
PRC2B	Protein PRRC2B GN=Prrc2b	2	2,2	160,8	8,9	110,6	13,69
Sep-09	Septin-9 GN=Sept9	2	2,6	65,5	9,7	65,3	10,35
PEX5	Peroxisomal targeting signal 1 receptor GN=Pex5	2	4,2	70,7	4,3	93,8	1,64
PUM2	Pumilio homolog 2 GN=Pum2	2	2,4	114,2	6,7	117,7	6,74

Annex 2: Complete list of identified proteins in the BirA*-mAGO2 sample

Protein identity	Protein description	Spectra # ▼	SC [%]	MW [kDa]	pI	Mascot Score	RMS [ppm]
SYRC	Arginine--tRNA ligase, cytoplasmic GN=Rars	2	3,6	75,6	8,4	76,9	2,56
UBP14	Ubiquitin carboxyl-terminal hydrolase 14 GN=Usp14	2	5,1	56	5	208,9	18,19
4ET	Eukaryotic translation initiation factor 4E transporter GN=Eif4enif1	2	1,9	107,9	8	37,4	8,27
SWP70	Switch-associated protein 70 GN=Swap70	2	5	69	5,7	97,8	18,29
ZFY16	Zinc finger FYVE domain-containing protein 16 GN=Zfyve16	2	1	166,6	4,5	65,3	8,52
AHSA1	Activator of 90 kDa heat shock protein ATPase homolog 1 GN=Ahsa1	2	9,5	38,1	5,3	94	12,78
RENT1	Regulator of nonsense transcripts 1 GN=Upf1	2	2,2	123,9	6,2	112	4,77
SPDLY	Protein Spindly GN=Spdl1	2	3,8	70,2	5,7	34,9	6,16
NDKB	Nucleoside diphosphate kinase B GN=Nme2	2	13,8	17,4	7,8	90,9	8,82
PIHD1	PIH1 domain-containing protein 1 GN=Pih1d1	2	4,1	32,2	5	37,7	7,04
PUF60	Poly(U)-binding-splicing factor PUF60 GN=Puf60	2	1,8	60,2	5,1	57,5	7,62
PGAM1	Phosphoglycerate mutase 1 GN=Pgam1	1	5,5	28,8	6,8	59,1	2,19
ISY1	Pre-mRNA-splicing factor ISY1 homolog GN=Isy1	1	5,3	33	5	64,8	0,71
NUDC1	NudC domain-containing protein 1 GN=Nudcd1	1	2,7	66,7	5	43,4	2,05
RS30	40S ribosomal protein S30 GN=Fau PE=3	1	16,9	6,6	12,6	35,6	5,25
MARE1	Microtubule-associated protein RP/EB family member 1 GN=Mapre1	1	6,7	30	5	38,7	4,21
NELL1	Protein kinase C-binding protein NELL1 GN=Nell1	1	1,1	89,4	5,7	34,8	18,9
EF1B	Elongation factor 1-beta GN=Eef1b	1	10,7	24,7	4,4	48,7	6,88
PLAK	Junction plakoglobin GN=Jup	1	2,4	81,7	5,7	36,9	25,88
SND1	Staphylococcal nuclease domain-containing protein 1 GN=Snd1	1	1,8	102	7,3	194,9	1,53
PP6R3	Serine/threonine-protein phosphatase 6 regulatory subunit 3 GN=Ppp6r3	1	1,8	94,6	4,3	120,9	20,17
GBLP	Guanine nucleotide-binding protein subunit	1	6,3	35,1	8,9	46,5	3,55

Annex 2: Complete list of identified proteins in the BirA*-mAGO2 sample

Protein identity	Protein description	Spectra # ▼	SC [%]	MW [kDa]	pI	Mascot Score	RMS [ppm]
	beta-2-like 1 GN=Gnb2l1						
TYB10	Thymosin beta-10 GN=Tmsb10	1	31,8	5	5,2	38,5	0,45
CPEB4	Cytoplasmic polyadenylation element-binding protein 4 GN=Cpeb4	1	2,2	80,1	6,7	38	12,19
MBB1A	Myb-binding protein 1A GN=Mybbp1a	1	0,8	151,9	9,8	73,7	7,19
CRKL	Crk-like protein GN=Crkl	1	4	33,8	6,3	61,8	0,87
RLA2	60S acidic ribosomal protein P2 GN=Rplp2	1	16,5	11,6	4,2	35,5	4,44
TWF1	Twinfilin-1 GN=Twf1	1	2,6	40,1	6,2	33,7	0,79
ZN574	Zinc finger protein 574 GN=Znf574	1	1,2	99,4	9,7	32,9	22,27
MARE2	Microtubule-associated protein RP/EB family member 2 GN=Mapre2	1	3,1	36,9	5,1	45,5	10,94
DNJA2	DnaJ homolog subfamily A member 2 GN=Dnaja2	1	7,8	45,7	6,1	41,7	1,32
RMP	Unconventional prefoldin RPB5 interactor GN=Uri1	1	2,4	59	4,8	40,1	2,63
VIME	Vimentin GN=Vim	1	4,5	53,7	4,9	54,3	3,42
RB6I2	ELKS/Rab6-interacting/CAST family member 1 GN=Erc1	1	2,2	128,3	5,6	47,8	4,53
PDLI1	PDZ and LIM domain protein 1 GN=Pdlim1	1	4,6	35,8	6,4	38,8	25,69
G3BP1	Ras GTPase-activating protein-binding protein 1 GN=G3bp1	1	3,2	51,8	5,3	133,3	3,89
SPR1A	Cornifin-A GN=Sprr1a	1	10,4	15,8	9,7	33,2	6,98
SON	Protein SON GN=Son	1	0,4	265,5	5,4	62,2	0,3
F91A1	Protein FAM91A1 GN=Fam91a1	1	1,1	93,4	5,9	130,4	13,37
TNR6B	Trinucleotide repeat-containing gene 6B protein GN=Tnrc6b	1	0,9	191,8	5,9	59,7	0,26
KTN1	Kinectin GN=Ktn1	1	1,2	152,5	5,6	54,5	3,04
ELP4	Elongator complex protein 4 GN=Elp4	1	4	46,3	9,8	35,4	2,41
SNX1	Sorting nexin-1 GN=Snx1	1	2,1	58,9	5	61	1,83
PLSI	Plastin-1 GN=Pls1	1	1,9	70,4	5,1	36,4	25,89

Spectra **#:** Number of fragmentation MS/MS spectra observed for a given protein. SC%: Sequence coverage expressed in percentage. MW: molecular weight of the identified protein in kDa. pI: isoelectric pH. RMS: Mass error expressed in ppm.

Annex 3: Complete list of identified proteins in mock, MCMV wt and MCMV mut168 infection

		Mock			MCMV wt			MCMV mut168		
Protein identity	**Protein description**	**R1**	**R2**	**R3**	**R1**	**R2**	**R3**	**R1**	**R2**	**R3**
SAV	Streptavidin	1307	1262	1339	1343	1316	1359	1371	1361	1356
PYC	Pyruvate carboxylase, mitochondrial	1009	1055	1057	1030	1018	1085	1062	1063	1084
PCCA	Propionyl-CoA carboxylase alpha chain, mitochondrial	378	377	392	333	315	342	341	363	353
MCCA	Methylcrotonoyl-CoA carboxylase subunit alpha, mitochondrial	141	143	130	127	87	88	96	116	100
AGO2_BIRA	Protein argonaute-2	112	121	121	101	89	103	103	106	107
ACACA	Biotin carboxylase	48	43	44	38	34	41	36	32	39
ACTG	Actin, cytoplasmic 2	25	35	35	20	27	31	28	25	25
TBA1B	Tubulin alpha-1B chain	25	24	25	18	17	19	19	19	20
HS90B	Heat shock protein HSP 90-beta	19	20	22	17	20	24	24	21	23
EDC4	Junction plakoglobin	18	20	24	27	28	20	32	27	28
TNR6C	Trinucleotide repeat-containing gene 6C protein	17	19	17	14	9	11	13	13	13
MYH9	Myosin-9	16	16	18	9	8	5	8	11	10
RTN4	Reticulon-4	16	16	13	11	16	15	18	19	17
TNR6B	Trinucleotide repeat-containing gene 6B protein	9	8	13	6	7	8	5	7	6
PCBP1	Poly(rC)-binding protein 1	8	6	8	6	6	8	8	9	8
IF4G1	Eukaryotic translation initiation factor 4 gamma 1	6	4	3	3	1		2		1
PCBP2	Poly(rC)-binding protein 2	6	4	4	3	4	3	6	4	4
TBB2A	Tubulin beta-2A chain	5	7	5	6	6	6	6	5	7
HS90A	Heat shock protein HSP 90-alpha	5	4	5	5	5	8	8	7	6
FLNC	Filamin-C	4		1						
RBP2	E3 SUMO-protein ligase RanBP2	4	2	3	1		2			
CNOT1	CCR4-NOT transcription complex subunit 1	4	2	4	1					1
HSP7C	Heat shock cognate 71 kDa protein	4	5	6	5	6	10	6	7	8
CSDE1	Cold shock domain-containing protein E1	4	6	5	4	3	3	4	4	6
KPYM	Pyruvate kinase PKM	4	4	3	2		2	2	2	
RL40	Ubiquitin-60S ribosomal protein L40	4	8	7			6	5	2	4
EF2	Elongation factor 2	4		3	1	3	6	3	2	5
STAM2	Signal transducing adapter molecule 2	4		1	3	2	2	1	2	

Annex 3: Complete list of identified proteins in mock, MCMV wt and MCMV mut168 infection

		Mock			MCMV wt			MCMV mut168		
Protein identity	**Protein description**	**R1**	**R2**	**R3**	**R1**	**R2**	**R3**	**R1**	**R2**	**R3**
FLNA	Filamin-A	3		1						
TCPQ	T-complex protein 1 subunit theta	3	2	3	5	2	3	2	3	3
RENT1	Regulator of nonsense transcripts 1	3	2	1		4	2		2	
SON	Protein SON	2	1	1						
TNR6A	Trinucleotide repeat-containing gene 6A protein	2		1						
PEX1	Peroxisome biogenesis factor 1	2								
COR1B	Coronin-1B	2	1	2						1
IF5	Eukaryotic translation initiation factor 5	2						2		
PLEC	Plectin	2	4	3	1		1	2		1
CRK	Adapter molecule crk	2	4	2	1	1	1	1		2
ENOA	Alpha-enolase	2	1		1	5	3	2	2	
TRAP1	Heat shock protein 75 kDa, mitochondrial	2	3	3	3	3	3	3	3	3
VIGLN	Vigilin	2	7	4	2	3	3	4	4	4
YAP1	Transcriptional coactivator YAP1	2	2	5	6	1	2	2	2	1
TLN1	Talin-1	2	2	1	1		2	3	3	2
ZSWM8	Zinc finger SWIM domain-containing protein 8	2	4	3	3		3		3	2
WIPI2	WD repeat domain phosphoinositide-interacting protein 2	2	2		1	3	1	1	2	2
DVL2	Segment polarity protein dishevelled homolog DVL-2	1	1							
CELF1	CUGBP Elav-like family member 1	1								
VCIP1	Deubiquitinating protein VCIP135	1								
MBB1A	Myb-binding protein 1A	1								
TCOF	Treacle protein	1								
CHD4	Chromodomain-helicase-DNA-binding protein 4	1	2	1						1
PERQ1	PERQ amino acid-rich with GYF domain-containing protein 1	1	1						1	
CNN2	Calponin-2	1	1	1	1					
UBP2L	Ubiquitin-associated protein 2-like	1		4	6	2	6		7	
GRP78	78 kDa glucose-regulated	1	1			1		2		1

Annex 3: Complete list of identified proteins in mock, MCMV wt and MCMV mut168 infection

		Mock			MCMV wt			MCMV mut168		
Protein identity	**Protein description**	**R1**	**R2**	**R3**	**R1**	**R2**	**R3**	**R1**	**R2**	**R3**
	protein									
PATL1	Protein PAT1 homolog 1	1				1		1	1	
D3XDW4	M142 protein OS=Murid herpesvirus				1	2				
H2A2B7	M86 protein OS=Murid herpesvirus 1				1	1				
PLAK	Junction plakoglobin		25							
CTNB1	Catenin beta-1		5							
DSG1A	Desmoglein-1-alpha		5							
THIO	Thioredoxin		3							
TPIS	Triosephosphate isomerase		2							
EF1A1	Elongation factor 1-alpha 1		1							
IF4A1	Eukaryotic initiation factor 4A-I		1							
NEST	Nestin		1							
NUP85	Nuclear pore complex protein Nup85		1							
PSB4	Proteasome subunit beta type-4		1							
ARFG1	ADP-ribosylation factor GTPase-activating protein 1			2						
SPR2B	Small proline-rich protein 2B			1						
TM263	Transmembrane protein 263				3	3	5	4	3	3
EF1D	Elongation factor 1-delta				3	2	2	2	3	3
S10AB	Protein S100-A11					1	1	1	1	1
PP6R3	Serine/threonine-protein phosphatase 6 regulatory subunit 3					1	3			2
TCPE	T-complex protein 1 subunit epsilon						1	1		
SPT6H	Transcription elongation factor SPT6				1					
INSRR	Insulin receptor-related protein					2				
RUVB1	RuvB-like 1					1				
GBB1	Guanine nucleotide-binding protein G(I)/G(S)/G(T) subunit beta-1							1		
RL35	60S ribosomal protein L35								4	2
RS30	40S ribosomal protein S30								1	
RL19	60S ribosomal protein L19								1	
RL29	60S ribosomal protein L29								2	

Annex 3: Complete list of identified proteins in mock, MCMV wt and MCMV mut168 infection

		Mock			MCMV wt			MCMV mut168		
Protein identity	**Protein description**	**R1**	**R2**	**R3**	**R1**	**R2**	**R3**	**R1**	**R2**	**R3**
H12	Histone H1.2								2	
H14	Histone H1.4								1	
H2A1F	Histone H2A type 1-F								2	
PERQ2	PERQ amino acid-rich with GYF domain-containing protein 2									1
ANXA2	Annexin A2		6							2
VIME	Vimentin		2		1	1				
4ET	Eukaryotic translation initiation factor 4E transporter		1	3	3	1	3	2	3	

Number of spectra for each identified protein is represented for each condition and replicates (R1 to R3).

Annex 4

OPEN ACCESS Freely available online

PLOS ONE

MiR-30a-3p Negatively Regulates BAFF Synthesis in Systemic Sclerosis and Rheumatoid Arthritis Fibroblasts

Ghada Alsaleh[1*9], Antoine François[1 9], Lucas Philippe[1], Ya-Zhuo Gong[1], Seiamak Bahram[1], Semih Cetin[2], Sébastien Pfeffer[2], Jacques-Eric Gottenberg[1], Dominique Wachsmann[1], Philippe Georgel[1], Jean Sibilia[1]

1 Immunorhumatologie moléculaire, INSERM UMR S_1109, Centre de Recherche en Immunologie et Hématologie, Faculté de Médecine, Fédération de Médecine Translationnelle de Strasbourg (FMTS), Université de Strasbourg, Strasbourg, France and Service de Rhumatologie, Centre National de Référence pour les Maladies Systémiques Autoimmunes Rares, Hôpitaux Universitaires de Strasbourg, Strasbourg, France, **2** Université de Strasbourg, UPR 9002 du CNRS Architecture et Réactivité de l'ARN, Institut de Biologie Moléculaire et Cellulaire, Strasbourg, France

Abstract

We evaluated micro (mi) RNA-mediated regulation of BAFF expression in fibroblasts using two concomitant models: (i) synovial fibroblasts (FLS) isolated from healthy controls (N) or Rheumatoid Arthritis (RA) patients; (ii) human dermal fibroblasts (HDF) isolated from healthy controls (N) or Systemic Sclerosis (SSc) patients. Using RT-qPCR and ELISA, we first showed that SScHDF synthesized and released BAFF in response to Poly(I:C) or IFN-γ treatment, as previously observed in RAFLS, whereas NHDF released BAFF preferentially in response to IFN-γ. Next, we demonstrated that miR-30a-3p expression was down regulated in RAFLS and SScHDF stimulated with Poly(I:C) or IFN-γ. Moreover, we demonstrated that transfecting miR-30a-3p mimic in Poly(I:C)- and IFN-γ-activated RAFLS and SScHDF showed a strong decrease on BAFF synthesis and release and thus B cells survival in our model. Interestingly, FLS and HDF isolated from healthy subjects express higher levels of miR-30a-3p and lower levels of BAFF than RAFLS and SScHDF. Transfection of miR-30a-3p antisense in Poly(I:C)- and IFN-γ-activated NFLS and NHDF upregulated BAFF secretion, confirming that this microRNA is a basal repressors of BAFF expression in cells from healthy donors. Our data suggest a critical role of miR-30a-3p in the regulation of BAFF expression, which could have a major impact in the regulation of the autoimmune responses occurring in RA and SSc.

Citation: Alsaleh G, François A, Philippe L, Gong Y-Z, Bahram S, et al. (2014) MiR-30a-3p Negatively Regulates BAFF Synthesis in Systemic Sclerosis and Rheumatoid Arthritis Fibroblasts. PLoS ONE 9(10): e111266. doi:10.1371/journal.pone.0111266

Editor: Shervin Assassi, University of Texas Health Science Center at Houston, United States of America

Received July 16, 2014; **Accepted** September 21, 2014; **Published** October 31, 2014

Data Availability: The authors confirm that all data underlying the findings are fully available without restriction. All relevant data are within the paper and its Supporting Information files.

Funding: Prof. Jean Sibilia's work was supported by grants from Bristol Myers Squibb, Roche, Pfizer, Courtin Foundation and CAMPLP. Sébastien Pfeffer's work was supported by the European Research Council (ERC-StG-260767) and Agence Nationale pour la Recherche (labex netRNA, ANR-10-LABX-36). The funders had no role in study design, data collection and analysis, decision to publish, or preparation of the manuscript.

Competing Interests: The authors have declared that no competing interests exist.

* Email: galfarhan@unistra.fr

9 These authors contributed equally to this work.

Introduction

TNFSF13B (also known as B cell-activating factor -BAFF, which will be the only nomenclature used thereafter in the manuscript) is a member of the TNF superfamily which plays a central role in the survival and homeostasis of transitional and naive B cells, plasmablasts and plasma cells [1]. BAFF is produced as a membrane-bound form or secreted by cells of hematopoietic origin, essentially monocytes, dendritic cells, macrophages and stimulated neutrophils [2,3]. However non-immune cells, such as astrocytes, can also constitutively produce BAFF [4].

The finding that BAFF transgenic mice develop autoimmune manifestations exhibiting similarities with systemic lupus erythematosus (SLE) and Sjögren's syndrom (SS) suggested a critical role for this cytokine in autoimmune diseases [5–7]. Consistent with this observation, auto-reactive B cells have a greater dependency for BAFF compared to naive mature B cells and elevated levels of BAFF were detected in the serum of patients with SLE, rheumatoid arthritis (RA) and SS [8]. In addition, these increased BAFF levels correlated with high auto-antibody titers and disease activity [9]. In patients with systemic sclerosis (SSc), increased levels of BAFF were associated with worsening of the skin sclerosis [10,11]. Similar results were obtained in experimental arthritis where overproduction of BAFF by dendritic cells and macrophages was demonstrated to play a crucial role in the disease [12]. Fibroblast-like synoviocytes isolated from RA patients (RAFLS) are characterized by their aggressive phenotype in response to various stimuli. In these inflammatory conditions, these cells also produce large amounts of cytokines including BAFF, thus enabling them to collaborate with autoimmune B cells [13]. Altogether, these data illustrate the central role played by BAFF in the pathogenesis of autoimmune diseases, which prompted the development of biological agents targeting BAFF. Belimumab, a humanized IgG1 monoclonal antibody which inhibits both soluble and membrane BAFF binding to BAFFR and TACI, was approved for the treatment of SLE [14–16].

However, modulation of BAFF activity for therapeutic purposes by targeting its synthesis has not yet been considered. The control of cytokine expression can occur at various levels including post-transcriptional regulation, which is now the focus of intense attention. The modulation of gene expression can take place at

several levels, among which regulation by microRNAs (miRNAs) has gained increased interest in the recent years. MiRNAs are an evolutionarily conserved class of endogenous small non-coding RNAs. They are produced from long precursor molecules by the consecutive action of the RNase III enzymes DROSHA and DICER, before being loaded on an ARGONAUTE protein within the RNA-induced-silencing complex (RISC). The mature miRNA acts a guide for RISC to mediate destabilization and/or translational repression of target mRNAs. The regulation of miRNA expression is itself controlled at various levels such as transcription, processing or stability and can be influenced by various stress factors including inflammation. In addition, emerging data have identified an important contribution of miRNA to the development and control of the inflammatory response which position these small non-coding RNAs at the heart of feedback and feed-forward loops controlling the inflammation process in both immune and non immune cells. Recently, microRNAs (miRNAs) have emerged as a new class of cytokines regulators, although computational analysis indicates that the 3′UTR (Three prime untranslated region) of many cytokines lacks miRNA target sites. Indeed, miRNAs could also regulate cytokine expression by targeting ARE-binding proteins (ARE machinery components) such as TTP, AUF1 and members of the HuR family [17,18].

In this study, we found that miR-30a-3p (and miR30d-3p and e-3p, which exhibit high sequence homology) is predicted to bind the 3′UTR region of BAFF transcripts. In SSc patients, we observed concomitant up-regulation of BAFF transcripts and decreased expression of miR-30a-3p in skin fibroblasts (HDF) isolated from SSc patients after cell stimulation with Poly (I:C) or IFN-γ. Analysis of synovial fibroblasts from RA patients yielded similar results. The prediction provided by bioinformatic tools and this inverse correlation between miR-30 family members and BAFF expression prompted us to analyze their likely direct interaction. To this end, we used reporter constructs containing a luciferase gene fused to the wild type or mutated full length human BAFF 3′UTR. Co-transfection of these reporter plasmids with miRNA mimic in cultured cells confirmed direct interaction. Furthermore, transfection of miR-30a-3p mimic or inhibitor in fibroblasts isolated from the skin or the synovium of healthy donors or from patients confirmed that this miRNA modulate IFN-γ- and Poly (I:C)-dependent BAFF expression. Finally, we report that miRNA-modulated BAFF secretion by activated skin or synovial fibrocytes significantly reduces the capacity of these cells to promote B cells survival, which provides physiological significance to our findings. Altogether, our data describe a novel mechanism involved in the regulation of BAFF expression and potentially provide an additional level of intervention for future therapeutic purposes.

Materials and Methods

Reagents

Cell culture media (RPMI 1640, M199 and DMEM), fetal calf serum (FCS), L-glutamine, penicillin, streptomycin, amphotericin B, TRIzol reagent and $DiOC_6$ (3,3′-Dihexyloxacarbocyanine Iodide) were from Invitrogen (Cergy-Pontoise, France). LPS from *Salmonella abortus equi* and Propidium Iodide (PI) solution was obtained from Sigma Aldrich (Saint-Quentin-Fallavier, France). Synthetic bacterial lipopeptide Pam_3CSK_4 (BLP) was obtained from EMC Microcollections GmbH (Tuebingen, Germany). Polyinosine-Polycytidylic acid (Poly(I:C)) was obtained from InvivoGen (Toulouse, France). iScript cDNA Synthesis Kit and SsoAdvanced SYBR Green Supermix from Bio-Rad (Marnes-la-Coquette, France). The miScript System, miRNA mimc and Allstars negative control siRNA were obtained from Qiagen (Courtabeuf, France). miR-30a-3p antagonists were from Fisher scientific (Illkirch Cedex, France). Human Dermal Fibroblast Nucleofector kit was from Lonza (Cologne, Germany). The enzyme immunoassay kits for human BAFF, APRIL and IL-6 detection and recombinant IFN-γ were from R&D systems (Lille, France).

Cell culture

Human FLS were isolated from synovial tissues from five different RA patients and from five healthy subjects at the time of knee joint arthroscopic synovectomy. RA patients were 3 female and two male, the average age is 49 years, and had all FR positive but only three were antiCCP positive. Human dermal fibroblasts (HDF) were obtained by biopsy of 4 mm diameter from the affected areas (dorsal forearm) of four patients with SSc (SScHDF)and from the corresponding area of three healthy subjects (NHDF). All SSc patients were female (average age52 years) and had diffuse cutaneous systemic sclerosis and anti-Scl70-positive antibodies. The total modified Rodnan skin scores were 29, 8, 25 and 14, and that for the biopsy area were 2, 1, 2, 2.Blood B cells were isolated from 6 healthy donors. Institutional ethics committee of the Hopitaux Universitaires de Strasbourg specifically approved this study.Written informed consent was obtained by all the participants of this study (patients and healthy donors). The diagnosis of RA and SSc was conformed to the revised criteria of the American College of Rheumatology (ACR). FLS, HDF and HEK293 cultures were done as previously described [19]. Experiments were performed between the 3rd and the 9th passage. During that time, cultures were constituted of a homogeneous population of fibroblastic cells, negative for CD16 as determined by FACS analysis. HEK293 cells were purchased from the American type culture collection (ATCC) and maintained in DMEM supplemented with 10% heat-inactivated FBS, 2 mM of L-glutamine, 40 U/ml penicillin and 50 mg/ml streptomycin. Cell number and cell viability were checked by the MTT (3-(4,5 dimethylthiazol-2-yl)-2,5-diphenyltetrazolium bromide) assay. Blood mononuclear cells were isolated from healthy blood donors by Ficoll-Paque centrifugation as described in standard protocols. B cells were then selected by negative sorting using EasySep Human B Cell Enrichment Kit (Stemcell Technologies). The efficacy of B cell isolation was determined by FACS analysis using anti-CD19 antibodies. The yield of isolated B cells was composed of 99% $CD19^+/CD3^-$ B cells and 0.01% of $CD19^-/CD3^+$ T cells.

Stimulation of cells for total RNA extraction

FLS (2.10^5 cells) and HDF (2.10^5 cells) were seeded in 24-well plates and stimulated with medium alone or medium containing LPS (1 μg/mL), BLP (1 μg/mL), Poly(I:C) (10 μg/mL) and IFN-γ (0.1, 1 or 5 ng/mL). After a 6 h, 48 h and 72 h incubation period, total RNA was extracted using TRIzol according to the manufacturer's instruction.

Real-time quantitative PCR (RT-qPCR)

Total RNA was reverse transcribed using the iScript cDNA Synthesis Kit according to the manufacturer's instructions (BioRad). Real-time quantitative RT-qPCR was performed in a total volume of 20 μL using SsoAdvanced SYBR Green Supermix (BioRad) and gene-specific primers: BAFF: 5′-TGAAACAC-CAACTATACAAAAAG-3′ and 5′-TCAATTCATCCCCAAA-GACAT-3′;

April: 5′- CTCTGCTGACCCAACAAACA-3′ and 5′-CTCCTTTTCCGGGATCTCTC-3′;

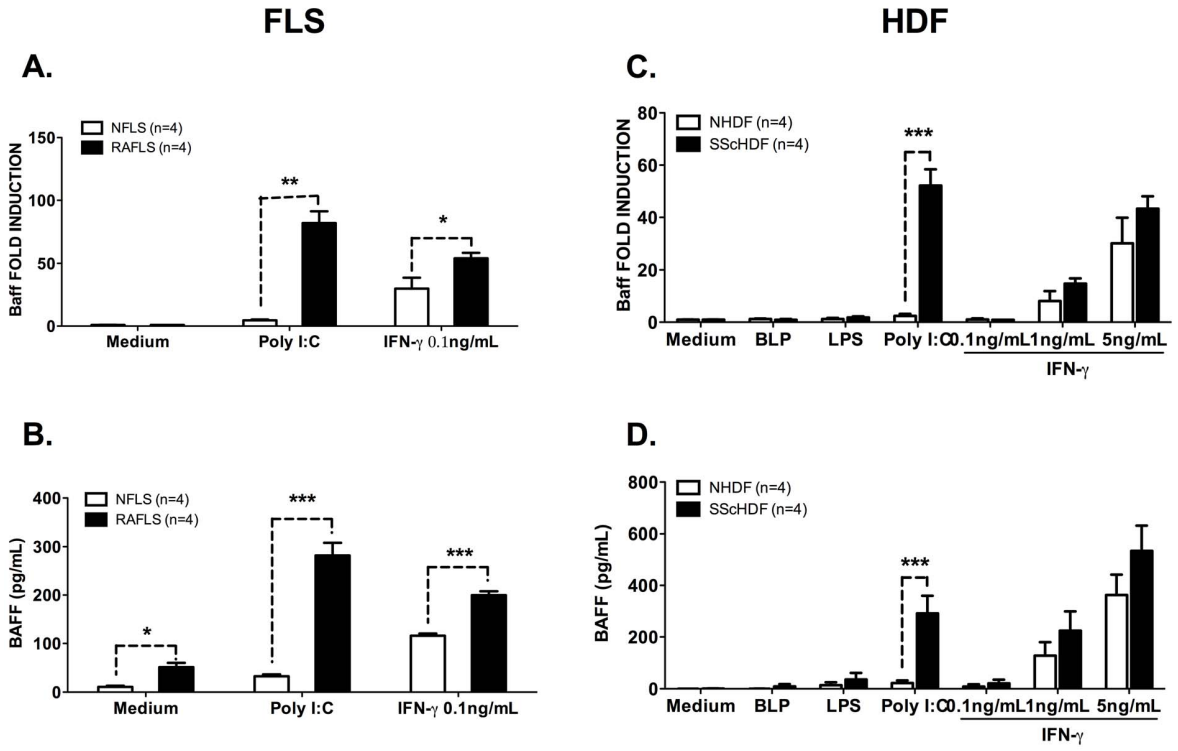

Figure 1. BAFF expression and secretion are up-regulated in Poly (I:C)- and IFN-γ-stimulated rheumatoid arthritis (RA) fibroblast-like synoviocytes (FLS) and systemic sclerosis (SSc) human dermal fibroblast (HDF). A, C. BAFF mRNA expression was determined by RT-qPCR in NFLS(n = 4) and RAFLS(n = 4) (A) or NHDF(n = 3) and SScHDF (n = 4) (C) stimulated (depending of the cell types) with BLP (1 μg/ml), LPS (1 μg/ml), Poly (I:C) (10 μg/mL) or IFN-γ (0.1, 1 or 5 ng/mL) for 72 h. Results were normalized to Gapdh and expressed as fold change compared with samples from cells incubated in medium. B, D. BAFF release was quantified by ELISA in culture supernatants of NFLS (n = 4) and RAFLS(n = 4) (B) or NHDF(n = 3) and SScHDF (n = 4) (D) in the same conditions as panels A and C. Data are expressed as the mean of triplicate samples ± SEM. *p<0.05, **p<0.01, ***p<0.001.
doi:10.1371/journal.pone.0111266.g001

Gapdh: 5′-GGTGAAGGTCGGAGTCAACGGA-3′ and 5′-GAGGGATCTCGCTCCTGGAAGA-3′

After an initial denaturing at 96°C for 10 min, the temperatures used were 95°C for 10 s, 60°C for 15 s, 72°C for 25 s using a Rotor-Gene 6000 real-time PCR machine (Corbett Life Science). Amplification products were detected as an increased fluorescent signal of SYBR Green during the amplification cycles. Results were obtained using Rotor-Gene 6000 Series Software and evaluated using Excel (Microsoft). Melting-curve analysis was performed to assess the specificity of PCR products.

Real-time quantitative PCR analyses for miRNAs were performed using the miScript System and the primers (Qiagen). RNA concentrations were determined with a NanoDrop instrument (NanoDrop Technologies). 500 ng of RNA per sample was used for the assays. Reverse transcriptase reactions and RT-qPCR were performed according to the manufacturer's protocols. Expression of endogenous U6snRNA was used for normalization. Relative expression was calculated using the comparative threshold cycle (Ct) method and fold induction in cells activated by Poly(I:C) or IFN-γ was obtained by calculating $2^{-\Delta\Delta Ct}$.

Transfections and luciferase assay

Transient transfection of FLS or HDF with miR-30a-3p mimic (20 pM/sample), miR-30a-3p antagonists or with the negative controls was performed using the Human Dermal Fibroblast Nucleofector kit from Lonza as previously described [20]. Transfection of HEK293 cells was performed using Lipofectamine 2000 (Invitrogen) as previously described [19].

B cells viability assay

FLS or HDF were transfected with miR-30a-3p mimic, miR-30a-3p antagonists or with the negative controls as described above and stimulated with medium alone or medium with Poly(I:C) (10 μg/mL) or IFN-γ (5 ng/mL) for 72 h. Supernatants (800 μL) were harvested and used to culture B cells (5×10^5) for 72 h. In some experiments, anti-human BAFF antibodies or control IgG (R&D Systems) were added (10 ng/mL) to the supernatant. Then, B cells were stained with 3,3-dihexyloxacarbocyanine iodide ($DiOC_6$) to assess the mitochondrial transmembrane potential, and with Propidium Iodide (PI) to assess membrane permeability, as described [21]. Briefly, cell suspensions were incubated with 40 nmol/L $DiOC_6$ and 1 μg/ml PI for 15 min at 37°C, washed with FACS buffer and then analyzed on FACSCalibur (BD Biosciences). A lymphocyte gate was set using forward-angle and side-angle light scatter characteristics of lymphocytes. The vital B cells were brightly positive when stained with $DiOC_6$ and excluded PI.

Statistical analysis

Student's t test (two-tailed unpaired) was used to compare two independent groups using GraphPad 5 software. A probability (p) value of <0.05 was considered significant. *p<0.05; **p<0.01; ***p<0.001.

Annex 4

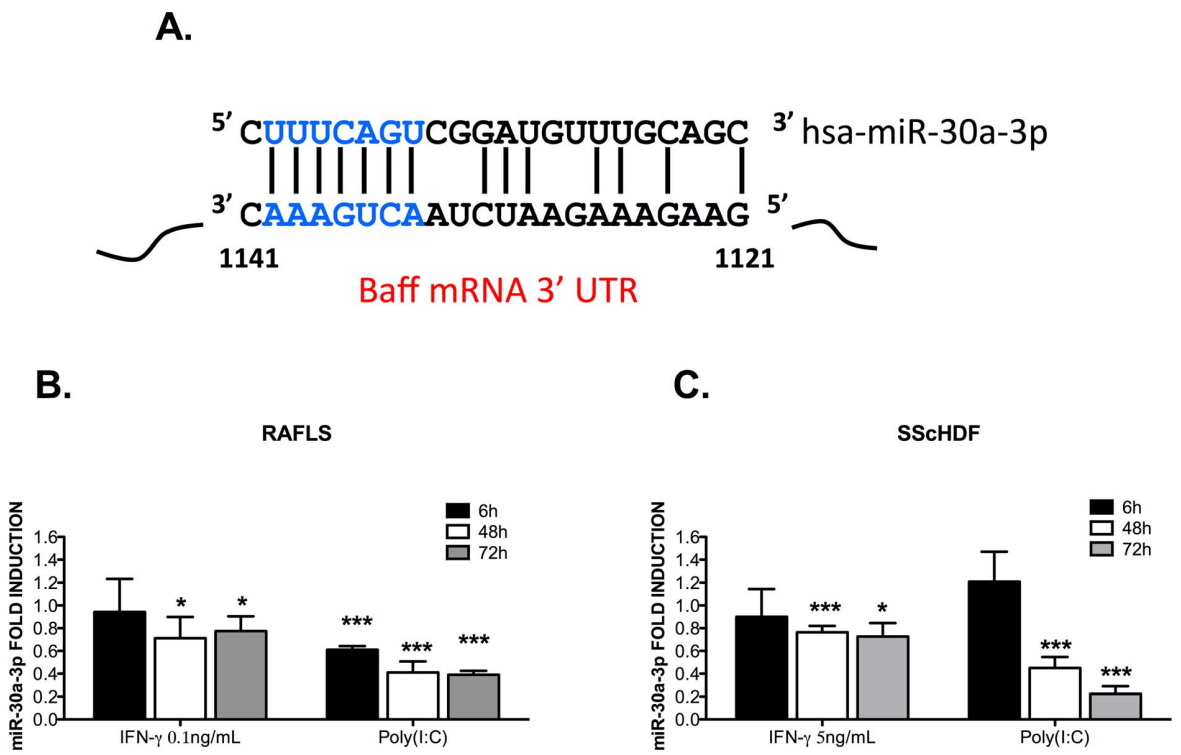

Figure 2. miR-30a-3p expression is down-regulated in Poly (I:C)- and IFN-γ-stimulated RAFLS and SScHDF. A. miR-30a-3p is predicted to target BAFF 3′ UTR mRNA. B, C. miR-30a-3p expression was determined by RT-qPCR in RAFLS (n = 4) (B) and SScHDF (n = 4) (C) stimulated with Poly (I:C) (10 μg/mL) or IFN-γ (0.1 or 5 ng/mL) for 6 h, 48 h and 72 h. Results were normalized to U6snRNA and expressed as fold change compared with samples from cells incubated in medium. Data are expressed as the mean of triplicate samples ± SEM. *p<0.05, ***p<0.001.
doi:10.1371/journal.pone.0111266.g002

Results

Increased BAFF secretion by SScHDF after stimulation with Poly(I:C) or IFN-γ

Upregulation of BAFF expression by Poly (I:C)- and IFN-γ-activated RAFLS, but not upon TLR2 or TLR4 activation, has been previously reported [13,22]. To gain more insights into the physiopathological consequences of this observation, we first compared BAFF expression in FLS isolated from healthy donors or RA patients. As shown in figure 1A and B, we observed that IFN-γ-dependent BAFF expression reaches maximum levels in RAFLS, whereas FLS isolated from healthy donors (NFLS) exhibit reduced cytokine expression at both mRNA and protein levels. Of note, Poly (I:C) stimulation induced very limited BAFF expression and secretion by NFLS, while RAFLS appeared extremely responsive to this stimulus. Next, we tested whether this difference between a healthy and a pathological (inflammatory) state could also be observed in another fibroblastic cell type and for this, we chose Human Dermal Fibroblasts (HDF) isolated from skin biopsies harvested from healthy donors (NHDF) or from patients suffering from systemic sclerosis (SScHDF). IFN-γ stimulation (1 and 5 ng/mL) resulted in a comparable increased expression of BAFF transcripts (figure 1C) and cytokine secretion (figure 1D) by NHDF or SScHDF. Interestingly, up-regulation of BAFF transcripts and protein release in response to TLR3 triggering by Poly (I:C) was only detectable in SScHDF and not from healthy individuals. We also investigated here the ability of Bacterial LipoProteins (BLP, Pam_3CSK4) or LipoPolysaccharide (LPS), which are respectively ligands for TLR2 and 4, to stimulate BAFF synthesis by NHDF and SScHDF. As seen in figure 1C and D, these PAMPs (Pathogen Associated Molecular Pattern) are not activators of BAFF transcription.

Thus, these results show that FLS and HDF from both healthy donors and RA or SSc patients can produce BAFF in response to IFN-γ stimulation, whereas BAFF transcription and protein secretion upon Poly (I:C) triggering occurred only in fibroblasts isolated from RA or SSc patients.

miR-30a-3p is down-regulated in Poly(I:C)- and IFN-γ-activated RAFLS and SScHDF

To understand the mechanisms underlying Poly (I:C)- and IFN-γ-dependent BAFF induction, we then focused our work on miRNA-driven post-transcriptional regulation. A computer-assisted search for miRNAs predicted to target BAFF mRNA performed using microCosm (http://www.ebi.ac.uk/enright-srv/microcosm/htdocs/targets/v5) identified several miRNAs candidates: miR-144*, miR-452, miR-340, miR-202, miR-500, miR-626, miR-330-3p, miR-302c* and miR-30 family members (miR-30a, d and e which share the same seed sequence). To evaluate the possible involvement of these miRNAs in BAFF regulation, we first performed RT-qPCR analysis to quantify their expression in RAFLS and SScHDF treated with Poly(I:C) or IFN-γ for 6 h, 48 h and 72 h. This analysis revealed that miR-144*, miR-30d-3p, miR-340, miR-626, miR-330-3p and miR-302c* could not be detected in RAFLS and SScHDF (figure 1S). miR-202 and miR-500 were expressed constitutively but their expression did not change after activation by Poly(I:C) or IFN-γ in both cell type. Finally, miR-452 was upregulated in Poly (I:C) treated RAFLS.

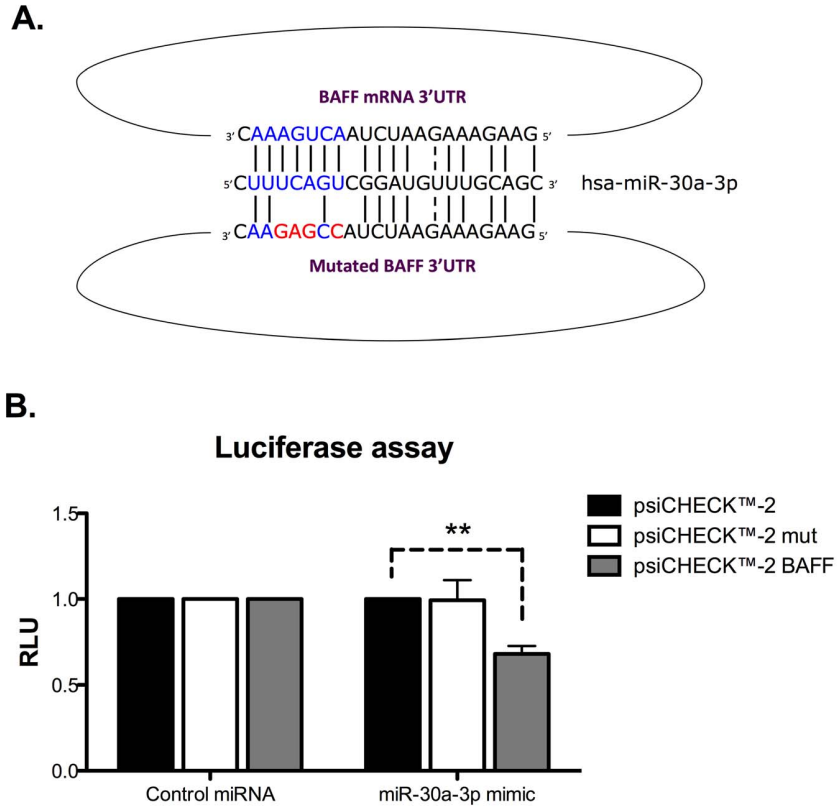

Figure 3. miR-30a-3p directly targets the 3′UTR of BAFF mRNA. A. Luciferase reporter constructs with wild-type or mutated (for miR-30-3p binding sites) BAFF 3′UTR were generated. B. HEK293 cells were transiently co-transfected with reporter constructs and with miR-30a-3p mimic (20 pM). Firefly Luciferase activities were measured 48 h after transfection and normalized to Renilla Luciferase expressed by the control psi-CHECK-2 vector devoid of 3′UTR sequences. Data are expressed as the mean of triplicate samples ± SEM and are representative of three independent experiments. **p<0.01.
doi:10.1371/journal.pone.0111266.g003

Interestingly, we noted that both miR-30a-3p and miR-30e-3p (data not shown), were significantly down-regulated in Poly (I:C)- and IFN-γ-activated, RAFLS (Figure 2B) and SScHDF (figure 2C) 48 h and 72 h after stimulation. These data, together with those illustrated in figure 1, indicate that BAFF transcripts and miR-30a-3p exhibit opposite expression patterns, therefore suggesting potential interactions. Given the strong similarities between miR-30a-3p and miR-30e-3p, we decided to focus on miR-30a-3p.

miR-30a-3p directly interacts with the 3′UTR of BAFF mRNA

To validate the involvement of miR-30a-3p in the regulation of *BAFF* expression, we generated luciferase reporter constructs (derived from the pSI-CHECK2 vector) containing the firefly luciferase gene fused to the entire human BAFF 3′UTR sequence and the renilla luciferase for normalization. We also generated a reporter construct in which a mutated version, designed to disrupt the predicted seed-match for miR-30a-3p of the human BAFF 3′UTR, was inserted (figure 3A). These plasmids were co-transfected in HEK293 cells with miR-30a-3p mimic or AllStars negative control siRNA (CT). In the presence of miR-30a-3p mimic, we observed a significant down regulation of the BAFF 3′UTR-controlled luciferase sensor, whereas luciferase expression upon transfection of the mutated form of the reporter vector remained unchanged (figure 3B). Altogether, these data suggest that BAFF transcripts can be directly targeted by miR-30a-3p for post-transcriptional regulation.

miR-30a-3p modulates BAFF expression in RAFLS and SScHDF

To assess the effect of miR-30a-3p on BAFF expression, we measured the production of BAFF mRNA by RT-qPCR in RAFLS and SScHDF transfected with miR-30a-3p mimic or with the AllStars negative siRNA control (CT). 24 h after transfection, cells were stimulated with Poly (I:C) or IFN-γ for 72 h. As seen in Figure 4, we found that overexpression of miR-30a-3p led to a global decrease in BAFF mRNA production and protein secretion by Poly (I:C)- and IFN-γ-activated RAFLS and SScHDF (panels A–D). Of note, transfection of miR-30a-3p mimic did not modulate IL-6 secretion by RAFLS and SScHDF activated with Poly (I:C) or IFN-γ (figure 4E–F), which is another major cytokine involved in B cells proliferation [23]. This indicates that miR-30a-3p does not interact with transcripts encoding factors involved in cytokine expression or inflammatory responses, but rather specifically interferes with BAFF mRNA in these cells, hence strengthening a potential role for BAFF in this process. Similar results were obtained upon transfection of miR-30e-3p and miR-30d-3p (data not shown).

These data demonstrate that miR-30a-3p is implicated in the negative regulation of BAFF synthesis in Poly (I:C)- and IFN-γ-activated FLS and HDF.

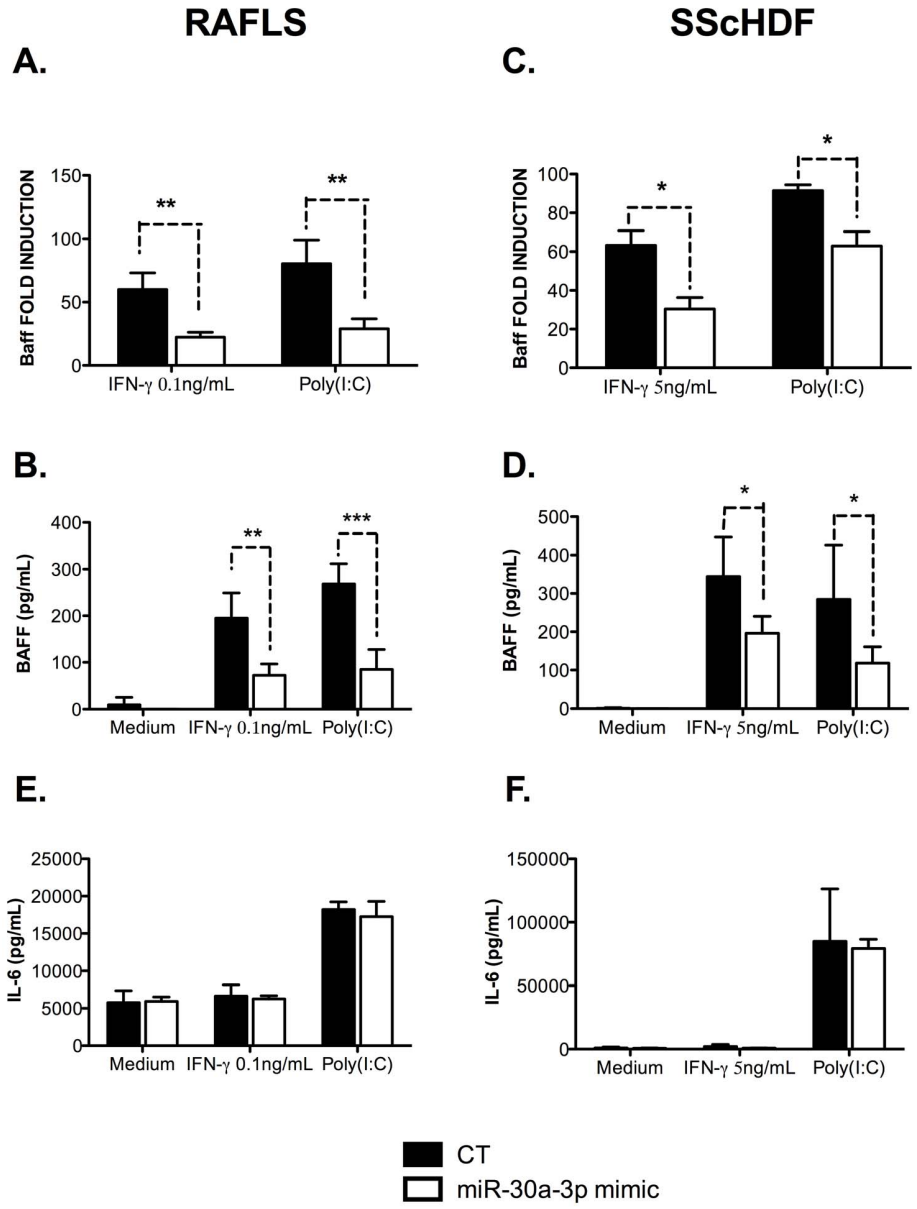

Figure 4. miR-30a-3p transfection affects BAFF mRNA expression and BAFF secretion in RAFLS and SScHDF. A, C. RAFLS (n = 5) (A) and SScHDF (n = 4) (C) were transfected with miR-30a-3p mimic (20 pM/sample) or with an AllStars negative control (CT). After 24 h, cells were activated with Poly (I:C) (10 μg/mL), IFN-γ (0.1 or 5 ng/mL, depending on cell types) or medium for 72 h. BAFF mRNA expression was determined by RT-qPCR. Results were normalized to Gapdh and expressed as fold change compared with samples from cells incubated with medium. B, D. BAFF release was determined by ELISA in culture supernatants in the same conditions as panel A and C. E, F. IL-6 release was determined by ELISA in culture supernatants in the same conditions as panel A and C. Data are expressed as the mean of triplicate samples ± SEM. *$p<0.05$; **$p<0.01$; ***$p<0.001$.
doi:10.1371/journal.pone.0111266.g004

miR-30a-3p specifically represses BAFF-dependent B cells survival

Next, we checked the physiological relevance of BAFF regulation by miR-30a-3p. To this end, we measured the faculty of stimulated RAFLS and SScHDF to promote B cells survival following transfection of miR-30a-3p mimic. RAFLS and SScHDF were transfected with miR-30a-3p mimic or with the AllStars negative control siRNA (CT) for 24 h and then activated with IFN-γ for 72 h. The supernatants (conditioned medium) were harvested and added in the culture medium of B cells. After 3 days, survival of CD19-gated B cells was assessed by FACS analysis. As shown in figure 5, addition of supernatant from IFN-γ-stimulated fibroblasts significantly ($p<0.05$) increases the proportion of viable B cells, which shifts from 10 to 26% in the case of RAFLS supernatant and from 35 to 56% in the case of SScHDF. Importantly, increasing miRNA activity upon transfection of miR-30a-3p mimic in activated fibroblasts lowers B cells viability (15% and 35%, respectively. $p<0.05$). Additionally, we analyzed the supernatant of Poly (I:C)-activated RAFLS and SScHDF but we could not detect any difference in B cells survival (data not shown). Indeed, Poly (I:C), unlike IFN-γ, is also a potent inducer of IL-6 release by RAFLS and SScHDF (figure 4 E–F) which could

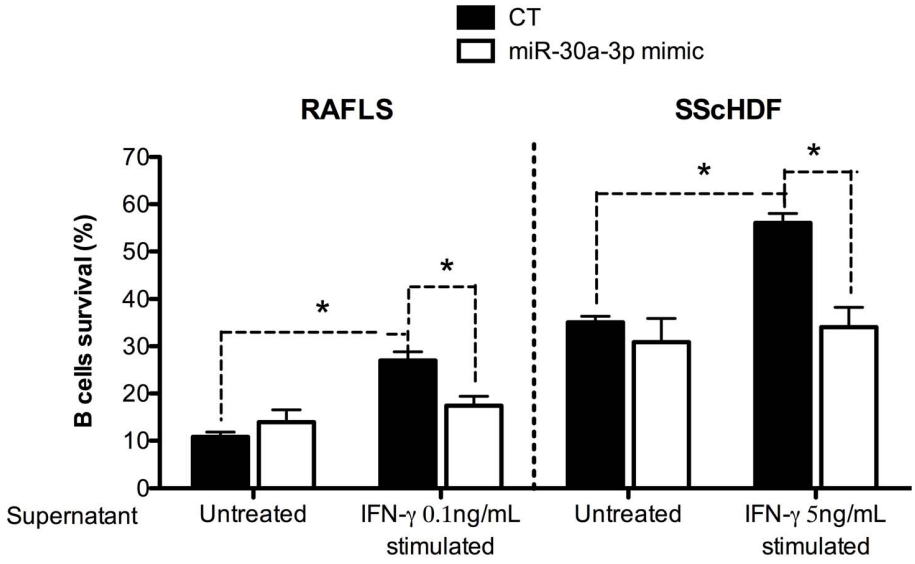

Figure 5. miR-30a-3p expression in RAFLS and SScHDF regulates BAFF-dependent B cells survival in vitro. RAFLS (n = 4) (left) and SScHDF (n = 4) (right) were transfected with miR-30a-3p mimic (20 pM/sample) or with an AllStars negative control (CT). After 24 h, cells were activated with IFN-γ (0.1 or 5 ng/mL depending on the cell type) or medium for 72 h. Then, supernatants were harvested and cultured with purified blood B cells isolated from healthy subjects. B cells viability was determined by FACS analysis; vital B cells were brightly positive when stained with DiOC6 and excluded PI. Data are expressed as the mean of triplicate samples ± SEM. *p<0.05.
doi:10.1371/journal.pone.0111266.g005

regulate B cells survival. Similar results were obtained upon transfection of miR-30e-3p and miR-30d-3p (data not shown).

This experiment reveals that the modulation of miR-30a-3p activity induces important physiological changes with potentially relevant immune repercussions within the frame of autoimmune diseases.

miR-30a-3p is a basal repressors of BAFF expression in non-inflammatory fibroblasts (NFLS and NHDF)

Finally, we considered the possibility that miR-30a-3p family members could represent an essential mechanism to maintain BAFF expression at a very low level necessary in healthy conditions. Indeed, excessive BAFF secretion leading to increased B cells activation constitutes a major trigger promoting auto-immunity. A first insight into this model is provided by our initial observation of augmented BAFF secretion in the supernatant of RAFLS compared to NFLS in response to Poly(I:C) and IFN-γ (figure 1B). Therefore, we compared the expression of miR-30a-3p between healthy donor and patients cells in response to Poly(I:C) and IFN-γ for 48 h and 72 h. Interestingly, we showed that control NFLS as well as Poly(I:C)- and IFN-γ-stimulated cells expressed higher levels of miR-30a-3p compared to RAFLS under the same conditions (figure 6A). Moreover, NHDF which did not release BAFF in response to Poly(I:C) (figure 1D), also expressed higher levels of miR-30a-3p in the same conditions (figure 6B). These observations strongly suggest that miR-30a-3p could be a basal repressor of BAFF expression in these cells. Similar results were obtained upon transfection of miR-30e-3p (data not shown).

To test this hypothesis, we next lowered the activity of miR-30a-3p by transfecting specific antagonists (antisense 2′O methylated oligoribonucleotides) or negative controls (CT) in NFLS and NHDF. 24 h after transfection, cells were stimulated with Poly(I:C) or IFN-γ for 72 h. As illustrated in figure 6C, treatment with Poly(I:C) significantly induced higher levels of BAFF release by activated NHDF transfected with antisense oligonucleotides targeting miR-30a-3p compared to activated NHDF transfected with control (CT) (113,15±23,75 *vs* 30,75±3,25 pg/ml). A similar increase in BAFF secretion was obtained in NFLS transfected with antisense oligonucleotides targeting miR-30a-3p stimulated with Poly(I:C) (122±22 vs 38,2±5,5 pg/ml) and IFN-γ (109,45±20,85 vs 29,65±4,85 pg/ml). This experiment suggests that miR-30a-3p could represent an essential mechanism to maintain BAFF expression at a very low level necessary in healthy conditions. Moreover, we checked whether BAFF transcripts modulation upon miR-30a-3p inhibition also positively impacts on B cells survival. For this, we added anti-BAFF antibodies to poly (I:C)-stimulated NHDF treated with miR-30-3p antagomiRs. As seen in figure 6D, addition of anti-BAFF antibodies significantly (p<0.01 **) eradicates miR-30a-dependant-B cells survival improvement, thereby demonstrating that miR-30a-3p specifically modulates BAFF expression.

Discussion

The role of B cells in autoimmunity has undergone a major renaissance after the demonstration of the efficacy of B cells depletion in RA [24]. BAFF plays a pivotal role in B cells activation in autoimmune diseases and is secreted by resident cells of target organs such as fibroblast-like synoviocytes [22,25,26]. On the other hand, the pivotal role of innate immunity in the initiation of autoimmune diseases is now well established, which prompted our present investigation on the role of innate immune receptors ligands and interferon-γ on BAFF secretion. We performed our analysis in fibroblasts isolated either from the skin (HDF) of healthy donors or from patients suffering from SSc or from the synovium (FLS) of RA patients or controls. Our results clearly show that, while Poly (I:C) stimulation induces high levels of BAFF transcription, LPS or BLP (respectively ligands of TLR4 and TLR2) remain poor activators of BAFF expression and secretion. Likewise, Poly (I:C) as well as LPS or BLP did not induce the synthesis of APRIL (a proliferation inducing ligand), which regulates also lymphocyte survival and activation (data not shown).

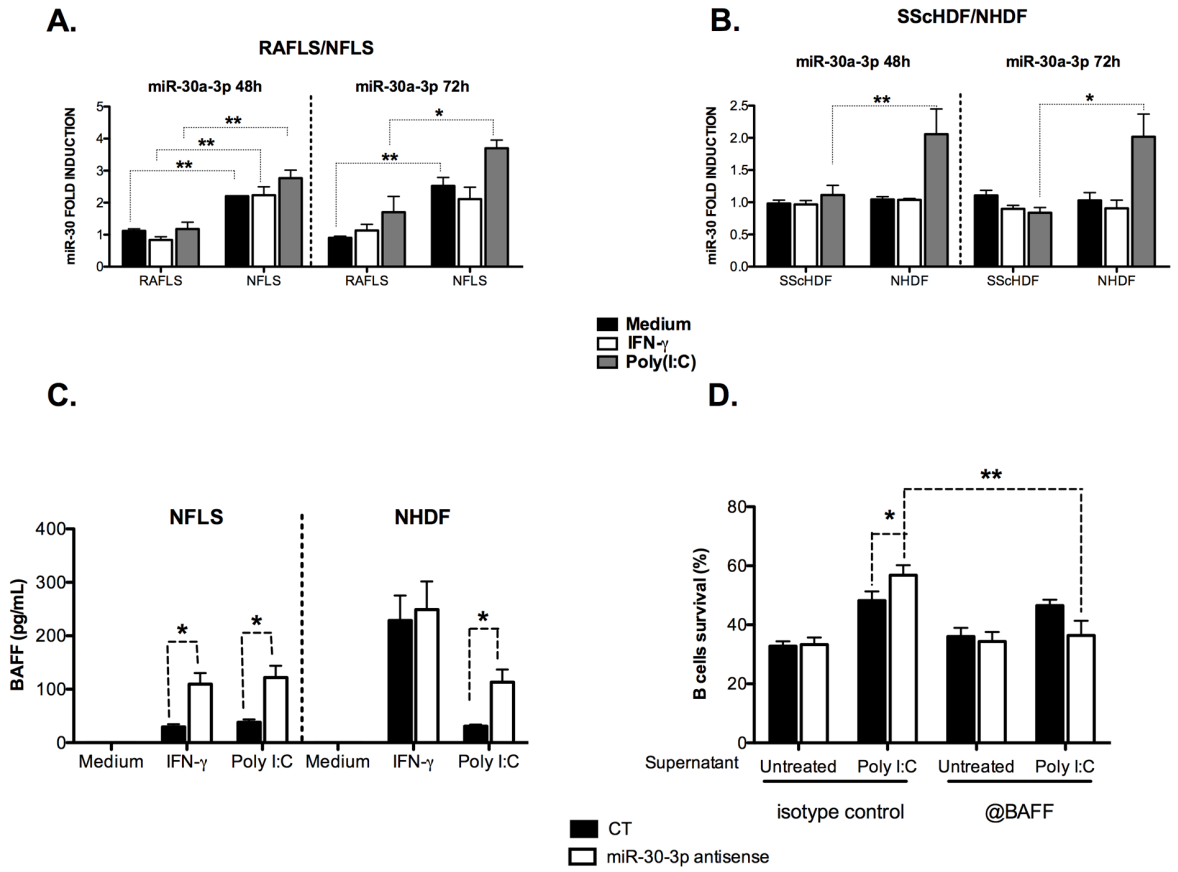

Figure 6. MiR-30a-3p represses BAFF secretion by healthy FLS and HDF. A, B. miR-30a-3p expression was determined by RT-qPCR in NFLS (n = 4)/RAFLS (n = 4) (A) and NHDF (n = 3)/SScHDF (n = 4) (B) stimulated with Poly(I:C) (10 μg/mL), IFN-γ (0.1 or 5 ng/mL) or medium for 48 h and 72 h. Results were normalized to U6snRNA and expressed as fold change compared with samples from RAFLS (A) or SScHDF (B) incubated with medium. C. NFLS (n = 3) and NHDF (n = 3) were transfected with miR-30-3p antisense oligonucleotides (20 pM/sample) or with an AllStars negative control (CT). After 24 h, cells were activated with Poly(I:C) (10 μg/mL), IFN-γ (0.1 or 5 ng/mL) or medium for 72 h. BAFF release was determined by ELISA in culture supernatants. D. NHDF (n = 3) transfected with miR-30-3p antisense, were stimulated with poly (I:C). The supernatant was then treated with control IgG or with anti-BAFF antibodies and added to purified B cells. B cells survival was next evaluated as in panel Figure 5. *p<0.05; **p<0.01.
doi:10.1371/journal.pone.0111266.g006

This finding is consistent with results from our group which proposed that TLR2, 4 and 9 ligands failed to induce BAFF mRNA and protein in rheumatoid FLS [22]. Likewise, stimulation of salivary gland epithelial cells (SGEC) obtained from patients with primary Sjögren's syndrome (pSS) or bronchial epithelial cells with TLR2, 7 and 9 ligands does not induce BAFF transcription and secretion [27,28]. Therefore, a first important result of this study is our description of specific Poly (I:C)-dependent BAFF transcriptional induction and subsequent secretion by SScHDF. This observation provides a conceptual framework whereby pathogens, such as herpesviruses which are capable of triggering a TLR3-dependent response [29] and have been associated to many autoimmune diseases [30], can initiate BAFF secretion and ignite a vicious circle leading to pathogenic auto-antibodies production. In line with this hypothesis, Ittah et al. suggested that PKR is the major mediator of BAFF expression and secretion after dsRNA virus infection or Poly (I:C) stimulation by salivary epithelial cells of pSS [31].

Next, we investigated the mechanisms involved in the regulation of BAFF production by FLS and HDF. miRNAs, which are considered as efficient fine tuners of immune responses because they usually modulate gene expression by a factor 1.2 to 4 [32], exhibit abnormal expression associated with inflammatory disorders such as RA [33,34], SLE [35,36] and SSc [37,38]. In an initial attempt to identify miRNAs involved in the control of BAFF expression, we performed RT-qPCR analysis of Poly (I:C)- and IFN-γ-activated RAFLS and SScHDF to quantify the expression of 9 miRNAs that were predicted to target BAFF transcripts. Among these candidates, miR-30a-3p was selected for further analysis because its expression was down regulated in Poly (I:C)- and IFN-γ-activated RAFLS and SScHDF; such inverse correlation with the expression of BAFF transcripts in the same cells and the same conditions indicated that miR-30-3p family members might have a role in the regulation of BAFF expression. We next demonstrated by several complementary approaches that miR-30a-3p actually bind specifically to the 3′UTR of BAFF transcripts and modulate cytokine expression. Importantly, additional results (data not shown) indicate that additional members (and closely related) of the miR-30a-3p family (miR30-d-3p and -e-3p) also regulate BAFF expression in RAFLS and SScHDF stimulated with Poly (I:C) or IFN-γ. Therefore, our study additionally suggests a novel mechanism for the regulation of BAFF expression at the posttranslational level in response to inflammatory stimuli but the transcriptional regulation of BAFF expression must also be considered. Usually, miRNAs can function together with RNA-binding proteins to regulate mRNA expression through the AU-

rich elements (AREs) that are found in numerous cytokine-encoding mRNAs. For example, TNF-α and IL-10 mRNAs both contain long AREs that are targeted by the RNA-binding protein tristetraprolin (TTP) [39]. Our group previously showed that blocking miR-346 decreases TTP expression and re-established mature TNF-α intracellular expression in LPS-activated RAFLS [40,41]. Although evidence for the direct targeting of cytokine mRNAs by miRNAs is limited [39], we demonstrated in this study that miR 30a-3p directly regulates BAFF mRNA.

Importantly, we also analyzed in our study the functional outcome of miRNA-dependent BAFF regulation. We demonstrated that IFN-γ stimulation of fibroblasts favors an extracellular milieu that promotes B cells survival. Importantly, our experiments (illustrated in Figure 5) demonstrated that specifically altering BAFF secretion (with miR-30a mimic or upon anti-BAFF antibodies addition following antagomiRs transfection) reduces the B cells survival capacity of supernatant from IFN-γ stimulated RAFLS or SScHDF back to normal (as observed in control cells). This indicates that BAFF (and not IL-6) is the major B cells survival factor expressed by these fibrocytes upon IFN-γ stimulation. Similar to our findings, Ohata et al reported that FLS treated with IFN-γ and/or TNF-α had a greater capacity to support B cells survival than did untreated FLS [26]. B cells survival could be inhibited by BAFF-R:Fc, indicating that BAFF/BAFF-R interactions were involved in B cells survival [26]. Altogether, this work provides a mechanistic explanation to the control of BAFF transcripts expression and demonstrates that cytokine secretion by resident cells of target organs of autoimmune diseases can be negatively regulated at the post-transcriptional level by miRNAs. A tentative model describing these interactions is depicted in Figure 2S. The understanding of these complex pathways has important implications for the development of future therapeutic applications. Indeed, the success of Belimumab in the treatment of patients with RA and ongoing clinical trials in SSc (NCT01670565) suggest that therapeutic targeting of BAFF could be of interest [42]. Our present study suggests that miR-30a-3p (and others family members) mimic could be used to target BAFF mRNA in autoimmune diseases. Recently, patients chronically infected with hepatitis C virus (HCV) treated with locked nucleic acid (modified antisense oligonucleotides) against miR-122 showed a prolonged dose-dependent reductions in HCV RNA levels without evidence of viral resistance [43], which suggests that miRNA modulation in patients could become a new therapeutic option in the future.

Supporting Information

Figure S1 miRNAs expression in RAFLS and SScHDF. MiR-144*, miR-30d-3p, miR-452, miR-340, miR-202, miR-500, miR-626, miR-330-3p and miR-302c* expression was determined by RT-qPCR in RAFLS (n = 3) and SScHDF (n = 3) stimulated with Poly (I:C) (10 μg/mL) or IFN-γ (0.1 or 5 ng/mL) for 72 h. Results were normalized to U6snRNA and expressed as fold change compared with samples from RAFLS or SScHDF incubated with medium.
(TIFF)

Figure S2 Model describing the role of miR-30a-3p in BAFF secretion by FLS (A) and HDF (B) from RA or SSc patients and healthy subjects.
(TIFF)

Acknowledgments

The authors are grateful to Angélique Pichot for technical help and to Prof. François Bonnomet, (Service de chirurgie orthopédique, Strasbourg Hospital) Dr. Emmanuel Chatelus and Dr. Christelle Sordet (service de rheumatology, Strasbourg hospital) for patients' biopsies.

Author Contributions

Conceived and designed the experiments: GA AF SP DW PG. Performed the experiments: GA AF LP YZG SC. Analyzed the data: GA AF SP PG. Contributed reagents/materials/analysis tools: SP SB JS. Wrote the paper: GA AF SP PG JEG JS.

References

1. Mackay F, Schneider P, Rennert P, Browning J (2003) BAFF AND APRIL: a tutorial on B cell survival. Annu Rev Immunol 21: 231–264. doi:10.1146/annurev.immunol.21.120601.141152.
2. Nardelli B, Belvedere O, Roschke V, Moore PA, Olsen HS, et al. (2001) Synthesis and release of B-lymphocyte stimulator from myeloid cells. Blood 97: 198–204.
3. Scapini P, Nardelli B, Nadali G, Calzetti F, Pizzolo G, et al. (2003) G-CSF-stimulated neutrophils are a prominent source of functional BLyS. J Exp Med 197: 297–302.
4. Krumbholz M, Theil D, Derfuss T, Rosenwald A, Schrader F, et al. (2005) BAFF is produced by astrocytes and up-regulated in multiple sclerosis lesions and primary central nervous system lymphoma. J Exp Med 201: 195–200. doi:10.1084/jem.20041674.
5. Kalled SL (2005) The role of BAFF in immune function and implications for autoimmunity. Immunol Rev 204: 43–54. doi:10.1111/j.0105-2896.2005.00219.x.
6. Mackay F, Woodcock SA, Lawton P, Ambrose C, Baetscher M, et al. (1999) Mice Transgenic for Baff Develop Lymphocytic Disorders along with Autoimmune Manifestations. Journal of Experimental Medicine 190: 1697–1710. doi:10.1084/jem.190.11.1697.
7. Seyler TM, Park YW, Takemura S, Bram RJ, Kurtin PJ, et al. (2005) BLyS and APRIL in rheumatoid arthritis. J Clin Invest 115: 3083–3092. doi:10.1172/JCI25265.
8. Mackay F, Schneider P (2009) Cracking the BAFF code. Nat Rev Immunol 9: 491–502. doi:10.1038/nri2572.
9. Pers J-O, Daridon C, Devauchelle V, Jousse S, Saraux A, et al. (2005) BAFF overexpression is associated with autoantibody production in autoimmune diseases. Ann N Y Acad Sci 1050: 34–39. doi:10.1196/annals.1313.004.
10. Matsushita T, Hasegawa M, Matsushita Y, Echigo T, Wayaku T, et al. (2007) Elevated serum BAFF levels in patients with localized scleroderma in contrast to other organ-specific autoimmune diseases. Exp Dermatol 16: 87–93. doi:10.1111/j.1600-0625.2006.00485.x.
11. Matsushita T, Fujimoto M, Hasegawa M, Tanaka C, Kumada S, et al. (2007) Elevated serum APRIL levels in patients with systemic sclerosis: distinct profiles of systemic sclerosis categorized by APRIL and BAFF. J Rheumatol 34: 2056–2062.
12. Zhang M, Ko K-H, Lam QLK, Lo CKC, Srivastava G, et al. (2005) Expression and function of TNF family member B cell-activating factor in the development of autoimmune arthritis. Int Immunol 17: 1081–1092. doi:10.1093/intimm/dxh287.
13. Alsaleh G, François A, Knapp A-M, Schickel J-N, Sibilia J, et al. (2011) Synovial fibroblasts promote immunoglobulin class switching by a mechanism involving BAFF. Eur J Immunol 41: 2113–2122. doi:10.1002/eji.201041194.
14. Baker KP, Edwards BM, Main SH, Choi GH, Wager RE, et al. (2003) Generation and characterization of LymphoStat-B, a human monoclonal antibody that antagonizes the bioactivities of B lymphocyte stimulator. Arthritis Rheum 48: 3253–3265. doi:10.1002/art.11299.
15. Chan AC (2011) B cell immunotherapy in autoimmunity–2010 update. Mol Immunol 48: 1344–1347. doi:10.1016/j.molimm.2010.11.021.
16. Chugh PK, Kalra BS (2013) Belimumab: targeted therapy for lupus. Int J Rheum Dis 16: 4–13. doi:10.1111/1756-185x.12002.
17. Jing Q, Huang S, Guth S, Zarubin T, Motoyama A, et al. (2005) Involvement of microRNA in AU-rich element-mediated mRNA instability. Cell 120: 623–634. doi:10.1016/j.cell.2004.12.038.
18. Asirvatham AJ, Magner WJ, Tomasi TB (2009) miRNA regulation of cytokine genes. Cytokine 45: 58–69. doi:10.1016/j.cyto.2008.11.010.
19. Philippe L, Alsaleh G, Pichot A, Ostermann E, Zuber G, et al. (2013) MiR-20a regulates ASK1 expression and TLR4-dependent cytokine release in rheumatoid fibroblast-like synoviocytes. Ann Rheum Dis 72: 1071–1079. doi:10.1136/annrheumdis-2012-201654.
20. Alsaleh G, Suffert G, Semaan N, Juncker T, Frenzel L, et al. (2009) Bruton's tyrosine kinase is involved in miR-346-related regulation of IL-18 release by lipopolysaccharide-activated rheumatoid fibroblast-like synoviocytes. J Immunol 182: 5088–5097. doi:10.4049/jimmunol.0801613.

Annex 4

21. Zamzami N, Marchetti P, Castedo M, Zanin C, Vayssière JL, et al. (1995) Reduction in mitochondrial potential constitutes an early irreversible step of programmed lymphocyte death in vivo. J Exp Med 181: 1661–1672.
22. Alsaleh G, Messer L, Semaan N, Boulanger N, Gottenberg J-E, et al. (2007) BAFF synthesis by rheumatoid synoviocytes is positively controlled by alpha5beta1 integrin stimulation and is negatively regulated by tumor necrosis factor alpha and Toll-like receptor ligands. Arthritis Rheum 56: 3202–3214. doi:10.1002/art.22915.
23. Kishimoto T (2005) Interleukin-6: from basic science to medicine–40 years in immunology. Annu Rev Immunol 23: 1–21. doi:10.1146/annurev.immunol.23.021704.115806.
24. Finnegan A, Ashaye S, Hamel KM (2012) B effector cells in rheumatoid arthritis and experimental arthritis. Autoimmunity 45: 353–363. doi:10.3109/08916934.2012.665526.
25. Moisini I, Davidson A (2009) BAFF: a local and systemic target in autoimmune diseases. Clin Exp Immunol 158: 155–163. doi:10.1111/j.1365-2249.2009.04007.x.
26. Ohata J, Zvaifler NJ, Nishio M, Boyle DL, Kalled SL, et al. (2005) Fibroblast-like synoviocytes of mesenchymal origin express functional B cell-activating factor of the TNF family in response to proinflammatory cytokines. J Immunol 174: 864–870.
27. Ittah M, Miceli-Richard C, Gottenberg J-E, Sellam J, Eid P, et al. (2008) Viruses induce high expression of BAFF by salivary gland epithelial cells through TLR- and type-I IFN-dependent and -independent pathways. Eur J Immunol 38: 1058–1064. doi:10.1002/eji.200738013.
28. Kato A, Truong-Tran AQ, Scott AL, Matsumoto K, Schleimer RP (2006) Airway epithelial cells produce B cell-activating factor of TNF family by an IFN-beta-dependent mechanism. J Immunol 177: 7164–7172.
29. Zhang S-Y, Jouanguy E, Sancho-Shimizu V, Von Bernuth H, Yang K, et al. (2007) Human Toll-like receptor-dependent induction of interferons in protective immunity to viruses. Immunol Rev 220: 225–236. doi:10.1111/j.1600-065X.2007.00564.x.
30. Ferraccioli G, Tolusso B (2007) Infections, B cell receptor activation and autoimmunity: different check-point impairments lead to autoimmunity, clonal B cell expansion and fibrosis in different immunological settings. Autoimmun Rev 7: 109–113. doi:10.1016/j.autrev.2007.02.013.
31. Ittah M, Miceli-Richard C, Gottenberg J-E, Sellam J, Lepajolec C, et al. (2009) B-cell-activating factor expressions in salivary epithelial cells after dsRNA virus infection depends on RNA-activated protein kinase activation. Eur J Immunol 39: 1271–1279. doi:10.1002/eji.200839086.
32. Mukherji S, Ebert MS, Zheng GXY, Tsang JS, Sharp PA, et al. (2011) MicroRNAs can generate thresholds in target gene expression. Nat Genet 43: 854–859. doi:10.1038/ng.905.
33. Stanczyk J, Pedrioli DML, Brentano F, Sanchez-Pernaute O, Kolling C, et al. (2008) Altered expression of MicroRNA in synovial fibroblasts and synovial tissue in rheumatoid arthritis. Arthritis Rheum 58: 1001–1009. doi:10.1002/art.23386.
34. Ceribelli A, Nahid MA, Satoh M, Chan EKL (2011) MicroRNAs in rheumatoid arthritis. FEBS Lett 585: 3667–3674. doi:10.1016/j.febslet.2011.05.020.
35. Dai Y, Huang Y-S, Tang M, Lv T-Y, Hu C-X, et al. (2007) Microarray analysis of microRNA expression in peripheral blood cells of systemic lupus erythematosus patients. Lupus 16: 939–946. doi:10.1177/0961203307084158.
36. Tang Y, Luo X, Cui H, Ni X, Yuan M, et al. (2009) MicroRNA-146A contributes to abnormal activation of the type I interferon pathway in human lupus by targeting the key signaling proteins. Arthritis Rheum 60: 1065–1075. doi:10.1002/art.24436.
37. Li H, Yang R, Fan X, Gu T, Zhao Z, et al. (2012) MicroRNA array analysis of microRNAs related to systemic scleroderma. Rheumatol Int 32: 307–313. doi:10.1007/s00296-010-1615-y.
38. Maurer B, Stanczyk J, Jüngel A, Akhmetshina A, Trenkmann M, et al. (2010) MicroRNA-29, a key regulator of collagen expression in systemic sclerosis. Arthritis Rheum 62: 1733–1743. doi:10.1002/art.27443.
39. O'Neill LA, Sheedy FJ, McCoy CE (2011) MicroRNAs: the fine-tuners of Toll-like receptor signalling. Nat Rev Immunol 11: 163–175. doi:10.1038/nri2957.
40. Alsaleh G, Suffert G, Semaan N, Juncker T, Frenzel L, et al. (2009) Bruton's tyrosine kinase is involved in miR-346-related regulation of IL-18 release by lipopolysaccharide-activated rheumatoid fibroblast-like synoviocytes. J Immunol 182: 5088–5097. doi:10.4049/jimmunol.0801613.
41. Semaan N, Frenzel L, Alsaleh G, Suffert G, Gottenberg J-E, et al. (2011) miR-346 controls release of TNF-α protein and stability of its mRNA in rheumatoid arthritis via tristetraprolin stabilization. PLoS ONE 6: e19827. doi:10.1371/journal.pone.0019827.
42. Stohl W, Merrill JT, McKay JD, Lisse JR, Zhong ZJ, et al. (2013) Efficacy and safety of belimumab in patients with rheumatoid arthritis: a phase II, randomized, double-blind, placebo-controlled, dose-ranging Study. J Rheumatol 40: 579–589. doi:10.3899/jrheum.120886.
43. Janssen HLA, Reesink HW, Lawitz EJ, Zeuzem S, Rodriguez-Torres M, et al. (2013) Treatment of HCV Infection by Targeting MicroRNA. N Engl J Med. doi:10.1056/NEJMoa1209026.

Caractérisation moléculaire du mécanisme de dégradation des microARN par un transcrit cible

Résumé de thèse en français

Semih CETIN

Introduction

Les microARN (miARN) sont des petits ARN non codants d'environ 22 nucléotides qui jouent un rôle de régulateurs de l'expression génique chez les eucaryotes. À ce jour, plus de 1500 miARN impliqués dans de nombreux processus cellulaires ont été identifiés chez l'homme. La biogenèse des miARN s'effectue par un clivage séquentiel d'un transcrit primaire par les ribonucléases de type III Drosha (Lee et al., 2003) et Dicer (Hutvágner et al., 2001) pour former un duplexe miARN (Figure 1). Un des brins de ce duplexe va être incorporé dans une protéine Argonaute (AGO) (Chendrimada et al., 2005; Gregory et al., 2005; Maniataki and Mourelatos, 2005) qui va guider le complexe effecteur RISC (RNA induced silencing complex) vers des messagers cellulaires cibles pour réguler négativement leur expression en réprimant leur traduction et/ou en les déstabilisant (Jonas and Izaurralde, 2015) (Figure 1 et 2). La biogenèse et le mode d'action des miARN ont été intensivement étudiés, ce qui a permis de comprendre la complexité de cette voie de régulation d'expression génique. Par ailleurs, la compréhension des mécanismes permettant de réguler les miARN eux-mêmes a récemment reçu beaucoup d'attention. Les données publiées indiquent que cette régulation a lieu à plusieurs niveaux de la biogenèse et de l'activité des miARN (Ha and Kim, 2014). Cependant, il y a encore très peu d'information concernant la régulation de la stabilité des miARN. Ces derniers ont en effet longtemps été considérés comme des molécules très stables (Baccarini et al., 2011; Bail et al., 2010; Gantier et al., 2011; Rooij et al., 2007). Toutefois, plusieurs exemples illustrant la nécessité de contrôler la stabilité des miARN, notamment en cas d'adaptation aux stress biotiques et abiotiques, commencent à apparaître dans la littérature. Ainsi, il a été observé au laboratoire qu'au cours d'une infection par le cytomégalovirus murin (MCMV), un transcrit viral (m169) induit la dégradation spécifique d'un miARN cellulaire (miR-27) suite à la formation d'espèces plus courtes ('trimming') et plus longues ('tailing') de miR-27 (Marcinowski et al., 2012).

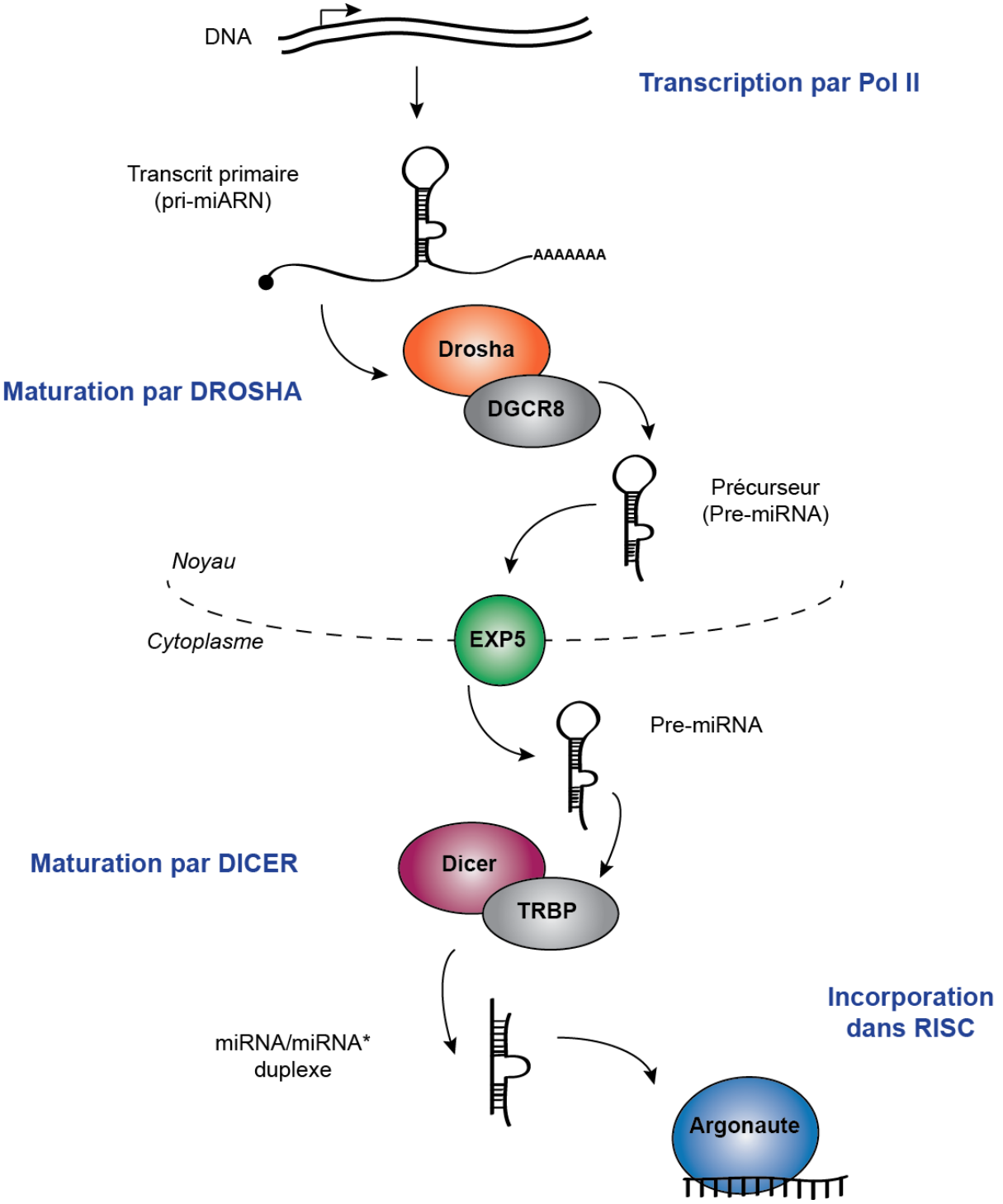

Figure 1 : Biogenèse des microARN

Schéma de la biogenèse des miARN. Après la production du transcrit primaire d'un miARN (pri-miARN), deux clivages séquentiels se produisent, d'abord par DROSHA qui forme le précurseur (pré-miARN), suivi de son export dans le cytoplasme par EXP5 (exportin-5), ensuite par DICER qui génère le duplexe de miARN mature (miARN/miARN*). Un des brins de ce duplexe sera incorporé dans une protéine Argonaute qui formera le 'RNA-induced silencing complex' (RISC).

Un phénomène similaire de *tailing-trimming* des miARN a été décrit récemment chez la drosophile et l'importance du degré de complémentarité de séquence entre l'ARN messager cible et le miARN modifié a été démontrée (Ameres et al., 2010). Ce mécanisme est appelé TDMD pour *'target-RNA directed miRNA degradation'*. Le projet de thèse a consisté à élucider le mécanisme moléculaire du TDMD en suivant deux grands axes de recherche. Tout d'abord, j'ai étudié et caractérisé les déterminants moléculaires et les facteurs cellulaires impliqués dans ce mécanisme de *tailing-trimming* de miR-27 au cours de l'infection par le MCMV (Chapitre I). Dans un second temps, j'ai entrepris une approche différente afin d'identifier directement les partenaires de la protéine AGO2 dans des cellules infectées ou non par le MCMV (Chapitre II).

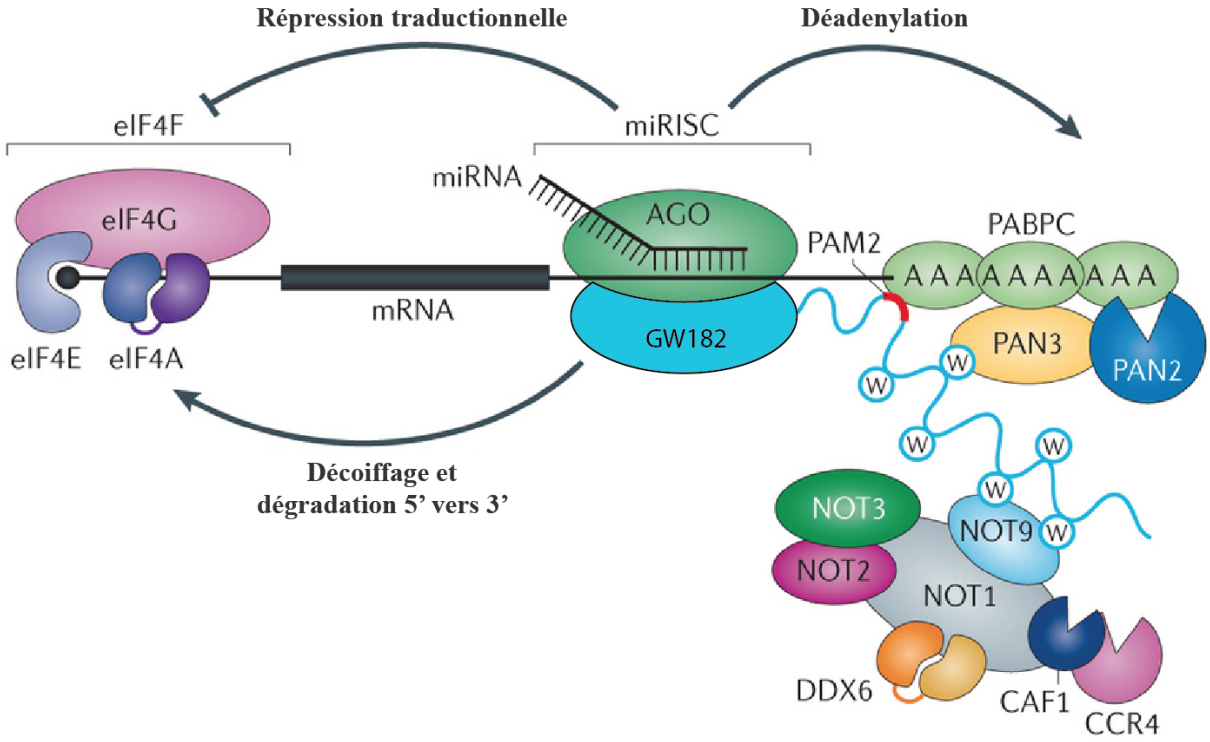

Figure 2 : Mécanismes de régulation d'un ARN messager par les miARN
Après la reconnaissance d'un ARN messager cible par AGO, elle recrute la protéine GW182, qui agit comme une plateforme interagissant avec PABPC (cytoplasmic poly(A)-binding protein) et les complexes de déadenylation PAN2-PAN3 et CCR4-NOT. Quand la déadenylation est complète, le messager est rapidement décoiffé et dégradé par XRN1 (5' to 3' exoribonuclease 1). De plus, les miARN peuvent aussi induire la répression traductionnelle de leur messagers cibles, bien que le mécanisme sous-jacent soit peu clair. PAM2 : PABP-interacting motif, W : Domaine riche en résidus de tryptophane recrutant divers complexes au RISC. D'après (Jonas and Izaurralde, 2015).

Chapitre I

Dans un premier temps, nous avons voulu étudier l'effet de l'appariement entre le miARN et le transcrit viral afin de déterminer les prérequis pour l'induction de ce mécanisme. Les expériences ont montré que le *tailing-trimming* d'un miARN existe aussi dans les cellules humaines, mais également qu'il peut être induit simplement par un oligonucléotide qui mime une interaction parfaite. L'appariement entre miR-27 et m169 n'est pas parfait, l'interaction entre ces deux ARN implique la région 5' (seed) et un appariement fort en 3' du miARN. Après transfection d'oligoribonucléotides anti-sens mimant l'interaction miR-27/m169 sauvage et mutants, nous avons observé que l'interaction miR-27/m169 présente déjà l'appariement minimum en 3' puisque la mutation du nucléotide 3' proximal entraîne la perte de l'effet. Par ailleurs, nous avons observé que l'appariement de trois nucléotides en 3' du miARN en plus de l'appariement de la région 'seed' permet toujours d'induire le tailing-trimming de miR-27.

Le site de liaison à miR-27 sur m169 est capable d'induire la dégradation de miR-27 mais permet cependant également la répression traductionnelle de m169 par miR-27. Nous avons voulu étudier plus en détail la double fonction de ce site de liaison. A l'aide de rapporteurs luciférase contenant la région 3'UTR du transcrit viral m169, nous avons tout d'abord confirmé que le site de liaison de miR-27 était fonctionnel pour induire la régulation de la cible en parallèle de la dégradation du miARN. En multipliant le nombre de sites de fixation de miR-27 dans la 3' UTR des rapporteurs nous avons observé comme attendu une répression accrue due à la coopérativité entre ces sites successifs. En revanche, la multiplication des sites n'affecte pas le TDMD de miR-27, démontrant que ce dernier est un phénomène non cumulatif.

Au laboratoire, nous avons utilisé une approche protéomique pour identifier les facteurs cellulaires impliqués dans le mécanisme de TDMD. La transfection de cellules HeLa

par un oligoribonucléotide antisens couplé à la biotine nous a permis d'une part d'induire spécifiquement la dégradation de miR-27 *in vivo* et d'autre part de précipiter les facteurs cellulaires attachés au complexe dans le lysat cellulaire. En effectuant une spectrométrie de masse, ces facteurs protéiques ont été identifiés. Cette analyse a permis, en plus de plusieurs protéines connues de la voie des miARN, d'identifier deux candidats particulièrement prometteurs pour être impliqué dans le mécanisme de TDMD, une Terminal-Uridylyl-Transferase (TUT1), et une 3'-5' exoribonucléase DIS3 like 2 (DIS3L2). TUT1 est un des sept membres de la famille des TUTases chez les mammifères et DIS3L2 est une 3'-5' exonucléase agissant indépendamment de l'exosome.

Ces facteurs découverts dans les cellules HeLa par la spectrométrie de masse sont conservés chez la souris. Les expériences de co-immunoprécipitation ont montré que ces deux candidats interagissaient entre eux et avec la protéine AGO2 dans les lignées cellulaires humaines mais également murines. Nous avons par la suite effectué des expériences visant à valider l'implication de ces facteurs dans le TDMD de miR-27 en contexte d'infection par MCMV. Dans un premier temps, nous avons réalisé des expériences d'extinction de l'expression de ces facteurs par transfection de siARN dans les cellules murines suivi de l'infection par MCMV. Ces expériences n'ont pas produit de résultats significatifs concernant la stabilisation de miR-27, probablement due à une extinction incomplète de ces facteurs protéiques et/ou à la haute processivité de DIS3L2 et à la redondance des TUTases.

Un mutant catalytique de DIS3L2 a été auparavant décrit dans la littérature (Faehnle et al., 2014), ce mutant incapable de dégrader l'ARN, est toujours capable de se lier à celui-ci. Nous avons donc surexprimé ce mutant catalytique pour obtenir un effet dominant négatif. Par cette approche, nous avons pu observer une stabilisation partielle mais significative des isoformes de miR-27 durant l'infection par MCMV. Ces résultats ont été inclus dans un

manuscrit sur lequel je suis co-premier auteur et qui a été publié dans la revue *Nucleic Acids Research* début 2016 (Haas et al., 2016).

Chapitre II

Nous avons voulu mettre en place une approche protéomique afin de déterminer les protéines partenaires d'AGO2 durant l'infection par MCMV. Cette approche nous a permis dans un premier temps d'identifier des protéines candidates qui fonctionneraient avec AGO2 durant l'infection. Par ailleurs, nous avons également comparé l'infection par un virus MCMV sauvage (MCMVwt) ou mutant n'induisant pas la dégradation de miR-27 (appelé par la suite MCMVmut), ce dans le but d'identifier des facteurs impliqués dans le TDMD. Pour réaliser cette étude, nous avons opté pour une approche dite 'étiquetage par proximité' permettant le marquage par la biotinylation in vivo des protéines proximales à la protéine d'intérêt (Roux et al., 2012) (Figure 3). Pour cela nous avons exprimé la protéine AGO2 murine (mAGO2) fusionnée à une version mutante de la protéine d'origine bactérienne BirA (biotin ligase) (appelé par la suite BirA*) permettant le marquage par la biotine des protéines dans un rayon de 10 nm de la protéine de fusion. Une étape d'enrichissement des protéines biotinylées par des billes couplées à la streptavidine est nécessaire avant de passer à l'identification par spectrométrie de masse.

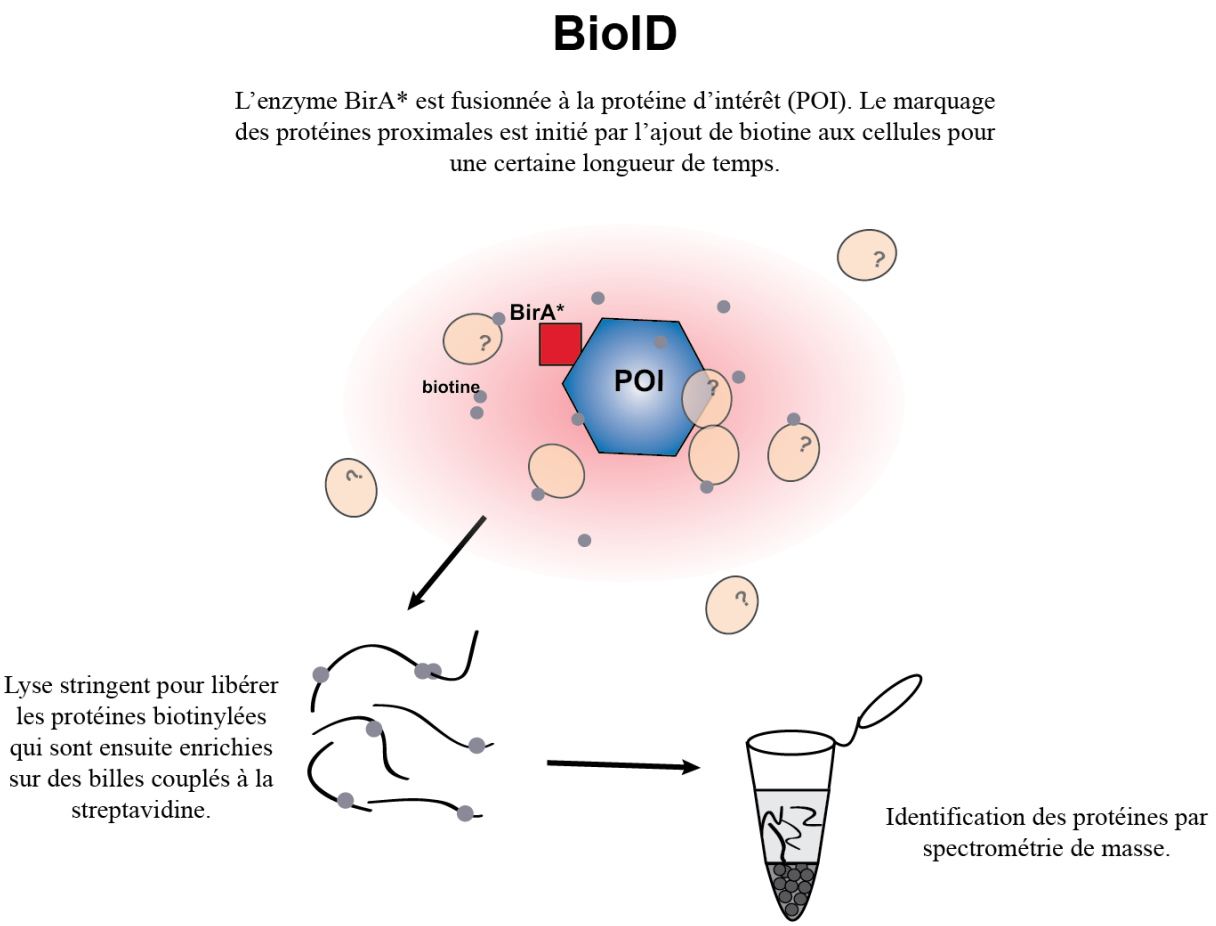

Figure 3 : Technique d'étiquetage par proximité (BioID)
Approche d'étiquetage enzymatique d'un rayon d'activité restreint. Grâce à la protéine d'origine bactérienne BirA* fusionnée à la protéine d'intérêt, les protéines proximales sont marquées par la biotine et enrichies par une chromatographie d'affinité à la streptavidine permettant leur identification. POI : Protéine d'intérêt. Adapté depuis (Mehta and Trinkle-Mulcahy, 2016).

Dans un premier temps nous avons mis au point l'étape de l'expression transitoire de la fusion BirA*-mAGO2 dans une lignée cellulaire de souris en absence d'infection (Figure 4-A), suivi de la mise au point du marquage par la biotine et les conditions d'enrichissement par streptavidine des protéines proximales (Figure 4-B et C). Une fois les étapes de mise au point effectuées, l'analyse par spectrométrie de masse nous a permis d'identifier les partenaires connus de AGO2 impliqués entre autres dans l'incorporation de miARN dans le complexe RISC comme HSP90/HSC70 (Iwasaki et al., 2010; Johnston et al., 2010) et dans la

régulation des messagers cibles comme TNRC6B (Lian et al., 2009; Pfaff et al., 2013), EDC4 (Jonas and Izaurralde, 2013), PABP (Jinek et al., 2010; Zekri et al., 2009).

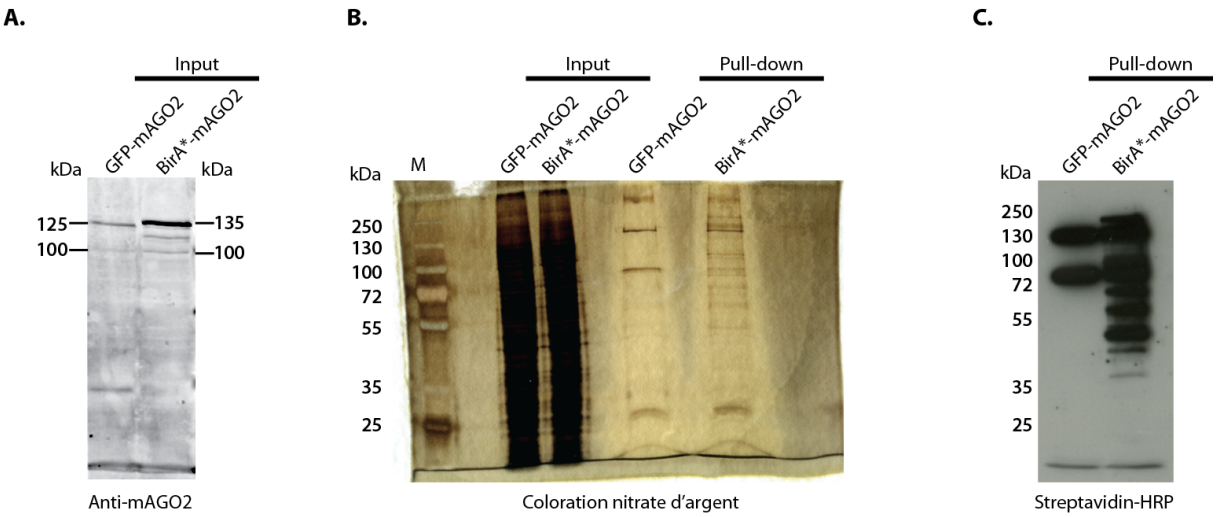

Figure 4 : Enrichissement des protéines proximales marquées par la biotine dans les cellules Hepa 1.6.
A. Niveau d'expression de la protéine mAGO2 endogène (100kDa) et des protéines mAGO2 fusionnées à la GFP (125 kDa) et BirA* (135 kDa) révélé par Western blot. **B.** Coloration nitrate d'argent après l'enrichissement et élution des protéines marquées à la biotine. **C.** Révélation par la Streptavidin-HRP des protéines biotinylées par Western blot.

Par la suite, nous avons voulu créer une lignée stable exprimant la protéine de fusion BirA*-mAGO2. Pour créer cette lignée, nous sommes partis d'une lignée cellulaire appelée MEF-AGO2-/-, une lignée de fibroblastes embryonnaires de souris (MEF) issue de souris 'knock-out' pour AGO2 (Liu et al., 2004). Cette lignée stable nous permettrait d'avoir l'expression de la fusion BirA*-mAGO2 sans bruit de fond provenant de l'expression de la protéine AGO2 endogène et comparée à l'expression transitoire, il n'y aurait pas d'inertie d'incorporation *de novo* de miARN dans les protéines AGO2. Après la vérification de plusieurs colonies sélectionnées durant la générations de lignées stables, nous avons pu obtenir une seule colonie de cellules positive, exprimant la fusion BirA*-mAGO2 (Figure 5).

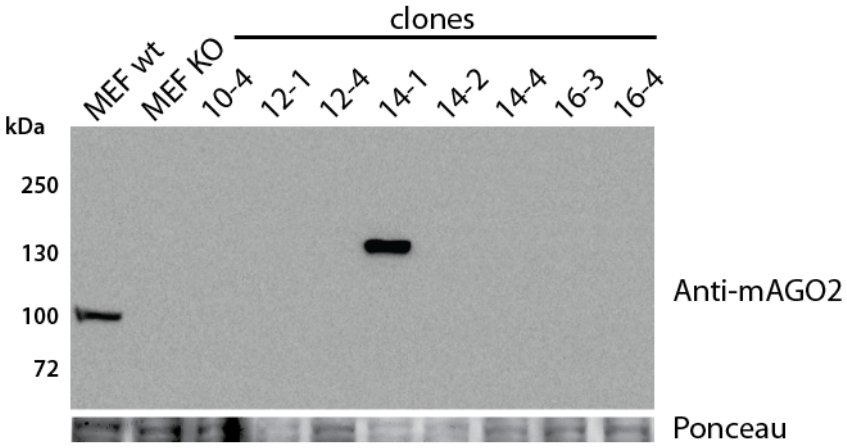

Figure 5 : Vérification de l'expression de la protéine de fusion BirA*-mAGO2 dans les clones MEF AGO2 -/-.
Analyse par Western blot des colonies sélectionnées pour l'expression de la protéine de fusion BirA*-mAGO2. L'échantillon MEF WT est issu des cellules MEF de souris sauvage et sert de control pour le niveau d'expression de la protéine AGO2 endogène. L'échantillon MEF KO est issu des cellules MEF AGO2-/- qui ont servi comme les cellules parentales pour la génération des colonies et sert comme contrôle négative. La coloration Ponceau est présentée comme contrôle de charge.

Suivant l'obtention de cette lignée stable, nous avons effectué l'expérience dans trois conditions, une condition sans infection servant de contrôle négatif (mock), une avec l'infection par MCMVwt et une par MCMVmut, trois réplicas techniques pour chacune des conditions (R1-3). A l'issue de l'analyse par spectrométrie de masse, nous avons constaté malheureusement que les échantillons contenaient beaucoup de résidus de streptavidine. Cela présente un problème pour l'identification des peptides car le signal est noyé par les peptides provenant de la streptavidine. Néanmoins, l'analyse par la spectrométrie de masse a permis l'identification de plusieurs partenaires connus d'AGO2 (Tableau 1), et également que certains de ces partenaires montraient un taux d'identification différentiel dépendant des conditions d'infection. Ce résultat en soi est encourageant car il montre que notre approche est fonctionnelle et elle permet l'identification quantitative de partenaires d'AGO2. Nous avons également recherché des protéines d'origine virale dans nos données, mais n'avons pu n'en identifier que deux. Cela peut être dû au fait que le virus n'exprime pas de protéines

interagissant avec AGO2 ou à la contamination par la streptavidine qui a empêché l'identification d'un plus grand nombre de protéines.

Tableau 1 : Les spectres de masse identifiés pour AGO2 et certains de ses partenaires directes et indirectes connus.

		Mock			**MCMV wt**			**MCMV mut**		
L'identité de la protéine	**Description de la protéine**	**R1**	**R2**	**R3**	**R1**	**R2**	**R3**	**R1**	**R2**	**R3**
Ago2	Protein argonaute-2 (BirA* fusion)	112	121	121	101	89	103	103	106	107
Hsp90ab1	Heat shock protein HSP 90-beta	19	20	22	17	20	24	24	21	23
Hsp90aa1	Heat shock protein HSP 90-alpha	5	4	5	5	5	8	8	7	6
Hspa8	Heat shock cognate 71 kDa protein	4	5	6	5	6	10	6	7	8
Tnrc6b	Trinucleotide repeat-containing gene 6B	9	8	13	6	7	8	5	7	6
Tnrc6c	Trinucleotide repeat-containing gene 6C	17	19	17	14	9	11	13	13	13
Edc4	Enhancer of mRNA-decapping protein 4	18	20	24	27	28	20	32	27	28
Cnot1	CCR4-NOT transcription complex subunit 1	4	2	4	1					1

Conclusion et perspectives

Les résultats obtenus au cours de cette thèse nous ont permis d'élargir notre compréhension du mécanisme de TDMD. Ce mécanisme dépend du degré d'appariement entre le miARN et sa cible ainsi que de leur abondance relative. De plus, à l'inverse de la répression d'une cible par miARN, il s'agit d'un processus non cumulatif. Nous avons identifié et démontré l'implication dans le TDMD de la protéine DIS3L2, la surexpression du mutant catalytique de cette enzyme permettant une stabilisation de miR-27 durant l'infection par MCMV. DIS3L2 est déjà impliquée dans la dégradation d'autres types de transcrit comme les mARN (Lubas et al., 2013; Malecki et al., 2013), des précurseurs de certains miARN (Chang et al., 2013; Ustianenko et al., 2013) et encore d'autres ARN non codants (Pirouz et al., 2016; Łabno et al., 2016) nos résultats élargissent la gamme de transcrit que cette enzyme peut réguler.

L'approche protéomique que nous avons mise en place semble être prometteuse pour l'identification des partenaires de AGO2 durant l'infection par MCMV. Elle nous a permis d'identifier certains des partenaires de AGO2, même si nous pouvons encore optimiser les conditions pour l'analyse par spectrométrie de masse. Enfin, la lignée cellulaire stable exprimant la fusion BirA*-mAGO2 pourrait être infectée dans l'avenir par différents virus pour identifier des partenaires généraux de AGO2 associé à l'infection ou des partenaires spécifiques associé un virus ou une famille de virus spécifique. De plus, cette lignée pourrait aussi servir à étudier la dynamique des partenaires de AGO2 dans des conditions de stress autre que l'infection virale.

Références

Ameres, S.L., Horwich, M.D., Hung, J.H., Xu, J., Ghildiyal, M., Weng, Z., and Zamore, P.D. (2010). Target RNA-directed trimming and tailing of small silencing RNAs. Science *328*, 1534–1539.

Baccarini, A., Chauhan, H., Gardner, T.J., Jayaprakash, A.D., Sachidanandam, R., and Brown, B.D. (2011). Kinetic analysis reveals the fate of a microRNA following target regulation in mammalian cells. Curr. Biol. *21*, 369–376.

Bail, S., Swerdel, M., Liu, H., Jiao, X., Goff, L.A., Hart, R.P., and Kiledjian, M. (2010). Differential regulation of microRNA stability. RNA N. Y. N *16*, 1032–1039.

Chang, H.-M., Triboulet, R., Thornton, J.E., and Gregory, R.I. (2013). A role for the Perlman syndrome exonuclease Dis3l2 in the Lin28-let-7 pathway. Nature *497*, 244–248.

Chendrimada, T.P., Gregory, R.I., Kumaraswamy, E., Norman, J., Cooch, N., Nishikura, K., and Shiekhattar, R. (2005). TRBP recruits the Dicer complex to Ago2 for microRNA processing and gene silencing. Nature *436*, 740–744.

Faehnle, C.R., Walleshauser, J., and Joshua-Tor, L. (2014). Mechanism of Dis3l2 substrate recognition in the Lin28-let-7 pathway. Nature *514*, 252–256.

Gantier, M.P., McCoy, C.E., Rusinova, I., Saulep, D., Wang, D., Xu, D., Irving, A.T., Behlke, M.A., Hertzog, P.J., Mackay, F., et al. (2011). Analysis of microRNA turnover in mammalian cells following Dicer1 ablation. Nucleic Acids Res. *39*, 5692–5703.

Gregory, R.I., Chendrimada, T.P., Cooch, N., and Shiekhattar, R. (2005). Human RISC couples microRNA biogenesis and posttranscriptional gene silencing. Cell *123*, 631–640.

Ha, M., and Kim, V.N. (2014). Regulation of microRNA biogenesis. Nat. Rev. Mol. Cell Biol. *15*, 509–524.

Haas, G., Cetin, S., Messmer, M., Chane-Woon-Ming, B., Terenzi, O., Chicher, J., Kuhn, L., Hammann, P., and Pfeffer, S. (2016). Identification of factors involved in target RNA-directed microRNA degradation. Nucleic Acids Res. *44*, 2873–2887.

Hutvágner, G., McLachlan, J., Pasquinelli, A.E., Balint, E., Tuschl, T., and Zamore, P.D. (2001). A cellular function for the RNA-interference enzyme Dicer in the maturation of the let-7 small temporal RNA. Science *293*, 834–838.

Iwasaki, S., Kobayashi, M., Yoda, M., Sakaguchi, Y., Katsuma, S., Suzuki, T., and Tomari, Y. (2010). Hsc70/Hsp90 chaperone machinery mediates ATP-dependent RISC loading of small RNA duplexes. Mol. Cell *39*, 292–299.

Jinek, M., Fabian, M.R., Coyle, S.M., Sonenberg, N., and Doudna, J.A. (2010). Structural insights into the human GW182-PABC interaction in microRNA-mediated deadenylation. Nat. Struct. Mol. Biol. *17*, 238–240.

Johnston, M., Geoffroy, M.-C., Sobala, A., Hay, R., and Hutvagner, G. (2010). HSP90 protein stabilizes unloaded argonaute complexes and microscopic P-bodies in human cells. Mol. Biol. Cell *21*, 1462–1469.

Jonas, S., and Izaurralde, E. (2013). The role of disordered protein regions in the assembly of decapping complexes and RNP granules. Genes Dev. *27*, 2628–2641.

Jonas, S., and Izaurralde, E. (2015). Towards a molecular understanding of microRNA-mediated gene silencing. Nat. Rev. Genet. *16*, 421–433.

Łabno, A., Warkocki, Z., Kuliński, T., Krawczyk, P.S., Bijata, K., Tomecki, R., and Dziembowski, A. (2016). Perlman syndrome nuclease DIS3L2 controls cytoplasmic non-coding RNAs and provides surveillance pathway for maturing snRNAs. Nucleic Acids Res.

Lee, Y., Ahn, C., Han, J., Choi, H., Kim, J., Yim, J., Lee, J., Provost, P., Radmark, O., Kim, S., et al. (2003). The nuclear RNase III Drosha initiates microRNA processing. Nature *425*, 415–419.

Lian, S.L., Li, S., Abadal, G.X., Pauley, B.A., Fritzler, M.J., and Chan, E.K.L. (2009). The C-terminal half of human Ago2 binds to multiple GW-rich regions of GW182 and requires GW182 to mediate silencing. RNA *15*, 804–813.

Liu, J., Carmell, M.A., Rivas, F.V., Marsden, C.G., Thomson, J.M., Song, J.J., Hammond, S.M., Joshua-Tor, L., and Hannon, G.J. (2004). Argonaute2 is the catalytic engine of mammalian RNAi. Science *305*, 1437–1441.

Lubas, M., Damgaard, C.K., Tomecki, R., Cysewski, D., Jensen, T.H., and Dziembowski, A. (2013). Exonuclease hDIS3L2 specifies an exosome-independent 3'-5' degradation pathway of human cytoplasmic mRNA. EMBO J. *32*, 1855–1868.

Malecki, M., Viegas, S.C., Carneiro, T., Golik, P., Dressaire, C., Ferreira, M.G., and Arraiano, C.M. (2013). The exoribonuclease Dis3L2 defines a novel eukaryotic RNA degradation pathway. EMBO J. *32*, 1842–1854.

Maniataki, E., and Mourelatos, Z. (2005). A human, ATP-independent, RISC assembly machine fueled by pre-miRNA. Genes Dev *19*, 2979–2990.

Marcinowski, L., Tanguy, M., Krmpotic, A., Rädle, B., Lisnić, V.J., Tuddenham, L., Chane-Woon-Ming, B., Ruzsics, Z., Erhard, F., Benkartek, C., et al. (2012). Degradation of cellular mir-27 by a novel, highly abundant viral transcript is important for efficient virus replication in vivo. PLoS Pathog. *8*, e1002510.

Mehta, V., and Trinkle-Mulcahy, L. (2016). Recent advances in large-scale protein interactome mapping. F1000Research *5*.

Pfaff, J., Hennig, J., Herzog, F., Aebersold, R., Sattler, M., Niessing, D., and Meister, G. (2013). Structural features of Argonaute-GW182 protein interactions. Proc. Natl. Acad. Sci. U. S. A. *110*, E3770-3779.

Pirouz, M., Du, P., Munafò, M., and Gregory, R.I. (2016). Dis3l2-Mediated Decay Is a Quality Control Pathway for Noncoding RNAs. Cell Rep.

Rooij, E. van, Sutherland, L.B., Qi, X., Richardson, J.A., Hill, J., and Olson, E.N. (2007). Control of Stress-Dependent Cardiac Growth and Gene Expression by a MicroRNA. Science *316*, 575–579.

Roux, K.J., Kim, D.I., Raida, M., and Burke, B. (2012). A promiscuous biotin ligase fusion protein identifies proximal and interacting proteins in mammalian cells. J. Cell Biol. *196*, 801–810.

Ustianenko, D., Hrossova, D., Potesil, D., Chalupnikova, K., Hrazdilova, K., Pachernik, J., Cetkovska, K., Uldrijan, S., Zdrahal, Z., and Vanacova, S. (2013). Mammalian DIS3L2 exoribonuclease targets the uridylated precursors of let-7 miRNAs. RNA *19*, 1632–1638.

Zekri, L., Huntzinger, E., Heimstädt, S., and Izaurralde, E. (2009). The Silencing Domain of GW182 Interacts with PABPC1 To Promote Translational Repression and Degradation of MicroRNA Targets and Is Required for Target Release. Mol. Cell. Biol. *29*, 6220–6231.

Semih CETIN

Caractérisation moléculaire du mécanisme de dégradation des microARN par un transcrit cible

Résumé

La littérature indique que les miARN sont régulés à plusieurs niveaux de leur biogenèse et de leur activité. Cependant, il existe très peu d'information concernant la régulation de la stabilité des miARN. Le projet de thèse a consisté à étudier la dégradation spécifique d'un miRNA cellulaire (miR-27) induite par un transcrit viral (m169) au cours de l'infection par le cytomégalovirus murin (MCMV). Ce miARN est déstabilisé par un mécanisme moléculaire appelé *'target-RNA directed miRNA degradation'* (TDMD). En suivant deux grands axes de recherche j'ai entrepris : premièrement l'étude et la caractérisation des déterminants moléculaires et des facteurs cellulaires impliqués dans le mécanisme de TDMD ; puis dans un second temps, la mise en place d'une approche protéomique permettant l'identification des partenaires de la protéine AGO2 potentiellement impliqué dans le TDMD dans des cellules infectées ou non par le MCMV.

Mots-clés : microARN – TDMD – MCMV - BioID

Résumé en anglais

Several regulatory mechanisms have been uncovered at every level of the biogenesis and the activity of miRNAs. However, there is less information about the regulation of the stability of miRNAs. The PhD project entailed the study of a process, which specifically enables the degradation of a cellular miRNA (miR-27) induced by a viral transcript (m169) during an infection by the mouse cytomegalovirus (MCMV). This miRNA is destabilized by a process called 'target-RNA directed miRNA degradation' (TDMD). I first undertook the study and the characterization of the molecular determinants and the cellular factors implicated in TDMD. Moreover, I started to set up a protocol in order to identify AGO2 partners of viral or host origin during MCMV infection, which would potentially be implicated in TDMD.

Keywords: microRNA – microRNA – MCMV – BioID